

CAPITAL UNIVERSITY OF SCIENCE AND  
TECHNOLOGY, ISLAMABAD



# Electric Machine Control Design for Hybrid Electric Vehicles

by

Athar Hanif

A thesis submitted in partial fulfillment for the  
degree of Doctor of Philosophy

in the

Faculty of Engineering

Department of Electrical Engineering

2018

# Electric Machine Control Design for Hybrid Electric Vehicles

By

Athar Hanif

(PE131003)

Dr. Matthew C. Turner

University of Leicester, UK

Dr. Codrin-Gruie Cantemir

The Ohio State University, OH, USA

Dr. Aamer Iqbal Bhatti

(Thesis Supervisor)

Dr. Noor Muhammad Khan

(Head, Department of Electrical Engineering)

Dr. Imtiaz Ahmed Taj

(Dean, Faculty of Engineering)

DEPARTMENT OF ELECTRICAL ENGINEERING  
CAPITAL UNIVERSITY OF SCIENCE AND TECHNOLOGY  
ISLAMABAD

2018

Copyright © 2018 by Athar Hanif

All rights reserved. No part of this thesis may be reproduced, distributed, or transmitted in any form or by any means, including photocopying, recording, or other electronic or mechanical methods, by any information storage and retrieval system without the prior written permission of the author.



**CAPITAL UNIVERSITY OF SCIENCE & TECHNOLOGY  
ISLAMABAD**

Expressway, Kahuta Road, Zone-V, Islamabad  
Phone: +92-51-111-555-666 Fax: +92-51-4486705  
Email: [info@cust.edu.pk](mailto:info@cust.edu.pk) Website: <https://www.cust.edu.pk>

**CERTIFICATE OF APPROVAL**

This is to certify that the research work presented in the thesis, entitled “**Electric Machine Control Design for Hybrid Electric Vehicles**” was conducted under the supervision of **Dr. Aamir Iqbal Bhatti**. No part of this thesis has been submitted anywhere else for any other degree. This thesis is submitted to the **Department of Electrical Engineering, Capital University of Science and Technology** in partial fulfillment of the requirements for the degree of Doctor in Philosophy in the field of **Electrical Engineering**. The open defence of the thesis was conducted on **March 13, 2018**.

Student Name: Mr. Athar Hanif (PE131003)

The Examining Committee unanimously agrees to award PhD degree in the mentioned field.

**Examination Committee :**

(a) External Examiner 1: Dr. Adeel Mehmood  
Assistant Professor,  
CIIT, Islamabad

(b) External Examiner 2: Dr. Muhammad Rehan  
Assistant Professor  
PIEAS, Islamabad

(c) Internal Examiner : Dr. Muhammad Ashraf  
Associate Professor  
CUST, Islamabad

**Supervisor Name :** Dr. Aamir Iqbal Bhatti  
Professor  
CUST, Islamabad

**Name of HoD :** Dr. Noor Muhammad Khan,  
Professor  
CUST, Islamabad

**Name of Dean :** Dr. Imtiaz Ahmad Taj  
Professor  
CUST, Islamabad

## AUTHOR'S DECLARATION

I, **Mr. Athar Hanif** (Registration No. PM-131003), hereby state that my PhD thesis titled, '**Electric Machine Control Design for Hybrid Electric Vehicles**' is my own work and has not been submitted previously by me for taking any degree from Capital University of Science and Technology, Islamabad or anywhere else in the country/ world.

At any time, if my statement is found to be incorrect even after my graduation, the University has the right to withdraw my PhD Degree.



(Mr. Athar Hanif)

Dated: **13** March, 2018

Registration No : PE131003

## PLAGIARISM UNDERTAKING

I solemnly declare that research work presented in the thesis titled “**Electric Machine Control Design for Hybrid Electric Vehicles**” is solely my research work with no significant contribution from any other person. Small contribution/ help wherever taken has been duly acknowledged and that complete thesis has been written by me.

I understand the zero tolerance policy of the HEC and Capital University of Science and Technology towards plagiarism. Therefore, I as an author of the above titled thesis declare that no portion of my thesis has been plagiarized and any material used as reference is properly referred/ cited.

I undertake that if I am found guilty of any formal plagiarism in the above titled thesis even after award of PhD Degree, the University reserves the right to withdraw/ revoke my PhD degree and that HEC and the University have the right to publish my name on the HEC/ University Website on which names of students are placed who submitted plagiarized thesis.

Dated: 13 March, 2018

  
\_\_\_\_\_  
(Mr. Athar Hanif)  
Registration No. PE131003

This thesis is dedicated to;  
Abu, Ammi, Hina, Moawaz, Moaaz, Afra, Fatima & Khadija

---

# *List of Publications*

It is certified that following publication(s) have been made out of the research work that has been carried out for this thesis:-

## **Journal Publications**

1. **A. Hanif**, A. I. Bhatti and Q. Ahmed, “Managing the Thermally Derated Torque of an Electrified Powertrain through LPV Control,” *IEEE/ASME Transaction on Mechatronics*, Vol. 23, no. 1, pp. 364-376, 2018. **impact factor: 4.357**
2. **A. Hanif**, Q. Ahmed, A. I. Bhatti and G. Rizzoni “Linear Parameter Varying based Field-oriented Control for an Induction Machine based Electrified Powertrain,” *International Journal of Robust and Nonlinear Control*, (Under Review), 2017.

## **Conference Publications**

1. **A. Hanif**, A. I. Bhatti, Q. Ahmed and G. Rizzoni, “Genetic Algorithms optimized Multi-objective Controller for an Induction Machine based Electrified Powertrain,” *In Control Technology and Applications (CCTA), 2017 IEEE Conference on 2017*, pp. 853-858. *IEEE*, Hawaii, USA.
2. **A. Hanif**, A. I. Bhatti and Q. Ahmed, “Estimation of thermally de-rated torque of an HEV drive using robust LPV observer”, in American Control Conference, 2016. Proceedings of the 2016, pp. 1530-1535, July 2016.
3. **A. Hanif**, A. I. Bhatti and Q. Ahmed, “Compensating the Performance and Loss of Life of an Induction Machine based Electrified Powertrain using Robust LPV Controller”, in American Control Conference, 2018. Proceedings of the 2018, Accepted, June 2018.

4. **A. Hanif**, S. M. N. Ali, Q. Ahmed, A. I. Bhatti, G. Yin, and M. H. Jaffery, “Effect of variation in rotor resistance on the dynamic performance of induction motor”, in 2016 35th Chinese Control Conference (CCC), pp. 9524-9529, July 2016.
5. **A. Hanif**, Aamer Iqbal Bhatti, Abdul Rehman Yasin, Ghulam Murtaza, and Qadeer Ahmed, “Sliding Mode Based Robust Observer Design for Field-oriented Control of 3-phase Induction Machine Drive for Applications in Hybrid Electric Vehicles”, in Control Conference (CCC), 2014 33rd Chinese, pp. 263-268, IEEE, 2014.
6. **A. Hanif**, Aamer Iqbal Bhatti, and Qadeer Ahmed, “LPV Based Robust Observer and Controller Design for Field-oriented Control of 3-phase Induction Machine Drive for Applications in Hybrid Electric Vehicles”. Presented in WEC-2013, NUST, 2013, Islamabad, Pakistan.

**Athar Hanif**

(Registration No.:PE131003)

## *Acknowledgements*

First and foremost I would like to thank Allah Subhana Wataallahu, who gave me the strength, guidance and opportunity to carry on my postgraduate studies in Pakistan. The perseverance granted by Almighty Allah helped me to bear the hard times in writing this thesis.

I acknowledge intimate support of my parents who kept me motivated and assured every kind of moral and financial support throughout my doctoral studies. I also appreciate my spouse and children for their cooperation, support and providing stress free atmosphere during my doctorate's tenure.

I am very much grateful to my supervisor Prof. Dr. Aamer Iqbal Bhatti, who's keen observance and directives helped me to develop and enhance my skills and research work well in time. His exceptional guidance has always enabled me to get out of difficulties of research work.

I extend my special thanks to my co-supervisor; Dr. Qadeer Ahmed for their invaluable support and technical guidance to make this research a success.

I would like to extend my gratitude to Prof. Dr. Giorgio Rizzoni, Center for Automotive Research (CAR), The Ohio State University, Columbus, USA; for inviting and giving me very good technical exposure at the world leading center in automotive research.

Special thanks to Dr. Abdul Rehman Kashif for providing the hardware setup for the validation of proposed control scheme.

Special thanks to the foreign evaluators: Prof. Dr. Matthew C. Turner and Dr. C. G. Cantemir.

I am also thankful to Dr. Amir Qayyum, Dr. Imtiaz Taj, Dr. Raza Sammar, Dr. Noor Muhammad Khan, Dr. Fazal ur Rehman and Dr. Muhammad Ashraf for their support and precious guidance during my postgraduate studies.

I also recognize the constructive comments and suggestions of Control and Signal Processing Research Group members: Dr. Ali Arshad, Dr. Safdar Hussain, Dr. Imran Khan, Dr. Ghulam Murtaza, Raheel Anjum, Salman Ali Shaukat and many others, who contributed a lot in improving this research work.

I am also greatly indebted to my parents in law for their sincere prayers.

In the last, I acknowledge the Higher Education Commission (HEC), Islamabad for financial support for this research work.

# *Abstract*

In order to achieve fuel efficiency and reduce emissions into the atmosphere, the automobile manufacturers have decided to escalate modern technologies such as Electric Vehicles (EVs) and Hybrid Electric Vehicle (HEVs). Vehicles with electrified powertrain exhibit degraded performance when operated in hot environments. When the operating and ambient temperatures rise, an electric drive suffers from torque derating, poor efficiency and loss of lifetime (aging) as its parameters change. Electric machine is the main component of an electrified powertrain. Among the available electric machines, induction machine has been used for the traction system of EVs and HEVs because of the advantages including reasonable cost, simpler control, enhanced power density and efficiency, consistent operation over wide speed range, elevated initial torque, technological development and universal availability. Induction machines are also very robust, have rugged construction and require little maintenance. Moreover, induction machines are inherently de-excited with respect to inverter fault hence highly recommended to be used in automobile industries for precautionary measures. This manuscripts presents the novel control schemes based on linear parameter varying theory for enhancing the performance of an induction machine based electrified powertrain. Linear parameter varying control theory is extensively used in time varying plants. Linear parameter varying observers and controllers based on linear parameter varying dynamics deliver robust platform for the estimation and control of electric drive system variables. In this dissertation, linear parameter varying based observer is designed for an electrified powertrain. The designed observer is used to estimate the thermally derated torque and flux of an electric powertrain. This estimation is extremely helpful in controller design for the performance improvement of electric drive system. Secondly, a robust control scheme is designed and developed in this thesis to address the torque derating problem. The designed observer-controller pair is used to manage the thermally derated torque of an electrified powertrain. The performance of the proposed linear parameter varying based observer-controller pair is evaluated for a light duty electric vehicle against

Federal Urban Driving Schedule (FUDS) operating at various ambient temperatures, which is a common controller evaluation approach adapted by automotive community. Experiments are carried out on an induction machine electric drive, realized by the NI myRIO-1900, using FUDS driving cycle to investigate that the proposed technique is effective and delivers robust performance. Another contribution of this manuscript is the design and development of degradation control scheme for an electric powertrain. In the synthesis of this control scheme, meeting the road loads, ensuring efficient powertrain operation and minimizing the loss of lifetime (aging) of an electric machine are considered as three essential but conflicting targets. The effectiveness of the proposed control framework is tested for a direct drive electrified powertrain of a three-wheeled vehicle commonly found in urban transportation for Asian countries. The urban driving schedule based simulation results confirm that the lifetime of induction machine can be enhanced by appropriate controller design without compromising its performance.

# Contents

<b>Author’s Declaration</b>	<b>v</b>
<b>Plagiarism Undertaking</b>	<b>vi</b>
<b>List of Publications</b>	<b>vii</b>
<b>Acknowledgements</b>	<b>ix</b>
<b>Abstract</b>	<b>xi</b>
<b>List of Figures</b>	<b>xvii</b>
<b>List of Tables</b>	<b>xxi</b>
<b>Abbreviations</b>	<b>xxii</b>
<b>Symbols</b>	<b>xxiii</b>
<b>1 Introduction</b>	<b>1</b>
1.1 Background . . . . .	1
1.2 Hybrid Electric Vehicles . . . . .	3
1.2.1 Types of Hybrid Electric Vehicles . . . . .	4
1.2.1.1 Parallel hybrid . . . . .	4
1.2.1.2 Split hybrid . . . . .	4
1.2.1.3 Series hybrid . . . . .	6
1.3 Electric Machine . . . . .	6
1.3.1 Induction Machine . . . . .	6
1.4 Degradation Control . . . . .	8
1.5 Motivation and Objectives . . . . .	8
1.6 Contributions . . . . .	10
1.7 Organization of the Thesis . . . . .	10
<b>2 Electric Machines in Hybrid and Electric Vehicles</b>	<b>14</b>
2.1 Introduction . . . . .	15
2.2 Propulsion Electric Machine Topologies . . . . .	18

2.2.1	Induction Machines . . . . .	19
2.2.2	Permanent Magnet Machines . . . . .	20
2.2.3	Switched Reluctance Machines . . . . .	22
2.3	Traction Operation Versus Industrial Operation . . . . .	23
2.4	Induction Machine for Traction System . . . . .	26
2.5	Research Scope in Induction Machine Control . . . . .	28
2.5.1	Parameter Variations Effects . . . . .	29
2.5.2	Review of Existing Estimators and Controllers . . . . .	30
2.5.2.1	Estimation Problem . . . . .	32
2.5.2.2	Control Problem . . . . .	35
2.6	Conclusion . . . . .	38
<b>3</b>	<b>Mathematical Modeling of Induction Machine</b>	<b>39</b>
3.1	Construction and Principle of Induction Machine . . . . .	40
3.2	Induction Machine Modeling . . . . .	42
3.2.1	d-q Model of a Three-phase Induction Machine . . . . .	45
3.2.1.1	d-q Model of a Three-phase Induction Machine in Synchronously Rotating Reference Frame . . . . .	46
3.2.1.2	d-q Model of a Three-phase Induction Machine in Stationary Reference Frame . . . . .	48
3.2.1.3	The Complete Dynamics of an Induction Machine . . . . .	51
3.3	Hybrid Electric Vehicle Drive System and Control . . . . .	51
3.3.1	Field-oriented Or Vector Control of a Three-phase Induction Machine Drive . . . . .	52
3.3.1.1	Direct or Feedback Field-oriented Control . . . . .	53
3.4	Load Torque Profile . . . . .	55
3.5	Model Based Analysis and Simulation . . . . .	57
3.5.1	Model Simulation and Discussion . . . . .	57
3.5.1.1	Positive Load Torque-Motoring Operation . . . . .	58
3.5.1.2	Positive and Negative Load Torque-Motoring and Generating Operation . . . . .	60
3.6	LPV Modeling of Induction Machine . . . . .	61
3.6.1	LPV Model Validation . . . . .	66
3.7	Conclusion . . . . .	69
<b>4</b>	<b>Estimation of Thermally de-rated Torque of an Electrified Powertrain</b>	<b>71</b>
4.1	Benefits of Thermally Derated Torque Estimation . . . . .	72
4.2	Advantage of LPV Control Technique . . . . .	72
4.3	Linear Parameter Varying Observer for Electrified Powertrain . . . . .	73
4.4	Current and Flux Dynamics . . . . .	75
4.4.1	Linear Parameter Varying Dynamics . . . . .	76
4.4.2	LPV Robust Observer . . . . .	76
4.4.2.1	Structure of Robust LPV Observer . . . . .	76
4.4.2.2	Observer Stability . . . . .	77

---

4.4.2.3	Observer Construction . . . . .	78
4.4.2.4	Synthesizing the Robust LPV Flux Observer . . . . .	79
4.4.2.5	Selection of Observer Gain . . . . .	80
4.5	Evaluation of Estimation Scheme . . . . .	80
4.5.1	Theoretical Scenario . . . . .	81
4.5.2	HEV Powertrain . . . . .	82
4.5.3	Thermally derated torque estimation . . . . .	84
4.6	Conclusion . . . . .	86
<b>5</b>	<b>Managing Thermally Derated Torque of an Electrified Powertrain</b>	<b>87</b>
5.1	Introduction . . . . .	88
5.2	Vehicle Dynamics and IM Modeling . . . . .	90
5.2.1	Vehicle Modeling and Dynamics . . . . .	90
5.2.2	Dynamics of IM . . . . .	91
5.2.3	LPV Modeling of Induction Machine . . . . .	92
5.3	EV Performance Constraints and IM Parameter Estimation . . . . .	92
5.3.1	Performance Criteria . . . . .	92
5.3.2	IM Performance Curve . . . . .	93
5.3.3	Rotor and Stator Resistance Estimation . . . . .	94
5.4	Control Design . . . . .	95
5.4.1	Controller Structure . . . . .	96
5.4.2	Robust LPV Current Controller . . . . .	97
5.4.3	Design Methodology . . . . .	100
5.4.4	Robust Torque and Flux Controller . . . . .	102
5.4.5	Reference Current Calculation . . . . .	106
5.4.6	Reference Flux Calculation . . . . .	107
5.4.7	Selection of Controller Gain . . . . .	108
5.5	Comparison With Sliding Mode Control . . . . .	108
5.6	Standard Driving Cycle Analysis . . . . .	110
5.6.1	EV Specifications and Simulation Detail . . . . .	111
5.6.2	Control Evaluation . . . . .	112
5.7	Experimental Verification . . . . .	118
5.7.1	Experimental Setup . . . . .	118
5.7.2	Open Loop Torque Derating Confirmation . . . . .	120
5.7.3	Comparison with Sliding Mode Controller . . . . .	120
5.7.4	Torque Derating Compensation against FUDS Cycle . . . . .	122
5.8	Conclusion . . . . .	124
<b>6</b>	<b>Degradation Control for an Induction Machine based Electrified Powertrain</b>	<b>126</b>
6.1	Introduction . . . . .	127
6.2	Brief Theoretical Background of Multi-objective Control Problem . . . . .	130
6.3	Proposed LPV based FOC Framework for Traction Induction Machine . . . . .	131
6.4	Modeling of Electrified Powertrain . . . . .	132

---

6.4.1	Vehicle Dynamics and Drivetrain Modeling . . . . .	133
6.4.2	Mathematical Model of IM . . . . .	134
6.5	Calculations for the Upper Limits on Stator Voltages . . . . .	137
6.6	The Multi-objective Functions . . . . .	138
6.6.1	Case-1 . . . . .	138
6.6.2	Case-2 . . . . .	139
6.6.3	Constraints . . . . .	139
6.6.4	Efficiency of Electrified Powertrain . . . . .	140
6.6.5	Road Load Error . . . . .	140
6.6.6	Aging . . . . .	140
6.6.7	Temperature Measurement . . . . .	141
6.7	LPV based FOC Control Design . . . . .	142
6.7.1	Torque and Flux Estimation . . . . .	142
6.7.2	Multi-objective LPV Controller Synthesis . . . . .	143
6.7.3	Robust Flux and Torque Controller . . . . .	147
6.7.4	Calculation for Reference Flux . . . . .	147
6.8	Performance Evaluation . . . . .	148
6.8.1	Vehicle specifications and simulation detail . . . . .	148
6.8.2	Simulation Results . . . . .	150
6.9	Conclusion . . . . .	158
<b>7</b>	<b>Conclusion and Future Directions</b>	<b>159</b>
7.1	Conclusions . . . . .	159
7.2	Contributions . . . . .	161
7.3	Future Directions . . . . .	162
<b>8</b>	<b>Appendices</b>	<b>164</b>
8.1	Appendix A . . . . .	164
8.1.1	Close-loop stability and synthesis of controller . . . . .	164
8.2	Appendix B . . . . .	167
8.2.1	Induced L-2 norm of LPV systems . . . . .	167
8.3	Appendix C . . . . .	167
8.3.1	Thermally derated torque's observer gains . . . . .	167
8.4	Appendix D . . . . .	170
8.4.1	LPV current controllers gains . . . . .	170
8.4.2	Torque and flux controllers gains . . . . .	173
	<b>Bibliography</b>	<b>174</b>

# List of Figures

1.1	Oil Production, Demand and Import by Pakistan[2]. . . . .	2
1.2	Based on the powertrain components arrangement, there are basically three schemes for the hybrid electric vehicles. (a)Parallel hybrid, (b)Split hybrid, and (c)Series hybrid . . . . .	5
2.1	Parallel HEV Configuration. . . . .	16
2.2	Schematic of an electric vehicle (EV) powertrain . . . . .	16
2.3	Electric Traction Motor (a) Torque-Speed Curve (b) Propulsive Effort Versus Speed [33]. . . . .	17
2.4	Motor Characteristics [33]. . . . .	18
2.5	Major traction and industrial machines. . . . .	19
2.6	Hybrid and electric vehicles. . . . .	24
2.7	Variations in (a) Drive cycle (b) Ambient temperature (c) Payloads and (d) Operating temperature. . . . .	25
2.8	(a) Rotor and stator resistance variations (b) Operating voltages imbalances and (c) Operating currents imbalances. . . . .	26
2.9	Effect of ambient and operating temperatures on the dynamic torque-speed characteristic curve for unipolar load torque. . . . .	31
2.10	Effect of ambient and operating temperatures on the dynamic torque-speed characteristic curve for bipolar load torque. . . . .	31
2.11	Direct Field-oriented Control Block Diagram With Rotor Flux Orientation [13]. . . . .	36
3.1	Idealized two pole three-phase wound-rotor induction machine [100].	40
3.2	Coupling effect in three-phase stator and rotor windings of the wound-rotor induction machine [13]. . . . .	42
3.3	Equivalent two-phase machine. . . . .	43
3.4	Stationary frame $a - b - c$ to $ds - qs$ axes transformation. . . . .	44
3.5	Location of rotating $d - q$ axes relative to stationary $d - q$ axes. . . . .	45
3.6	Dynamic $d - q$ equivalent circuits of a $3 - \phi$ induction machine [13].	46
3.7	Proposed Induction Machine Drive Structure with Direct or Feedback Field-oriented Control. . . . .	54
3.8	Phasor Diagram for Direct Field-oriented Control in Synchronously Rotating Reference Frame (SRRF)[13]. . . . .	55
3.9	Aerodynamic drag force, Rolling resistance force, Road grade force on a Vehicle . . . . .	56
3.10	Load Torque. . . . .	58

3.11	Induction machine load torque, electromagnetic generated torque, rotor speed. . . . .	59
3.12	Induction machine three phase current for the unipolar load torque. . . . .	59
3.13	Dynamic behavior of induction machine: Torque-speed curve. . . . .	60
3.14	Bipolar load torque. . . . .	61
3.15	Induction machine phase currents for bipolar torque. . . . .	61
3.16	Induction machine load torque, electromagnetic generated torque, rotor speed for bipolar torque. . . . .	62
3.17	Dynamic behavior of induction machine: Torque-speed curve. . . . .	62
3.18	Open-loop time response of an LPV model. Unit step demand in $u_{ds}$ , for 10 equally spaced values of $n_r, r_r, r_s$ . . . . .	66
3.19	Input voltages $u_{ds}$ and $u_{qs}$ to validate the nonlinear model and LPV model . . . . .	67
3.20	Load torque input $\tau_L$ to validate the nonlinear model and LPV model . . . . .	68
3.21	Validation plots of output currents $i_{ds}$ and $i_{qs}$ of the original nonlinear model and the LPV model. . . . .	68
3.22	Validation plots of states $\phi_{dr}$ and $\phi_{qr}$ of the original nonlinear model and the LPV model. . . . .	69
4.1	Overall scheme . . . . .	74
4.2	Robust LPV observer estimated results of : $d$ -axis flux(Top), $q$ -axis flux(Middle) and Torque derating(Bottom) at $-20^{\circ}C$ , $20^{\circ}C$ and $40^{\circ}C$ . . . . .	81
4.3	Robust LPV observer convergence results of actual and estimated: $d$ -axis flux(Top), $q$ -axis flux(Middle) and Torque derating(Bottom). . . . .	82
4.4	(a) 3-phase Input voltages to the electric drive system. (b) $u_{ds}$ and $u_{qs}$ for the electric drive system. . . . .	83
4.5	Robust LPV observer estimated results for shortened FUDS test cycle of : $d$ -axis flux(Top), $q$ -axis flux(Middle), and Torque derating(Bottom) at $-20^{\circ}C$ , $20^{\circ}C$ and $40^{\circ}C$ . . . . .	84
4.6	Robust LPV observer convergence results for shortened FUDS test cycle of actual and estimated: $d$ -axis flux(Top), $q$ -axis flux(Middle), and Torque derating(Bottom). . . . .	85
4.7	(a) 3-phase Input voltages to the electric drive system. (b) $u_{ds}$ and $u_{qs}$ for the electric drive system. . . . .	85
4.8	Robust LPV observer estimated torque derating under different operating conditions. . . . .	86
5.1	Induction motor (used in this work) performance curve at $25^{\circ}C$ and $40^{\circ}C$ (Torque derating at $40^{\circ}C$ is vivid). . . . .	94
5.2	Inner and outer loop strategy in induction machine. . . . .	96
5.3	Constraints on $S, T$ , and $KS$ in term of a generalized plant. . . . .	100
5.4	Simulation result for closed loop rotor velocity performance. (a) Load torque taken in closed loop simulation. (b) Rotor velocity tracking: reference (red) and actual (blue). . . . .	109
5.5	Vehicle level system architecture. . . . .	111

---

5.6	Simulation results: Temperature profile for the controller observer pair evaluation at different ambient temperatures. . . . .	113
5.7	Tracking of vehicle speed profile via a change profile of temperature (at ambient temperature of $40^{\circ}C$ ) with LPV controller observer pair. . . . .	114
5.8	Induction machine speed. . . . .	114
5.9	Simulation results: Rotor and stator resistance variations over the entire period of operation at different ambient temperatures. . . . .	115
5.10	Simulation results: Tracking of torque request profile via a change profile of temperature (at ambient temperature of $40^{\circ}C$ ) with LPV controller observer pair. . . . .	116
5.11	Simulation results: Tracking of flux request profile via a change profile of temperature (at ambient temperature of $40^{\circ}C$ ) with LPV controller observer pair. . . . .	116
5.12	Simulation results: Induction machine direct and quadrature axis (a) stator currents. (b) stator voltages: corresponding to the operation of electrified powertrain at $40^{\circ}C$ . . . . .	117
5.13	Experimental setup of an IM drive system. . . . .	119
5.14	Experimental result: Induction motor (used in this work) performance curve at $40^{\circ}C$ (Torque derating at $40^{\circ}C$ is vivid). . . . .	120
5.15	Actual (blue) and estimated (red) experimental results for a reference (trapezoidal-wave) of $\pm 10$ Nm. (a) Torque tracking. (b) Stator resistance variation. (c) Stator current. (d) Rotor flux. . . . .	121
5.16	Experimental result: Tracking of induction machine speed profile via a change profile of temperature (at ambient temperature of $40^{\circ}C$ ) with LPV controller observer pair. . . . .	122
5.17	Experimental results: Tracking of torque request profile via a change profile of temperature (at ambient temperature of $40^{\circ}C$ ) with LPV controller observer pair. . . . .	123
5.18	Experimental results: Tracking of flux request profile via a change profile of temperature (at ambient temperature of $40^{\circ}C$ ) with LPV controller observer pair. . . . .	123
5.19	Experimental results: RMSE and NRMSE values of induction machine: (a) Speed tracking (b) Torque tracking (c) Flux tracking. . . . .	124
6.1	Proposed LPV based FOC control framework for a traction induction machine. . . . .	132
6.2	Closed loop system block diagram . . . . .	144
6.3	IM winding temperature and resistance over the entire period of operation. . . . .	150
6.4	Vehicle speed profile for the validation of multi-objective LPV controller with and without aging compensation during the operation of electrified powertrain. . . . .	151
6.5	IM speed under the validation driving schedule with and without aging compensation. . . . .	152
6.6	Vehicle torques with multi-objective LPV controller: without and with aging compensation. . . . .	152

---

6.7	Power efficiency for an electrified powertrain after the compensation of change in operating conditions with multi-objective LPV controller.	153
6.8	Induction machine direct and quadrature axis (a) stator currents. (b) stator voltages with aging. . . . .	154
6.9	Induction machine direct and quadrature axis (a) stator currents. (b) stator voltages without aging. . . . .	155
6.10	IM winding temperature: simulation of driving cycle. . . . .	155
6.11	IM winding temperature: simulation of driving cycle with cooling phase. . . . .	156
6.12	(a) Average efficiency of an electrified powertrain. (b) RMSE values of vehicle torque. (c) loss of lifetime of an IM. . . . .	157
8.1	Generalized plant diagram. . . . .	164
8.2	Closed-loop system. . . . .	164

# List of Tables

2.1	Electric Traction Systems Evaluation . . . . .	27
3.1	State Variables Used in the Modeling of The Induction Machine . .	48
3.2	Induction Machine Specifications . . . . .	57
3.3	Accuracy of the LPV model in comparison to the nonlinear model .	69
4.1	Induction Machine Specifications . . . . .	80
5.1	Performance comparison of FOC-HOSMC and FOC-LPV to stator resistance variations . . . . .	110
5.2	Performance comparison of FOC-HOSMC and FOC-LPV to rotor resistance variations . . . . .	110
5.3	Specifications of an induction machine and a light duty electric vehicle	111
5.4	Performance indices comparison for proposed LPV based FOC con- trol framework at different ambient temperature . . . . .	117
6.1	Specifications of the three-wheeled vehicle induction machine . . . .	149
6.2	Specifications of a three-wheeled vehicle used in urban transporta- tion for Asian countries . . . . .	149
6.3	Optimal Value of Weighting Matrices coefficients . . . . .	150
6.4	Loss of lifetime of IM at ambient temperature of $40^{\circ}C$ and $20^{\circ}C$ . .	157

# Abbreviations

<b>IM</b>	Induction Machine
<b>EVs</b>	Electric Vehicles
<b>FOC</b>	Field-oriented Control
<b>DFOC</b>	Direct Field-oriented Control
<b>EPTP</b>	Electrical Power Transmission Path
<b>MPTP</b>	Mechanical Power Transmission Path
<b>PMM</b>	Permanent Magnet Machine
<b>PMSM</b>	Permanent Magnet Synchronous Machine
<b>PM BLDC</b>	Permanent Magnet Brushless DC
<b>SRM</b>	Switched Reluctance Machine
<b>HF</b>	Hybridization Factor
<b>PEM</b>	Power of Electric Machine
<b>PICE</b>	Power of Internal Combustion Engine
<b>PHEV</b>	Power to push the Hybrid Electric Vehicle
<b>SRRF</b>	Synchronously Rotating Reference Frame
<b>SRF</b>	Stationary Reference Frame
<b>d-axis</b>	Direct axis
<b>GHG</b>	Green House Gases
<b>q-axis</b>	Quadrature Axis
<b>HEVs</b>	Hybrid Electric Vehicles
<b>ICE</b>	Internal Combustion Engine
<b>LPV</b>	Linear Parameter Varying
<b>SMC</b>	Sliding Mode Control
<b>FUDS</b>	Federal Urban Driving Schedule

# Symbols

$n_r$	Rotor angular speed
$\phi_{dr}$	Rotor flux of direct (d)-axis
$\phi_{qr}$	Rotor flux of quadrature (q)-axis
$i_{ds}$	Stator current of direct (d)-axis
$i_{qs}$	Stator current of quadrature (q)-axis
$n_e$	Synchronous speed
$\tau_e$	Electromagnetic generated torque
$\tau_{eref}$	Reference electromagnetic generated torque
$\phi_{ref}$	Reference rotor flux
$\tau_L$	Load Torque
$v(t)$	Vehicle's instantaneous velocity
$P_{TR}(t)$	Instantaneous tractive power
$r_s$	Stator resistance
$r_r$	Rotor resistance
$\chi_s$	Stator leakage inductance
$\chi_M$	Magnetizing Inductance
$\chi_r$	Rotor leakage inductance
$n_p$	Number of pole pairs
$J$	Inertia
$b$	Damping
$n_M$	Mechanical Speed
$\rho_{air}$	Air mass density
$C_d$	Aerodynamic drag coefficient

$A_f$	Frontal surface area of the vehicle
$f_{ad}$	Aerodynamic drag force
$M$	Mass of the vehicle
$g$	Gravity acceleration
$C_r$	Rolling resistance coefficient
$\alpha_g$	Grade angle
$f_{roll}$	Rolling resistance
$f_{grade}$	Road grade force
$R_w$	Radius of the wheel
$R_f$	Ratio between the motor shaft and differential axle of the vehicle
$f_e$	Electrical frequency

# Chapter 1

## Introduction

This chapter provides the preliminary knowledge to understand the rest of the thesis.

### 1.1 Background

The world is facing severe energy crisis from the last few decades. As well as, harmful emissions produced due to the burning of oil are polluting the environment. Due to the both problems, peoples are much attentive toward the energy savings and environmental protection now a days. Use of oil in the transportation sector is much high than the other available energy resources. Therefore, it is producing the major problem for the both motives of energy savings and environmental protection. Currently, a study is conducted by the Energy Information Administration (EIA) [1], in United States, transportation sector is using 68% of available amount of the petroleum resources from which 66% of these assets were imported.

Correspondingly, in Pakistan (a developing country), Figure 1.1 depicts the oil production, demand, and import [2]. It can be observed in Figure 1.1 that there is a large gap between the oil production and its demand, in result, Pakistan spending billions of USD to import fuels to meet its power demand. Oil is the

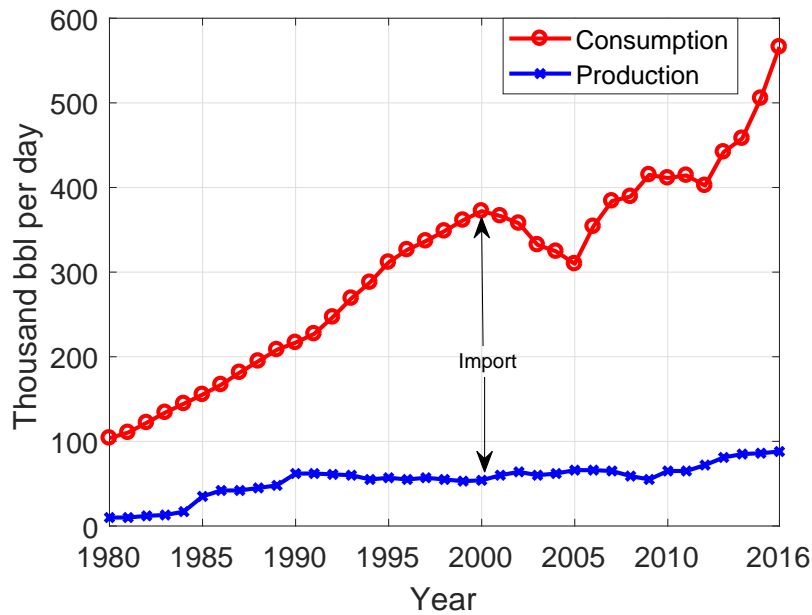


FIGURE 1.1: Oil Production, Demand and Import by Pakistan[2].

biggest contributor to transport sector in Pakistan, almost 48% of the oil resources are used in this sector [2]. So it can be concluded that utilizing the oil inefficiently is not an economically feasible energy strategy.

Moreover, the submission of numerous limiting legislations to manage the pollutant emissions, particularly the greenhouse gases (GHG) is also important element of this discussion. For illustration, an international agreement (Kyoto protocol) has been signed by all the countries to diminish the pollutant emissions especially carbon emissions upto 5.2% by 2012 than the value of carbon emissions in 1990 and so on [1]. It is clear from the literature that the transportation sector has very poor energy conversion efficiency of about 20% [1]. Therefore, due to the increasing nature of the energy requirements, limited availability of energy resources, lowest efficiency of energy conversion and inflexible rules about emission [3], the automotive leading industry is continuously practicing unusual traction systems (practical technologies) to reduce the dependence of transportation on the non-renewable energy types ,as well as they are trying to improve the fuel savings and the vehicle's efficiency. Electric machine has been used in vehicles as an alternative to the Internal Combustion Engine (ICE) by the automotive industry. The electric means of transport was preferable because of its calm, consistency

and most significantly the soundless operation, at the start of the 20th century. However, electric means of transport was removed from the market, excluding for some special uses due to the development of the ICE. Now a days, to reduce the fuel consumption and diminish the exhaust emissions, the hybridization of existing vehicles and electric powertrain is one of the viable solutions.

## 1.2 Hybrid Electric Vehicles

The vehicles with electric machine and internal combustion engine propulsion are known as Hybrid Electric Vehicles (HEVs). HEVs utilize the electrical energy from the batteries for its electric traction system with the combination of Atkinson Cycle Combustion Engine (ACCE) in series or parallel to the former traction system. The first hybrid vehicle was built in 1898 by Dr. Ferdinand P. This vehicle had an ICE to rotate the generator to charge the batteries. These batteries provide the electric power to the electric motor to drive the vehicle [4, 5]. However, hybrid vehicles have been ignored initially due the presence of heavy availability of the fossil fuel at very low cost, lack of knowledge regarding the harmful emissions and the development of the ICE technologies. These days the availability of oil is becoming shorter and shorter. Also the cost of oil and insertion of harmful emissions to environment is becoming high day by day. These are the alarming notions for the automotive industry to deploy the alternative energy resources in the vehicle as well as to meet the emission constraints imposed by the environment governing bodies. Therefore, the automotive industry is constantly evolving to meet two major demands of the world: (1) to meet consumer expectations and (2) to meet Environmental Protecting Agency (EPA) requirements. HEVs have successfully addressed the trade off between environmental and energy needs and consumer demand for performance and utility. A hybrid vehicle contains two power sources, usually a ICE is supplemented by one or more electric machines powered by electricity stored in a battery. This not only helps in providing the desired performance, decrease in emissions, and improved fuel efficiency, but also enables to recover energy wasted during braking. In summary, a HEV enables

fuel savings: (1) by avoiding engine idle (the engine is shut off whenever the vehicle is stationary); (2) by allowing for downsizing of the ICE without losing any performance; (3) by enabling electric-only drive mode for short distances under operating conditions that would normally correspond to very low engine efficiency; and (4) by allowing for the recovery of kinetic energy. The composite effect is a significant reduction in vehicle fuel consumption, typically highest for vehicles that are predominantly used in urban cycles [6]. It may be kept in mind that the peak ICE efficiency is not more than 30% while comparing it with that of the electric drives which is typically greater than 60%.

## 1.2.1 Types of Hybrid Electric Vehicles

According to the arrangement of components (ICE, Battery, Electric Machine Drive) used in the power train of the EVs and HEVs, there are broadly three types[5, 7, 8]:

### 1.2.1.1 Parallel hybrid

In Figure 1.2(a), an electric machine which act as a generator and motor is connected to the ICE through mechanical coupling. It behaves like a generator to charge the battery bank and behaves as motor to propel the vehicle whenever a boost is required in the speed. It also acts as a motor below the speed of  $60\text{Km/h}$ . Therefore, in this type of hybrid vehicles, engine is used at its optimal (highest) efficiency operating point. Brake energy is converted to the useful energy to charge the battery as shown in Figure 1.2(a).

### 1.2.1.2 Split hybrid

In Figure 1.2(b), type planetary gear set is used to connect the generator and engine, with third shaft is going to the vehicle's wheels. The engine charges the battery bank and it provides the power to the electric machine connected

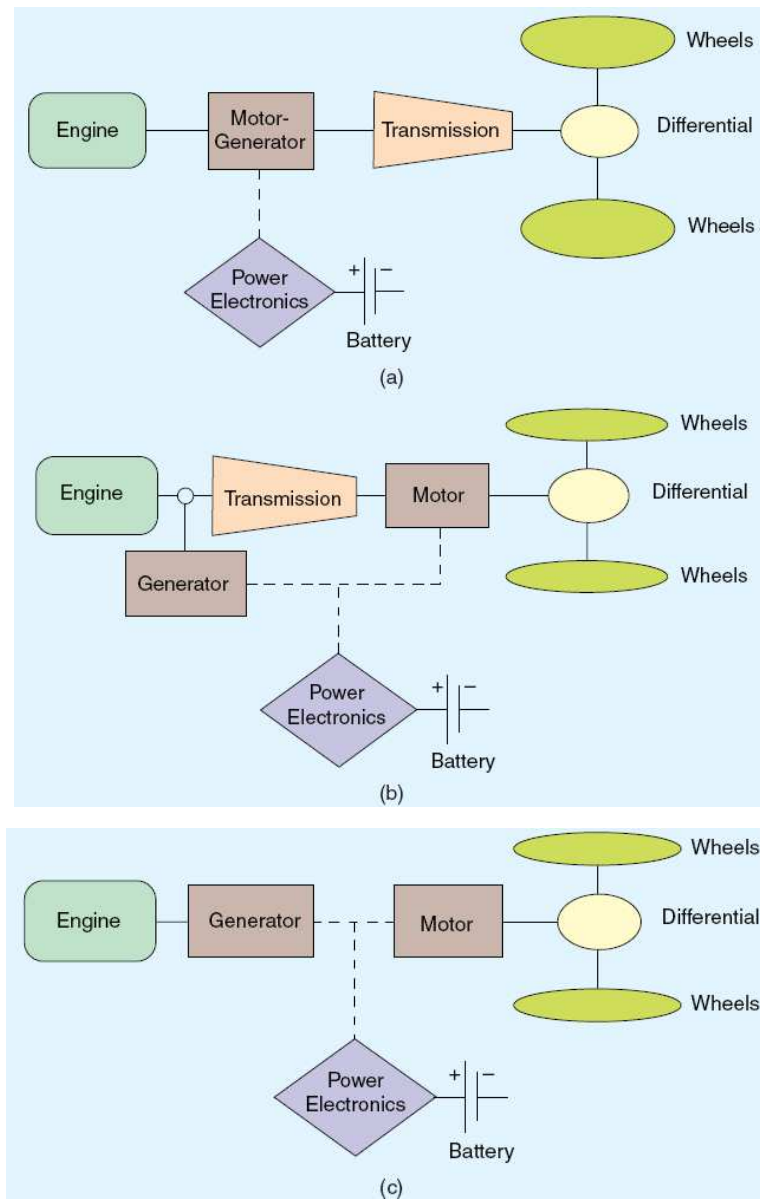


FIGURE 1.2: Based on the powertrain components arrangement, there are basically three schemes for the hybrid electric vehicles. (a)Parallel hybrid, (b)Split hybrid, and (c)Series hybrid

to the wheels through the power electronics circuits. Therefore, in this type of hybrid vehicles, engine directly drives the vehicle through the planetary gear and through the electrical path between generator, battery, and motor as shown in Figure 1.2(b).

### 1.2.1.3 Series hybrid

In Figure 1.2(c), engine has no connection with the transmission but it is used to run the generator to charge the battery bank. The battery bank provides the power to the electric motor to drive the vehicle as shown in the Figure 1.2(c). Therefore, this type of powertrain technology is also adopted for pure electric and plug in type hybrid vehicles.

## 1.3 Electric Machine

Matured manufacturing and elevated efficiency of electric machines have widened their scope of applications in industry, domestic appliances, and in modern automotive systems. The electric machine converts the electrical energy stored in the battery bank of the electrical vehicles (EVs) and hybrid electric vehicles (HEVs) into mechanical energy to achieve the efficient operation of electric drive (traction) system. The uses of electric machine in the automotive other than the propulsion include fuel pump, starter, power steering, alternator, etc. Now a days, electric machines are used in different drive systems of hybrid electric vehicles (HEVs) and electric vehicles (EVs) due to their availability in high power. Induction machines, DC machines, switched reluctance machines, permanent magnet machines, all are suitable applicants for the traction system as well as for high power starter-generator used in the electric and hybrid electric vehicles. Due to the heavy use of high power electric machines in automotive, efficient operation of control algorithms is the most crucial area of research to improve the torque performance, efficiency and lifetime of the machine and vehicle in the presence of rise in surrounding and operating temperatures.

### 1.3.1 Induction Machine

The induction machine has advantages over the other electric machines used in electric and hybrid electric vehicles. For example, it has wide speed range, low

cost, ruggedness, reliable, and complete deenergization because it has no brushes, one piece rotor shaft inherently, availability, and its safer operation in hazardous environment. Therefore, it is best suited for the hybrid and electric vehicles [9–12]. However, the control of the induction machine is not straightforward. Due to this, development of induction machine based drive system is complex. Initially, drive system were built using the scalar control method in which only the magnitude of the control variables are controlled. But these techniques are only useful for the constant speed operation [13]. In 1970's, a new field-oriented control (FOC) technique was developed by Haase and Blaschke to achieve the high performance drive system based on induction machine [14]. In this technique, both the magnitude and phase of the control variable are changed to control the machine operation. This technique is based on the machine's model in a rotor reference frame. Instead of having superior performance over scalar control, this method also suffers from some severe drawbacks, when it is adopted for high dynamic performance applications like hybrid and electric vehicles where exact and precise tracking is needed. These drawbacks include: the machine model is highly non linear, components of rotor flux which are the two states of the machine's model are actually not accessible, and some of the machine's parameters (rotor resistance, stator resistance etc.) change significantly during the operation. These changes have severe effect on the field-oriented control (FOC) of induction machine drive system for the applications in hybrid and electric vehicle than in other industrial applications. Because the operating conditions in hybrid and electric vehicles change constantly depending upon the traffic situations, drive cycles, load on the vehicle, and temperature, causing wide variations in speed. A significant change in rotor and stator resistances occurs linearly with the change in ambient and operating temperatures, depending upon the temperature coefficient of the resistance of the material as well as these are also effected by the skin effect [13, 15, 16]. The variations in rotor and stator resistances as well as wide variation in speed make the overall performance of the direct field-oriented control (DFOC) based induction machine traction system for HEVs and EVs poor. Because the whole operation of the induction machine propulsion system based on direct field-oriented control (DFOC)

is dependent on the exact and precise generation of the unit vectors ( $\cos\theta_e$  and  $\sin\theta_e$ ). Various methods are described in [7, 9, 10, 17–19] to overcome the rotor resistance variations only.

## 1.4 Degradation Control

Conventionally, the electric machine acts as prime mover in hybrid and electric vehicles, as discussed in Section 1.2. It is the most rugged and most reliable component over the whole electrified powertrain. It has expected life of 15 years or 20,000 hours without degrading with respect to its efficiency and power transferring capability. It is only possible by using high purity copper in windings. Due to this, it is most expensive component in electric and hybrid vehicle powertrain. Therefore, a compromise exists between the rate of degradation and the cost of the design of a traction machine for hybrid and electric vehicles [20, 21]. Degradation in winding insulation [22, 23], bearing [24, 25] and magnets [26] is associated with a traction machine used in electric and hybrid vehicles. The aforementioned degradations are high in traction machines. Traction machines have to fulfill the changing torque and speed demands unlike the industrial machines which are operated at static load conditions. Therefore, there is a genuine need to have a degradation-aware control techniques that will use to mitigate the aging, improve the torque tracking performance and efficiency of the an electric machine used in electrified powertrain of electric and hybrid vehicles. To achieve the degradation control, optimal methods can be used in traction machine control. The degradation metric will be discussed later in Chapter-6.

## 1.5 Motivation and Objectives

With the hasty development in automotive engineering, the researchers in automotive field have struggled hard to build up the schemes and make use of the diverse novel technologies to achieve fuel economy improvement and decrease in

the emission of vehicles. For these purposes the efficient control of the powertrain of vehicle has been of impressive significance.

Therefore, the foremost motivation of this research is to achieve the overall better torque performance, efficiency and minimizing the loss of lifetime (aging) of a traction induction machine based electrified powertrain deployed in the electric vehicles (EVs) and hybrid electric vehicles (HEVs) with the design and implementation of advanced and robust controllers. Secondly, this research also addresses and provides the optimum solution against the parameter variations of induction machine. The induction machine parameters change as the operating condition changes. Operating conditions for HEV propulsion system will change constantly. Traffic situations, driving cycles, etc. are the reasons of the variation in speed. Also temperature has the effect on parameters, which is influenced by ambient season, loading, etc. In spite of all these, induction machine must track the reference flux, which is desired to reduce the energy consumption in HEVs and EVs. Also torque demanded by the controller must be exact and efficient.

The primary objective of this research is to develop the novel (robust and advanced) controllers for the efficient control of the hybrid and electric vehicle's traction machine. The others objectives are:

- Design and implementation of a novel and robust observer for induction machine to estimate the thermally derated torque to achieve the efficient control of traction system.
- Design and implementation of novel and robust controller based on the novel and robust observer to manage the thermally derated torque (improve the performance) of traction system for hybrid and electric vehicles.
- Design and implementation of degradation control of an traction induction machine for hybrid and electric vehicles.

## 1.6 Contributions

The main contribution of this thesis is the development of robust control schemes to estimate and manage the thermally derated torque, enhance the efficiency of an electrified powertrain and minimize the loss of lifetime (aging) of a traction machine. The designed control scheme for HEV and EV powertrain overcomes the surrounding and operating temperatures effects on torque generating capability of a traction machine by delivering higher performance. Another control scheme is proposed to maximize the powertrain efficiency and mitigate the electric machine based electrified powertrain degradation while simultaneously providing the desired closed loop performance.

The presented and conducted research work has following main contributions:

- Development of Linear Parameter Varying (LPV) model for traction induction machine to cope with the change in operating and ambient temperatures.
- Estimation of thermally derated torque and flux of an traction drive.
- Development of method for confirmation of torque derating in traction machine.
- Compensation of thermally derated torque.
- Efficiency improvement control technique.
- Traction machine aging minimizing control technique.

## 1.7 Organization of the Thesis

Rest of the thesis is organized as discussed below:

**Chapter 2** discusses the types of the propulsion machines, their pros and cons, and their comparison based on the controllability, reliability, power density, technological maturity, efficiency, availability, and cost. A study based on aforementioned factors is done and concludes that induction machine is the excellent and decent choice for the Electric Vehicles (EVs) and Hybrid Electric Vehicles (HEVs). This chapter also describes the primary requirements of the electric traction drive for EVs and HEVs. The effects of change in operating and surrounding temperatures on the performance of an electric machine used for traction is also described. A detailed literature survey is presented for the existing estimators and controllers that have been used in induction machine based electric drive in general and for EVs and HEVs. The literature survey explains the past efforts of the researchers to estimate and control the flux, torque and speed of the induction machine based electric drive for industrial and traction applications. Moreover, it has been argued that estimating and managing of thermally derated torque in induction machine based electric drive is rare. The development of control technique for the degradation control of traction induction machine in EVs and HEVs is limited to improve the efficiency, performance and loss of life time (aging). It is still an open research task for a traction electric drive.

**Chapter 3** is devoted to the development of a mathematical model of the Induction Machine which has been chosen as a propulsion machine as detailed in chapter-2. This model will be used in propulsion drive needed for the hybrid and electric vehicles. It provides the background details needed for better understanding the induction machine from a dynamical system viewpoint. This model will be subsequently used for observer and controller design. A two-phase representation of a three-phase induction machine is described in this chapter. The voltage, flux, and current equations which are helpful in obtaining the induction machine model in arbitrary rotating reference frame and stationary reference frame are presented. The 5th order nonlinear model of induction machine, both in stationary reference frame and arbitrary rotating reference frame is derived. This model is used to derive the Linear Parameter Varying (LPV) model of an induction machine. Later on, this model will be used for the design of robust controllers and observers which

are necessarily required for the efficient operation of field-oriented control (FOC) of  $3 - \phi$  induction machine drive for the application in hybrid and electric vehicles. In the end, it is also simulated in Matlab<sup>®</sup>/Simulink software to appreciate its advantages from efficient operation viewpoint and model validation viewpoint as well.

**Chapter 4** deals with the estimation of thermally derated torque of an induction machine based electrified powertrain. This estimation is based on the LPV model presented in the preceding chapter. The estimation of thermally derated torque is more critical for obtaining the precise control to manage the thermally derated torque, improve the efficiency and minimize the loss of life time (aging) of an induction machine based electrified powertrain. Along with the estimation of thermally derated torque, flux of an induction machine based electric drive is also estimated. These objectives have been obtained by using a robust LPV based estimation technique. The LPV observer operates on a highly nonlinear currents and flux dynamics. Initially, the proposed estimation technique has been successfully tested by creating a theoretical scenario. Later on, estimation technique is investigated using shortened Federal Urban Driving Schedule (FUDS) test cycle for Hybrid Electric Vehicle (HEV) electric powertrain.

**Chapter 5** presents the Linear parameter varying based estimation scheme, discussed in Chapter 4 is used here to design linear parameter varying control technique to manage and compensate the thermally derated torque for an induction machine based electrified powertrain. The proposed scheme has the capability to retain the nominal performance even in the face of severe rise in the operating and surrounding temperatures. Due to the variations in ambient and operating temperatures, reasons are discussed in Section 2.3, proposed linear parameter varying control scheme reschedules its control signals to attain effective performance. The efficacy of the proposed algorithm is demonstrated for an EV operating in Federal Urban Driving Schedule (FUDS) with a dynamic temperature profile. The nonlinear simulation results confirm the LPV observer capability to successfully estimate the flux and derated torque in an EV drive system. The proposed technique, after

validating in simulation environment, is verified experimentally on an Induction Machine (IM) drive controlled by NI myRIO-1900.

**Chapter 6** describes a degradation control technique that is proposed to mitigate the electric machine based electrified powertrain degradation while simultaneously providing the desired closed loop performance. The performance of an electrified powertrain in extreme operating conditions is greatly compromised. This is due to the fact that meeting the road loads, ensuring efficient powertrain operation and minimizing the loss of lifetime (aging) of an electric machine are three essential but conflicting targets. In this chapter, a multi-objective Linear Parameters Varying (LPV) based Field-oriented Control (FOC) is proposed to address the problem of conflicting objectives mentioned above. The effectiveness of the proposed control framework is tested for a direct drive electrified powertrain of a three-wheeled vehicle commonly found in urban transportation for Asian countries. The urban driving schedule based simulation results confirm that the lifetime of induction machine can be enhanced by appropriate controller design without compromising its performance.

**Chapter 7** concludes the dissertation through outlining the main contributions and list of directions that can be accomplished in the future research.

## Chapter 2

# Electric Machines in Hybrid and Electric Vehicles

This chapter discusses the types of the propulsion machines, their pros and cons, and their comparison based on the controllability, reliability, power density, technological maturity, efficiency, availability, and cost. A study based on aforementioned factors is done and concludes that induction machine is the excellent and decent choice for the Electric Vehicles (EVs) and Hybrid Electric Vehicles (HEVs). This chapter also describes the primary requirements of the electric traction drive for EVs and HEVs. The effects of change in operating and surrounding temperatures on the performance of an electric machine used for traction is also described. A detailed literature survey is presented for the existing estimators and controllers that have been used in induction machine based electric drive in general and for EVs and HEVs. The literature survey explains the past efforts of the researchers to estimate and control the flux, torque and speed of the induction machine based electric drive for industrial and traction applications. Moreover, it has been argued that estimating and managing of thermally derated torque in induction machine based electric drive is rare. The development of control technique for the degradation control of traction induction machine in EVs and HEVs is limited to improve the efficiency, performance and loss of life time (aging). It is still an open research task for a traction electric drive.

## 2.1 Introduction

The propulsion electric machines and a ICE provides the traction power to the hybrid electric vehicles as shown in Figure 2.1. The traction power is delivered to the wheels through either the electrical power transmission path (EPTP) or the mechanical power transmission path (MPTP) or the combination of two. The vehicle electric machine drive subsystem must be capable of fulfilling the vehicle requirements at nominal load as well as extreme load conditions during starting and acceleration. The electric machine acts as motor and generator in either of the hybrid topology presented in Figure 1.2. The propulsion electric machine is the major component of an Electric Vehicle (EV). The schematic diagram of an electrified powertrain is shown in Figure 2.2. The traction motor can also recover the regenerative energy whenever the vehicle's brakes are applied. Therefore, the primary requirements of the electric traction drive for EVs and HEVs are the following: [27–32]:

- High torque density and power density
- High starting torque
- High Power
- High efficiency over wide torque and speed rang
- Very wide speed ranges
- Including constant torque and constant power regions
- High intermittent overload capacity
- Reasonable cost
- Reliability
- High efficiency for regenerative braking

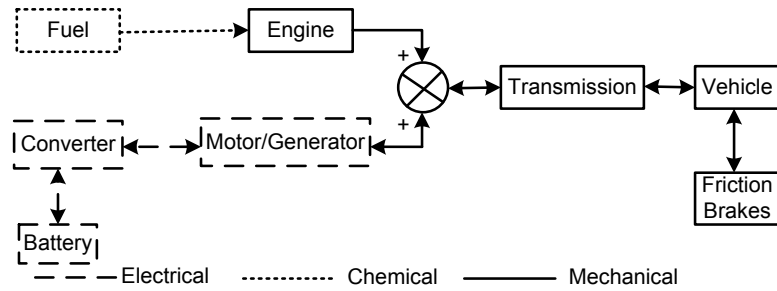


FIGURE 2.1: Parallel HEV Configuration.

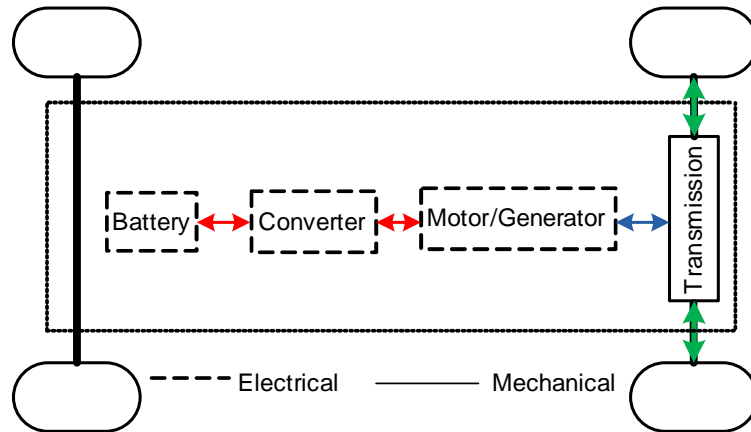
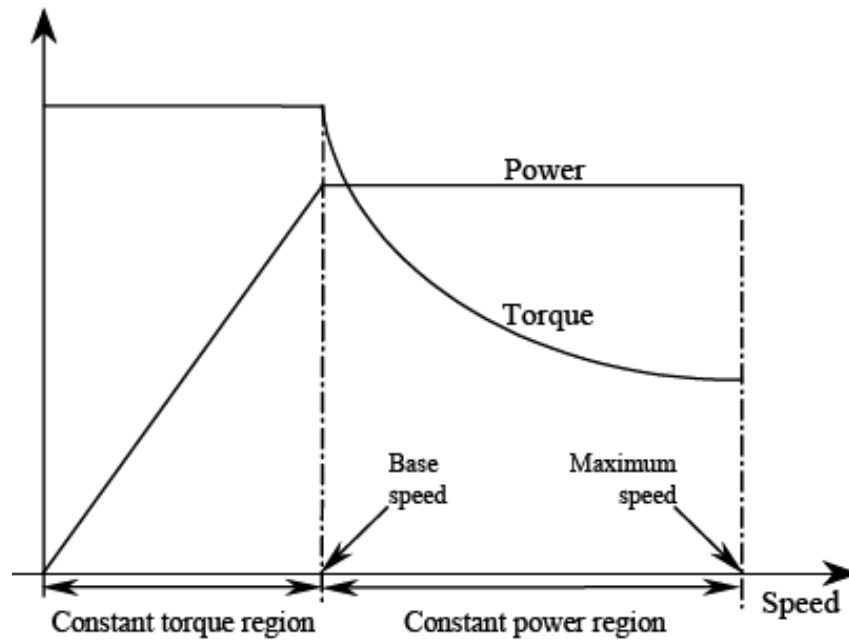


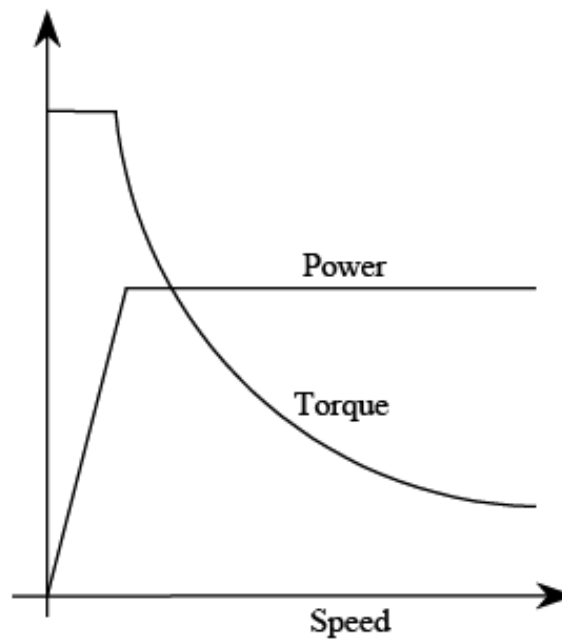
FIGURE 2.2: Schematic of an electric vehicle (EV) powertrain

The fuel efficiency and utilization time of the internal combustion engine in hybrid electric vehicle is based on precise and efficient utilization of electric machine. The selection of electric machine is based on appropriate torque-speed characteristics to deliver the demanded vehicle performance. The size of the electric machine is another important factor to be needed because it is to be packed and mounted inside the vehicle.

Figure 2.3 demonstrates the benchmark torque-speed curve of electric motor adopted in EVs and HEVs [33]. The propulsive effort versus speed that is required at the starting of vehicle from the electric motor is also shown in the Figure 2.3(b). It is clear from the curve that motor transmitted the maximum torque to the wheels upto the base speed where the maximum power condition of the motor is achieved. After this motor is not able to provide the rated torque. Modern power electronics circuits are used to operate the electric motor drive at any desired point inside the envelope of the torque-speed characteristics curve. Transmission gears are adopted



(a) Electric traction.



(b) Tractive effort versus speed.

FIGURE 2.3: Electric Traction Motor (a) Torque-Speed Curve (b) Propulsive Effort Versus Speed [33].

to match the lower rotations of the wheels to higher rotations of the electric motor in hybrid electric vehicles applications [34].

Figure 2.4 shows the the typical characteristics of an electric motor drive. High speed range operation with constant power beyond the rated speed is achieved by

flux-weakening. The torque speed characteristics shown in Figures 2.3 and 2.4 are bench mark for EVs.

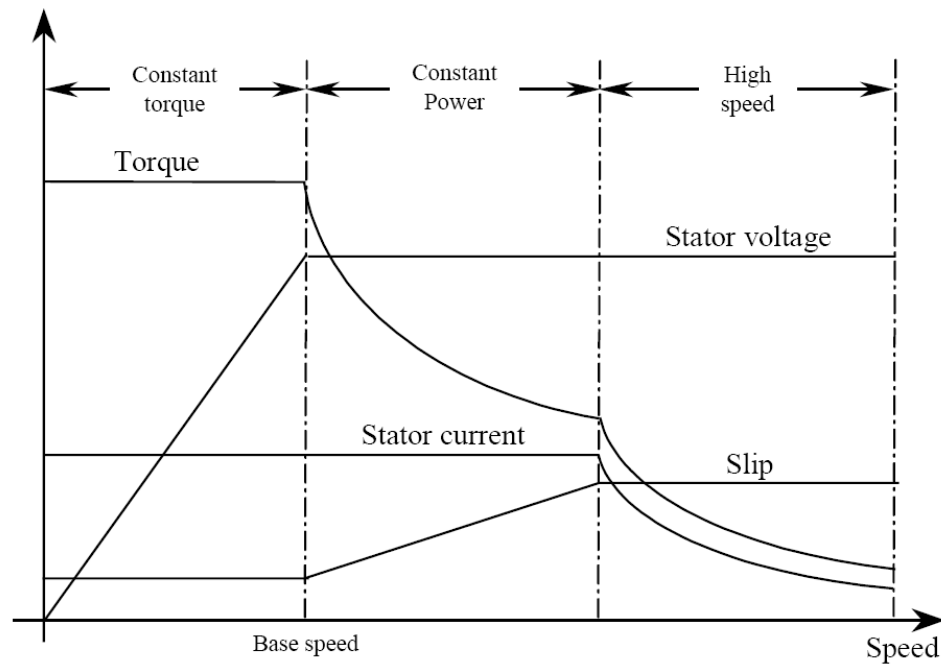


FIGURE 2.4: Motor Characteristics [33].

## 2.2 Propulsion Electric Machine Topologies

In recent vehicles, electric machines of more than 100 different types are used. Electric machines can be grouped as AC and DC types. Before 1980's, DC machines had wide applications in industries as well as in vehicles. DC machines are used in hybrid and electric vehicle technology because of variable torque-speed control and wide range of operation [35]. DC machines provide ease of control but they need commutator and brush maintenance, efficiency is low and also power to weight ratio is low. DC machines have been employed as for propulsion in Peugeot Partner (1990), Honda EV Plus(1997), Berlingo (1995) [12] and PSA Peugeot-Citreon (France) [33]. A prototype of plug-in type series hybrid electric vehicle using DC machine is implemented in [36].

After 1980, AC machines have started to replace the DC machine due the disadvantages of the later. At present, a great range of electric machines for use in vehicles

is commercially available. The possible candidate AC machines for HEVs and EVs are induction machines, permanent magnet machines and switched-reluctance machines [12, 37], as shown in Figure 2.5. Figure 2.5 also presents the cross-sections of the above mentioned machines. The main advantage of IMs, which are also known as asynchronous or squirrel-cage motors, is construction simplicity as shown in Figure 2.5 (a). PM motors are characterized by their constant rotor magnetization. PMs in the rotor induce high magnetic fields in the air gap, without excitation currents, leading to high power density as given in Figure 2.5 (b). The main characteristic of the switched-reluctance machine is the use of rotor salient poles as presented in Figure 2.5 (c).

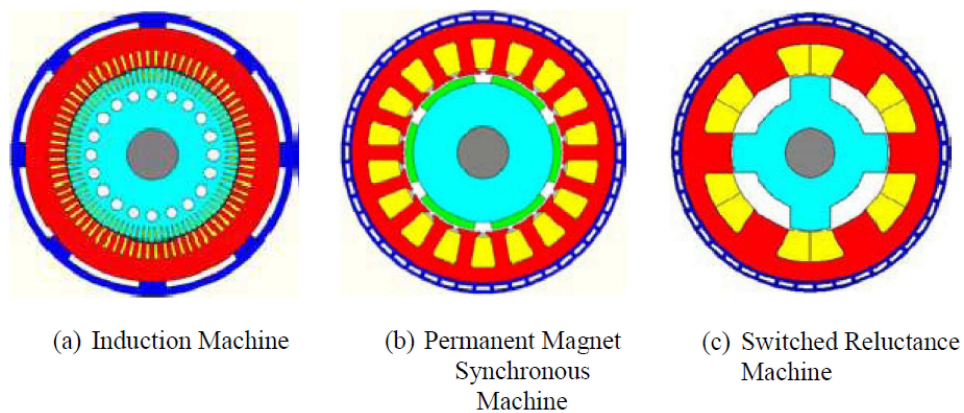


FIGURE 2.5: Major traction and industrial machines.

The next section will discuss these machines briefly.

### 2.2.1 Induction Machines

With much research and improvement activities over the last many decades, the technology of induction machine has become mature [38, 39]. Present growth in power electronics devices and digital signal processing chips, have made the control of induction machine like the separately-excited DC machine without the need of maintenance [40]. Induction machines are adopted in EVs, HEVs, and industry due to its low cost, reliability, ruggedness, robustness, high torque during starting and acceleration, high instant power, and wide range of speed of operation. Moreover, induction machines are inherently de-excited with respect to

inverter fault hence highly recommended to be used in automobile industries for precautionary measures [41]. The power to weight ratio of induction machines is much higher than the DC machines [12], therefore they are small in size as well. The induction machines also belong to the rotor and commutator less topology. Induction machines are of two kinds: wound-rotor and squirrel-cage. In wound-rotor type induction machine, the windings on the rotor are taken outside with the aid of slip rings. Due to this, external resistance can be added to change the rotor resistance. In squirrel-cage induction machine, the windings on the rotor are made of short-circuited aluminum or copper bars whose ends are welded to the copper rings. Automotive researchers show high interest in squirrel-cage induction machine for hybrid and electric vehicles. Induction machines are extensively used as a propulsion machine in hybrid and electric vehicles applications. Tesla Model (2012), Honda Fit EV (2012), Toyota RAV4 EV (2012), Renault/Kangoo (1998), BMW/X5 (Germany), Chevrolet (USA), Durango (USA), etc. [12, 33, 42]. In [43, 44], due to the simplicity, ruggedness, cheapness, low maintenance cost, high dynamic performance, and availability of enough starting torque and ability of acceleration, induction motor of squirrel-cage type is used as a propulsion motor in series HEVs. Chris Mi proposed induction machine of squirrel-cage type as a propulsion machine in hybrid and electric vehicles due to its small size as compared to DC machine, ease of fabrication, and high efficiency [45, 46]. Wide speed choice of operation can be achieved by flux-weakening with invariable power. Due to the occurrence of breakdown torque, the wide invariable power operation of induction machine is limited. This can be overcome by the use of multi-phase pole adjusting induction machines for the propulsion application [47, 48]. Tesla Motors have adopted induction machines for almost all types of hybrid and electric vehicles[10].

### **2.2.2 Permanent Magnet Machines**

Permanent magnet machines are widely used in traction, industry, and commercial applications. Permanent magnet machines are competing induction machine in the

hybrid and electric vehicle applications. Recently, permanent magnet machines are used by famous automaker for their hybrid electric vehicles. Toyota and Honda have adopted permanent magnet machines for more or less all types of hybrid and electric vehicles [10]. These machines have a various advantages such as high power density (for a known output power, there is a significance reduction in complete weight and volume), high efficiency (low losses), range of speed operation is wide, and compact size. It has small invariable power region. The primary difference between the permanent magnet machines and other kinds of rotating machine is the way in which they are excited. In permanent magnet machines, permanent magnets are used in the rotor as the field stimulant circuit, which is responsible for the production of air-gap magnetic flux. Therefore, the permanent magnets give the loss-less excitation without any external electric circuit. Conversely, because of permanent presence of flux from these permanent magnets, DC bus voltage method is much difficult for these types of machines as compared to the induction machines. The primary drawbacks of the PM machines are wrecked magnet chips and heating due to the rotor eddy currents at very high speed reduces the magnetization of the magnets [35].

Permanent magnet machine can be divided into two groups: permanent magnet synchronous machine (PMSM) and permanent magnet brushless DC (PM BLDC) machine. The major difference between the two is the stator winding [49–51]. In PMSM, sinusoidally distributed stator windings along the perimeter of the stator is producing the back-emf of sinusoidal nature. In PM BLDC, stator windings produce the back-emf of trapezoidal-shape. According to the shape and position of rotor's permanent magnet, PMSM are of three kinds: surface mount permanent magnet machine, interior permanent magnet machine, and unset permanent magnet machine. The only difference between the three kinds of permanent magnet synchronous machine is the placement of magnet into the rotor.

Permanent magnet machines are used as a propulsion machine in the hybrid and electric vehicles by famous automakers due to small size, low losses, and less weight in comparison to the induction machines [38, 39]. These have been used in Nissan Leaf (2010), Hyundai Blueon (2012), Mitsubishi iMiev (2009), Toyota Prius

(Japan), Nissan/Tino (Japan), Honda Insight (Japan) etc. [12, 33, 42]. The permanent magnets are needed for the permanent magnet machines which make them more costly as compare to the other types of the AC machines. At higher speed, rotor eddy currents increase the magnet heating, which is the source of demagnetization [35]. Placing the permanent magnet inside the rotor of the machine, improves the high speed operation due to the flux-weakening but cost will be increased [52].

### **2.2.3 Switched Reluctance Machines**

Another potential propulsion candidate for the hybrid and electric vehicles is the Switched Reluctance Machines (SRM). These machines have the advantages of simplicity, ruggedness, reliability, inexpensive, fault-tolerant control and operation, and excellent torque-speed envelope and large invariable power range. In switched reluctance machine, the phase inductance is maximum when stator and rotor poles are aligned and minimum in unaligned position. In motoring operation of SRM, the phase windings are energized during the instant when the inductance is increasing as the rotor moves. In generating operation of SRM, the phases are commutated on and off during the instant when the inductance is decreased as the rotor moves. In short, SRM needs the rotor pole arc slightly wider than that of the stator pole. The feasible stator/rotor pole number combinations (6/4, 8/6) of SRM are relatively less. Therefore, it requires special power converter topology and acoustic noise, high torque ripples, electromagnetic interference noise, and high bus current ripples are very high due to the sequential energization of diametrically opposite stator coils. The other disadvantages include: low torque for its volume, low efficiency, manufacturing complexity due to need of small air gap to maximize the power density and complex control technique in order to achieve the smooth torque. The above mentioned disadvantages are much critical for traction applications. Suitable solution to the aforementioned disadvantages are required to obtain a practicable switched reluctance motor based HEVs [53, 54]. The switched-reluctance machine has not yet been used in EVs and HEVs, but

it is successfully expressed as prototype [55]. The switched reluctance motor has been adopted in the Holden/ECOMmodore (Australia) hybrid electric vehicle for its traction system [33].

In the end, selection of traction motors for hybrid propulsion systems is a very important step that requires special attention. In fact, the automotive industry is still seeking for the most appropriate electric propulsion system for hybrid electric vehicles and even for electric vehicles. In this case, key features are efficiency, reliability and cost. The process of selecting the appropriate electric propulsion systems is however difficult and should be carried out at the system level. In fact, the choice of electric propulsion systems for HEVs and EVs mainly depends on three factors: driver expectation, vehicle constraint, and energy source. With these considerations, it is obvious that the overall motor operating point is not tightly defined. Therefore, selecting the most appropriate electric propulsion system for a HEV and EV is a challenging task [33].

## 2.3 Traction Operation Versus Industrial Operation

Vehicle with electrified powertrains exhibit degraded performance when operated in harsh environments. Conventionally, electric machine acts as a prime mover in EVs and HEVs as shown in Figure 2.1 and 2.2. It is one of the most reliable and most rugged component in the entire electric powertrain whether it is the powertrain of small car, delivery trucks, buses and vehicle used in construction as shown in Figure 2.6.

In Figure 2.6(a), a hybrid car is shown. Both electric machine (EM) and internal combustion engine (ICE) are used as propulsion systems. Parallel coupling of both (EM and ICE) components is common in hybrid electric vehicles, in which both components delivered propulsion torque to move the vehicle. Therefore in order to achieve the fuel economy and emission reduction, only electric motor provides the



FIGURE 2.6: Hybrid and electric vehicles.

traction force for the HEV within city (upto speed 40 Km/h). A similar concept and structure is deployed in urban delivery trucks as presented in Figure 2.6(b). Hybrid delivery trucks are used to distribute the mails within city and inter cities. Figure 2.6(c) and (d) represent the pure electric vehicle (electric truck and electric passenger bus). A high power electric machine with power modules and control circuitry is used to provide the transmission power to the wheels for propelling the vehicle. The schematic diagram of electric vehicle concept is shown in Figure 2.2. Electric passenger bus and electric truck are used to move the humans and goods within city respectively.

The causes which effect the operation of electric powertrain of an hybrid and electric vehicles are shown in Figure 2.7. In traction applications, electric machine has to be operate in different driving cycles such as Federal Urban Driving Schedule (FUDS). A complete FUDS driving cycle is shown in Figure 2.7 (a). It consists on number of frequent starts and stops, acceleration and de-acceleration and cruising and low speed intervals. This kind of driving cycles are used to evaluate the performance of electric and hybrid vehicles in America. The electric machine has

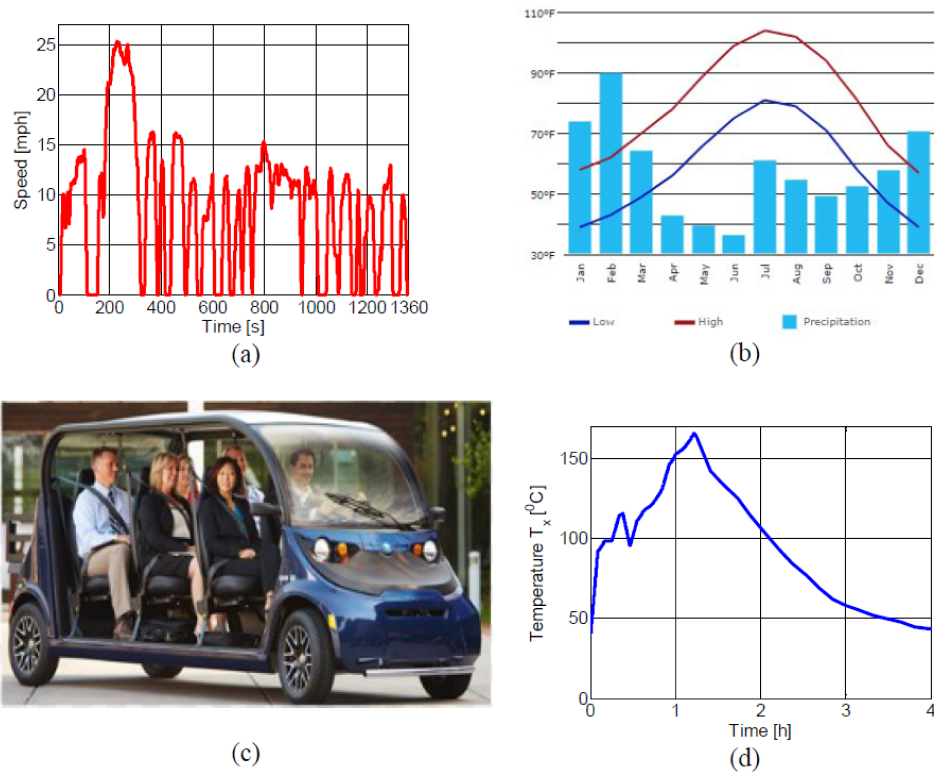


FIGURE 2.7: Variations in (a) Drive cycle (b) Ambient temperature (c) Payloads and (d) Operating temperature.

also supposed to be function under different ambient (surrounding) temperatures throughout the year. The ambient temperature profile for the city of Los Vegas in America is presented in Figure 2.7 (b). The payload on the vehicle is also continuously vary such as in electric and hybrid car and passenger bus. This is shown in Figure 2.7 (c). The operating temperature of an electric machine used in electric and hybrid vehicle vary continuously over the entire period of operation. The operating temperature profile of an electric machine in operating and stand-still conditions are shown in Figure 2.7 (d) [56, 57]. In short, electric machine has to operate under the different driving cycles, varying ambient temperatures, varying pay loads and varying operating temperatures conditions in comparison to the industrial operation of an electric machine.

As a result, all these conditions affect the winding resistances, produce the imbalance in the voltages and currents during the operation of traction machine for an electric powertrain [58–61] as shown in Figure 2.8. Figure 2.8 (a) gives the rotor and stator resistances variations for an electrified powertrain at different ambient

temperatures operating in FUDS driving cycle [62]. Figure 2.8 (b) and (c) show the zoomed version of electric machine voltage and current imbalances for an electrified powertrain functioning in FUDS driving cycle, respectively [62]. Due to these effects, the performance of a traction machine is deteriorated in following ways:

- Torque of an electric powertrain is thermally derated.
- Efficiency of an electric powertrain is reduced.
- Aging (loss of lifetime) of a traction machine is increased.

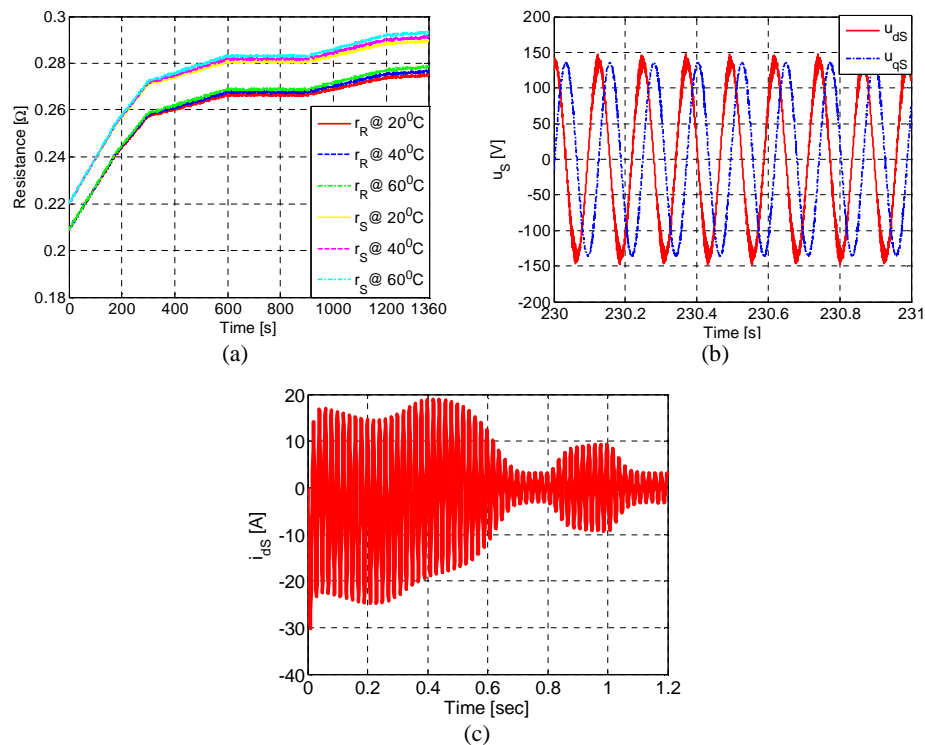


FIGURE 2.8: (a) Rotor and stator resistance variations (b) Operating voltages imbalances and (c) Operating currents imbalances.

## 2.4 Induction Machine for Traction System

In [12, 33], a complete comparison is accomplished among the induction machines, switched reluctance machines, and permanent magnet machines. The comparison

is based on the following factors: controllability, reliability, power density, technological maturity, efficiency, availability, and cost. In the aforementioned factors, controllability refers to the availability of matured control techniques and converter topologies used in the realization of electric machine control. The comparison has disclosed that the induction machine is the best appropriate choice for the applications in hybrid and electric vehicles although a hard competition exists with permanent magnet machines. The main advantages of adopting induction machine for EVs and HEVs are the availability of instant torque response only possible due the little leakage inductances, and capable to function in hostile environment. Induction machine has advantages of reliability, cheapness, ruggedness, and have an excellent invariable power region. The DC bus voltage control method is much feasible for the induction machines based propulsion drives as compared to the permanent magnet machines where constant source of flux is available to disturb this operation. Furthermore, it has very good efficiency along the broad range of speed operation. Table 2.1 provide the summary for the traction machines comparison. The comparison is based on the main characteristics of the HEV and EV electric propulsion presented in Section 2.1, each of them is graded from 1 to 10 points, where 10 points means the best. Indeed, this evaluation is an update of the one done in [33].

TABLE 2.1: Electric Traction Systems Evaluation

Sr. No.	Characteristics Vs Propulsion Systems	DC	IM	PM	SRM
1	Power Density	5	7	10	7
2	Efficiency	5	7	10	7
3	Controllability	10	10	8	6
4	Reliability	6	10	8	10
5	Technological maturity	10	10	8	8
6	Cost	8	10	6	8
7	Availability	8	10	8	5
	Total	42	64	58	56

As a result, induction machines is an excellent and decent choice for the hybrid and electric vehicles. Therefore, the primary objective of this research is to develop the novel (robust and advanced) controllers for the efficient control of the induction

machine based propulsion drive for the applications in hybrid and electric vehicles to achieve the high performance in the presence of conditions given in Section 2.3. The others objectives are:

- Design and implementation of a novel and robust observer for induction machine to estimate the thermally derated torque to achieve the efficient control of traction system.
- Design and implementation of novel and robust controller based on the novel and robust observer to manage the thermally derated torque (improve the performance) of traction system for hybrid and electric vehicles.
- Design and implementation of degradation control of an traction induction machine for hybrid and electric vehicles.

## **2.5 Research Scope in Induction Machine Control**

The traction machine is a necessary part of the drivetrain in the hybrid and electric vehicles. In order to optimize the operation of an electric powertrain, major efforts are in the direction of physical design of machine and improving its performance by means of closed-loop controllers. High performance induction machine based drive can be achieved by adopting the field-oriented control (FOC) method. But, the machine parameters needed for the implementation of field-oriented controller (FOC) should be exact and precise to obtain the good static and dynamic performance from the induction machine drive for the applications in electric vehicles and hybrid electric vehicles traction system. The IM parameters change as the operating conditions change. Operating conditions for an EV and HEV propulsion system change constantly. Traffic situations, driving cycles etc., are the reasons of variation in speed. Also temperature has the effect on parameters, which is influenced by ambient season and loading etc as elaborated in Section 2.3. Due to these effects, the flux and torque of an electrified powertrain is thermally derated

as compared to the industrial induction machines, where the variation in temperature and payload is very little. The effects of rise in operating and surrounding temperatures on the performance of induction machine drive has been studied in this research. In addition, a novel control techniques has been developed by considering the effects of rise in operating and surrounding temperatures to manage the thermally derated torque and to minimize the degradation on the performance of electric drive.

### **2.5.1 Parameter Variations Effects**

In direct or feedback field-oriented control (DFOC) method, the exact and precise measurement of rotor flux components is most critical and necessary. The generation of unit vectors which ensures the decoupling between d-axis and q-axis current components of the stator is dependent on these flux components. The model equations (3.29)-(3.36) given later show that the exact and precise values of rotor flux components is deteriorated by the variations in the following parameters.

- stator resistance
- rotor resistance
- wide variations in rotor speed

These variations are much sever for the operation of induction machine drive used in electric vehicles and hybrid electric vehicles. Both the resistances (stator and rotor) change due to the machine heating, skin effect, harmonics, and other non-idealities. Temperature shows significant effect on the stator resistance as well as on the rotor resistance. There will be a 20% to 60% change in the resistance when temperature changes from ambient temperature to the maximum operating temperature. The change in operating temperature is upto  $115C^o$  for high power induction machine [15, 16].

The conductor resistance temperature dependence is given as [62]:

$$R = R_{ref} (1 + \alpha (T - T_{ref})) \quad (2.1)$$

where,  $R$  is the conductor resistance at operating temperature,  $T(C^o)$ ,  $R_{ref}$  is the conductor resistance at ambient temperature,  $T_{ref}(C^o)$  and  $\alpha$  is the temperature coefficient. For copper conductor  $\alpha = 0.004041$  and for aluminum conductor  $\alpha = 0.004308$ .

The effects of rise in operating and ambient temperatures on the torque-speed characteristic curves of induction machine are studied in [63]. For this study, the induction machine's mathematical equations presented in fore-coming Section 3.2.1.3 are used. The unipolar and bipolar load torque disturbance are used with different ambient temperature conditions to investigate the study. At a high value of rotor resistance due to the elevated temperature, the starting torque and the slip of the motor is also quite high which results in the decrease in the amount of power in air-gap that actually converts into mechanical form. This phenomenon ultimately ends up with a lower efficiency of induction machine. The simulation study for three different ambient temperatures presented in Figures 2.9 and 2.10. Figures 2.9 and 2.10 depict the clear dynamic and steady-state behavior of an electric machine. In Figures 2.9 and 2.10, the zoomed portions of the plot represent the variation in dynamic performance of induction machine by the change in ambient temperature for unipolar and bipolar load torque.

## 2.5.2 Review of Existing Estimators and Controllers

In the hybrid and electric vehicle applications, the key problem is the performance of the electric traction system. The induction machine has been adopted for a propulsion system due to ease of control, reliability, high power density, technologically mature, high efficiency, ruggedness, availability of instant torque response during starting and acceleration, wide range of speed of operation, cost and inherently de-excited with respect to inverter fault. The feedback field-oriented control

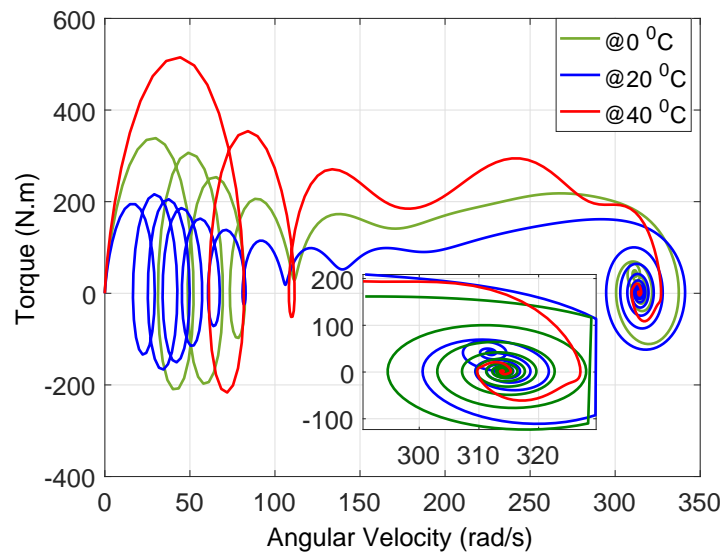


FIGURE 2.9: Effect of ambient and operating temperatures on the dynamic torque-speed characteristic curve for unipolar load torque.

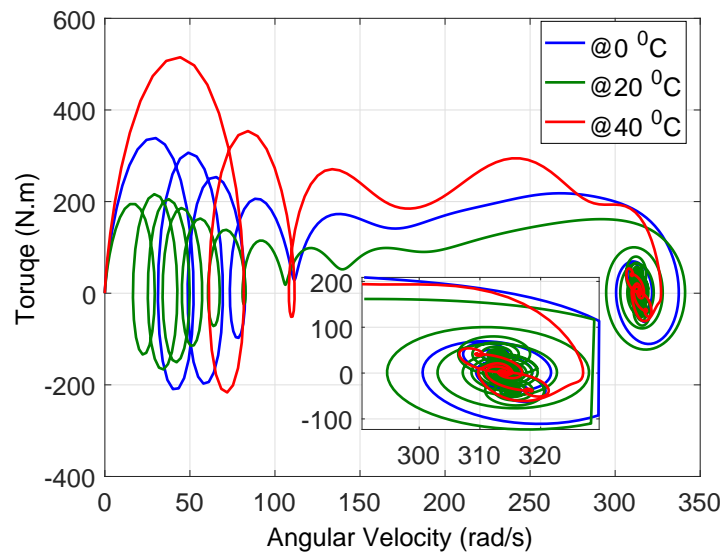


FIGURE 2.10: Effect of ambient and operating temperatures on the dynamic torque-speed characteristic curve for bipolar load torque.

of the induction machine is the most commonly adopted instantaneous speed/torque and flux control method for the hybrid and electric vehicle's propulsion system. The induction machine parameters change as the operating condition changes. Operating conditions for HEV propulsion system will change continuously. Traffic situations, driving cycles, etc. are the reason of variation in speed. Also temperature has the effect on parameters, which is influenced by ambient season, loading, etc. The feedback field-oriented control of induction machines

primarily depends upon the precise flux estimation. However, an accurate estimation of flux is hard due to the deviations in the machine's electrical parameters. Both the resistances (stator and rotor), which produces the imprecision in the flux estimation and in the generation of unit vectors ( $\cos\theta_e$  and  $\sin\theta_e$ ), increase linearly with temperature, depending upon the temperature co-efficient of the resistance of the material. The unit vectors are used to guarantee correct alignment of stator direct-axis current with the flux vector and stator quadrature-axis current perpendicular to it. This provides the decoupled control as in separately-excited DC machines. Secondly, unit vectors are used for the purpose of control. Therefore, the imprecision of the estimated flux will degrade the performance of torque/speed control.

Moreover, the HEV and EV electric machine torque generation capability is greatly affected by the surrounding thermal conditions as the motor parameters get altered [58]. Therefore, it is important to estimate the de-rated torque so that overall performance of the electric drive in an HEV can be monitored and later on it can be improved to meet the desired objectives.

Therefore, novel (robust and advance) observer-controller set is necessarily required for the efficient operation of induction machine based propulsion drive for the use in EVs and HEVs. As a result, torque compensation and degradation control of machine has been ensured.

### 2.5.2.1 Estimation Problem

An estimator (observer) is a supporting dynamical system which generates the estimate of the process's states by taking the input and output signal of the process. Then, this can be used to complete the closed loop control. Effective and suitable control techniques of induction machine propulsion systems need torque, speed and flux estimates in the presence of the parameter variations due to the change in surrounding and operating temperatures. In hybrid and electric vehicles, to achieve high performance, field-oriented control of induction motor drive is adopted. To implement the effective field-oriented control of induction motor

drive exact knowledge of rotor flux, torque as well as speed is required. Rotor flux, torque and speed are sensitive to the variation in rotor resistance, stator resistance, and load torque. Therefore robust observer is required. There are several methods available in the existing literature for the estimation of rotor flux and speed. The Luenberger and Kalman observers are the commonly adopted types of the induction machine observers [64–66]. The Luenbrger observer uses the stationary reference frame equations of induction machine model to estimate the the rotor flux and stator currents. The Luenberger observer’s gain matrix  $L$  is computed from the machine’s model. Therefore, it does not work efficiently due to the large variations in parameters due to the change in temperature as well as in measurements.

The current model flux estimator [67]–[68]–[69] and voltage model flux estimator [70] are extensively used for the flux estimation using the terminal quantities of the induction machine. The performance of current model flux estimator is deteriorated at high speed and the performance of voltage model flux observer is deteriorated at low speed due to the variation in the rotor resistance and stator resistance respectively. Because, the value of input signals are needed for voltage model flux observer which are very low at low speed and synthesis of rotor flux components with the help of speed and current signals are more easy at low speed. A hybrid model flux observer is suggested in [71], to use the current model flux estimator at low speed and voltage model flux estimator at high speed to overcome the problem of rotor and stator resistance variations. It does not completely overcome the dependency of observer on stator and rotor resistance.

Model referencing adaptive techniques are suggested in [72]–[73]–[74], two flux estimators are considered. One operates as a reference model, and other performs as an adaptive observer. The exact estimation of flux still remained as a problem. Another technique for the flux estimation is Extended Kalman filter as proposed in [66, 75, 76], where only motor terminal quantities are used. However, this technique has inherent problem of computation expense. Kubota, Matsuse and Nankano [65], used the full-order adaptive Luenberger flux observer to estimate

the stator currents and rotor fluxes with the help of fourth order part of the fifth-order induction machine model in stationary reference frame with constant rotor speed. Estimation of speed is done through the proportional plus integral formula.

Sliding mode has advantages of robustness and parameter invariance and order reduction [77]. Sliding mode observer of Derdiyok et al. [78] is used for the flux estimation with the same portion of induction machine model used in Kubota's observer. Sliding mode observer proposed by Utkin, Guldner, and Shi [77] is also used for the flux and speed estimation of induction machine. Utkin's observer is also based on the fourth order part of the fifth-order induction machine model in stationary reference frame. In the sliding mode technique based observers, the gain computation is tedious and trial basis. Sliding mode control technique has also the problem of chattering. In order to overcome the problem of chattering, higher-order sliding mode control (HOSM) techniques based observers are proposed and presented in [79–81]. But, the HOSM control technique is not robust like FOSMC method. For the implementation of HOSM control, ideal differentiator is needed which is not practicable and chattering is also appeared due to un-modeled fast dynamics sooner or later. In Verghese and Sander's flux observer [67], only flux estimation is focused by the authors. A fifth-order observer is also proposed in [82], to overcome the parameter's variation due to the abrupt change in operating conditions. In [83], the structure of the observer is inspired from the structure of Zak [84]. This observer faces the sever problem whenever the change in rotor speed is aggressive as in the case of hybrid and electric vehicles.

Another area of observer design in these days is the Linear Parameter Varying (LPV) technique. The main objective of the LPV control (gain scheduling) technique is to control the plant over the predefined operating range, but rather than simply being robust to variations in the plant, the controller is allowed to schedule itself based on some measurements. This is in opposite to the traditional Linear Time Invariant control technique which relies on the localized linear characteristics of the plant at a particular operating condition. The advantage of the LPV control structures lies in their explicit exploitation of knowledge of the actual plant dynamics, based on measurement. In addition to the measurement signal, the LPV

control technique takes the advantage of exogenous plant information to update its dynamics in real time. It is important to note that this information modifies not only the control signal, but also the way in which measurement signals are processed through the LPV control technique. As a consequence, LPV control technique can provide better robustness and performance properties than fixed controllers, which ignore the non-stationary nature of the plant. An LPV based rotor flux observer is presented in [85] but it only considered the rotor speed and rotor resistance variations. It does not consider the stator resistance variation in its observer design. In [86], LPV based observer for an induction machine is proposed and implemented which only takes the rotor resistance and load torque variations. In [87], only the stator resistance and rotor resistance variations have been taken into account.

From the above discussion, it can be seen that a variety of observer design techniques exist to address IM control in general. Some of them even consider limited parameter variations but not in the context of traction motor's flux and torque derating due to the change in operating and surrounding temperatures. It is worthwhile to mention that the study on estimating the thermally derated torque of an electrified powertrain is rare to the best of authors knowledge. As a result, in this research, a novel robust LPV based observer has been developed by taking into account the rotor resistance, stator resistance, and speed variations for the efficient control implementation of induction machine used in electric and hybrid vehicles.

### 2.5.2.2 Control Problem

Direct field-oriented control of an induction machine drive has two control loops: inner current loop, and outer flux and torque/speed control loops as shown in the Figure 2.11.

To realize these controller, Conventional Field-Oriented Control (FOC) is commonly used to ensure efficient operation of an IM based electric drive [10, 88]. The performance of conventional FOC is highly dependent on IM rotor and stator

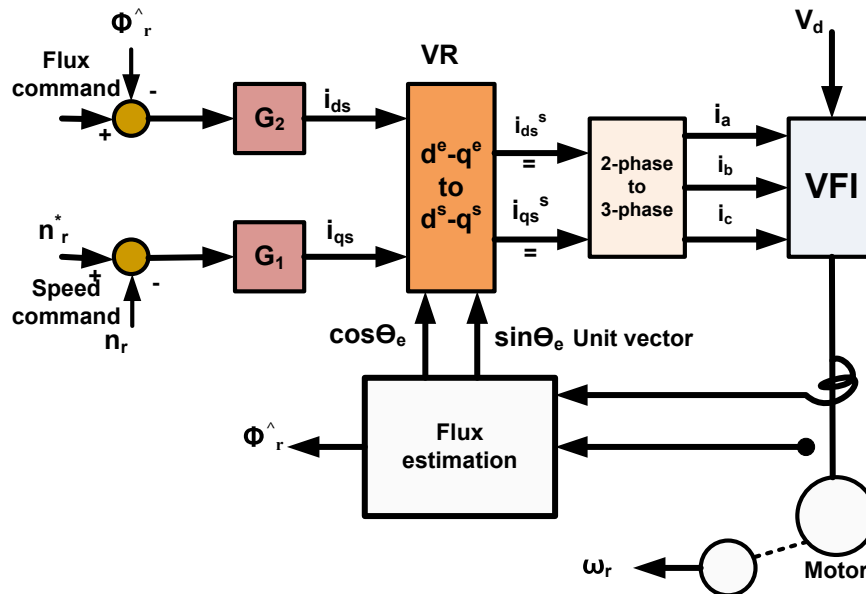


FIGURE 2.11: Direct Field-oriented Control Block Diagram With Rotor Flux Orientation [13].

parameters. These parameters are adversely affected in extreme operating conditions, part loads and variation in payloads. As a result, efficiency and torque of an electrified powertrain is also affected. Feedback linearization concept is used in [89–92] to compute the gains of the proportional plus integral controller for the flux and speed regulator. The robustness and parameter variations are not considered in the computation of controllers. As a consequence, performance of the control is deteriorated. Passivity based techniques [93–95], and First-order sliding mode control approaches [10, 96, 97] have been all studied and investigated. SMC technique is robust but it suffers from chattering problem. Due to the chattering in control, the optimal flux and torque is difficult to ensure for traction applications. The Higher Order Sliding Mode (HOSM) control based FOC is one of the possible solutions to minimize the chattering phenomenon and has been presented in [79–81]. But, the HOSM control technique is not robust like FOSMC method. For the implementation of HOSM control, ideal differentiator is needed which is not practicable and chattering is also appeared due to un-modeled fast dynamics sooner or later.

In [9], PI based field-oriented controller is implemented for the flux and torque tracking for the hybrid electric vehicle's applications. The resulting controller is

robust against the rotor resistance variations only. Adaptive anti-windup technique is deployed in [46], to design the flux and torque controller to implement the FOC of an induction machine for a hybrid electric vehicle. Machine parameter variations are not considered in the design process. Jalalifar, and Amir Farrokh in [43] implemented a controller based on input-output feedback linearization with the observer based on adaptive backstepping technique for the series hybrid electric vehicle. Field-oriented control based proportional plus integral controller has been proposed in [98], for the sensorless operation of induction machine drive for electric vehicle application. The output feedback controller is designed and validated in [99]. It addresses the limited parameter variations. Sensorless control techniques for electric vehicles are presented in [66, 76] for torque and flux tracking. In [85], linear parameter varying (LPV) feedback controller for the inner current loop is designed by taking into account the mechanical speed and the rotor resistance as the varying parameter. The outer flux and speed regulators are based on sliding mode control technique. In [86], linear parameter varying (LPV) feedback controller for the inner current loop is designed by taking into account the rotor speed as the varying parameter. The outer flux and speed regulators are designed classical linear techniques.

From the above discussion, it can be seen that a variety of control design techniques exist to address IM control in general. To the author best knowledge, in the current literature managing the thermally derated torque of an electrified powertrain is rare. The development of control technique to cater for the degradation (aging, efficiency, performance) as a joint criteria is limited as well. As a result, linear parameter varying (LPV) feedback controller for the inner current loop has been designed by taking into account the rotor speed, rotor resistance, and stator resistance as the varying parameters. The outer flux and speed regulators has been designed by solving the linear matrix inequalities. The development of advance, novel, and robust observer-controller set has been addressed in this research to cope with derated torque and powertrain degradation due to the rise in operating and ambient temperatures.

## **2.6 Conclusion**

To achieve the high performance of an electric drive in the presence of phenomenon discussed in Section 2.3, selection of the electric machine for the electric propulsion system of the EVs and HEVs is the most crucial step. Therefore, the selection of induction machine for the electric propulsion system of EVs and HEVs has been done on the basis of following parameters: controllability, reliability, power density, technological maturity, efficiency, availability, ruggedness and cost. Due to the parameters variations, the static and dynamic performance of induction machine, adopted as a propulsion machine in this research, is significantly affected, have been discussed. The existing techniques for the compensation of the effects due to the parameters variations on induction machine also have been described.

From this, it has been concluded that opportunities are exist in control, design and efficient use of induction machine drives in EVs and HEVs. As mentioned earlier, this research focuses on the design and development of novel (robust and advance) control techniques to estimating, managing the thermally derated torque, improving the efficiency of an electric powertrain and to minimize the loss of lifetime (aging) of an traction machine in the presence of adverse conditions presented in Section 2.3.

In the coming chapter, control-oriented non-linear model of an induction machine based drive will be formulated. An Linear Parameter Varying (LPV) model will be developed and presented for an induction machine based electric drive. Later on, LPV and non-linear models will be validated and analyzed for the parameters variations.

## Chapter 3

# Mathematical Modeling of Induction Machine

**Things of this world cannot be made known without Mathematics.**

Roger Bacon (1220-1292), Opus Majus, Transl. R. Burke 1928.

This chapter is devoted to the development of a mathematical model of the Induction Machine which has been chosen as a propulsion machine as detailed in chapter-2. This model will be used in propulsion drive needed for the hybrid and electric vehicles. It provides the background details needed for better understanding the induction machine from a dynamical system viewpoint. This model will be subsequently used for observer and controller design. A two-phase representation of a three-phase induction machine is described in this chapter. The voltage, flux, and current equations which are helpful in obtaining the induction machine model in arbitrary rotating reference frame and stationary reference frame are presented. The 5th order nonlinear model of induction machine, both in stationary reference frame and arbitrary rotating reference frame is derived. This model is used to derive the Linear Parameter Varying (LPV) model of an induction machine. Later on, this model will be used for the design of robust controllers and observers which are necessarily required for the efficient operation of field-oriented control (FOC)



slots and shorting rings are used to short it at either end. A wound rotor has a similar windings as of stator windings and rotor's shaft has slip rings which are used to tie the ends of the three rotor windings. The brushes are used to short the three phase rotor windings. If  $3 - \phi$  voltages are supplied to the windings of the stator. the three phase stator magnetomotive forces are developed and they produce the stator magnetic field. When the stator magnetic field cut the rotor conductors, it induces the voltage in the rotor side. The rotor currents will flow due to the induced voltages and as explained earlier rotor of the machine is short-circuited. The rotor currents will interact with the field of air-gap to induce the torque. Due to the induced torque, rotor will begin rotating. The direction of rotation is the same as that of the rotating field. The difference between synchronous speed (stator flux speed) and rotor speed is known as the slip speed. The slip,  $s$ , of the machine can be given as:

$$s = \frac{n_e - n_r}{n_e} \quad (3.1)$$

where  $n_e$  and  $n_r$  are the synchronous speed and rotor speed respectively.

The rotating field in the rotor circuit will be produced due to the induced currents and it can be given as:

$$f_r = s f_e \quad (3.2)$$

where  $f_r$  and  $f_e$  is the rotor frequency and stator frequency respectively.

The induced torque due to the relative motion between the stator and rotor magnetic fields are given as:

$$\tau_{ind} = k B_r \times B_s \quad (3.3)$$

where  $B_r$  and  $B_s$  are rotor and stator magnetic flux densities respectively.  $k$  is a constant depending on the machine construction. The induced torque will be zero when rotor is running at synchronous speed and in result the rotor slow down due to the frictional losses.

## 3.2 Induction Machine Modeling

Electromagnetic coupling exists between the stator and rotor circuits of the induction machine. Therefore, the coupling coefficient between the stator and rotor phases changes continuously with the change of rotor position  $\theta_r$ . This coupling effect can be removed by transferring/referring the stator and rotor variables to a common reference frame which may rotate at any speed (arbitrary reference frame) [13], [40]. For better graphical interpretation and simpler mathematical manipulation, a three-phase machine can be represented by an equivalent two-phase machine as shown in Figures 3.2 and 3.3. The variables in the equivalent two phase machine are: direct axis (d) and quadrature axis (q) variables as described in Figure 3.3.

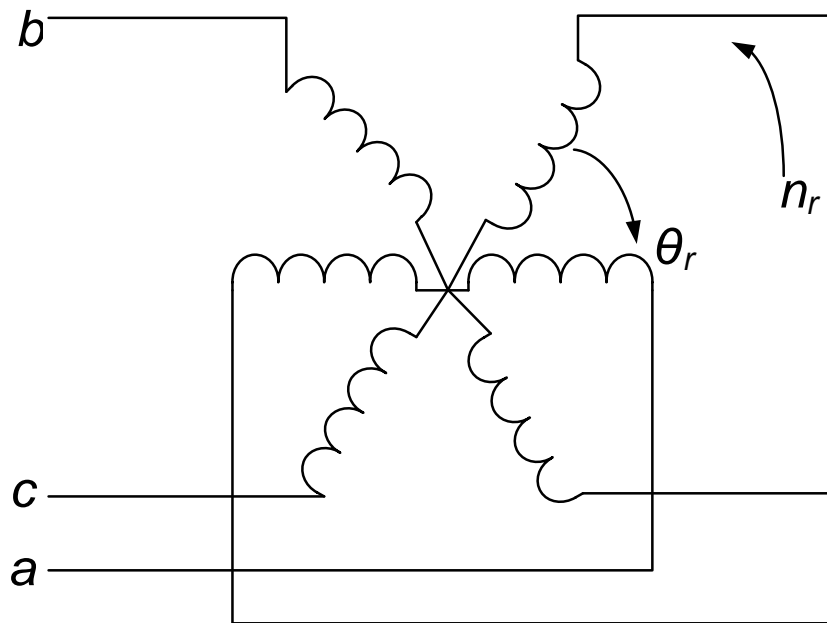


FIGURE 3.2: Coupling effect in three-phase stator and rotor windings of the wound-rotor induction machine [13].

In Figure 3.3,  $d^s - q^s$  correspond to stator direct and quadrature axes, and  $d^r - q^r$  correspond to rotor direct and quadrature axes. In Figure 3.2, the axes a, b, c are the stator abc reference frame and the rotor reference frame for the subscript of s and r attached to these axes respectively. If the synchronous speed,  $n_e$ , is zero, the common reference frame is said to be non-rotating and it is known as stationary reference frame (SRF) [13]. Similarly, if  $n_e$  is not zero, the common

reference frame is said to be a rotating and it is known as synchronously rotating reference frame (SRRF) [13].

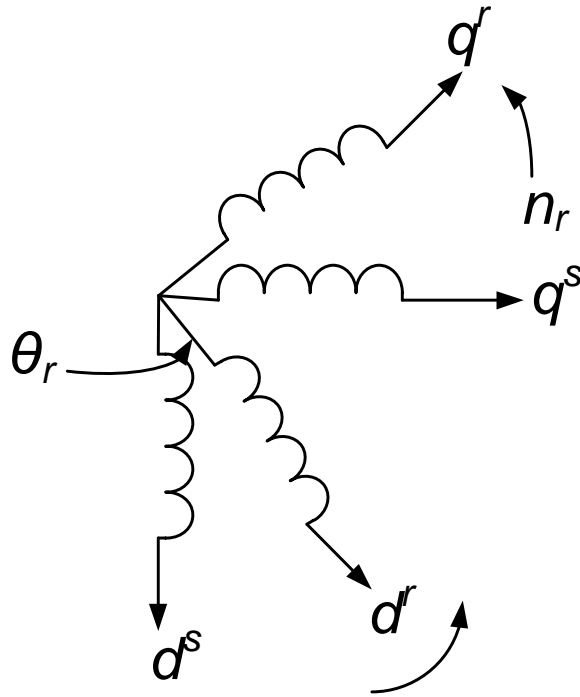


FIGURE 3.3: Equivalent two-phase machine.

The stator axes variables: a, b, c can be transformed to the  $d - q$  axes as shown in Figure 3.3 by the following equations.

$$f_{qs} = \frac{2}{3}[f_{as}\cos\theta + f_{bs}\cos(\theta - 120^\circ) + f_{cs}\cos(\theta + 120^\circ)] \quad (3.4)$$

$$f_{ds} = \frac{2}{3}[f_{as}\sin\theta + f_{bs}\sin(\theta - 120^\circ) + f_{cs}\sin(\theta + 120^\circ)] \quad (3.5)$$

Where the symbol  $f$  represent the current and the voltage of the three-phase and two-phase stator circuit.  $f_{qs}$  is the stator quadrature axes voltage or current,  $f_{ds}$  is the stator direct axes voltage or current,  $f_{as}$  is the stator phase  $a$  voltage or current,  $f_{bs}$  is the stator phase  $b$  voltage or current and  $f_{cs}$  is the stator phase  $c$  voltage or current.

Similarly, the stationary direct (d) and quadrature (q) axes quantities can be converted to synchronously rotating direct (d) and quadrature (q) axes quantities

as shown in Figure 3.4 by the following equations.

$$f_{ds}^e = f_{qs}^s \sin\theta_e + f_{ds}^s \cos\theta_e \quad (3.6)$$

$$f_{qs}^e = f_{qs}^s \cos\theta_e - f_{ds}^s \sin\theta_e \quad (3.7)$$

The rotating reference frame quantities can be converted to synchronously rotating reference frame by the following equations.

$$f_{ds}^s = -f_{qs}^e \sin\theta_e + f_{ds}^e \cos\theta_e \quad (3.8)$$

$$f_{qs}^s = f_{qs}^e \cos\theta_e + f_{ds}^e \sin\theta_e \quad (3.9)$$

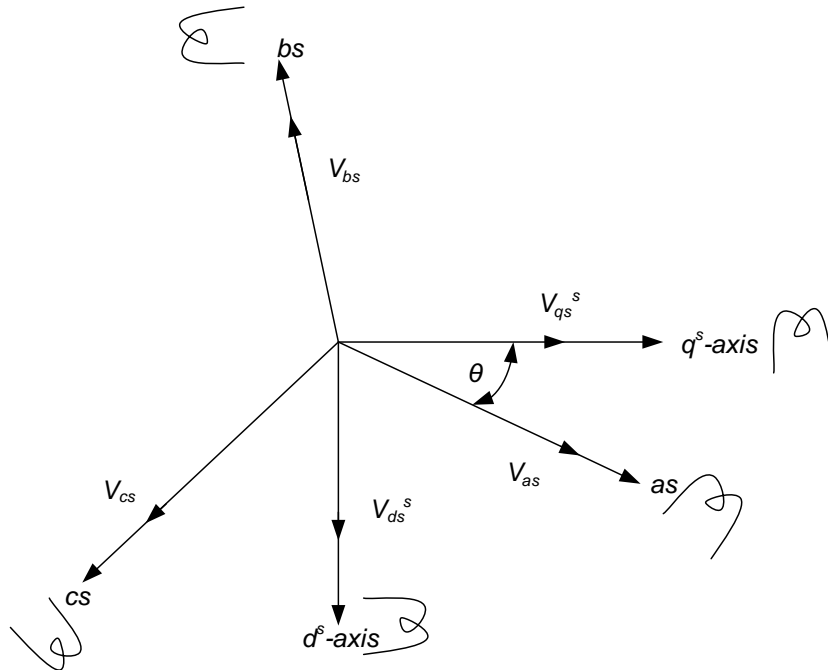


FIGURE 3.4: Stationary frame  $a - b - c$  to  $ds - qs$  axes transformation.

After the substitution of three-phase stator sinusoidal and balanced voltages in the (3.4) and (3.5), following equations yields.

$$f_{qs}^s = f_m \cos(\omega_e t + \phi) \quad (3.10)$$

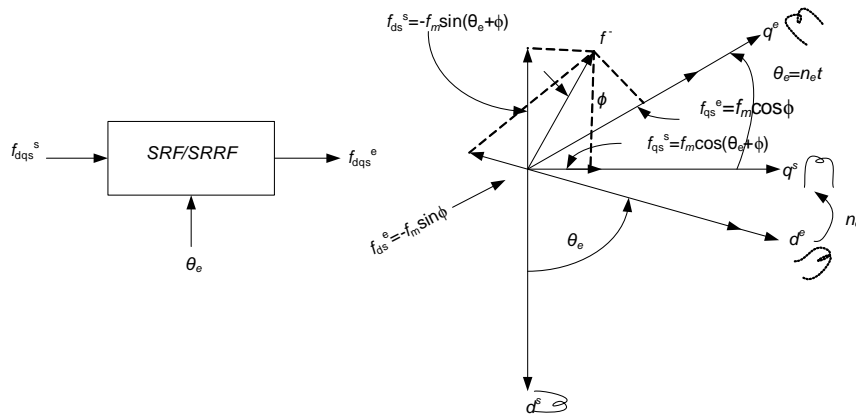


FIGURE 3.5: Location of rotating  $d - q$  axes relative to stationary  $d - q$  axes.

$$f_{ds}^s = -f_m \sin(\omega_e t + \phi) \quad (3.11)$$

Again, substituting (3.3) and (3.4) in (3.7) and (3.8), yields

$$f_{qs}^s = f_m \cos \phi \quad (3.12)$$

$$f_{ds}^s = -f_m \sin \phi \quad (3.13)$$

(3.10) and (3.11) show that  $f_{qs}^s$  and  $f_{ds}^s$  are balanced, two phase voltage or current of equal peak values and the latter is at  $\pi/2$  angle phase lead with respect to the other component. (3.12) and (3.13) show that the sinusoidal variables in stationary reference frame (SRF) appear as dc quantities in a synchronously rotating reference frame (SRRF).

### 3.2.1 d-q Model of a Three-phase Induction Machine

The field-oriented control (FOC) of induction machine adopted for the traction applications depend upon the (3.10)- (3.13) shown in the last section. Therefore, the  $d - q$  model of the induction machine will be presented and described in the following.

### 3.2.1.1 d-q Model of a Three-phase Induction Machine in Synchronously Rotating Reference Frame

The equivalent circuit of  $d$  axis and  $q$  axis of two-phase machine shown in Figure 3.3 [13] for the three-phase induction machine referred to a synchronously rotating reference frame (SRRF) at any arbitrary speed  $n_e$  as shown in Figure 3.6. The equivalent circuit of  $d$  axis and  $q$  axis are used to formulate the electrical differential equations of the induction machine. The  $d$ -axis and  $q$ -axis stator voltage equation can be described as:

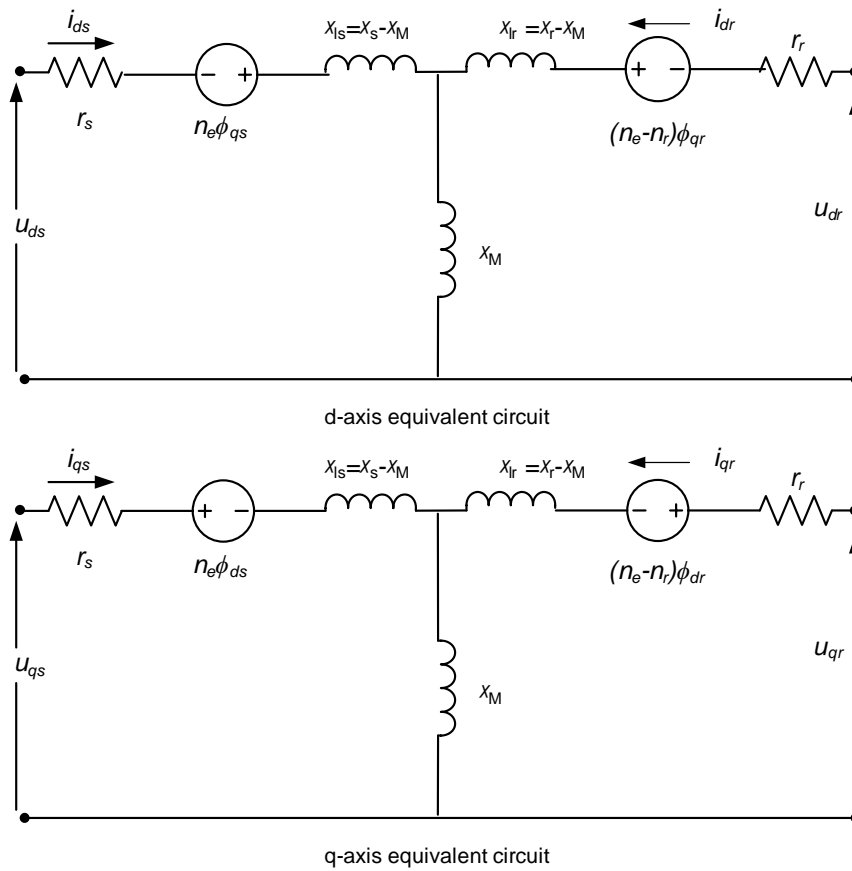


FIGURE 3.6: Dynamic  $d-q$  equivalent circuits of a 3- $\phi$  induction machine [13].

$$u_{ds} = r_s i_{ds} + \frac{d\phi_{ds}}{dt} - n_e \phi_{qs} \quad (3.14)$$

$$u_{qs} = r_s i_{qs} + \frac{d\phi_{qs}}{dt} + n_e \phi_{ds} \quad (3.15)$$

where

$$\phi_{qs} = \chi_{ls}i_{qs} + \chi_M(i_{qs} + i_{qr}) \quad (3.16)$$

$$\phi_{ds} = \chi_{ls}i_{ds} + \chi_M(i_{ds} + i_{dr}) \quad (3.17)$$

where all the variables are in rotating form.  $\phi_{qs}$  and  $\phi_{ds}$  are the q-axis and d-axis stator flux respectively.  $r_s$ ,  $n_e$ ,  $\chi_M$ , and  $\chi_{ls}$  are the stator resistance, synchronous speed, magnetizing inductance, and stator leakage inductance respectively.  $u_{ds}$  and  $u_{qs}$  are the d-axis and q-axis stator voltages respectively as well as these are the inputs of the system.  $i_{ds}$  and  $i_{qs}$  are the d-axis and q-axis stator currents respectively as well as these are the outputs of the system.  $i_{dr}$  and  $i_{qr}$  are the d-axis and q-axis rotor currents respectively.

Since the rotor of the machine is moving at the speed of  $n_e$ , the rotor  $d - q$  axes moves at the speed of  $n_e - n_r$  relative to the arbitrary (synchronously) rotating reference frame. So, the rotor equations are

$$u_{dr} = r_r i_{dr} + \frac{d\phi_{dr}}{dt} - (n_e - n_r)\phi_{qr} \quad (3.18)$$

$$u_{qr} = r_r i_{qr} + \frac{d\phi_{qr}}{dt} + (n_e - n_r)\phi_{dr} \quad (3.19)$$

where

$$\phi_{qr} = \chi_{lr}i_{qr} + \chi_M(i_{qs} + i_{qr}) \quad (3.20)$$

$$\phi_{dr} = \chi_{lr}i_{dr} + \chi_M(i_{ds} + i_{dr}) \quad (3.21)$$

$\phi_{qr}$  and  $\phi_{dr}$  are the q-axis and d-axis rotor flux respectively.  $r_r$ ,  $n_e$ ,  $n_r$ ,  $\chi_M$ , and  $\chi_{lr}$  are the rotor resistance, synchronous speed, rotor speed, magnetizing inductance, and rotor leakage inductance respectively.  $u_{dr}$  and  $u_{qr}$  are the d-axis and q-axis rotor voltages respectively.

The d-q representation presented above is used to derive the induction machine model in synchronously rotating reference frame. The definitions of control variables and states are presented in Table 3.1.

TABLE 3.1: State Variables Used in the Modeling of The Induction Machine

Symbol	Description	Units
$n_r$	Rotor angular speed	$r/s$
$\phi_{dr}$	Rotor flux of direct (d)-axis	$Wb$
$\phi_{qr}$	Rotor flux of quadrature (q)-axis	$Wb$
$i_{ds}$	Stator current of direct (d)-axis (state and output)	$A$
$i_{qs}$	Stator current of quadrature (q)- axis (state and output)	$A$
$u_{qs}$	Stator voltage of quadrature (q)- axis (input)	$V$
$u_{ds}$	Stator voltage of direct (d)-axis (in- put)	$V$

With the help of (3.16)- (3.21) and manipulation of these equations for the state (control) variable yields the following fourth-order electrical dynamics of the machine.

$$\frac{d\phi_{dr}}{dt} = -\frac{r_r}{\chi_r}\phi_{dr} + n_p(n_e - n_r)\phi_{qr} + \frac{\chi_M r_r}{\chi_r}i_{ds} \quad (3.22)$$

$$\frac{d\phi_{qr}}{dt} = -\frac{r_r}{\chi_r}\phi_{qr} - n_p(n_e - n_r)\phi_{dr} + \frac{\chi_M r_r}{\chi_r}i_{qs} \quad (3.23)$$

$$\frac{di_{ds}}{dt} = -\frac{(\chi_M^2 r_r + \chi_r^2 r_s)}{\sigma \chi_s \chi_r^2}i_{ds} + n_e i_{qs} + \frac{\chi_M r_r}{\sigma \chi_s \chi_r^2}\phi_{dr} + \frac{n_p \chi_M n_r}{\sigma \chi_s \chi_r}\phi_{qr} + \frac{1}{\sigma \chi_s}u_{ds} \quad (3.24)$$

$$\frac{di_{qs}}{dt} = -\frac{(\chi_M^2 r_r + \chi_r^2 r_s)}{\sigma \chi_s \chi_r^2}i_{qs} - n_e i_{ds} + \frac{\chi_M r_r}{\sigma \chi_s \chi_r^2}\phi_{qr} + \frac{n_p \chi_M n_r}{\sigma \chi_s \chi_r}\phi_{dr} + \frac{1}{\sigma \chi_s}u_{qs} \quad (3.25)$$

Equations (3.22)- (3.23) are the rotor flux and (3.24)- (3.25) are stator currents of d-axis and q-axis in the SRRF.

### 3.2.1.2 d-q Model of a Three-phase Induction Machine in Stationary Reference Frame

The dynamic model of a three-phase machine in stationary reference frame (SRF) can be obtained by simply putting the  $n_e = 0$  in the equations obtained for the three-phase machine moving in a arbitrary (synchronously) rotating reference frame. The model in SRF is required to implement the novel observer-controller set for the efficient operation of induction machine based propulsion drive. Therefore,

corresponding stationary reference frame equations at stator can be represented as

$$u_{ds} = r_s i_{ds} + \frac{d\phi_{ds}}{dt} \quad (3.26)$$

$$u_{qs} = r_s i_{qs} + \frac{d\phi_{qs}}{dt} \quad (3.27)$$

where

$$\phi_{qr} = \chi_{lr} i_{qr} + \chi_M i_{qs} \quad (3.28)$$

$$\phi_{dr} = \chi_{lr} i_{dr} + \chi_M i_{ds} \quad (3.29)$$

At rotor:

$$0 = r_r i_{dr} + \frac{d\phi_{dr}}{dt} + n_r \phi_{qr} \quad (3.30)$$

$$0 = r_r i_{qr} + \frac{d\phi_{qr}}{dt} - n_r \phi_{dr} \quad (3.31)$$

where the voltage of the rotor are,  $u_{dr} = u_{qr} = 0$ , for squirrel cage induction machine.

Now, d-q representation presented above is used to derive the induction machine model in stationary reference frame. This model will be used for the field-oriented control (FOC) of three-phase induction machine drive for the application in hybrid and electric vehicles. The definition of control variables and states are presented in Table 3.1.

Rotor flux equations:

Eliminating  $i_{dr}$  from (3.26) with the aid of (3.25) gives

$$\frac{d\phi_{dr}}{dt} = -\frac{r_r}{\chi_M} \phi_{dr} - n_p n_r \phi_{qr} + \frac{\chi_M r_r}{\chi_r} i_{ds} \quad (3.32)$$

Similarly, eliminating  $i_{qr}$  from (3.24) with the aid of (3.21) gives

$$\frac{d\phi_{qr}}{dt} = -\frac{r_r}{\chi_r} \phi_{qr} + n_p n_r \phi_{dr} + \frac{\chi_M r_r}{\chi_r} i_{qs} \quad (3.33)$$

To obtain the stator current equations, substituting the (3.24)- (3.25) and (3.28)- (3.29) in (3.22)- (3.23) respectively gives

Stator current equations:

$$\frac{di_{ds}}{dt} = -\frac{(\chi_M^2 r_r + \chi_r^2 r_s)}{\sigma \chi_s \chi_r^2} i_{ds} + \frac{\chi_M r_r}{\sigma \chi_s \chi_r^2} \phi_{dr} + \frac{n_p \chi_M n_r}{\sigma \chi_s \chi_r} \phi_{qr} + \frac{1}{\sigma \chi_s} u_{ds} \quad (3.34)$$

$$\frac{di_{qs}}{dt} = -\frac{(\chi_M^2 r_r + \chi_r^2 r_s)}{\sigma \chi_s \chi_r^2} i_{qs} + \frac{\chi_M r_r}{\sigma \chi_s \chi_r^2} \phi_{qr} + \frac{n_p \chi_M n_r}{\sigma \chi_s \chi_r} \phi_{dr} + \frac{1}{\sigma \chi_s} u_{qs} \quad (3.35)$$

Mechanical Equations:

The speed,  $n_r$ , in (3.28)- (3.31) can not be generally treated as a invariable. It is related to the torque of the machine as [13], [83]

$$\tau_e = \tau_L + J \frac{dn_M}{dt} + bn_r \quad (3.36)$$

and

$$n_M = \frac{2}{n_p} J \frac{dn_r}{dt} \quad (3.37)$$

Therefore, by substituting (3.37) in (3.36) yields

$$\frac{dn_r}{dt} = \frac{n_p}{2J} (\tau_e - \tau_L - bn_r) \quad (3.38)$$

In (3.38), the electromagnetic generated torque ( $\tau_e$ ) is given as

$$\tau_e = \frac{3}{2} \left( \frac{n_p}{2} \right) \frac{\chi_M}{\chi_r} (\phi_{dr} i_{qs} - \phi_{qr} i_{dr}) \quad (3.39)$$

where,  $\tau_e$ ,  $\tau_L$ ,  $J$ ,  $b$ ,  $n_M$  is the electromagnetic generated torque, load torque, rotor inertia, rotor damping, and rotor mechanical speed respectively.

The (3.32)- (3.35) represent the fourth order nonlinear electrical dynamics of the three-phase induction machine in stationary d-q reference frame. The (3.38) represent the mechanical dynamics of the the machine. Therefore, nonlinear dynamical model of the three-phase induction machine is of fifth-order.

### 3.2.1.3 The Complete Dynamics of an Induction Machine

The complete model at one place can be given as:

Electrical Equations:

$$\frac{d\phi_{dr}}{dt} = -\frac{r_r}{\chi_M}\phi_{dr} - n_p n_r \phi_{qr} + \frac{\chi_M r_r}{\chi_r} i_{ds} \quad (3.40)$$

$$\frac{d\phi_{qr}}{dt} = -\frac{r_r}{\chi_r}\phi_{qr} + n_p n_r \phi_{dr} + \frac{\chi_M r_r}{\chi_r} i_{qs} \quad (3.41)$$

$$\frac{di_{ds}}{dt} = -\frac{(\chi_M^2 r_r + \chi_r^2 r_s)}{\sigma \chi_s \chi_r^2} i_{ds} + \frac{\chi_M r_r}{\sigma \chi_s \chi_r^2} \phi_{dr} + \frac{n_p \chi_M n_r}{\sigma \chi_s \chi_r} \phi_{qr} + \frac{1}{\sigma \chi_s} u_{ds} \quad (3.42)$$

$$\frac{di_{qs}}{dt} = -\frac{(\chi_M^2 r_r + \chi_r^2 r_s)}{\sigma \chi_s \chi_r^2} i_{qs} + \frac{\chi_M r_r}{\sigma \chi_s \chi_r^2} \phi_{qr} + \frac{n_p \chi_M n_r}{\sigma \chi_s \chi_r} \phi_{dr} + \frac{1}{\sigma \chi_s} u_{qs} \quad (3.43)$$

Mechanical equation:

$$\frac{dn_r}{dt} = \frac{n_p}{2J} (\tau_e - \tau_L - bn_r) \quad (3.44)$$

$$\tau_e = \frac{3}{2} \left( \frac{n_p}{2} \right) \frac{\chi_M}{\chi_r} (\phi_{dr} i_{qs} - \phi_{qr} i_{ds}) \quad (3.45)$$

## 3.3 Hybrid Electric Vehicle Drive System and Control

A hybrid electric vehicle drive system consists of several major components including the propulsion (traction) machine. The components are sensors, power electronics converter, observers (estimators) to measure unknown parameters and states, controllers and any dedicated processor. The current sensors measure the

two phase currents and from this information current of third phase is computed. These currents are fed back to the controller. Speed sensor (encoder) may or may not be used to measure the angular position of the rotor. In some cases rotor fluxes and angular position of the rotor are estimated and used for the control of drive system. The controllers process the sensor and estimated data and control the power electronics converter for the desired efficient operation.

In hybrid and electric vehicle, control methodology can be speed control or torque control and flux control as shown in the Figure 3.7. In this work, there are two control loops. The outer loop is the flux control loop and speed control loop with indirect torque control loop i.e torque of the drive will be controlled indirectly. The inner control loop is the current loop. In this work, the actual speed and the actual flux of the machine is compared with the reference values to produce the reference currents of  $d$  and  $q$  axes. These currents are compared with the actual currents of  $d$  and  $q$  axes to generate the pulses for the pulse width modulation signals. In this research, field-oriented control of three-phase induction machine drive structure is used for the propulsion of hybrid and electric vehicles.

### 3.3.1 Field-oriented Or Vector Control of a Three-phase Induction Machine Drive

This section explains the field-oriented control of a three-phase induction machine for the applications in EVs and HEVs. In vector or Field-oriented Control (FOC) both the magnitude and phase alignment of the vector or control variables are controlled.  $d-q$  transformation is employed in field-oriented control to make the control easier and simpler.  $d-q$  transformation also decouples the two phases of the machine and machine behaves like a separately-excited DC machine in which field current vector,  $I_f$ , is used to control the flux of the machine and armature current vector,  $I_a$ , is used to control the torque of the DC machine respectively without disturbing control of each other. Similarly, by employing the  $d-q$  transformation, d-axis current of the machine's stator is used to control the flux of the three-phase machine and q-axis current of the machine's stator is used to control the torque of

the three-phase machine. Therefore, FOC is an attractive technique and provides better static and dynamic performance of induction machine drive for EVs and HEVs. The field-oriented control can be represented in both in any arbitrary rotating reference frame ( $n_{arbitrary}$ ) and in stationary reference frame. The  $d - q$  transformation, equivalent circuits, and model are detailed in previous sections. Field-oriented or vector control is of two types: (1) direct or feedback method, (2) indirect or feed forward method. The difference between the two method is how the unit vectors ( $\cos\theta_e$  and  $\sin\theta_e$ ) are generated to accomplish the control.

### 3.3.1.1 Direct or Feedback Field-oriented Control

Direct or feedback field-oriented control is used for the control of three-phase induction machine. The feedback (direct) field-oriented (vector) control is the most commonly adopted instantaneous speed/torque control method for the hybrid and electric vehicle's drive system. The proposed block diagram of the direct or feedback field-oriented control (DFOC) of the induction machine drive for the application in hybrid and electric vehicles is presented in Figure 3.7. The currents components,  $i_{ds}^*$ , and  $i_{qs}^*$  are the principle vector control parameters which are dc values in synchronously rotating reference frame (SRRF). These are converted to stationary reference frame (SRF) with the aid of unit vectors ( $\cos\theta_e$  and  $\sin\theta_e$ ). These unit vectors are generated from the rotor flux vector components  $\phi_{dr}^s$  and  $\phi_{qr}^s$ . The resulting  $d$  and  $q$  axis voltage signals are converted to phase voltages reference for the voltage fed inverter with the help of  $2 - \phi$  to  $3 - \phi$  transformation block. The flux components  $\phi_{dr}^s$  and  $\phi_{qr}^s$  are generated from the machine terminal voltages and currents with the aid of robust observer, which will be elaborated later. To achieve the precision control in flux, a flux control loop has been added. The control of torque is achieved indirectly in the outer speed loop. The torque is directly proportional to  $i_{qs}$ . It can be of positive and negative polarity. Field-weakening mode can be achieved by adjusting the flux command as a function of speed so that the inverter keeps itself in the PWM mode.

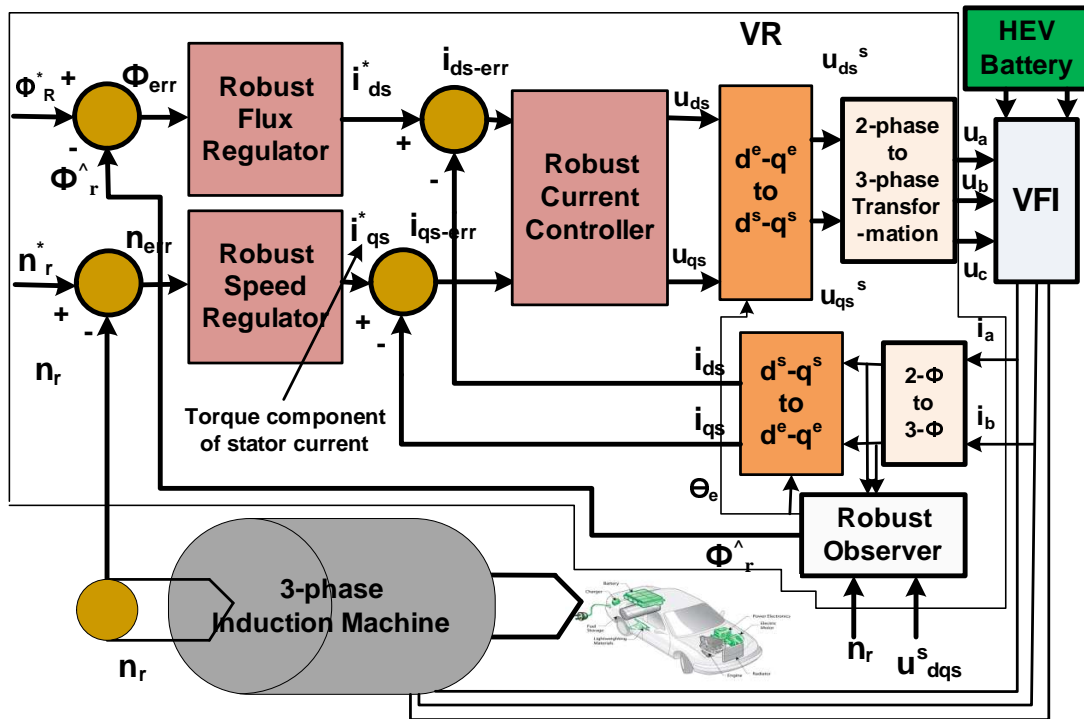


FIGURE 3.7: Proposed Induction Machine Drive Structure with Direct or Feedback Field-oriented Control.

The key and crucial point in the field-oriented control is that the  $d$  axis current  $i_{ds}$  must be aligned in the direction of rotor flux  $\hat{\phi}_r$  and the  $q$  axis current  $i_{qs}$  orthogonal to it. Figure 3.8 explains this alignment with the aid of the rotor flux components  $\phi_{dr}^s$  and  $\phi_{qr}^s$  in stationary reference frame. The stator  $d^s - q^s$  axes are fixed while the  $d^e - q^e$  axes are rotating at synchronous angular speed  $n_e$ . The angular position  $\theta_e$  is difference between  $d_e$  axis and  $q_e$  axis at any time, where  $\theta_e = n_e t$ . Figure 3.8 is showing the correct alignment of rotor flux signals and gives the following useful equations for direct field-oriented control.

$$\cos\theta_e = \frac{\phi_{dr}^s}{\hat{\phi}_r} \quad (3.46)$$

$$\sin\theta_e = \frac{\phi_{qr}^s}{\hat{\phi}_r} \quad (3.47)$$

and

$$\hat{\phi}_r = \sqrt{\phi_{dr}^s{}^2 + \phi_{qr}^s{}^2} \quad (3.48)$$

Therefore, exact and precise rotor flux is required to ensure that the  $d$  axis stator



through the air and given as [43]:

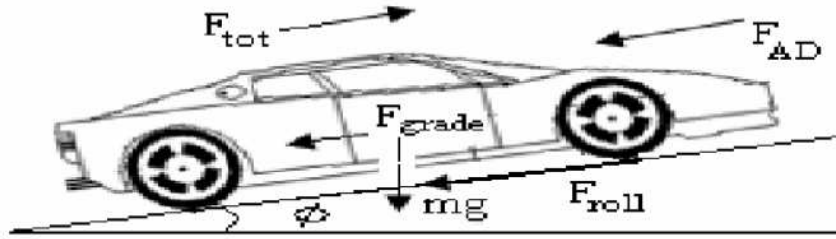


FIGURE 3.9: Aerodynamic drag force, Rolling resistance force, Road grade force on a Vehicle

$$f_{ad} = \frac{1}{2}\rho_{air}C_dA_fv^2 \quad (3.49)$$

Where  $\rho_{air}$  is the air mass density,  $C_d$  is the aerodynamic drag coefficient,  $A_f$  is the frontal surface area of the vehicle, and  $v$  is the velocity of the vehicle.

The rolling resistance is because of the damping of the vehicle tires on the road and given as:

$$f_{roll} = mgC_r\cos\alpha_g \quad (3.50)$$

Where  $m$  is the mass of the vehicle,  $g$  is the gravity acceleration,  $C_r$  is the rolling resistance coefficient, and  $\alpha_g$  is the grade angle.

The force due to the slope of the road is known as road grade force and is given as:

$$f_{grade} = mgsin\alpha_g \quad (3.51)$$

Therefore, load torque can be modeled by taking in account the rolling resistance force, road grade force and aerodynamic drag force and is given as:

$$\tau_L = \frac{R_{tire}}{R_f} \left[ \frac{1}{2}\rho_{air}C_dA_fv^2 + mgC_r\cos\alpha_g + mgsin\alpha_g \right] \quad (3.52)$$

Where  $R_{tire}$  is the radius of the tire, and  $R_f$  is the total ratio between the motor shaft and differential axle of the vehicle.

## 3.5 Model Based Analysis and Simulation

In this section, the developed model and FOC based drive structure of three-phase induction machine presented in section 3.2.1.2 and section 3.2.2.2 for the applications in hybrid and electric vehicles has been implemented and verified through the Matlab<sup>®</sup>/Simulink software.

### 3.5.1 Model Simulation and Discussion

The analysis of the developed model for the three-phase induction machine is performed with the parameters of 30KW, 2-pole pair, 280 line to line voltage, and 50 Hz electrical frequency. Table 3.2 gives the parameters values for three-phase induction machine. The simulation model has been developed for the machine to analyze its different characteristics such as phase currents, fluxes, phase voltages, speed and torque under different load conditions.

TABLE 3.2: Induction Machine Specifications

Symbol	Description	Value/Units
$P$	Power	30 KW
$n_p$	Number of pole pair	2
$f_e$	Electrical frequency	50 Hz
$u_L$	Line to line voltage	280 V
$r_r$	Rotor resistance	0.228 $\Omega$
$\chi_r$	Rotor inductance	0.8 mH
$r_s$	Stator resistance	0.087 $\Omega$
$\chi_s$	Stator inductance	0.8 mH
$\chi_M$	Mutual inductance	34.7 mH
$J$	Inertia	1.662 kg.m <sup>2</sup>
$b$	Damping	0.01 N.m.s.r <sup>-1</sup>

To validate the presented dynamic model of the three-phase induction machine, two cases are considered.

### 3.5.1.1 Positive Load Torque-Motoring Operation

In this case a positive load torque of  $40\text{N.m}$  is applied at  $t = 1\text{ms}$  and it becomes again zero at  $t = 1.5\text{ms}$  to simulate the presented dynamic model of induction machine to observe its motoring behavior. The profile of the applied load torque is shown in the Figure 3.10. Three phase supply voltages which are  $120^\circ$  apart from each other is applied as the input. In the case of hybrid and electric vehicle, these three phase voltages come from the inverter output whose input is the battery bank voltages. Behavior of the electromagnetic generate torque, motor speed is

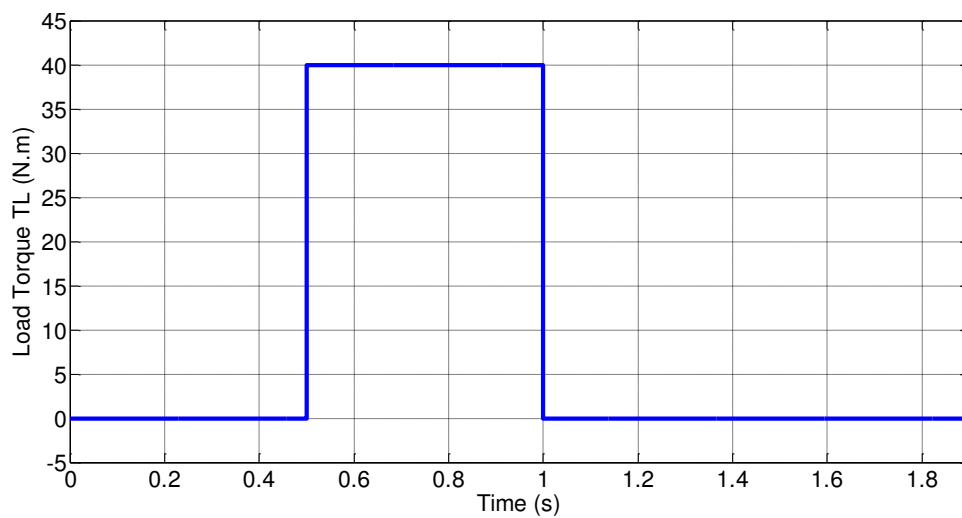


FIGURE 3.10: Load Torque.

shown in the Figure 3.11 when a load torque is applied. At time  $t = 1\text{ms}$ , the electromagnetic generated torque is  $\tau_e > (\tau_L + bn_m)$ . Figure 3.12 gives the induction machine current in SRF. It is clear from the Figure 3.12 that as the demanded electromagnetic generated torque from the motor at  $t = 1\text{ms}$ , the q-axis current component increases to meet the requirement of the demanded torque from the machine. Therefore, it is basically the torque component of the induction machine drive. Figure 3.12 shows the dynamic behavior of the d-axis and q-axis currents components in SRF and effect of the load torque is evident from the plots. Three phase currents of induction machine are presented in Figure 3.12 to show the load torque effects.

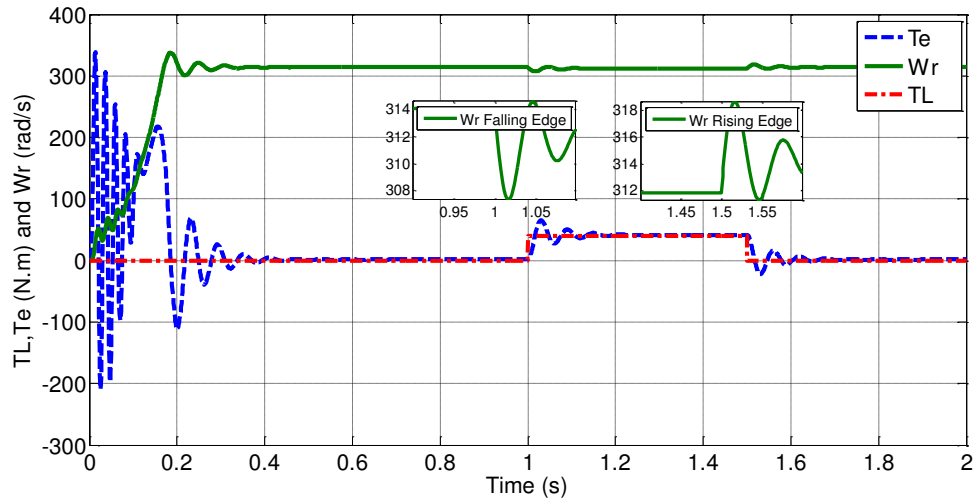


FIGURE 3.11: Induction machine load torque, electromagnetic generated torque, rotor speed.

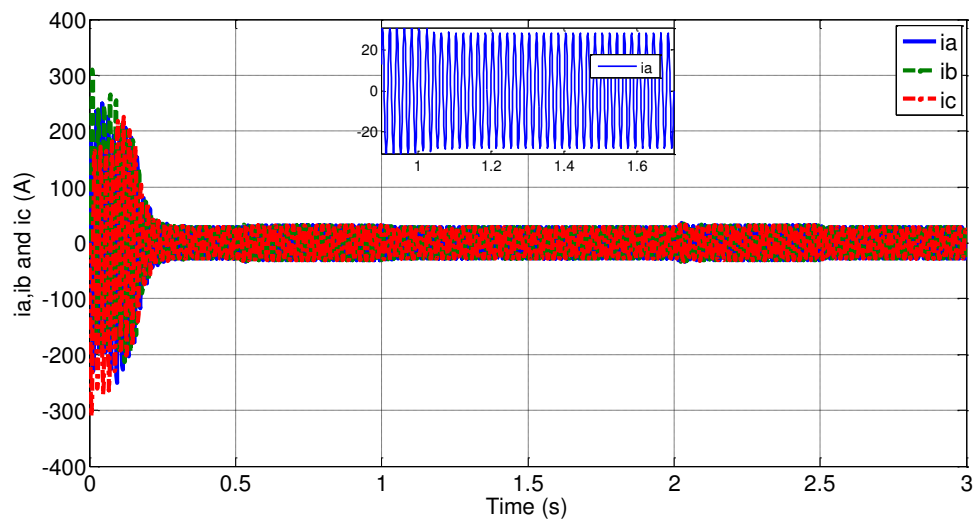


FIGURE 3.12: Induction machine three phase current for the unipolar load torque.

The dynamic behavior of the machine can also be observed by plotting the  $\tau_e$  versus  $n_r$  as shown in Figure 3.13. The motoring behavior of the machine is also clear from this plot. Zoomed version of this plot shows that first steady state point occurs when load torque is zero and second steady state point occurs when load torque is 40 N.m. Again the motor settles at first steady state point as the load torque is removed.

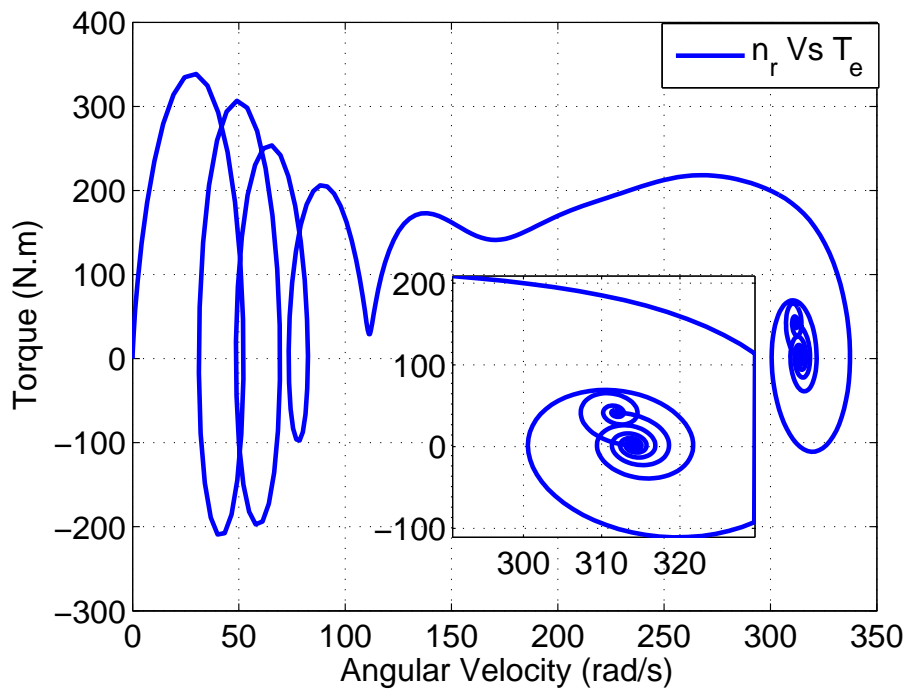


FIGURE 3.13: Dynamic behavior of induction machine: Torque-speed curve.

### 3.5.1.2 Positive and Negative Load Torque-Motoring and Generating Operation

In this case a positive load torque of 40N.m is applied at  $t = 1\text{ms}$ , it becomes again zero at  $t = 1.5\text{ms}$ , its value is  $-40\text{N.m}$  at 2ms and it becomes again zero at  $t = 2.5\text{ms}$  to simulate the presented dynamic model of induction machine to observe its motoring and generating behavior. The profile of the applied load torque is shown in the Figure 3.14. Figure 3.15 presents the plot of the three-phase stator current with application of load torque of Figure 3.14. Zoomed version of the stator currents is given in Figure 3.15 to show the variation in these currents during the motoring and generating operation of the machine. Figure 3.16 is plot for the electromagnetic generate torque, machine's speed and the load torque. Dynamic behavior of this machine as a generator and as a motor is evident from the plot between  $\tau_e$  and  $n_r$  as shown in the Figure 3.17. Zoomed version of this plot shows that first steady state point occurs when load torque is zero and second steady state point occurs when load torque is 40 N.m. This is the motoring behavior of the machine. Again the motor settles at first steady state point as the load torque

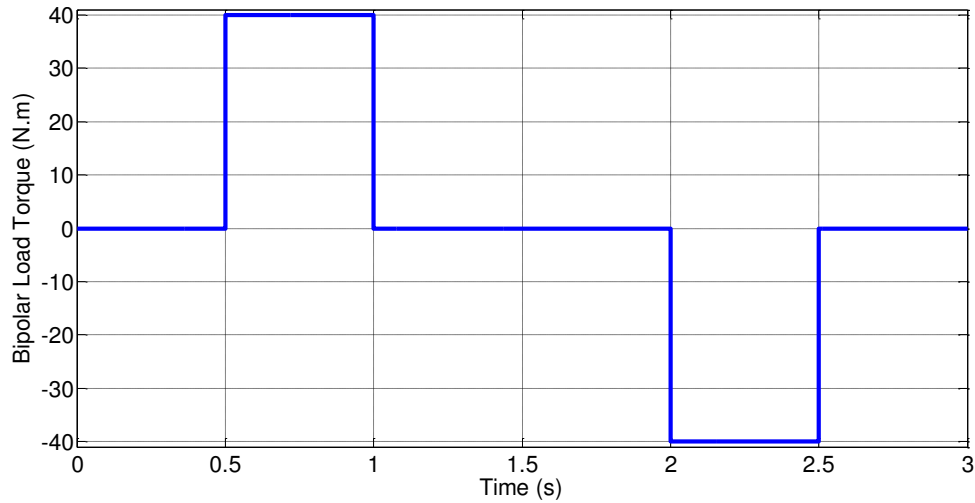


FIGURE 3.14: Bipolar load torque.

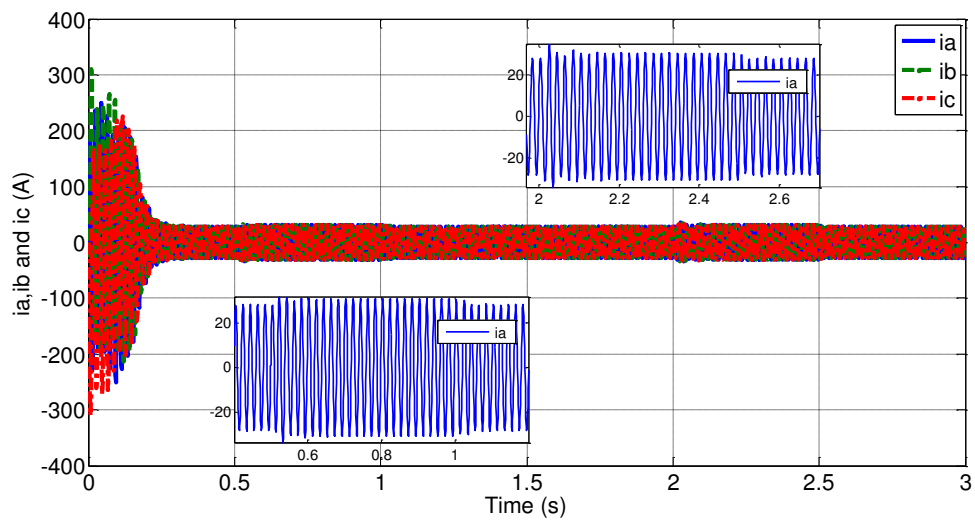


FIGURE 3.15: Induction machine phase currents for bipolar torque.

is zero at  $t = 1.5$  ms. A third steady state point occurs when the load torque is  $-40$  N.m. This is the generating behavior of the machine. Again the machine settles at first steady state point as the load torque is zero at  $t = 2.5$  ms.

### 3.6 LPV Modeling of Induction Machine

In this section, LPV modeling of induction machine is presented. The general representation of the group of LPV system in which state space matrices depend

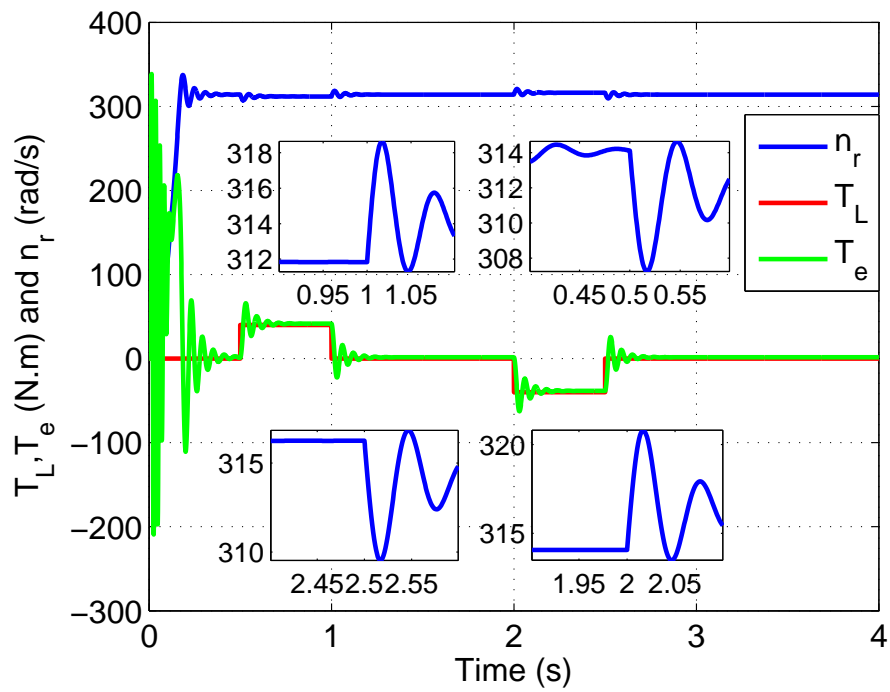


FIGURE 3.16: Induction machine load torque, electromagnetic generated torque, rotor speed for bipolar torque.

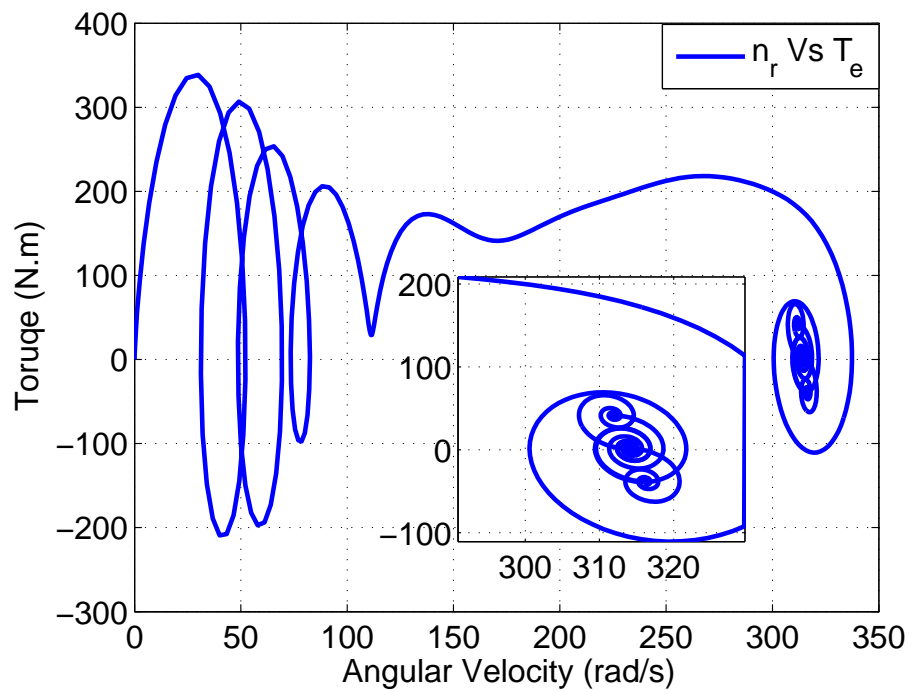


FIGURE 3.17: Dynamic behavior of induction machine: Torque-speed curve.

on the parameter vector is described by

$$\frac{dx(t)}{dt} = A(\rho(t))x(t) + B(\rho(t))u(t) \tag{3.53}$$

$$y = C(\rho(t))x(t) + Du(t) \quad (3.54)$$

where,

$x \in \mathcal{R}^n$  are the system state vector.

$\rho \in \mathcal{R}^s$  are the time varying parameter vector.

$u \in \mathcal{R}^{m_2}$  are the system input vector.

$y \in \mathcal{R}^{p_2}$  are the system output vector.

The matrices  $A(\cdot)$ ,  $B(\cdot)$ ,  $C(\cdot)$  and  $D(\cdot)$  are continuous matrix valued functions of appropriate dimensions of the time varying parameter vector  $\rho$ . In (3.53) and (3.54), the system matrix, input matrix and output matrix can be written as:

$$A(\rho(t)) = A_0 + \sum_{i=1}^{i=N} \rho_i(t)A_i \quad (3.55)$$

and

$$B(\rho(t)) = B_0 + \sum_{i=1}^{i=N} \rho_i(t)B_i \quad (3.56)$$

$$C(\rho(t)) = C_0 + \sum_{i=1}^{i=N} \rho_i(t)C_i \quad (3.57)$$

The time varying parameter vector,  $\rho(t)$  can be expressed in the form given as

$$\rho(t) = (\rho_1, \rho_2, \dots, \rho_m)^T, \quad \rho_{-i} \leq \rho_i \leq \rho^{-i}, i = 1, 2, \dots, m \quad (3.58)$$

In order to develop the LPV model for the induction machine; in [85]- [87] only the rotor speed and rotor resistance variations are modeled. In [86], only rotor resistance are considered to obtain LPV model. In this work, the rotor resistance,  $r_r$ , the stator resistance,  $r_s$ , and the rotor speed,  $n_r$  are taken as linear varying parameters. The state vector,  $x(t)$ , derivative of the state vector,  $\frac{dx(t)}{dt}$ , input vector,  $u(t)$  and output vector,  $y(t)$  for the induction machine LPV model of (3.53) and (3.54) can be given as:

$$x(t) = \begin{bmatrix} i_{ds} & i_{qs} & \phi_{dr} & \phi_{qr} \end{bmatrix}^T \quad (3.59)$$

$$x(t) = \begin{bmatrix} \dot{i}_{ds} & \dot{i}_{qs} & \dot{\phi}_{dr} & \dot{\phi}_{qr} \end{bmatrix}^T \quad (3.60)$$

$$u(t) = \begin{bmatrix} u_{ds} & u_{qs} \end{bmatrix}^T \quad (3.61)$$

$$y(t) = \begin{bmatrix} i_{ds} & i_{qs} \end{bmatrix}^T \quad (3.62)$$

The state space matrices  $A(\rho)$ ,  $B(\rho)$ ,  $C(\rho)$ , and  $D$  for the induction machine LPV model of (3.53) and (3.54) can be given as:

$$A(\rho(t)) = A_0 + \sum_{i=1}^{i=3} \rho_i(t) A_i \quad (3.63)$$

where

$$[\rho_1, \dots, \rho_3] := [r_r, r_s, n_r] \quad (3.64)$$

The LPV system matrix is given by

$$A(\rho) = \begin{bmatrix} a_{11}(\rho) & 0 & a_{13}(\rho) & a_{14}(\rho) \\ 0 & a_{22}(\rho) & a_{23}(\rho) & a_{24}(\rho) \\ a_{31}(\rho) & 0 & a_{33}(\rho) & a_{34}(\rho) \\ 0 & a_{42}(\rho) & a_{43}(\rho) & a_{44}(\rho) \end{bmatrix} \quad (3.65)$$

where

$$\left\{ \begin{array}{l} a_{11}(\rho) = -\frac{\chi_M^2 \rho_1 + \chi_r^2 \rho_2}{\sigma \chi_s \chi_r^2} \\ a_{13}(\rho) = \frac{\chi_M \rho_1}{\sigma \chi_s \chi_r^2} \\ a_{14}(\rho) = \frac{n_p \chi_M \rho_3}{\sigma \chi_s \chi_r} \\ a_{22}(\rho) = -\frac{\chi_M^2 \rho_1 + \chi_r^2 \rho_2}{\sigma \chi_s \chi_r^2} \\ a_{31}(\rho) = \frac{\chi_M \rho_1}{\chi_r} \\ a_{23}(\rho) = -\frac{n_p \chi_M \rho_3}{\sigma \chi_s \chi_r} \\ a_{24}(\rho) = \frac{\chi_M \rho_1}{\sigma \chi_s \chi_r^2} \\ a_{42}(\rho) = \frac{\chi_M \rho_1}{\chi_r} \\ a_{33}(\rho) = -\frac{\rho_1}{\chi_r} \\ a_{34}(\rho) = -n_p \rho_3 \\ a_{43}(\rho) = n_p \rho_3 \\ a_{44}(\rho) = -\frac{\rho_1}{\chi_r} \end{array} \right. \quad (3.66)$$

$$\left\{ \begin{array}{l} B = \beta \begin{bmatrix} I \\ O \end{bmatrix} \\ C = \begin{bmatrix} I & O \end{bmatrix} \\ D = \begin{bmatrix} O \end{bmatrix} \end{array} \right. \quad (3.67)$$

where,

$$\beta = \frac{1}{\sigma\chi_s} \quad (3.68)$$

In (3.67),  $I$  is  $2 \times 2$  identity matrix, and  $O$  is  $2 \times 2$  zero matrix.

In this LPV model of induction machine,  $\rho$  is the time varying parameter vector and  $P_0$  is a convex polytopes with vertices,  $\rho_i, i = 1, 2, \dots, N.$ , and can be defined as:

$$P_0 = Co\{\rho_{v1}, \rho_{v2}, \dots, \rho_{vL}\} \quad (3.69)$$

where,  $\rho_{vi}$  are the vertices,  $i = 1, 2, \dots, L.$   $L = 2^p$  are the number of vertices.  $Co$  is a convex hull, i.e, the set of all convex combinations of  $\rho_{vi}$  (all points inside and on the boundary of the polytopes).

The convex form of time varying parameter vector in the case of FOC of 3- $\phi$  induction machine drive for the applications in EVs and HEVs becomes

$$\rho(t) = \sum_{i=1}^{i=8} \alpha_i \rho_i \quad (3.70)$$

The matrix  $A(\rho)$  depends upon the linear time varying parameters and matrices,  $B, C,$  and  $D$  are constant. The matrix  $A(\rho)$  can be given as

$$A(\rho(t)) = A_0 + A_1\rho_1 + A_2\rho_2 + A_3\rho_3 \quad (3.71)$$

and

$$A(r_r, r_s, n_r) = A_0 + A_1r_r + A_2r_s + A_3n_r \quad (3.72)$$

The time varying parameters  $\rho_1, \rho_2$  and  $\rho_3$  are assumed to vary in the ranges

$$r_r \in [0.5r_r, 1.5r_r] \quad (3.73)$$

$$r_s \in [0.5r_s, 1.5r_s] \quad (3.74)$$

$$n_r \in [-160, 160] \quad (3.75)$$

### 3.6.1 LPV Model Validation

Figure 3.18 shows the open-loop step responses for the developed LPV model for the various values of  $n_r$ ,  $r_r$  and  $r_s$ . It is vivid from the responses that the

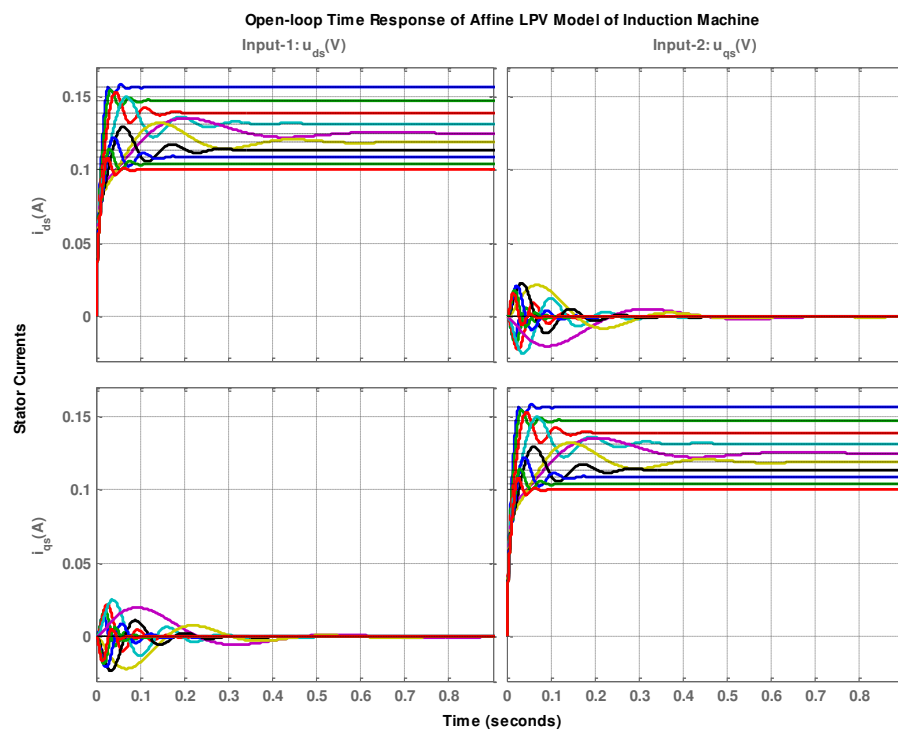


FIGURE 3.18: Open-loop time response of an LPV model. Unit step demand in  $u_{ds}$ , for 10 equally spaced values of  $n_r, r_r, r_s$ .

induction machine exhibits the prominent cross-coupling and badly damped poles whose frequencies vary considerably with the rotor resistance, stator resistances and rotor speed.

The obtained LPV model is validated in closed-loop against the original nonlinear model presented in (3.40)- (3.44). Two input signal  $u_{ds}$  and  $u_{qs}$  are generated with the sufficient amplitude to energize the closed-loop system as reference signals and

are given by:

$$u_{ds} = u_m \cos \phi \quad (3.76)$$

$$u_{qs} = -u_m \sin \phi \quad (3.77)$$

The reference voltage signals and load torque are shown in Figures 3.19 and 3.20.

The scheduling parameter  $n_r$  is considered as an internal signal. The value of the

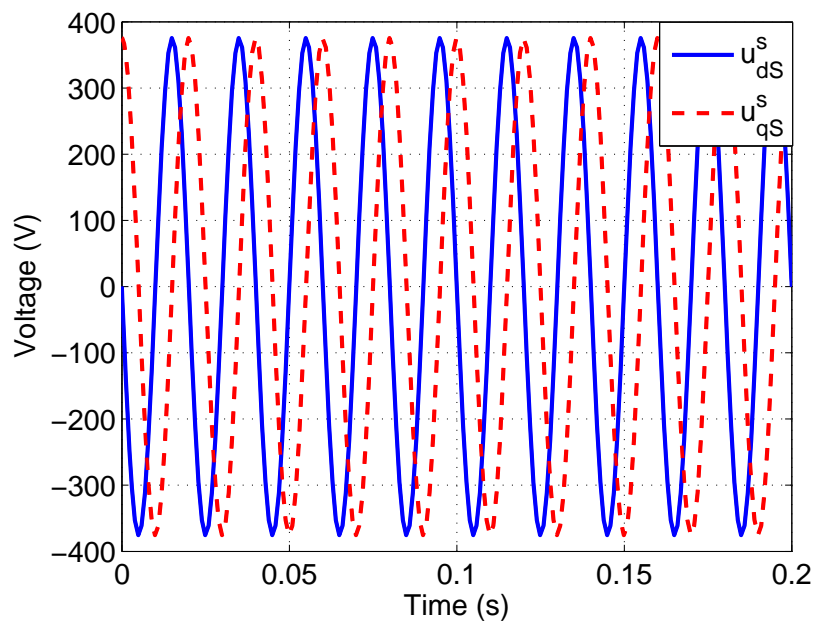


FIGURE 3.19: Input voltages  $u_{ds}$  and  $u_{qs}$  to validate the nonlinear model and LPV model

$r_r$  and  $r_s$  is kept constant. The validation plots for the output signals and states signal are shown in Figure 3.21 and Figure 3.22 respectively. Plots show that the LPV model confines the dynamics of nonlinear model well within the required range of operation.

Root Mean Square Error (RMSE) and Normalized Root Mean Square Error (NRMSE) are used as performance indices to measure the validity of the LPV model against the nonlinear model. Table 3.3 gives RMSE and NRMSE values of LPV model and nonlinear model.

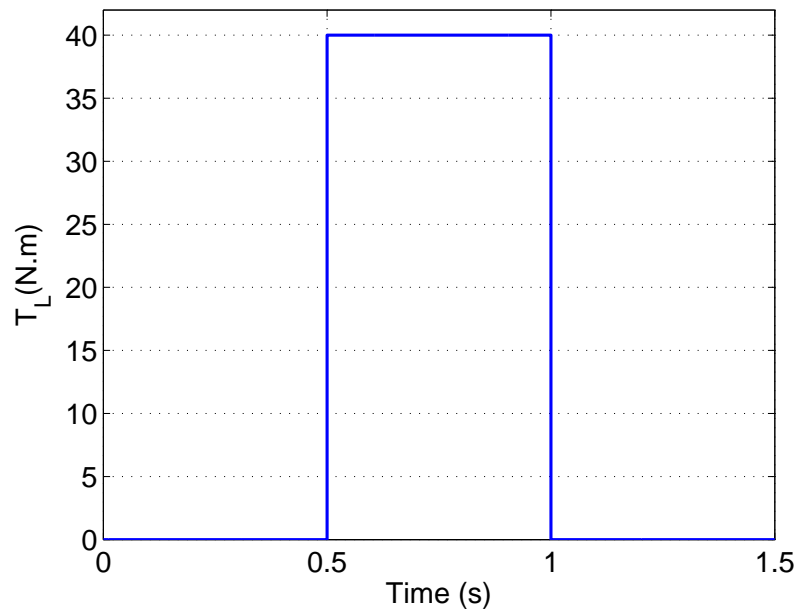


FIGURE 3.20: Load torque input  $\tau_L$  to validate the nonlinear model and LPV model

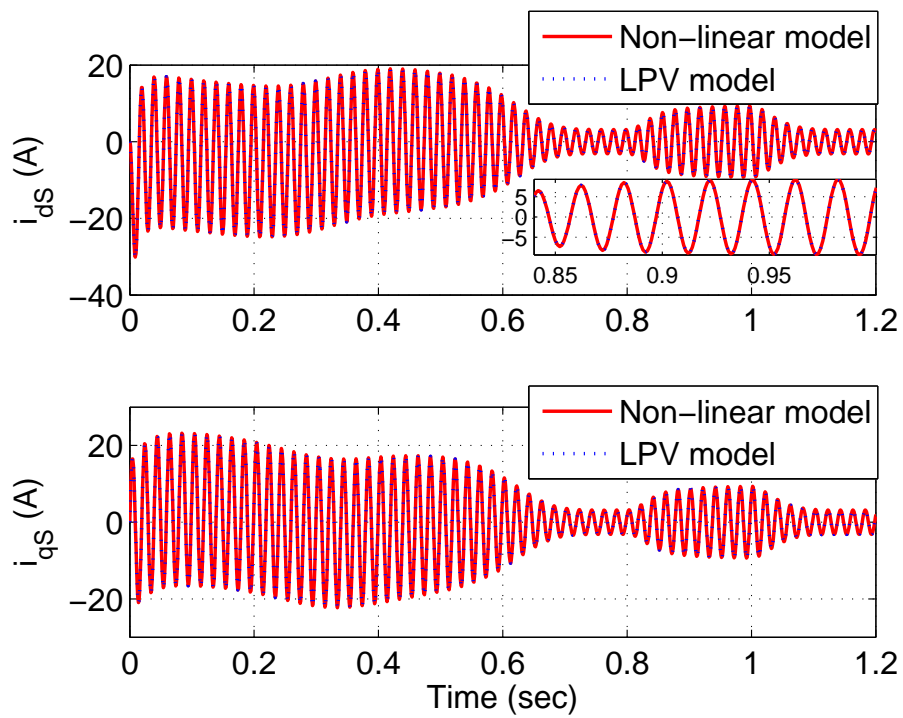


FIGURE 3.21: Validation plots of output currents  $i_{ds}$  and  $i_{qs}$  of the original nonlinear model and the LPV model.

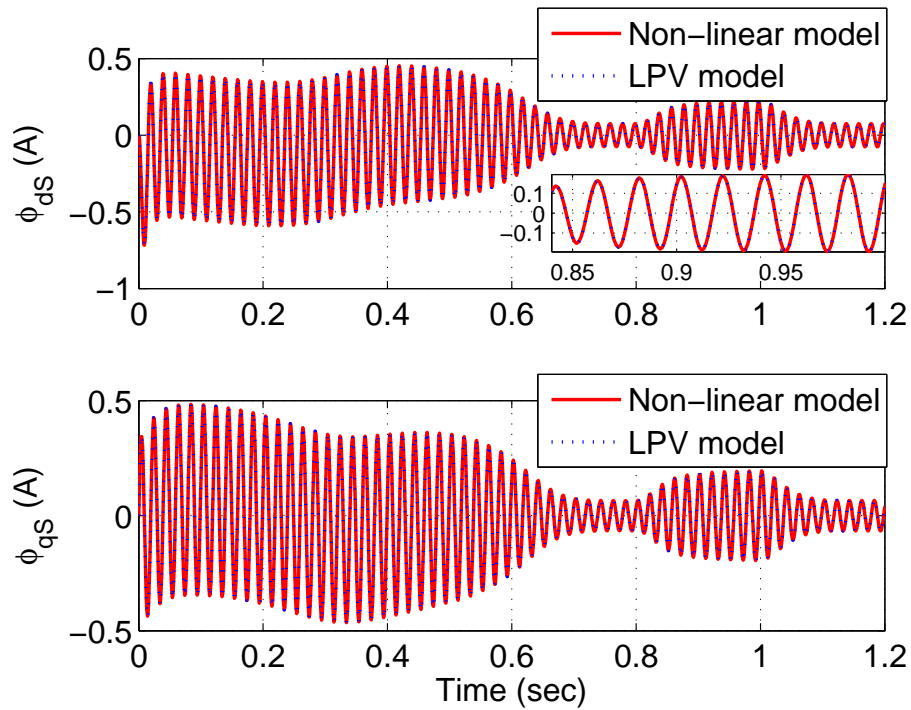


FIGURE 3.22: Validation plots of states  $\phi_{dr}$  and  $\phi_{qr}$  of the original nonlinear model and the LPV model.

TABLE 3.3: Accuracy of the LPV model in comparison to the nonlinear model

Model states	Cost Function	
	RMSE	NRMSE
$i_{ds}$	1.9375e-004	0.9998
$i_{qs}$	1.8993e-004	0.9998
$\phi_{dr}$	9.6877e-005	0.9999
$\phi_{qr}$	9.4966e-005	0.9999

### 3.7 Conclusion

The mathematical modeling of an induction machine has been presented which will be used in the propulsion system of hybrid and electric vehicles. The LPV derivation of the non-linear model is also presented. This model will be subsequently used in the design of novel (robust and advance) control techniques to estimate and manage the thermally derated torque in induction machine based electric powertrain for EVs and HEVs. This model will be also used in designing a control technique to improve the performance, efficiency and loss of life time

(aging) of an electric powertrain. A direct field-oriented control based structure of induction machine propulsion drive has been proposed. Load torque profile has been discussed which is useful for the determination of size of electric machine. At the end, model based analysis and simulation of both an induction machine and an induction machine based propulsion drive has been given. The results present the motoring and generating behavior which is needed in hybrid and electric vehicles. The RMSE and NRMSE are used as performance indices to show the effectiveness of LPV model with non-linear model.

In the coming chapter, an LPV based estimator will be formulated and designed for the estimation of thermally derated torque in EVs and HEVs electric powertrain.

## Chapter 4

# Estimation of Thermally de-rated Torque of an Electrified Powertrain

This chapter deals with the estimation of thermally derated torque of an induction machine based electrified powertrain. This estimation is based on the LPV model presented in the preceding chapter. The estimation of thermally derated torque is more critical for obtaining the precise control to manage the thermally derated torque, improve the efficiency and minimize the loss of life time (aging) of an induction machine based electrified powertrain. Along with the estimation of thermally derated torque, flux of an induction machine based electric drive is also estimated. These objectives have been obtained by using a robust LPV based estimation technique. The LPV observer operates on a highly nonlinear currents and flux dynamics. Initially, the proposed estimation technique has been successfully tested by creating a theoretical scenario. Later on, estimation technique is investigated using shortened Federal Urban Driving Schedule (FUDS) test cycle for Hybrid Electric Vehicle (HEV) electric powertrain.

## **4.1 Benefits of Thermally Derated Torque Estimation**

The torque performance of an induction machine based electrified powertrain deteriorates under the vast uncertainties in rotor and stator resistance due to the temperature variations during the HEV operation. Similar worsening of the response is expected due to the wide variations in rotor speed in HEV application. These problems can be resolved by employing state-of-art estimation techniques. The significant benefits of the thermally derated torque estimation are:

- Efficient torque compensation control can be accomplished by the estimation of thermally derated torque.
- Meeting the road loads, ensuring efficient powertrain operation and minimizing the loss of lifetime (aging) of an electric machine are three essential but conflicting targets. Conflicting objectives control technique can be developed by estimating the thermally derated torque.
- Instead of installing another sensor, virtual sensors can be developed to sense a phenomena in parallel to real sensors (A cheaper solution). This reduces dependence on a single sensor and can also help in sensor health monitoring

## **4.2 Advantage of LPV Control Technique**

The main objective of the LPV control (gain scheduling) technique is to control the plant over the predefined operating range, but rather than simply being robust to variations in the plant, the controller is allowed to schedule itself based on some measurements. This is in opposite to the traditional Linear Time Invariant control technique which relies on the localized linear characteristics of the plant at a particular operating condition. The advantage of the LPV control structures lies in their explicit exploitation of knowledge of the actual plant dynamics, based on

measurement. In addition to the measurement signal, the LPV control technique takes the advantage of exogenous plant information to update its dynamics in real time. It is important to note that this information modifies not only the control signal, but also the way in which measurement signals are processed through the LPV control technique.

Several benefits from employing the LPV methodology are immediately apparent.

- As mentioned above, LPV control technique provides additional freedom to achieve the performance and robustness objectives.
- The classical approach to gain scheduling employs point wise interpolation or heuristically based switching strategies. These techniques are potentially hazardous, since they obliterate the time-varying nature of the plant and lack systematic theoretical guarantees on performance.
- LPV control techniques are direct extension of well-known LTI synthesis techniques, so some engineering insight is preserved.
- Some LPV plant are not stabilizable via fixed controller hence the practical need of gain scheduling.

As a consequence, LPV control technique can provide better robustness and performance properties than fixed controllers, which ignore the non-stationary nature of the plant.

### **4.3 Linear Parameter Varying Observer for Electrified Powertrain**

Keeping in view the importance for estimation of thermally derated torque discussed in Section 4.1 and the potential attributes of the LPV control technique discussed in Section 4.2, an LPV based observer is designed to estimate the thermally derated torque in an electrified powertrain. The proposed estimation strategy is

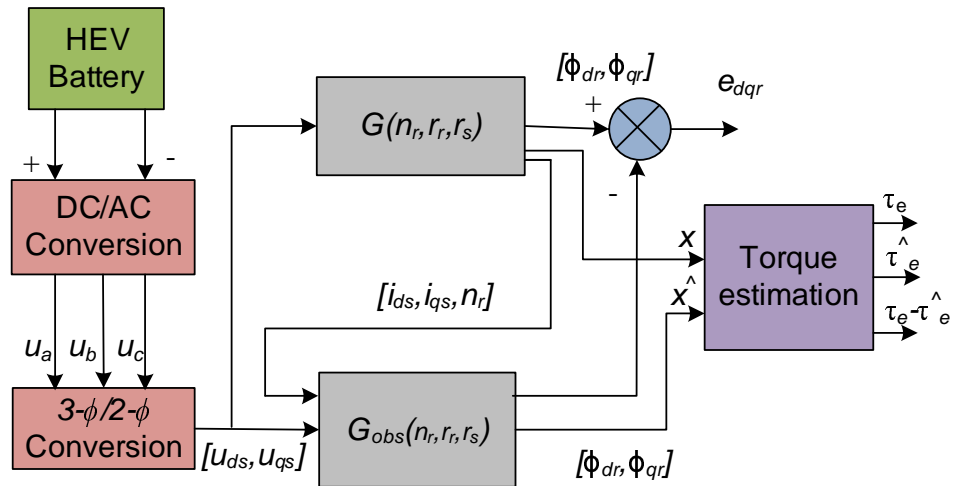


FIGURE 4.1: Overall scheme

shown in Figure 4.1. In this scheme, it is assumed that the currents and rotor speed measurements are available from the current and speed sensors respectively. The machine terminal voltages are available at the output of voltage sensor for use. Based upon these measurements, rotor flux and torque de-rating are estimated to enhance the performance of hybrid and electric vehicle drive.

The LPV observer based estimation technique is not only computationally cheap but also has the potential for on-line implementation (See Chapter 5). Now we will design the LPV observer for the estimation of flux and thermally derated torque of an electric drive using the stator current dynamics ( (3.42)- (3.43)) and rotor flux dynamics ( (3.40)- (3.41)) of the induction machine model given in Section 3.2.1.3. The induction machine model presented in Section 3.2.1.3 is stable but has the prominent cross-coupling and badly damped poles whose frequencies vary considerably with the rotor resistance, stator resistances and rotor speed as shown in Figure 3.18.

## 4.4 Current and Flux Dynamics

The validated stator current and rotor flux dynamics can be written as:

$$\begin{bmatrix} \dot{i}_s \\ \dot{\phi}_r \end{bmatrix} = \begin{bmatrix} A_{11} & A_{12} \\ A_{21} & A_{22} \end{bmatrix} \cdot \begin{bmatrix} i_s \\ \phi_r \end{bmatrix} + \begin{bmatrix} U_1 \\ U_2 \end{bmatrix} u_s \quad (4.1)$$

In (4.1),  $i_s$ ,  $\phi_r$ , and  $u_s$  are the stator current, rotor flux, and stator voltage vectors in stationary reference frame respectively.

$$i_s = \begin{bmatrix} i_{ds} \\ i_{qs} \end{bmatrix}, \phi_r = \begin{bmatrix} \phi_{dr} \\ \phi_{qr} \end{bmatrix}, u_s = \begin{bmatrix} u_{ds} \\ u_{qs} \end{bmatrix} \quad (4.2)$$

$$A_{11} = \begin{bmatrix} -\frac{\chi_M^2 r_r + \chi_r^2 r_s}{\sigma \chi_s \chi_r^2} & 0 \\ 0 & -\frac{\chi_M^2 r_r + \chi_r^2 r_s}{\sigma \chi_s \chi_r^2} \end{bmatrix} \quad (4.3)$$

$$A_{22} = \begin{bmatrix} -\frac{r_r}{\chi_r} & -n_p n_r \\ n_p n_r & -\frac{r_r}{\chi_r} \end{bmatrix} \quad (4.4)$$

$$A_{21} = \begin{bmatrix} \frac{\chi_M r_r}{\chi_r} & 0 \\ 0 & \frac{\chi_M \chi_r}{\chi_r} \end{bmatrix} \quad (4.5)$$

$$A_{12} = \begin{bmatrix} \frac{\chi_M r_r}{\sigma \chi_s \chi_r^2} & n_p \frac{\chi_M n_r}{\sigma \chi_s \chi_r^2} \\ -n_p \frac{\chi_M n_r}{\sigma \chi_s \chi_r^2} & \frac{\chi_M r_r}{\sigma \chi_s \chi_r^2} \end{bmatrix} \quad (4.6)$$

$$U_1 = \begin{bmatrix} \frac{1}{\sigma \chi_s} & 0 \\ 0 & \frac{1}{\sigma \chi_s} \end{bmatrix} \quad (4.7)$$

$$U_2 = \begin{bmatrix} 0 & 0 \\ 0 & 0 \end{bmatrix} \quad (4.8)$$

where  $n_e$  is the stator supply frequency,  $n_r$  is the rotor speed,  $n_p$  is the number of pole pairs,  $r_s$  is the stator resistance,  $r_r$  is the rotor resistance,  $\chi_s$  is the stator inductance,  $\chi_r$  is the rotor inductance,  $\chi_M$  is the mutual inductance between stator and rotor and  $\sigma = 1 - \frac{\chi_M^2}{\chi_s \chi_r}$ , is the leakage factor.

The definition of rotor speed, electromagnetic generated torque and load torque are given in (3.44), (3.45) and (3.52) respectively.

#### 4.4.1 Linear Parameter Varying Dynamics

The LPV model of the current and flux dynamics is required for the design of LPV observer. The LPV dynamics are given in Section 3.6 by taking the rotor resistance, stator resistance and rotor speed as time varying parameters. The ranges of the variations of these parameters are given in (3.73)- (3.75).

#### 4.4.2 LPV Robust Observer

After presenting the current and flux dynamics and their corresponding LPV dynamics, an observer based on [101] is proposed to estimate the flux and thermally derated torque.

##### 4.4.2.1 Structure of Robust LPV Observer

The observer written here for the system in presented in Section 3.6 is:

$$\begin{bmatrix} \dot{\hat{i}}_s \\ \dot{\hat{\phi}}_r \end{bmatrix} = A(\rho) \begin{bmatrix} \hat{i}_s \\ \hat{\phi}_r \end{bmatrix} + B(\rho)u_s + L(\rho)(i_s - \hat{i}_s) \quad (4.9)$$

$$\hat{i}_s = C(\rho) \begin{bmatrix} \hat{i}_s \\ \hat{\phi}_r \end{bmatrix} \quad (4.10)$$

$$\begin{bmatrix} \dot{\hat{i}}_s \\ \dot{\hat{\phi}}_r \end{bmatrix} = A(\rho) \begin{bmatrix} \hat{i}_s \\ \hat{\phi}_r \end{bmatrix} + B(\rho)u_s + L(\rho)(i_s - C(\rho) \begin{bmatrix} \hat{i}_s \\ \hat{\phi}_r \end{bmatrix}) \quad (4.11)$$

For performing the computation for the observer gain, the observer error is defined as:

$$e = \begin{bmatrix} i_s \\ \phi_r \end{bmatrix} - \begin{bmatrix} \hat{i}_s \\ \hat{\phi}_r \end{bmatrix} \quad (4.12)$$

The state space equation of the error,  $e$  is then given as:

$$\dot{e} = (A(\rho) - L(\rho)C(\rho))e \quad (4.13)$$

#### 4.4.2.2 Observer Stability

To ensure the stability of the observer error (4.13), the following theorem is proposed.

**Theorem 1:** *The system (4.11) is an observer for (3.53) and (3.54), if there exist appropriate matrices  $P$ , and  $Q$  such that*

$$\begin{cases} A_i^T P - C_i^T Q_i^T + P A_i - Q_i C_i \prec 0, i = 1, \dots, 2^p \\ P = P^T \succ 0 \end{cases} \quad (4.14)$$

and consequently  $\begin{bmatrix} \hat{i}_s \\ \hat{\phi}_r \end{bmatrix}$  will converge to  $\begin{bmatrix} i_s \\ \phi_r \end{bmatrix}$ .

The LMIs in (4.14) are for the induction machine based electrified powertrain.

**Proof:** Consider the Lyapunov function  $V(e(t)) = e^T(t)Pe(t)$  with  $P = P^T$ , where,  $(\cdot)^T$  denotes the transpose of the matrix. The derivative of the Lyapunov function with respect to time along the system states (4.13) is:

$$\frac{dV(e(t))}{dt} = e^T(t)Pe(t) + e^T(t)Pe(t) \quad (4.15)$$

Putting error dynamics of (4.13) in (4.15), we have

$$\frac{dV(e(t))}{dt} = (A(\rho) - L(\rho)C(\rho))^T Pe(t) + e^T(t)P(A(\rho) - L(\rho)C(\rho)) \quad (4.16)$$

$$\frac{dV(e(t))}{dt} = (A^T(\rho)P - C^T(\rho)L^T(\rho))e(t) + e^T(t)(PA(\rho) - PL(\rho)C(\rho)) \quad (4.17)$$

$$\frac{dV(e(t))}{dt} = e^T(t)(PA(\rho) - PL(\rho)C(\rho) + A^T(\rho)P - C^T(\rho)L^T(\rho))e(t) \quad (4.18)$$

Quadratic stability is guaranteed if  $V(\dot{e}(t)) < 0, \forall(t) \neq 0$  [102]. This condition is verified if

$$((A^T(\rho)P - C^T(\rho)L^T(\rho)P^T) + (PA(\rho) - PL(\rho)C(\rho))) < 0 \quad (4.19)$$

The (4.19) is the bi-linear matrix inequality (BMI) and it can be converted to the LMI by considering  $Q(\rho) = PL(\rho)$ .

The (4.19) becomes:

$$A^T(\rho)P - C^T(\rho)Q(\rho)^T + PA(\rho) - Q(\rho)C(\rho) < 0 \quad (4.20)$$

(4.20) is an infinite LMI condition. However, the dependence on the  $\rho$  is affine, (4.20) can be converted to a finite LMI problem by solving only at the vertices of the polytopes.

**Definition 1:** The polytopic system  $(A(\rho), P_\rho)$ , with  $\rho \in P_\rho = Co(\rho_1, \rho_2, \dots, \rho_{2^\rho})$  is quadratically stable if there exists common Lyapunov matrix  $P = P^T$  such that

$$A_i^T P - C_i^T Q_i^T + P A_i - Q_i C_i < 0, i = 1, \dots, 2^\rho \quad (4.21)$$

Finally, if there exist appropriate matrices P, and Q, then it is obvious that (4.21) holds and consequently the system in (4.11) is affine quadratically stable.

#### 4.4.2.3 Observer Construction

If  $\rho$  is measurable, at each vertex, design of local observer is possible. Then, the linear combination of local observer gives the design of an LPV observer. Following equation gives the gain of local observer.

$$L_i = P^{-1}Q_i \quad (4.22)$$

LPV observer is computed as:

$$L = \sum_{i=1}^{i=2^p} c_i L_i \quad (4.23)$$

where,  $c_i(t) \geq 0$ , and

$$\sum_{i=1}^{i=2^p} c_i = 1 \quad (4.24)$$

#### 4.4.2.4 Synthesizing the Robust LPV Flux Observer

**Definition 2:** If the time varying parameter vector,  $\rho$ , contains the measurable and immeasurable components. The immeasurable components are taken as parameters uncertainties and only the range of their variations are known. The parameter vector,  $\rho$ , is defined as:

$$\begin{bmatrix} \rho_m^T & \rho_{um}^T \end{bmatrix} \quad (4.25)$$

where  $\rho_m$  is a vector which contains measurable components and  $\rho_{um}$  is a vector which contains immeasurable components.

**Theorem 2:** If  $\rho_i^m$ ,  $i = 1, \dots, N_m$  are the vertices that define the polytope of the measurable components and  $\rho_j^{um}$ ,  $j = 1, \dots, N_{um}$  are the vertices that define the polytopic of the immeasurable components. Then, the robust LPV flux observer can be synthesized as:

$$A_{ij}^T P - C_{ij}^T Q_{ij}^T + P A_{ij} - Q_{ij} C_{ij} \prec 0, i = 1, \dots, N_m, j = 1, \dots, N_{um} \quad (4.26)$$

where,  $P = P^T \succ 0$ .

The gain of robust polytopic observer is computed as described in (4.22) and (4.24).

**Theorem 3:** If the flux estimation is exact and precise, and the flux error  $\begin{bmatrix} \phi_{dr} \\ \phi_{qr} \end{bmatrix}$  converges towards zero then the estimation of torque de-rating will also

be exact and precise and torque de-rating error  $[\tau_e - \hat{\tau}_e]$  will also converge towards zero.

The estimated torque is given as:

$$\hat{\tau}_e = \frac{3}{2}(n_p) \frac{\chi_M}{\chi_r} (\hat{\phi}_{dr} i_{qs} - \hat{\phi}_{qr} i_{ds}) \quad (4.27)$$

#### 4.4.2.5 Selection of Observer Gain

We selected the observer gains using (4.22)- (4.24) which were computed by solving the LMI in (4.21). The LMI optimization delivered a LPV observer with 8 vertices, each vertex being an LTI regulator with four states.

The observer gains at each vertex are given in Appendix-C.

## 4.5 Evaluation of Estimation Scheme

The simulation of the proposed and designed robust LPV observer for the estimation of thermal torque derating in HEV drive has been tested in two ways. The values of different parameters are given in Table 4.1.

TABLE 4.1: Induction Machine Specifications

Symbol	Description	Value/Units
$P$	Power	3 KW
$n_p$	Number of pole pair	2
$f_e$	Electrical frequency	50 Hz
$u_L$	Line to line voltage	280 V
$r_r$	Rotor resistance	0.39 $\Omega$
$\chi_r$	Rotor inductance	0.91 mH
$r_s$	Stator resistance	0.153 $\Omega$
$\chi_s$	Stator inductance	0.91 mH
$\chi_M$	Mutual inductance	39.47 mH
$J$	Inertia	0.662 kg.m <sup>2</sup>
$b$	Damping	0.04 N.m.sec.rad <sup>-1</sup>

### 4.5.1 Theoretical Scenario

In this case, the input voltages  $u_{ds}$  and  $u_{qs}$  ( (3.76) and (3.77) ) to the plant and observer are generated from mathematical relations. Then the designed robust LPV observer is simulated for different initial conditions, and for ambient temperature of  $-20^{\circ}C$ ,  $20^{\circ}C$  and  $40^{\circ}C$  to verify its convergence and estimation performance. Simulation results show excellent performance of the designed robust LPV observer in the presence of vast variations in rotor resistance, stator resistance, and rotor speed which are severe in HEV application. The derated torque due to thermal effects has been estimated as seen in Figure 4.2(bottom).

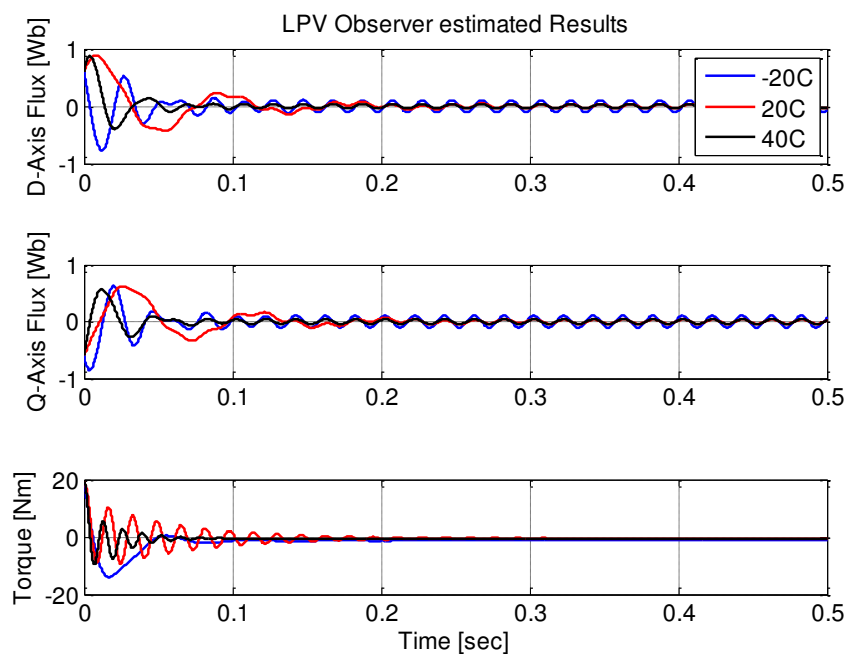


FIGURE 4.2: Robust LPV observer estimated results of :  $d$ -axis flux(Top),  $q$ -axis flux(Middle) and Torque derating(Bottom) at  $-20^{\circ}C$ ,  $20^{\circ}C$  and  $40^{\circ}C$ .

Derated torque scenario due to thermal effects is more vivid at 0.01 seconds. It is clear from the Figure 4.3, the convergence time of the robust LPV observer is 0.16 seconds. As a result, precise and exact estimation of flux is available for the efficient estimation of machine's electromagnetic generated torque and operation of HEV drive system. From Figure 4.2, it is clear that the estimation of flux and torque derating is guaranteed at different ambient temperature. The three-phase

input and  $dq$  voltages to the electric drive system are given in Figure 4.4. These results also proved the stability of proposed robust LPV observer. Hence, the robust LPV observer proves to be a useful tool to estimate the derated torque.

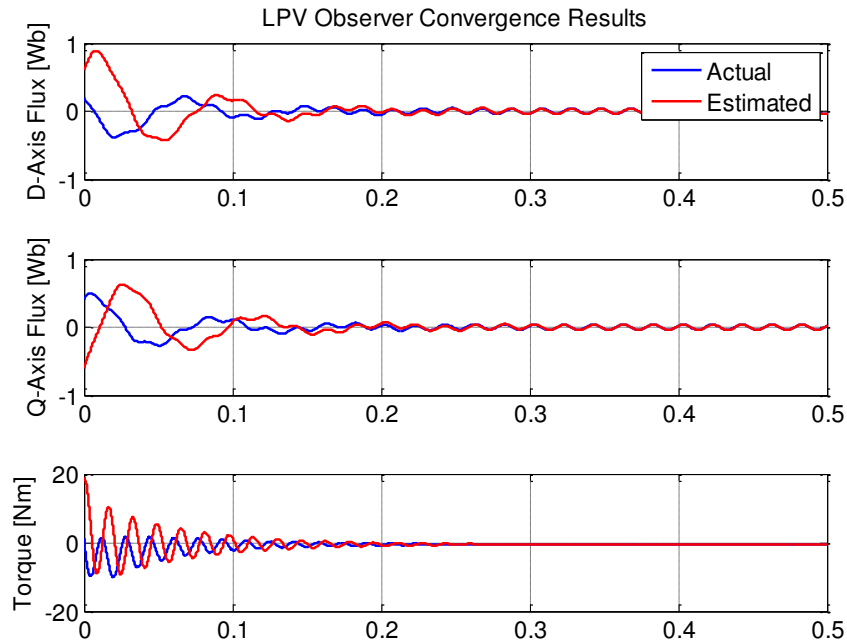


FIGURE 4.3: Robust LPV observer convergence results of actual and estimated:  $d$ -axis flux(Top),  $q$ -axis flux(Middle) and Torque derating(Bottom).

The LPV model of induction machine presented in Section 3.6 is used in the implementation and evaluation of the proposed LPV observer. Therefore, the observer performance responses, presented in Figures 4.2 and 4.3, exhibit the oscillations. These oscillations are due to the presence of prominent cross-coupling and badly damped poles whose frequencies vary considerably with the rotor resistance, stator resistances and rotor speed in an induction machine.

#### 4.5.2 HEV Powertrain

In this case, the input voltages  $u_{ds}$  and  $u_{qs}$  to the plant and observer in Figure 4.1 has been extracted from HEV electric powertrain developed at Center for Automotive Research (CAR), The Ohio State University using FUDS driving cycle. The

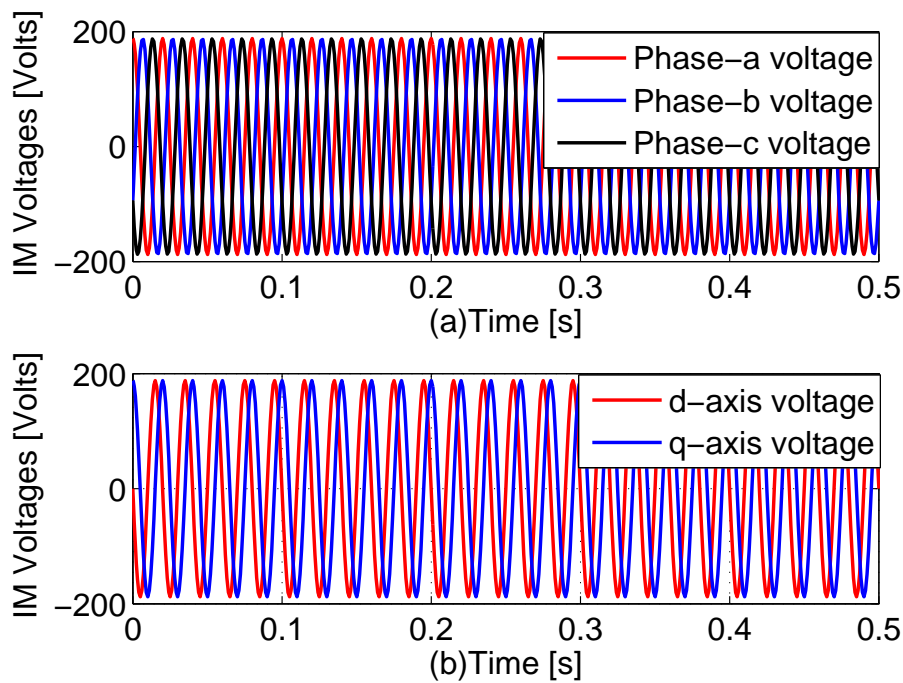


FIGURE 4.4: (a) 3-phase Input voltages to the electric drive system. (b)  $u_{ds}$  and  $u_{qs}$  for the electric drive system.

profile of the  $u_{ds}$  and  $u_{qs}$  which are extracted from this HEV electric powertrain are shown in Figure 4.7. The purpose of using the extracted voltage profile is to investigate the performance of designed LPV observer using practical data.

This evaluation is conducted for shortened FUDS test cycle. Then, for different initial conditions and for ambient temperature of  $-20^{\circ}C$ ,  $20^{\circ}C$  and  $40^{\circ}C$ , the designed robust LPV observer is simulated to verify its convergence and estimation performance. Simulation results show excellent performance of the designed robust LPV observer for the shortened FUDS test cycle for HEV electric power-train in the presence of vast variations in rotor resistance, stator resistance, and rotor speed. The derated torque due to thermal effects has been estimated as seen in Figure 4.5(bottom).

Derated torque scenario due to thermal effects is more vivid at 0.01 seconds. It is clear from the Figure 4.6, the convergence time of the robust LPV observer is 0.18 seconds. As a result, precise and exact estimation of flux is available for the efficient estimation of machine's electromagnetic generated torque and operation

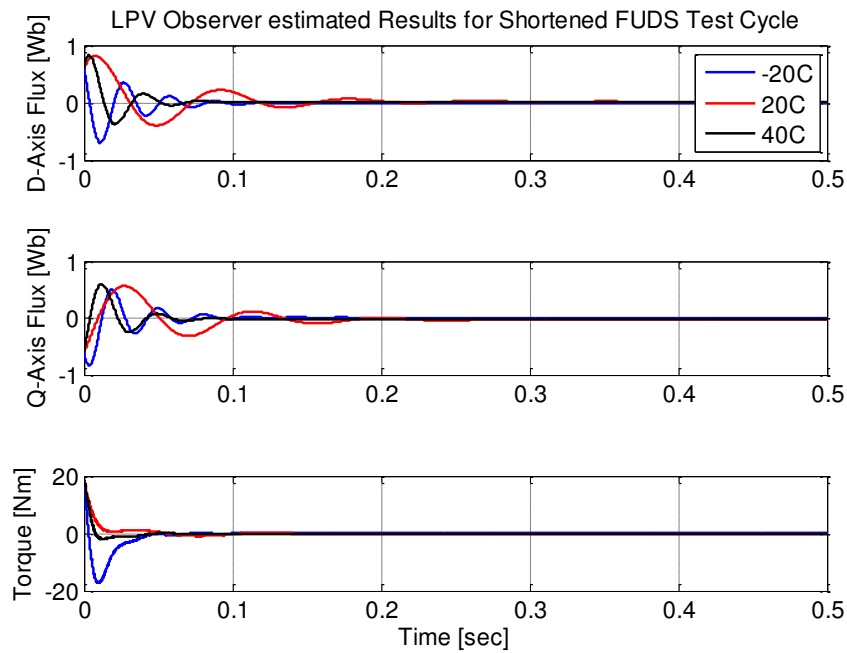


FIGURE 4.5: Robust LPV observer estimated results for shortened FUDS test cycle of :  $d$ -axis flux(Top),  $q$ -axis flux(Middle), and Torque derating(Bottom) at  $-20^{\circ}C$ ,  $20^{\circ}C$  and  $40^{\circ}C$ .

of HEV's drive system. From Figure 4.5, it is clear that the estimation of flux and torque de-rating is guaranteed at different ambient temperature. The three-phase input and  $dq$  voltages to the electric drive system for shortened FUDS driving cycle are shown in Figure 4.7. These results also proved the stability of proposed robust LPV observer in the practical scenario. Hence, the robust LPV observer proves to be a useful tool to estimate the de-rated torque in the HEV electric power-train.

### 4.5.3 Thermally derated torque estimation

Figure 4.8 shows the performance of the proposed and designed observer in estimating the thermally derated torque due to the the change in ambient temperature. It can be seen that the torque delivering capability is adversely affected by the temperature and operating speed. Moreover, the estimation results also exhibit the torque de-rates non-linearly with respect to temperature.

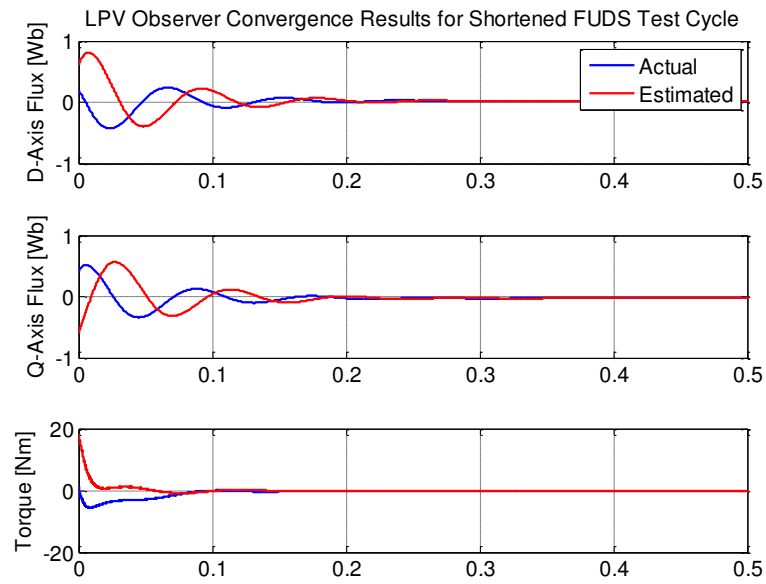


FIGURE 4.6: Robust LPV observer convergence results for shortened FUDS test cycle of actual and estimated:  $d$ -axis flux(Top),  $q$ -axis flux(Middle), and Torque derating(Bottom).

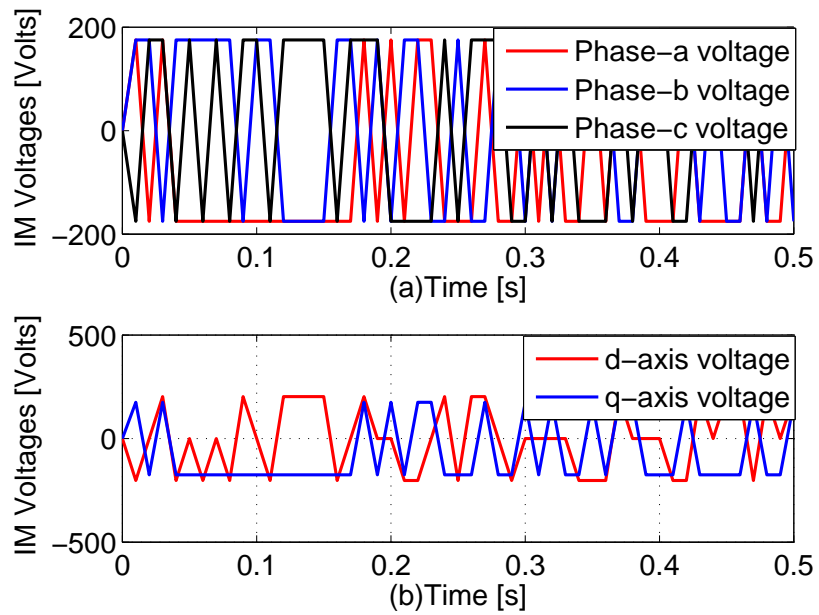


FIGURE 4.7: (a) 3-phase Input voltages to the electric drive system. (b)  $u_{ds}$  and  $u_{qs}$  for the electric drive system.

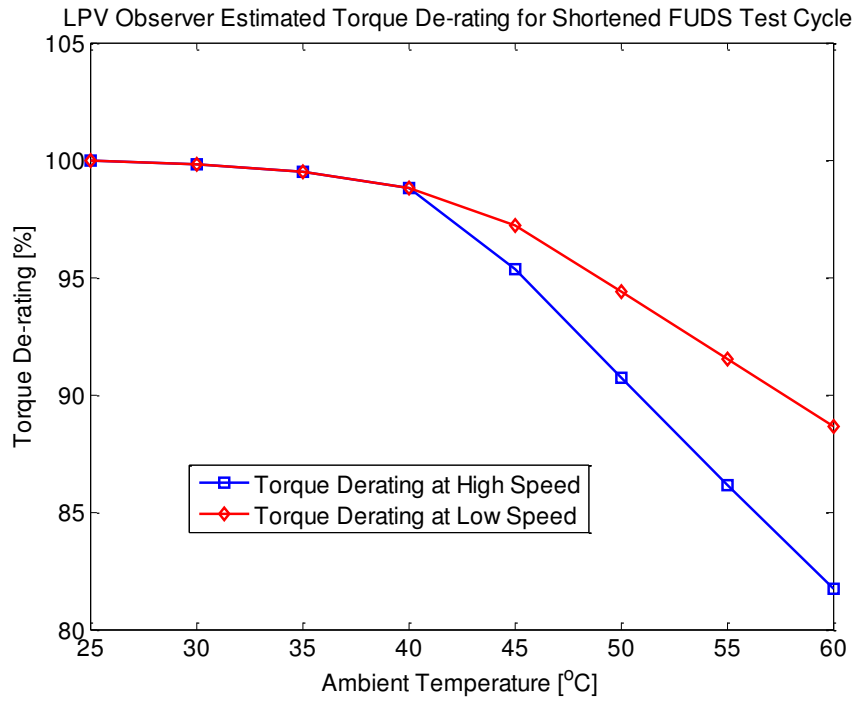


FIGURE 4.8: Robust LPV observer estimated torque derating under different operating conditions.

## 4.6 Conclusion

An LPV based robust observer has been proposed and designed to estimate the rotor flux and torque de-rating by utilizing the measurements of the stator currents and the rotor speed. Efficient and exact rotor flux and torque de-rating is necessary for the implementation of FOC HEV drive. Simulation study is carried out to investigate the performance of the designed robust LPV observer in theoretical scenario and practical scenario for shortened FUDS test cycle for HEV electric powertrain, demonstrating the efficacy of the observer.

In the coming chapter this observer will be used to design a robust control technique for managing the thermally derated torque in EVs and HEVs electric powertrain.

## Chapter 5

# Managing Thermally Derated Torque of an Electrified Powertrain

Linear parameter varying based estimation scheme, discussed in Chapter 4 is used here to design linear parameter varying control technique to manage and compensate the thermally derated torque for an induction machine based electrified powertrain. The proposed scheme has the capability to retain the nominal performance even in the face of severe rise in the operating and surrounding temperatures. Due to the variations in ambient and operating temperatures, reasons are discussed in Section 2.3, proposed linear parameter varying control scheme reschedules its control signals to attain effective performance. The efficacy of the proposed algorithm is demonstrated for an EV operating in Federal Urban Driving Schedule (FUDS) with a dynamic temperature profile. The nonlinear simulation results confirm the LPV observer capability to successfully estimate the flux and derated torque in an EV drive system. The proposed technique, after validating in simulation environment, is verified experimentally on an Induction Machine (IM) drive controlled by NI myRIO-1900.

## 5.1 Introduction

In order to achieve fuel efficiency and reduce emissions into the atmosphere, the automobile manufacturers have decided to escalate modern technologies such as EV and Hybrid Electric Vehicle (HEV) [103]. HEV has Atkinson cycle engine based traction system and EM propulsion system [104, 105]. In order to achieve fuel economy and emission reduction, only EM propulsion provides the traction force for EV and HEV. Among the available EMs, Induction Machine (IM) has been used for the traction system of EV and HEV because of the advantages including reasonable cost, simpler control, enhanced power density and efficiency, consistent operation over wide speed range, elevated initial torque, technological development and universal availability. IMs are also very robust, have rugged construction and require little maintenance [106, 107]. Moreover, IMs are inherently de-excited with respect to inverter fault hence highly recommended to be used in automobile industries for precautionary measures [41]. Production level vehicles have IM as an electric traction system [108].

In EV and HEV applications, where accurate and precise tracking is needed, a major problem is the operation of the electric traction system. FOC technique used for torque and flux control of IM is sensitive to parameter variations. The IM parameters change as the operating conditions change. Operating conditions for an EV and HEV propulsion system change constantly. Traffic situations, driving cycles etc., are the reasons of variation in speed. Also temperature has the effect on parameters, which is influenced by ambient season and loading etc. Due to these effects, the flux and torque of an electrified powertrain is thermally derated as compared to the industrial induction machines, where the variation in temperature and payload is very little [58–61]. Flux and torque tracking performance of a conventional FOC is deteriorated. Therefore, to attain high performance in EVs and HEVs, effective implementation of FOC for an EV and HEV electric traction system requires accurate and precise knowledge of thermally derated torque and flux.

The primary requirement for the FOC technique is a robust and accurate estimation of flux and torque in presence of extreme variations in the parameters. In order to meet the requirement, a robust LPV based observer has been developed and discussed by authors in [109] to estimate the thermal flux and torque derating by taking into account the rotor resistance, stator resistance, and speed variations for efficient control implementation of an EV and HEV electric traction system.

Mostly conventional Field-Oriented Control (FOC) is used to ensure efficient operation of an IM based electric drive [88]. The performance of conventional FOC is highly dependent on IM rotor and stator parameters. These parameters are adversely affected in extreme operating conditions, part loads and variation in payloads. As a result, flux and torque of an electrified powertrain is also affected. To overcome the problem of parameter variations on the torque and flux performance of an electrified powertrain, a robust controller based on LPV gain scheduling technique for the estimation and control of thermal flux and torque derating in an electrified powertrain and its evaluation under Standard Driving Cycle (SDC) has been proposed. This technique addresses the problem of flux and torque derating due to the change in operating and surrounding temperatures of an electrified powertrain. The performance of the proposed LPV based controller has been evaluated for a light duty electric vehicle against Federal Urban Driving Schedule (FUDS) operating at various ambient temperatures, which is a common controller evaluation approach adapted by automotive community [110] and [111]. Experiments are carried out on an IM drive, realized by the NI myRIO-1900, using FUDS driving cycle to investigate that the proposed technique is effective and delivers robust performance.

The rest of the chapter is structured as follows: Section 5.2 briefly describes the vehicle dynamics and nonlinear mathematical modeling of IM. EV performance constraints and IM parameters (rotor and stator resistance) estimation is presented in Section 5.3. Section 5.4 elaborates the control structure which includes the robust LPV current controller, robust flux and torque controllers derivation and its stability. Optimal flux calculation and reference current calculation are presented also in Section 5.4. Comparison of the proposed LPV control strategy

with Sliding Mode Control (SMC) technique is established in Section 5.5. The evaluation of proposed controller based on SDC is presented in Section 6.8 followed by experimental verification in Section 5.7. The concluding comments are presented in Section 5.8.

## 5.2 Vehicle Dynamics and IM Modeling

### 5.2.1 Vehicle Modeling and Dynamics

The proposed observer-controller pair strategy takes into consideration the EV aerodynamics and is not applied to the induction motor alone. The vehicle model is based on mechanics and aerodynamics principles [66].

The load torque ( $\tau_L$ ) of a vehicle is given by

$$\tau_L = \underbrace{(F_a + F_g + F_r + F_w)}_{F_t} R_w \quad (5.1)$$

where,  $F_a$  is the aerodynamic resistance force,  $F_g$  is the grade resistance force,  $F_r$  is the rolling resistance force,  $F_w$  is the acceleration resistance force,  $F_t$  is the total road load, and  $R_w$  is the wheel radius.

The following speed dynamics in the motor referential is used to describe the wheel drive:

$$\frac{dn_M}{dt} = \frac{n_p}{J}(\tau_e - \tau_L - bn_M) \quad (5.2)$$

where,  $n_M$  is the motor mechanical speed,  $\tau_e$  is the motor generated torque,  $n_p$  is the number of pole-pair,  $J$  is the total inertia (rotor and load), and  $b$  is the friction.

Moreover, the EV speed ( $v_w$ ) is proportional to the IM speed ( $n_M$ ), which can be expressed in term of wheel radius  $R_w$ , and the gear box ratio ( $G_R$ ) as follows:

$$v_w = \frac{R_w}{G_R} n_M \quad (5.3)$$

and the vehicle torque ( $\tau_w$ ) is given by

$$\tau_w = \tau_e G_R \eta_t \quad (5.4)$$

where,  $\eta_t$  is the transmission efficiency.

## 5.2.2 Dynamics of IM

Induction machine dynamics, presented in Section 3.2.1.3 based on  $d$ - $q$  axis coordinate can be written as [63, 109, 112]:

$$\begin{cases} \dot{i}_{ds} = -k_1 i_{ds} + k_2 \phi_{dr} + k_3 n_r \phi_{qr} + k_4 u_{ds} \\ \dot{i}_{qs} = -k_1 i_{qs} + k_2 \phi_{qr} - k_3 n_r \phi_{dr} + k_4 u_{qs} \\ \dot{\phi}_{dr} = -k_5 \phi_{dr} - n_p n_r \phi_{qr} + k_6 i_{ds} \\ \dot{\phi}_{qr} = -k_5 \phi_{qr} + n_p n_r \phi_{dr} + k_6 i_{qs} \end{cases} \quad (5.5)$$

where,  $d$  and  $q$  stand for direct and quadrature axis respectively and

$$\begin{cases} k_1 = \frac{(\chi_M^2 r_r + \chi_r^2 r_s)}{\sigma \chi_s \chi_r^2} \\ k_2 = \frac{\chi_M r_r}{\sigma \chi_s \chi_r^2} \\ k_3 = \frac{n_p \chi_M}{\sigma \chi_s \chi_r} \\ k_4 = \frac{1}{\sigma \chi_s} \\ k_5 = \frac{r_r}{\chi_r} \\ k_6 = \frac{\chi_M r_r}{\chi_r} \\ k_7 = \frac{b}{J} \\ k_8 = \frac{n_p}{J} \\ \sigma = 1 - \frac{\chi_M^2}{\chi_s \chi_r} \end{cases} \quad (5.6)$$

where  $\sigma = 1 - \frac{\chi_M^2}{\chi_s \chi_r}$  is the leakage factor.  $n_r$ ,  $r_r$ ,  $r_s$ ,  $\chi_r$ ,  $\chi_s$ ,  $\chi_M$  and  $n_p$  are the synchronous speed ( $r/m$ ), rotor speed ( $r/m$ ), rotor and stator resistances ( $\Omega$ ), rotor and stator inductances ( $H$ ), mutual inductance ( $H$ ) and the number of pole pairs respectively.

The electromagnetic generated torque, rotor speed and rotor flux can be expressed as

$$\begin{cases} \tau_e = \frac{3}{2}n_p \frac{\chi_M}{\chi_r} (\phi_{dr} i_{qs} - \phi_{qr} i_{ds}) \\ n_r = n_p n_M \\ \phi_r = \sqrt{\phi_{dr}^2 + \phi_{qr}^2} \end{cases} \quad (5.7)$$

where,  $n_r$  is the rotor electrical speed and  $\phi_r$  is the rotor flux.

### 5.2.3 LPV Modeling of Induction Machine

The design of a robust LPV control technique for the IM based EV drive is based on an LPV state space model of the form

$$\begin{cases} \frac{dx(t)}{dt} = A(\rho(t))x(t) + B(\rho(t))u(t) \\ y = C(\rho(t))x(t) + D(\rho(t))u(t) \end{cases} \quad (5.8)$$

where  $x \in \mathcal{R}^n$ ,  $\rho \in \mathcal{R}^s$ ,  $u \in \mathcal{R}^{m_2}$  and  $y \in \mathcal{R}^{p_2}$  are state, time varying parameter, input and output vectors respectively. The matrices  $A(\cdot)$ ,  $B(\cdot)$ ,  $C(\cdot)$  and  $D(\cdot)$  are continuous matrix valued functions of appropriate dimensions of the time varying parameter vector  $\rho$ . The validated LPV dynamics and definition of matrices are given in Section 3.6. In this model,  $r_r$ ,  $r_s$  and  $n_r$  are taken as scheduling signals.

## 5.3 EV Performance Constraints and IM Parameter Estimation

### 5.3.1 Performance Criteria

To have a smooth EV performance, the following criteria need to be observed:

- The (5.9) that describes the vehicle must track the speed profile of the driving cycle.

$$\min_{i_{ds}, i_{qs}, n_e} \|v(t) - v_{cycle}(t)\| \quad (5.9)$$

where,  $v(t)$  and  $v_{cycle}(t)$  are the actual vehicle speed and desired vehicle speed respectively.

- The (5.10) that describes the torque requirement must be exact and precise for the smooth operation of EVs.

$$\min_{i_{ds}, i_{qs}, n_e} \|\tau_e(t) - \tau_{ref}(t)\| \quad (5.10)$$

where  $\tau_e(t)$  and  $\tau_{ref}(t)$  are the actual and reference torque of IM over the entire range of operation.

- The (5.11) describes that the IM drive system must track the reference flux to reduce the fuel consumption in EVs.

$$\min_{i_{ds}, i_{qs}, n_e} \|\phi_r(t) - \phi_{ref}(t)\| \quad (5.11)$$

where  $\phi_r(t)$  and  $\phi_{ref}(t)$  are the actual and reference flux of IM over the entire range of operation.

### 5.3.2 IM Performance Curve

Induction motor performance curve is generated by rapidly loading the motor from the no-load condition to the locked rotor condition using fixed terminal voltages. Figure 5.1 represents the motor performance curve (plot of the motor shaft speed as a function of torque of the motor) at room temperature ( $25^{\circ}C$ ) which is used as a baseline. This is very useful information for EV application that needs intermittent function with a lengthy rest interval between every duty cycle. In this experiment, the rotor slip is 1.548 percent at rated voltage.

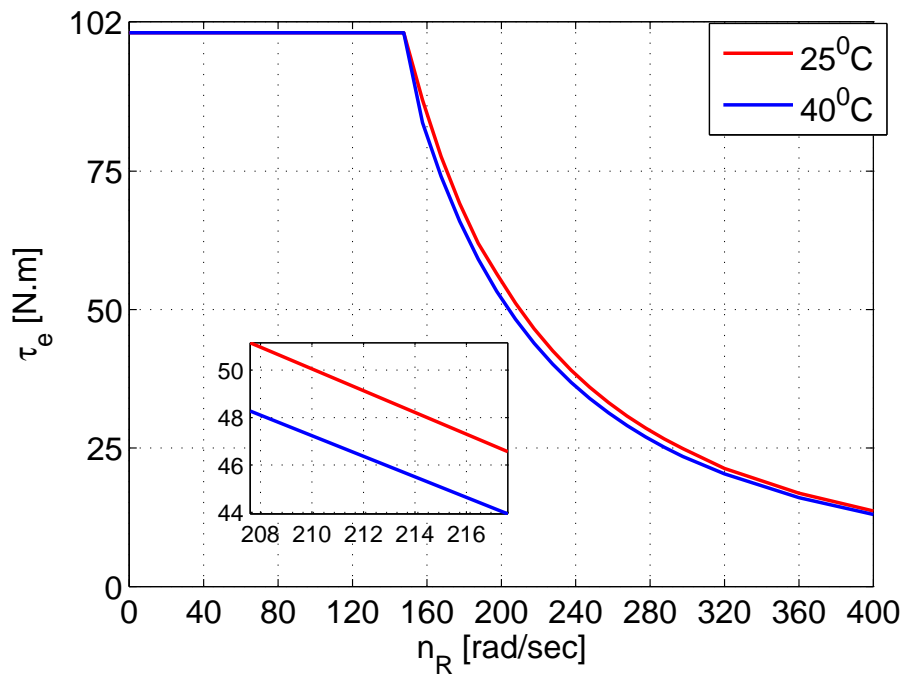


FIGURE 5.1: Induction motor (used in this work) performance curve at 25°C and 40°C (Torque derating at 40°C is vivid).

In EV and HEV applications, frequent starts and stops of high inertial loads exist. Due to this, EM temperature increases and the rotor and stator resistances also increase. This means that the motor performance curve at room temperature is inadequate. Figure 5.1 also shows the EM performance curve at high temperature (40°C). It is clear that torque of EM is derated due to the change in one or both temperatures. Therefore, an LPV control technique is proposed in this work to minimize the torque derating problem due to the temperature effects.

### 5.3.3 Rotor and Stator Resistance Estimation

The estimation of rotor and stator resistance are required for the design of the proposed observer-controller pair strategy. To estimate the rotor resistance, model based approach has been adopted from [113, 114]. It is further assumed that rotor speed, stator voltages and currents measurements are available for use from the

speed, voltage and current sensors respectively.

$$r_r = \sqrt{n_{sl}^2 \chi_r \left[ \frac{n_e \chi_M^2}{\frac{Q}{I_s^2} + n_e \chi_s} - \chi_r \right]} \quad (5.12)$$

where

$n_{sl}$  is the slip frequency and given as:

$$n_{sl} = n_e - n_r \quad (5.13)$$

$Q$  is the reactive power and can be calculated as:

$$Q = u_{ds} i_{qs} - u_{qs} i_{ds} \quad (5.14)$$

The estimation of stator resistance is given by [113]:

$$r_s = k r_r \quad (5.15)$$

$$k = \frac{r_s n}{r_{rn}} \quad (5.16)$$

where,  $r_{rn}$ ,  $r_{sn}$  are the nominal values of rotor and stator resistance, respectively.

The temperature dependence of rotor and stator resistance is given by [63]:

$$r = r_0 [1 + \alpha \Delta T] \quad (5.17)$$

where,  $r_0$  is the resistance at reference temperature ( $T_0 = 25^\circ C$ ),  $\alpha$  is the temperature coefficient of resistance, and  $\Delta T$  is the temperature increase.

## 5.4 Control Design

In this section, the design of robust LPV current controllers for inner feedback loop is presented. Robust flux and torque controllers are designed and presented

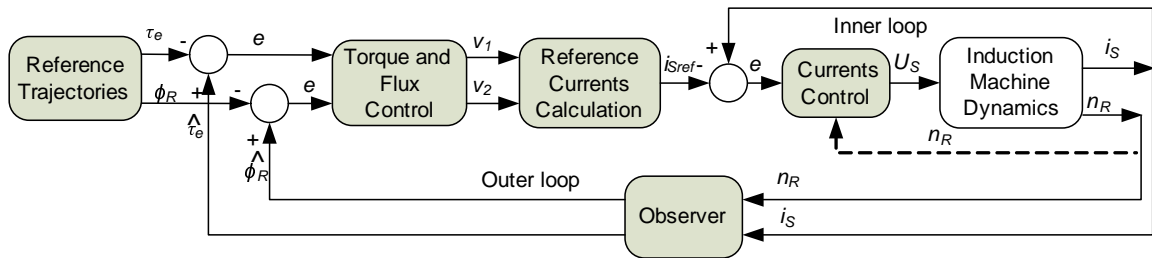


FIGURE 5.2: Inner and outer loop strategy in induction machine.

for outer feedback loop. It is designed using the LPV dynamics of IM presented in Section 5.2.3.

### 5.4.1 Controller Structure

The overall control structure considered in this work is presented in Figure 6.1. It consists of four components. Each component is designed individually. Currents control block is a stator current feedback controller which tracks the desired current set point  $i_{sref}$ . It is a robust LPV output feedback controller. Its inputs are the two stator currents available from measurement. It is scheduled with the rotor speed  $n_r$ , rotor resistance  $r_r$  and stator resistance  $r_s$ . Currents control block ensures good tracking over the entire operating range. LMIs are formulated for the computation of this controller. It permits to take the advantage of LPV formulation of the machine to design the robust LPV flux observer and stator current controller. The construction of observer and controller is simple and easy to implement. This structure also gives the robust controllers for outer flux and torque loop which is another advantage of this structure. A robust LPV observer is designed to estimate the thermal flux and derated torque and it is presented in Chapter 4. Input Output Feedback Linearization (IOFL) is used to generate the reference current vector and to linearize and decouple the rotor flux and torque as shown in Figure 6.1 [102]. Finally, the diagonal gains for torque and flux control are designed by formulating an LMI using the concept of Robust Input Output Feedback Linearization (RIOFL). These controllers ensure the robust tracking of the rotor flux and EM torque.

The major advantage of this control structure is that overall control problem is subdivided into four independent sub-control problems. The closed-loop stability of each independent sub-control problem is proved. Reference torque trajectory is generated by the driver and powertrain controller blocks as described in Section 5.6.1. The flux request is calculated from the torque request to achieve the fuel economy and its derivation is given in Section 5.4.6.

## 5.4.2 Robust LPV Current Controller

In this section, an LPV current feedback controller is synthesized for an LPV model of IM presented in Section 5.2.3. This LPV current control design technique is practically valid. LPV control is an extended form of  $H_\infty$  optimal control to nonlinear or time varying systems that can be represented in LPV framework [115]. Actuator constraints, disturbance rejection, and reference tracking are the design specifications on the control system. These are the control sensitivity function, complementary sensitivity function and sensitivity function to shape the design specifications.  $H_\infty$  norm can be adopted to ensure these specifications.  $L_2$ -gain of the closed-loop system is an alternate to  $H_\infty$  norm in the LPV framework. The idea of ‘generalized plant’ is commonly adopted in LPV control to express design specifications.

Consider an LPV plant with state space representation:

$$\begin{cases} \dot{x} = A(\rho)x + B_1(\rho)w + B_2(\rho)u \\ z = C_1(\rho)x + D_{11}(\rho)w + D_{12}(\rho)u \\ y = C_2(\rho)x + D_2(\rho)w \end{cases} \quad (5.18)$$

where  $w$  and  $z$  are the external input and controlled output vectors, respectively. The time varying parameter  $\rho(t)$  can be expressed in the form  $\rho(t) = (\rho_1, \rho_2, \dots, \rho_L)^T$  and the range of each parameter  $\rho_i$  is given as

$$\rho_i(t) \in [\rho_{-i}, \rho^{-i}] \quad (5.19)$$

$\mathcal{P}$  is a convex polytopes with vertices,  $\rho_i, i = 1, 2, \dots, N$ , and can be defined as

$$\mathcal{P} = Co\{\rho_{v1}, \rho_{v2}, \dots, \rho_{vL}\} \quad (5.20)$$

where  $\rho_{vi}$  are the vertices,  $i = 1, 2, \dots, L$ .  $L = 2^p$  are the number of vertices.  $Co$  is a convex hull ,i.e, the set of all convex combinations of  $\rho_{vi}$  (all points inside and on the boundary of the polytopes).

The objective is to design the gain schedule LPV output feedback control. The state space representation of the dynamic controller is:

$$\begin{cases} \dot{x}_K = A_K(\rho)x_K + B_K(\rho)y \\ u = C_K(\rho)x_K + D_K(\rho)y \end{cases} \quad (5.21)$$

which ensures the internal stability and a guaranteed  $L_2$ -gain bound  $\gamma$  for the closed-loop operator ((5.18) and (5.21)) from the disturbance signal  $w$  to the error signal  $z$ , that is

$$\int_0^T z^T z d\tau \leq \gamma^2 \int_0^T w^T w d\tau, \forall T \geq 0 \quad (5.22)$$

Next, LPV controller with guaranteed  $L_2$ -gain performance is presented in the following theorem:

**Theorem 3.** Consider the LPV plant ((5.18)) with parameter trajectories constrained as in (6.20). There exist an LPV output feedback controller ((5.21)) enforcing closed-loop stability and an upper bound  $\gamma > 0$  on the  $L_2$ -gain of the closed-loop system ((5.18) and (5.21)) from  $w$  to  $z$ , if there exist parameter dependent symmetric matrices  $X(\rho)$  and  $Y(\rho)$  and a parameter dependent quadruple of state space data  $(\tilde{A}_K(\rho), \tilde{B}_K(\rho), \tilde{C}_K(\rho), \tilde{D}_K(\rho))$  such that

$$\begin{bmatrix} A(i)Y(i) + B_2(i)\tilde{C}_K(i) + * & * & * & * \\ \tilde{A}_K^T(i) + A(i) & A^T(i)X(i) + \tilde{B}_K(i)C_2(i) + * & * & * \\ B_1(i) & X(i)B_1(i) + \tilde{B}_K(i)D_2(i) & -\gamma I & * \\ C_1(i)Y(i) + (D_{12}(i)\tilde{C}_K(i))^T & C_1(i) & D_{11}(i) & -\gamma I \end{bmatrix} < 0 \quad (5.23)$$

$$\begin{bmatrix} X(i) & I \\ I & Y(i) \end{bmatrix} > 0 \quad (5.24)$$

where  $*$  represents the terms required to achieve symmetry in matrix and  $\rho$  is dropped for simplicity.

The variables  $X$  and  $Y$  in (5.24) are the auxiliary variables. These are used to perform the linearizing the change of variables in output feedback.

**Proof.** See [116].

Based on the above theorem, the LPV controller synthesis problem can be solved by solving the optimization problem

$$\min_{X(\rho), Y(\rho), \tilde{A}_K(\rho), \tilde{B}_K(\rho), \tilde{C}_K(\rho)} \gamma \quad (5.25)$$

such that (6.60) and (6.61) hold  $\forall \rho \in \mathcal{P}$  and the controller of the form (5.21) can be computed by adopting the following two step scheme:

1) Solve  $R$  and  $S$  from the singular value decomposition of  $I - XY$

$$\begin{cases} I - XY = U\Sigma V^T \\ \Rightarrow R = U\sqrt{\Sigma}, S^T = \sqrt{\Sigma}V^T \end{cases} \quad (5.26)$$

2) Compute  $A_K$ ,  $B_K$  and  $C_K$  with

$$\begin{cases} C_K = (\tilde{C}_K - D_K C_2 Y)(S^T)^{-1} \\ B_K = (R)^{-1}(\tilde{B}_K - X B_2 D_K) \\ A_K = (R)^{-1}(\tilde{A}_K - R B_K C_2 Y - X B_2 C_K S^T \\ -X(A + B_2 D_K C_2)Y)(S^T)^{-1} \end{cases} \quad (5.27)$$

$D_K$  is zero for the output feedback control. Now, the scheduling parameter is given by (6.20) and the LPV model is affine, the constraints ((6.60) and (6.61)) constitute an LMI system. Hence, the construction of LPV controller with guaranteed  $L_2$ -gain performance can be reduced to an LMI problem and is numerically tractable.

So, the controller can be constructed as

$$\begin{bmatrix} A_K(\rho) & B_K(\rho) \\ C_K(\rho) & D_K(\rho) \end{bmatrix} = \sum_{i=1}^{i=2^p} c_i \begin{bmatrix} A_K(i) & B_K(i) \\ C_K(i) & D_K(i) \end{bmatrix} \quad (5.28)$$

### 5.4.3 Design Methodology

Depending on the results described in Section 6.7.2, an LPV output feedback controller is designed for the IM presented in Section 5.2.3. The objectives of this design are: (1) to achieve stability of the plant over the wide range of operation, (2) to get fast tracking with disturbance and noise rejection capability with little or no overshoot and (3) taking into account the control actuator constraints.

A mixed sensitivity loop shaping technique is adopted to meet the design objectives. Where  $W_T$  and  $W_S$  are the weighting gains which shape the output complementary sensitivity  $T(\rho)$  and sensitivity  $S(\rho)$  functions.  $W_K$  is the weighting gain used to express the upper bound on the control sensitivity  $K(\rho)S(\rho)$  function. The generalized plant is shown in Figure 6.2.

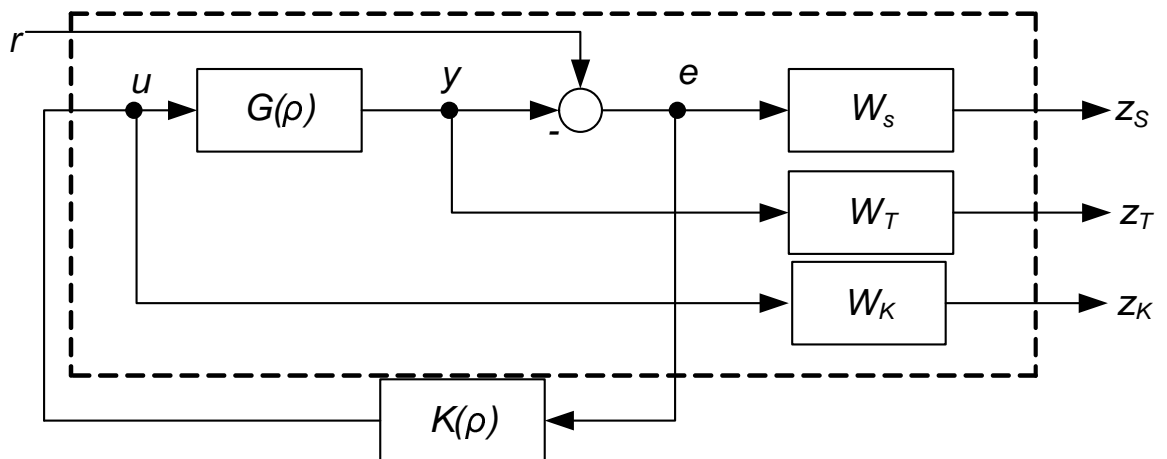


FIGURE 5.3: Constraints on  $S, T,$  and  $KS$  in term of a generalized plant.

These weighting gains are tuned iteratively until the design objectives are met satisfactorily. The values of these gains are

$$W_S = \begin{bmatrix} \frac{s+1.05}{0.45s+545} & 0 \\ 0 & \frac{s+1.05}{0.45s+545} \end{bmatrix} \quad (5.29)$$

$$W_T = \begin{bmatrix} 0.6 & 0 \\ 0 & 0.6 \end{bmatrix} \quad (5.30)$$

$$W_{KS} = \begin{bmatrix} 0.05 & 0 \\ 0 & 0.05 \end{bmatrix} \quad (5.31)$$

In this design,  $w$  in (5.18) describes the desired input  $r$ , which is the reference stator current  $i_{Sref}$ . Whereas  $z$  in (5.18) is a vector  $[z_S \ z_T \ z_K]^T$ , that has the output of the weighting matrices  $W_S$ ,  $W_T$  and  $W_K$ . These are used to shape the sensitivity (from  $r$  to  $e$ ), complementary sensitivity (from  $r$  to  $y$ ) and the control sensitivity (from  $r$  to  $u$ ) respectively.

Now, the LMI problem of (6.60) and (6.61) with the weighting functions given in (6.68), (5.65) and (5.31) is solved to achieve the LPV output feedback controller. LPV controller has six states (four come from the plant and two from  $W_S$ ). The achieved optimal value of  $\gamma$  is 1.023. The resultant controller is comparatively simple and easy to implement.

The performance and stability of the nonlinear system (original) presented in Section 5.2.2 are discussed with the designed LPV controller. It is observed in controller evaluation, Section 5.6.2, that better performance and stability are obtained for the closed-loop nonlinear system in the whole range of operation. Hence, this technique proves to provide the practical solution for the control of a highly nonlinear system (Section 5.2.2).

#### 5.4.4 Robust Torque and Flux Controller

To design a nonlinear control for tracking of torque and flux, the concept of Input Output Linearization (IOL) is adopted. The IOL gives linear differential relationship between output and input which is direct and simple [102]. For the control of IM, the relative degree and zero dynamics are well defined and are stable respectively [117]. Thus IOL can be adopted and performed. The input and output vectors for RIOL are

$$i_s = \begin{bmatrix} i_{ds} & i_{qs} \end{bmatrix}^T \quad (5.32)$$

$$y = \begin{bmatrix} \tau_e & \phi_r \end{bmatrix}^T \quad (5.33)$$

To ensure the decouple operation of FOC for IM

$$\phi_{qr} = 0 \quad (5.34)$$

To perform the RIOL, differentiating  $\tau_e$ , and  $\phi_r$  relations from (6.22) and putting (6.10) (only the two fluxes equations), it yields

$$\dot{\phi}_r = \frac{\phi_{dr}\dot{\phi}_{dr} + \phi_{qr}\dot{\phi}_{qr}}{\phi_r} \quad (5.35)$$

Now, by taking the two fluxes from ((6.10)) and using the definition:

$$n_e - n_r = \frac{r_r \chi_M}{\chi_r} \frac{i_{qs}}{\hat{\phi}_{dr}} \quad (5.36)$$

It yields:

$$\dot{\phi}_{dr} = -\frac{r_r}{\chi_r} \phi_{dr} + \frac{r_r \chi_M}{\chi_r} i_{ds} + \frac{r_r \chi_M}{\chi_r} \frac{i_{qs}}{\phi_{dr}} \phi_{qr} \quad (5.37)$$

and

$$\dot{\phi}_{qr} = -\frac{r_r}{\chi_r} \phi_{qr} \quad (5.38)$$

Now (5.35) yields

$$\dot{\phi}_r = -\frac{r_r}{\chi_r}\phi_r + \frac{r_r\chi_M/\chi_r(i_{ds}\hat{\phi}_{dr} + i_{qs}\hat{\phi}_{qr})}{\phi_r} \quad (5.39)$$

Time-derivative of the electromagnetic generated torque,  $\tau_e$  in (6.22) is

$$\dot{\tau}_e = \frac{3}{2}n_p\frac{\chi_M}{\chi_r}(\phi_{dr}\dot{i}_{qs} + i_{qs}\dot{\phi}_{dr} - \phi_{qr}\dot{i}_{ds} - i_{ds}\dot{\phi}_{qr}) \quad (5.40)$$

Putting (5.39) and (5.40) in matrix form

$$\begin{bmatrix} \dot{\tau}_e \\ \dot{\phi}_r \end{bmatrix} = G + H \begin{bmatrix} i_{ds} \\ i_{qs} \end{bmatrix} \quad (5.41)$$

where

$$G = \begin{bmatrix} -\frac{\tau_L}{J} - \frac{b}{J}n_r \\ -\frac{r_r}{\chi_r}\phi_r \end{bmatrix}, H = \begin{bmatrix} 0 & \frac{3}{2}n_p\frac{\chi_M}{J\chi_r}\hat{\phi}_{dr} \\ \frac{r_r\chi_M}{\chi_r\phi_r}\hat{\phi}_{dr} & 0 \end{bmatrix}$$

The estimation of rotor flux is affected by the variations in the rotor resistance, stator resistance and rotor speed. Therefore, uncertainty in flux estimation is considered to achieve the robust flux and torque controllers for the outer feedback loop in FOC of the electrified powertrain. Thus, by replacing  $\hat{\phi}_{dr}$  with  $\hat{\phi}_{dr} + \delta\phi_{dr}$ , (5.41) can be rearranged as

$$\begin{bmatrix} \dot{\tau}_e \\ \dot{\phi}_r \end{bmatrix} = \hat{G} + \hat{H} \begin{bmatrix} i_{ds} \\ i_{qs} \end{bmatrix} + \begin{bmatrix} \frac{3}{2}n_p\frac{\chi_M}{J\chi_r}\delta\phi_{dr}i_{qs} \\ -\frac{r_r}{\chi_r}\delta\phi_{dr} \end{bmatrix} \quad (5.42)$$

where

$$\hat{G} = \begin{bmatrix} -\frac{\hat{\tau}_L}{J} - \frac{b}{J}n_r \\ -\frac{r_r}{\chi_r}\hat{\phi}_{dr} \end{bmatrix}, \hat{H} = \begin{bmatrix} 0 & \frac{3}{2}n_p\frac{\chi_M}{J\chi_r}\hat{\phi}_{dr} \\ \frac{r_r\chi_M}{\chi_r} & 0 \end{bmatrix}$$

and Considering the following control law:

$$\begin{bmatrix} i_{ds} \\ i_{qs} \end{bmatrix} = -\frac{G}{H} + \frac{1}{H} \begin{bmatrix} u_{ds} \\ u_{qs} \end{bmatrix} \quad (5.43)$$

Putting (5.43) into (5.42), yields

$$\begin{bmatrix} \dot{\tau}_e \\ \dot{\phi}_r \end{bmatrix} = \begin{bmatrix} u_{ds} \\ u_{qs} \end{bmatrix} + \begin{bmatrix} \frac{3}{2} n_p \frac{\chi M}{J \chi_r} \delta \phi_{dr} i_{qs} \\ -\frac{r_r}{\chi_r} \delta \phi_{dr} \end{bmatrix} \cdot \begin{bmatrix} \delta \phi_{dr} i_{qs} \\ \delta \phi_{dr} \end{bmatrix} \quad (5.44)$$

Let the desired output vector be

$$y_d = \begin{bmatrix} \tau_{ed} & \phi_{rd} \end{bmatrix}^T \quad (5.45)$$

where  $\tau_{ed}$  is the desired torque and  $\phi_{rd}$  is the desired rotor flux.

The torque and rotor flux tracking errors are

$$e_{\tau_e} = \tau_e - \tau_{ed} \quad (5.46)$$

and

$$e_{\phi_r} = \phi_r - \phi_{rd} \quad (5.47)$$

From (5.44), the torque and flux controllers are

$$u_{ds} = -K_1 e_{\tau_e} + \dot{\tau}_{rd} \quad (5.48)$$

$$u_{qs} = -K_2 e_{\phi_r} + \dot{\phi}_{rd} \quad (5.49)$$

The closed-loop error dynamics becomes

$$\begin{bmatrix} \dot{e}_{\tau_e} \\ \dot{e}_{\phi_r} \end{bmatrix} = -K_e \begin{bmatrix} u_{ds} \\ u_{qs} \end{bmatrix} + B_e \begin{bmatrix} i_{qs} \\ \phi_{dr} \end{bmatrix} \quad (5.50)$$

where

$$K_e = \begin{bmatrix} K_1 & 0 \\ 0 & K_2 \end{bmatrix}, B_e = \begin{bmatrix} \frac{3}{2} \frac{n_p \chi M}{J \chi_r} & 0 \\ 0 & -\frac{r_r \chi M}{\chi_r} \end{bmatrix}$$

To convert the closed-loop error dynamics into an LMI, the definition of bounded real lemma is used [116] which is given as

$$\begin{bmatrix} A^T P + PA & PB & C^T \\ B^T P & -\gamma I & D^T \\ C & D & -\gamma I \end{bmatrix} \prec 0 \quad (5.51)$$

where  $P$  is a positive definite matrix,  $P = P^T$  and  $\gamma$  is greater than zero.

Putting closed loop error dynamics matrices from (5.50) into (5.51), yields

$$\begin{bmatrix} K_e^T P + PK_e & PB_e & I_2 \\ B_e^T P & -\gamma I_2 & 0 \\ I_2 & 0 & -\gamma I_2 \end{bmatrix} \prec 0 \quad (5.52)$$

This is a Bilinear Matrix Inequality (BMI). To deal with BMI, considering  $N = PK_e$ , the resultant LMI is

$$\begin{bmatrix} N^T + N & PB_e & I_2 \\ B_e^T P & -\gamma I_2 & 0 \\ I_2 & 0 & -\gamma I_2 \end{bmatrix} \prec 0 \quad (5.53)$$

The solution of (5.53) gives the  $N$  and  $P$ . From these, the gains of the torque and flux controllers can be constructed as:

$$K_e = P^{-1}N \quad (5.54)$$

The gains of torque and flux controllers are  $\text{diag}(-300, -230)$ .

### 5.4.5 Reference Current Calculation

The reference currents are calculated by differentiating the torque  $\tau_e$  and rotor flux  $\phi_R$  equations,

$$\dot{\phi}_r = \frac{-\frac{r_r}{\chi_r}\phi_{dr}^2 + \frac{\chi_{Mr_r}}{\chi_r}\phi_{dr}\dot{i}_{dr} - \frac{r_r}{\chi_r}\phi_{qr}^2 + \frac{\chi_{Mr_r}}{\chi_r}\phi_{qr}\dot{i}_{qr}}{\phi_r} \quad (5.55)$$

Let the first derivative of the torque  $\tau_e$  is  $v_1$  and the first derivative of the rotor flux  $\phi_R$  is  $v_2$ , it yields.

$$v_1 = \frac{3}{2}n_p \frac{\chi_M}{\chi_r} (\phi_{dr}\dot{i}_{qs} + i_{qs}\dot{\phi}_{dr} - \phi_{qr}\dot{i}_{ds} - i_{ds}\dot{\phi}_{qr}) \quad (5.56)$$

$$v_2 = \frac{-\frac{r_r}{\chi_r}\phi_{dr}^2 + \frac{\chi_{Mr_r}}{\chi_r}\phi_{dr}\dot{i}_{dr} - \frac{r_r}{\chi_r}\phi_{qr}^2 + \frac{\chi_{Mr_r}}{\chi_r}\phi_{qr}\dot{i}_{qr}}{\phi_r} \quad (5.57)$$

(5.56) and (5.57) can be re-written as

$$M \begin{bmatrix} \dot{i}_{ds} \\ \dot{i}_{qs} \end{bmatrix} = N \quad (5.58)$$

where

$$M = \begin{bmatrix} \frac{\chi_{Mr_r}}{\chi_r}\phi_{dr} & \frac{\chi_{Mr_r}}{\chi_r}\phi_{qr} \\ -n_p \frac{\chi_M}{\chi_r J} \phi_{qr} & n_p \frac{\chi_M}{\chi_r J} \phi_{dr} \end{bmatrix} \quad (5.59)$$

and

$$N = \begin{bmatrix} \phi_r(v_2 + \frac{r_r}{\chi_r}\phi_r) \\ v_1 + \frac{b}{J}n_r + \frac{1}{J}\tau_L \end{bmatrix} \quad (5.60)$$

From (5.58), the reference currents command can be calculated as

$$i_{sref} = \begin{bmatrix} \dot{i}_{dsref} \\ \dot{i}_{qsref} \end{bmatrix} = \frac{1}{|M|\phi_r^2} [M]^{-1} [N] \quad (5.61)$$

### 5.4.6 Reference Flux Calculation

The IM functions at different speeds and torques based on the operating conditions of the vehicle. Therefore, this section presents the reference flux calculation to optimize the electrical energy consumption. It is not possible to achieve the energy optimization with standard reference of flux. The standard flux reference is not adopted for the EVs and HEVs. In reality, for small torque demand, it is not useful to keep the flux reference at high level when a small flux reference can provide the same torque. Higher levels of flux demand the use of more current and therefore, more energy. In order to minimize the energy utilization, reference flux is computed using the torque reference. The machine steady-state losses on the stator and rotor sides are given by [9]:

$$P_{Loss} = \underbrace{\frac{3}{2}r_s(i_{ds}^2 + i_{qs}^2)}_{\text{Stator losses}} + \underbrace{\frac{3}{2}\frac{\chi_M}{\chi_r}(n_e - n_r)\phi_r i_{qs}}_{\text{Rotor losses}} \quad (5.62)$$

Putting the steady state values of  $i_{ds}$ ,  $i_{qs}$  and  $n_e - n_r$  taken from (6.10), in (5.62) gives

$$P_{Loss} = \frac{3}{2} \left[ r_s \left( \frac{\phi_r}{\chi_M} \right)^2 + \left( r_s + \left( \frac{\chi_M}{\chi_r} \right)^2 r_r \right) \left( \frac{\tau_e}{T_k \phi_r} \right) \right] \quad (5.63)$$

where,  $T_k = \frac{3}{2}n_p \frac{\chi_M}{\chi_r}$ . Optimal flux reference, to minimize the energy consumption, can be obtained by minimizing (5.63)

$$\begin{cases} \phi_{r_{ref}} = \lambda_{opt} \sqrt{|T_{e_{ref}}|} \\ \lambda_{opt} = \left( \frac{\chi_M}{T_k} \left( 1 + \left( \frac{\chi_M}{\chi_r} \right)^2 \frac{r_r}{r_s} \right)^{1/2} \right)^{1/2} \end{cases} \quad (5.64)$$

Moreover, the constraints on the stator voltages and currents are not considered in the analysis worked out here. Indeed, the stator voltages and currents cannot increase from their maximum physical values which is described by the weakening region in the standard flux reference selection. To solve the voltage and current constraints, the standard flux reference profile is used as a maximum value. The

standard flux reference signal is written as

$$\phi_m = \begin{cases} \phi_0 & \text{if } |n_r| \leq n_b \\ \frac{n_b}{|n_r|} \phi_0 & \text{if } |n_r| > n_b \end{cases} \quad (5.65)$$

where  $\phi_0$  is the maximum value of the flux without saturation and  $n_b$  is the base speed of IM.

To meet the constraints on the stator voltage and current, the optimum reference flux signal ((6.68)) does not exceed the standard reference flux signal ((5.65)) during the entire operation of the EV.

#### 5.4.7 Selection of Controller Gain

The LPV controller  $K_{lpv}$  was computed by solving the optimization problem of Equation (5.25) such that Eqs. (5.23) and (5.24) hold. With the weighting functions defined in Equations (5.29)-(5.31), the LMI optimization gave a LPV controller with eight vertices, each vertex being an LTI controller with six states. Four states come from the plant and two from WS: The achieved optimal value of performance index  $\gamma$  is 1.023.

The controller gains at each vertex are given in Appendix-D.

The torque and flux controllers were computed by solving the linear matrix inequality in Equation (5.53) and Equation (5.54) gives us the gains of controllers.

### 5.5 Comparison With Sliding Mode Control

In order to validate the effectiveness and robustness of proposed LPV control scheme, another technique is used for comparison. The technique is called ‘‘FOC HOSMC’’ in this paper and originally presented in [80]. It discusses the performance of IM by taking into account the rotor and stator resistances variations (one

parameter variation at a time) by utilizing the concept of Higher Order Sliding Mode (HOSMC) technique.

In order to evaluate the closed loop performance of the LPV control scheme with FOC-HOSMC scheme, two cases are studied. The first case is under similar load torque and velocity signal references are generated and utilized as in [80, 118] to observe the effectiveness of the LPV control scheme. The accuracy of both scheme is quantitatively assessed by considering the chattering in the output velocity profile. The LPV control technique has chattering of 0.0009 rad/sec as compared to 0.36 rad/sec chattering of the FOC-HOSMC scheme. Simulation result of actual and reference velocity signal is plotted together in Figure 5.4.

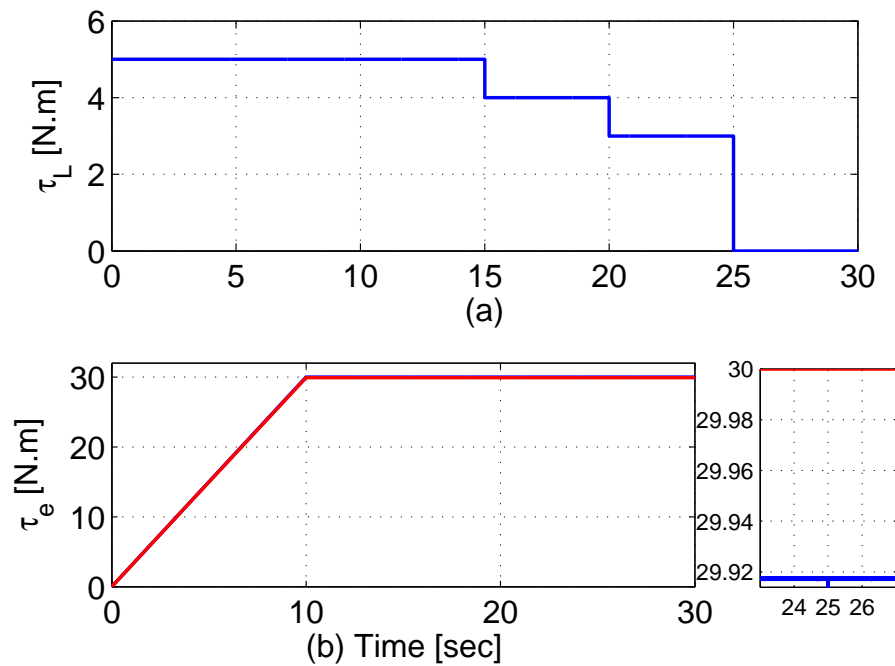


FIGURE 5.4: Simulation result for closed loop rotor velocity performance. (a) Load torque taken in closed loop simulation. (b) Rotor velocity tracking: reference (red) and actual (blue).

The second case is under the variations of stator and rotor resistances. The percent tracking error in the rotor velocity ( $\Delta z_1$ ) and the increment of the optimal rotor flux modulus ( $\Delta \phi_r$ ) with respect to steady state value obtained without motor parameter variations are used as performance indices. The simulation results are presented and summarized in Tables 6.3 and 6.4. From Tables 6.3 and 6.4, one

TABLE 5.1: Performance comparison of FOC-HOSMC and FOC-LPV to stator resistance variations

FOC-HOSMC			FOC-LPV		
$\Delta r_s$	$\Delta z_1$	$\Delta \phi_r$	$\Delta r_s$	$\Delta z_1$	$\Delta \phi_r$
20%	-0.12%	62%	20%	-0.10%	59.4%
40%	-0.2%	139%	40%	-0.17%	135.6%
60%	-0.3%	216%	60%	-0.23%	210%
80%	—	—	80%	-0.27%	230%

TABLE 5.2: Performance comparison of FOC-HOSMC and FOC-LPV to rotor resistance variations

FOC-HOSMC			FOC-LPV		
$\Delta r_r$	$\Delta z_1$	$\Delta \phi_r$	$\Delta r_r$	$\Delta z_1$	$\Delta \phi_r$
20%	-0.03%	7.82%	20%	-0.009%	6.2%
40%	-0.042%	17.33%	40%	-0.022%	11.42%
60%	-3.5%	1590%	60%	-0.40%	590%
80%	—	—	80%	-0.53%	729%

can examine that LPV control scheme performs well in the tracking of the rotor velocity in the presence of variations in stator and/or rotor resistance. On the other hand, the increase in the optimal rotor flux reference signal is significantly less in the presence of such variations. The proposed LPV control technique is also tested for more rotor and stator resistance variations ( $\pm 80\%$ ) and result are summarized in Tables 6.3 and 6.4.

## 5.6 Standard Driving Cycle Analysis

This section describes the effectiveness of the designed observer controller pair for a standard driving cycle. It is evaluated on a high fidelity EV simulator constructed in MATLAB/SIMULINK for an actual electric vehicle shown in Figure 5.5, as

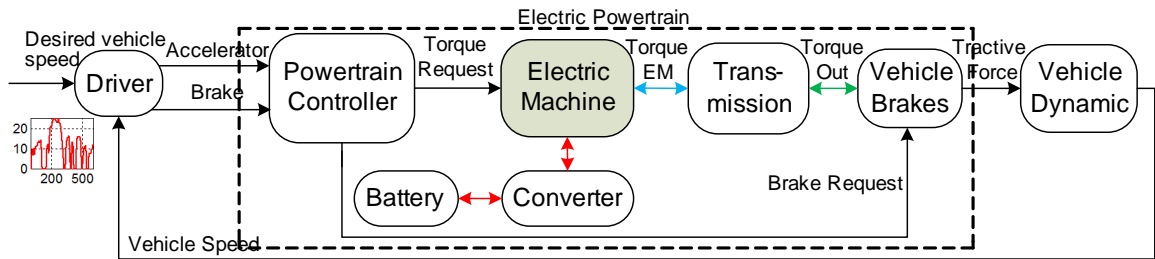


FIGURE 5.5: Vehicle level system architecture.

commonly exercised by automotive community to evaluate their control frameworks [119] and [120]. The evaluation is conducted at  $20^{\circ}C$ ,  $40^{\circ}C$  and  $60^{\circ}C$  ambient temperatures to show the effectiveness of the proposed control framework.

### 5.6.1 EV Specifications and Simulation Detail

The vehicle architecture considered in this article is shown in Figure 5.5. The specifications of a light duty EV and cage induction machine are given in Table 6.1.

TABLE 5.3: Specifications of an induction machine and a light duty electric vehicle

Induction Machine					
$n_p$	No. of pole pairs	2	$r_s$	Stator resistance	$0.22\Omega$
$r_r$	Rotor resistance	$0.209\Omega$	$\chi_s$	Stator inductance	$0.425H$
$\chi_r$	Rotor inductance	$0.043H$	$\chi_M$	Mutual inductance	$0.04H$
$J$	Inertia	$0.124Kg.m^2$			
$b$	Damping	$0.013N.m.s.rad^{-1}$			
Light duty Electric Vehicle					
$M$	Mass	350Kg			
$R_w$	Radius of wheel	0.205m			
$A_f$	Frontal area	$2.1m^2$			
$C_r$	Roll coefficient	0.013			
$C_d$	Drag coefficient	0.42			

The electric powertrain consists of powertrain controller, EM with transmission, battery and vehicle brakes. The flow of energy is from the battery and EM to the drive shaft and vice versa. The powertrain controller (1) drives the desired torque signal to the EM control unit; and (2) perform the transmission to the vehicle. The aim of the driver block is to simulate the decision of the driver on the braking pedal and the accelerator positions depending on the actual and desired vehicle speed and slope of the road. The desired vehicle speed is considered to be known by the particular driving cycle, FUDS in case of this work. A classical proportional plus integral controller has been adopted with proportional gain,  $k_p = 0.25$  and integral gain,  $k_i = 0.01$  to reproduce the reaction of driver regarding the tracking of the vehicle speed. The driver block takes the error between the actual and desired vehicle speeds as an input, and the output is a pedal signal with a saturated scale from  $-1$  to  $1$ . It is interpreted as a brake-pedal position and accelerator-pedal position when it is negative and positive respectively. In powertrain controller, the requested EM torque can be decided on the accelerator pedal position or the brake pedal position. The EM is supposed to deliver the requested torque through transmission to the vehicle efficiently. This study mainly focuses on managing of thermally derated torque of the electrified powertrain. The compensation of thermally de-rated torque of EM (electric powertrain) mainly . How to efficiently compensate the thermally de-rated torque in EM (electric powertrain) on the basis of the vehicle operating conditions and the powertrain operating condition is the main concern in this work and has been addressed through LPV control.

### 5.6.2 Control Evaluation

A predefined city driving cycle FUDS which has several starts and stops is used for evaluating the performance of proposed LPV control strategy regarding the managing of thermally derated torque of an electrified powertrain via a change profile of temperature. A validation temperature profile is shown in Figure 5.6.

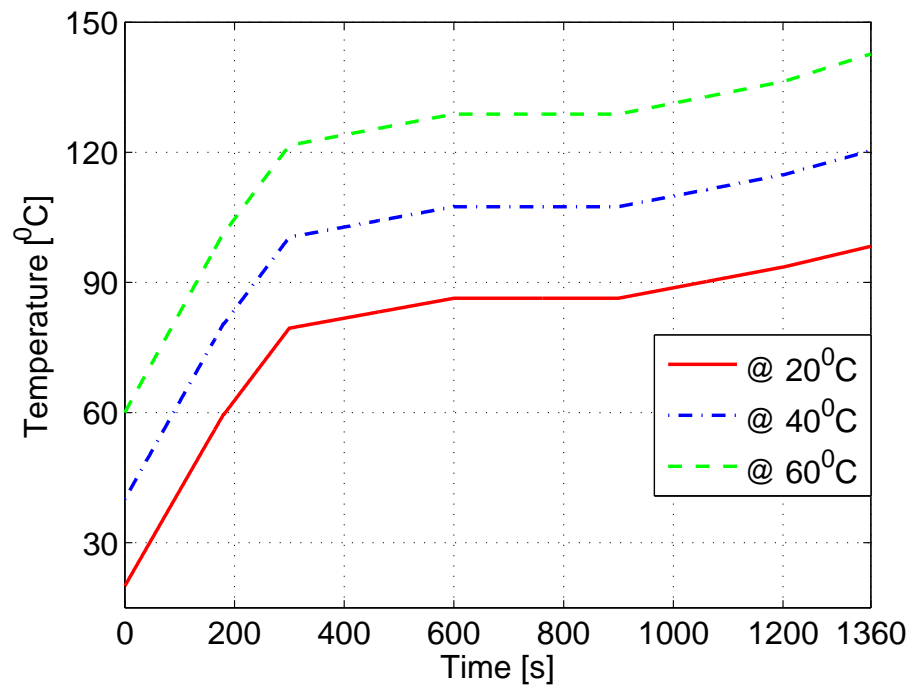


FIGURE 5.6: Simulation results: Temperature profile for the controller observer pair evaluation at different ambient temperatures.

It has a duration of 1360 s and exhibits the operating performance under very fast temperature, very low temperature and constant temperature. Very fast temperature, very low temperature and constant temperature operations can also be examined between 0-180, 900-1200 and 600-900 s, respectively. The temperature profile is realized from the stator voltages and currents, motor speed and power utilized over the entire driving cycle. Figure 5.7 gives the results for traction system. Figure 5.7 represents the vehicle speed tracking performance of the LPV control method via a change profile of temperature and shows clearly the different phases of constant speed, acceleration and deceleration. As the result signify, LPV control method accomplishes the vehicle speed tracking performance conditions well over the entire temperature profile (low, high and constant temperatures).

The rotational speed of IM is given in Figure 5.8.

The change in the IM drive system parameters (rotor and stator resistances at different ambient temperatures) for the light duty electric vehicle operated in a complete FUDS cycle are shown in Figure 5.9.

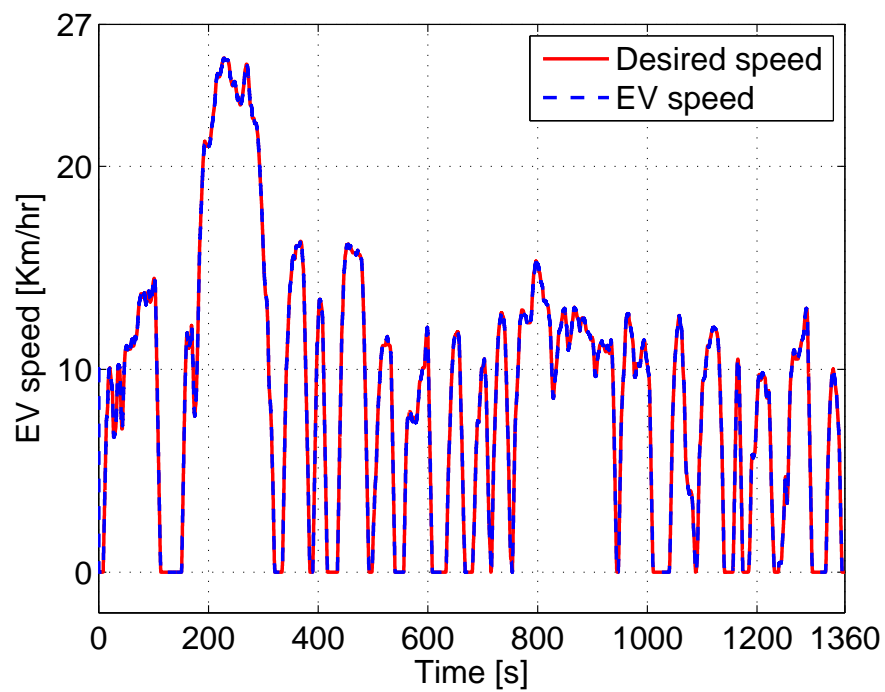


FIGURE 5.7: Tracking of vehicle speed profile via a change profile of temperature (at ambient temperature of  $40^{\circ}C$ ) with LPV controller observer pair.

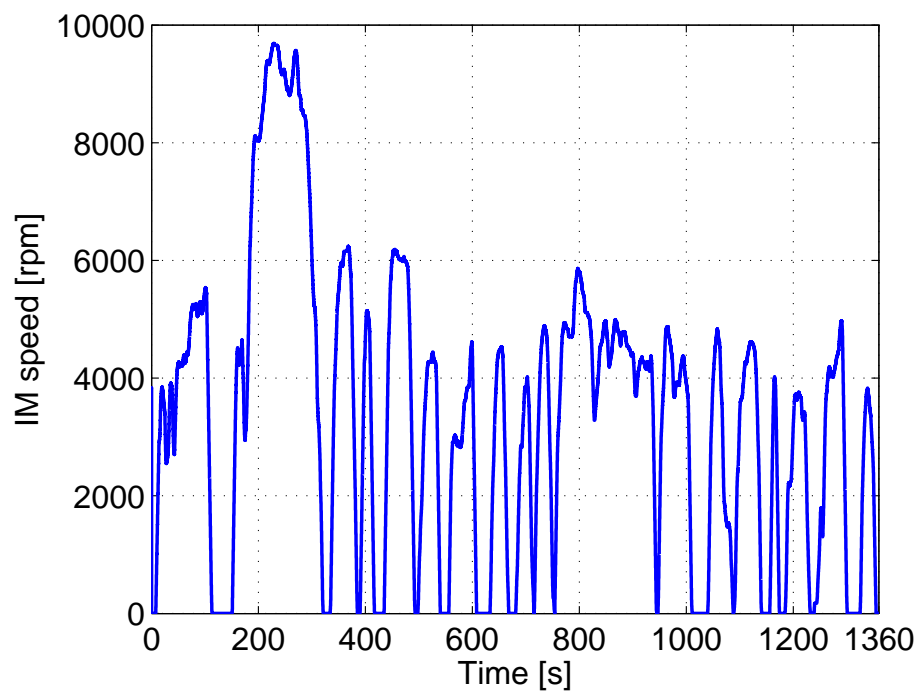


FIGURE 5.8: Induction machine speed.

The major component of the electric powertrain is an EM. To measure its performance the requested torque profile that is generated by the powertrain controller

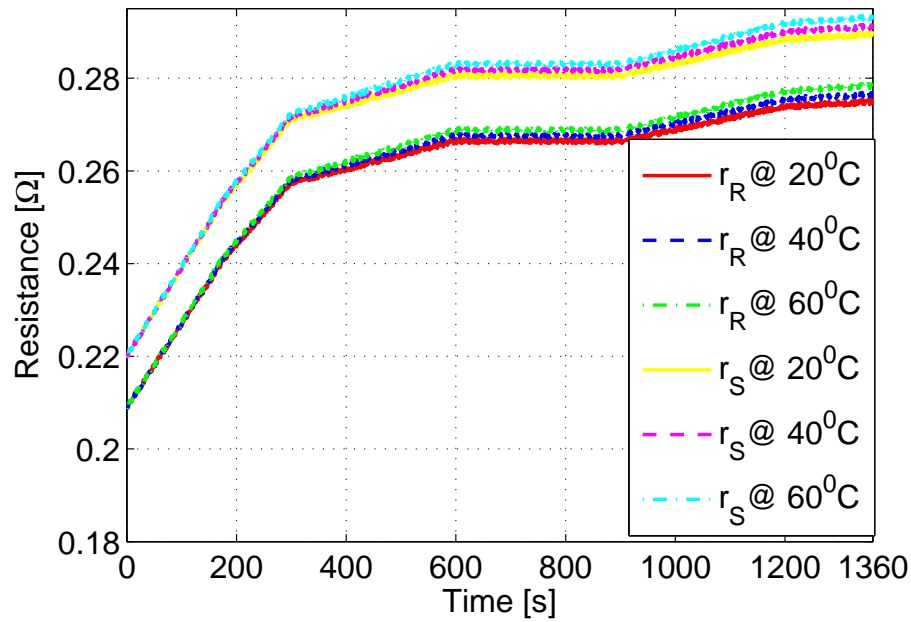


FIGURE 5.9: Simulation results: Rotor and stator resistance variations over the entire period of operation at different ambient temperatures.

depending upon the accelerator and brake pedal position is supposed to be tracked by the EM at all operating (temperature) conditions. Figure 5.10 gives the requested torque tracking with LPV control method via a change profile of temperature (in the presence of vast uncertainties in the stator and rotor resistances). As can be seen, torque tracking is excellent at all operating conditions in the presence of rapid changes in requested torque signal. These rapid changes are due to the high traffic situations in FUDS route. Consequently, a smoother operation of the vehicle is guaranteed. This also shows the accuracy of the estimation of thermally derated torque through LPV observer.

The optimal flux request for the EM is generated from the torque request signal as explained in Section 5.4.6. To achieve better efficiency from the electric powertrain, an EM is assumed to track the optimal flux request over the entire period of operation via a change profile of temperature. Figure 5.11 represents requested flux tracking. It is clear that the performance of an EM based on the requested flux tracking is more accurate and precise with the LPV control method at all temperature conditions. It is clear also from Figure 5.10 that the requested flux is less than the rated flux (0.55 Wb) over the entire driving cycle. It reduces the fuel

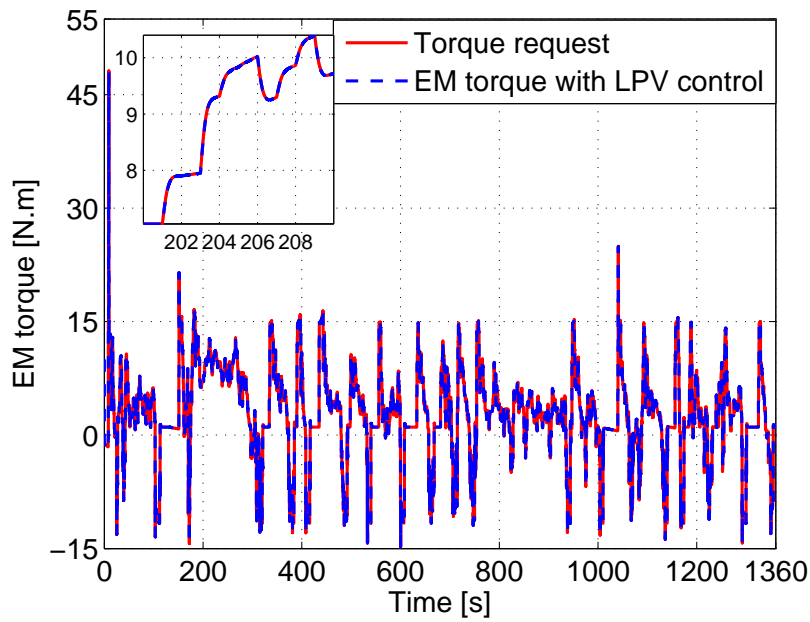


FIGURE 5.10: Simulation results: Tracking of torque request profile via a change profile of temperature (at ambient temperature of  $40^{\circ}\text{C}$ ) with LPV controller observer pair.

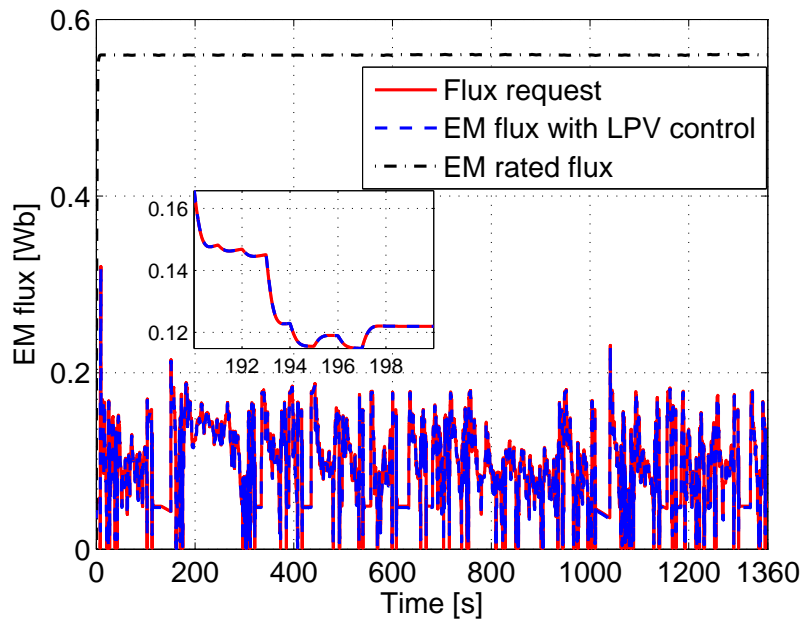


FIGURE 5.11: Simulation results: Tracking of flux request profile via a change profile of temperature (at ambient temperature of  $40^{\circ}\text{C}$ ) with LPV controller observer pair.

consumption in EVs. Figures. 5.7, 5.10 and 5.11 also illustrate the performance of the proposed LPV observer during the operation of EV.

It is worth notice also that stator voltages and currents never attained their upper limit during simulation because of the upper limit set on the flux reference in (6.68). A close up view in short time frame of stator voltages and currents in the IM is given in Figure 5.12. Therefore, improved performance of electric powertrain with respect to the compensation of thermally derated torque of an EM is ensured.

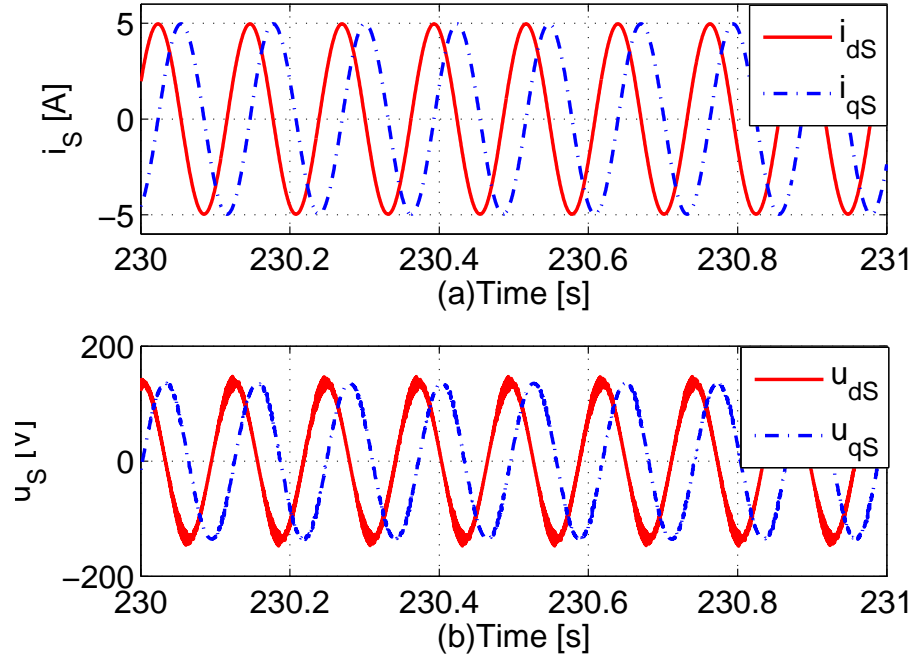


FIGURE 5.12: Simulation results: Induction machine direct and quadrature axis (a) stator currents. (b) stator voltages: corresponding to the operation of electrified powertrain at  $40^{\circ}C$ .

The performance of proposed LPV control method via a change profile of temperature is presented in Table 5.4 for three different ambient temperatures. RMSE and NRMSE are used as performance indices.

TABLE 5.4: Performance indices comparison for proposed LPV based FOC control framework at different ambient temperature

Performance indices	Vehicle Level			Machine Level					
	Speed profile tracking			Torque tracking			Flux tracking		
	Temperature								
	$20^{\circ}C$	$40^{\circ}C$	$60^{\circ}C$	$20^{\circ}C$	$40^{\circ}C$	$60^{\circ}C$	$20^{\circ}C$	$40^{\circ}C$	$60^{\circ}C$
RMSE	0.1551	0.1536	0.1451	0.1950	0.1956	0.1965	0.0099	0.00982	0.0097
NRMSE	0.8449	0.8464	0.8549	0.8050	0.8044	0.8035	0.9901	0.99018	0.9903

## 5.7 Experimental Verification

In the previous Sections it has been amply demonstrated that the proposed LPV scheme fully obviates the torque derating effects arising from the motor resistance variations arising from temperature changes. However, there is still a need to put this LPV controller to test on a hardware rig. For this purpose, a hardware test set-up consisting of an IM, a Controller Board and a Torque Measurement arrangement is employed to validate the controller test results. The current Section is essentially divided into four sub-sections. The first sub-section 5.7.1 describes the test set-up formed. The remaining three sections are dedicated to the hardware results of the three experiments performed. Practical observation of the open loop thermal torque effects (the first experiment) is discussed in the second sub-section 5.7.2. The third sub-section 5.7.3 addresses the excellent performance on the test bed of the LPV controller for a step demand on the torque, in contrast to the sliding mode based results reported in the literature [10], this experiment is performed on the raised temperature profile. The third and final experiment, aimed at validating controller for the harsh environment faced by an electrified powertrain in a challenging urban environment, is addressed in the last sub-section 5.7.4 of this Section. For this purpose the speed demand profile was generated from FUDS.

### 5.7.1 Experimental Setup

This section elaborates the experimental setup used for the validation of proposed estimation and control technique for an electrified powertrain. Figure 5.13 shows the experimental setup devised. The control algorithm was implemented on a control board based on NI myRIO-1900 from National Instruments. The setup also included the inverter to control the IM, sensors (voltage, current and speed), torque measurement, auto-transformer and electric brake to generate the load torque. The NI myRIO-1900 was interfaced to a PC. The data logging, downloading and data communication functions are performed by the microprocessor.



FIGURE 5.13: Experimental setup of an IM drive system.

The braking mechanism is realized by the magnetic powder brake (DL 1019P) of DE LORENZO group which consists on load cell (DL 2006E) with 150 N range. The powder brake is controlled by brake control unit (DL 1054TT) of same company. It allows measuring the rotating speed and the torque generated by an electric machine. It also provides the excitation voltage to the brake.

The electric machine drive system shown in Figure 5.13 is equipped with state of the art sensors. These sensors are heavily relied upon to monitor each of the electric machine drive subsystem precisely. Among number of sensors in machine test setup, the optical transducer (DL 2031M) for measuring the rotation speed through a slotted optical switch with encoder disc. The current of machine is sensed due to change in magnetic field using a hall effect sensor (ACS724).

### 5.7.2 Open Loop Torque Derating Confirmation

In EV and HEV applications, frequent starts and stops of high inertial loads exist. Due to this, EM temperature increases and the rotor and stator resistances also increase. This means that the motor performance curve at room temperature is inadequate. Figure 5.14 also shows the measured EM performance curve at high temperature ( $40^{\circ}\text{C}$ ). It is clear that torque of EM is derated due to the change in one or both temperatures.

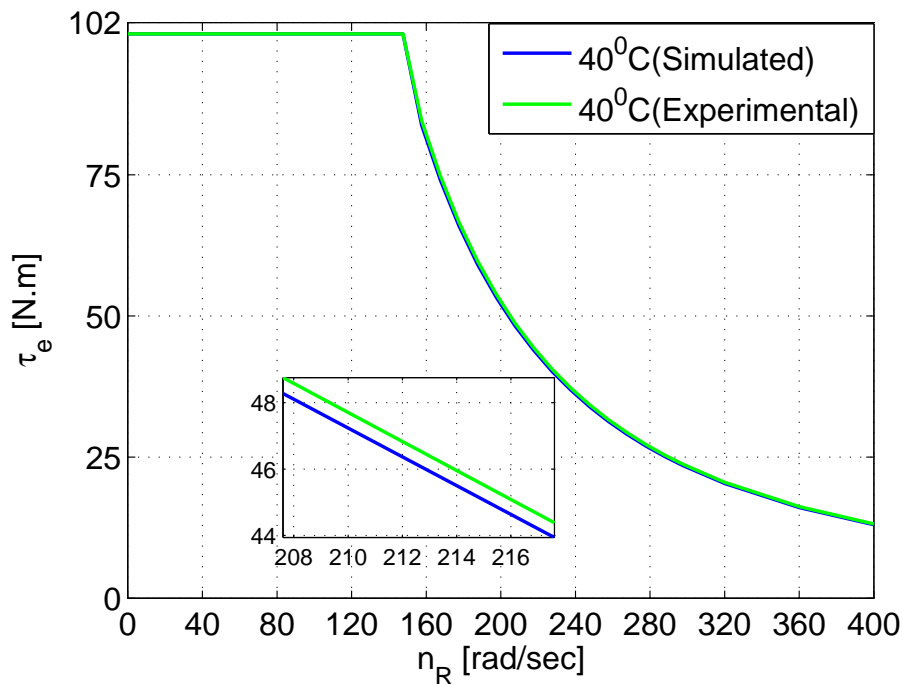


FIGURE 5.14: Experimental result: Induction motor (used in this work) performance curve at  $40^{\circ}\text{C}$  (Torque derating at  $40^{\circ}\text{C}$  is vivid).

### 5.7.3 Comparison with Sliding Mode Controller

In order to validate the effectiveness and robustness of proposed LPV control scheme, another technique is used for comparison and is originally presented in [10] and is named “FOC SMC” in this paper. It addresses the control, flux and torque estimation of IM based on first order Sliding Mode Control (SMC) technique. To compare the LPV control technique, presented in this paper, torque reference

similar to the profile used in [10] is generated. The resistance reference similar to profile used in [10] is used in controller computation. The accuracy of the proposed LPV control technique has quantitatively been assessed and is about 99.1% as compared to 97% accuracy of the FOC-SMC scheme. Experimental results of the actual and estimated quantities are plotted together in Fig. 5.15. The proposed LPV control technique is also tested for more rotor and stator resistance variations ( $\pm 80\%$ ). In a result, an accurate torque estimation and control is demonstrated.

This can be concluded that the proposed LPV control technique is more robust to  $r_S$  and  $r_R$  variations. The currents required to generate the reference torque are also less. Furthermore, chattering behavior of SMC is overcome by LPV, which leads to smaller flux and torque estimation error as well as better control stability. Consequently, the proposed LPV technique can give more accurate estimation and control, even when the rotor and stator resistance are bound to change.

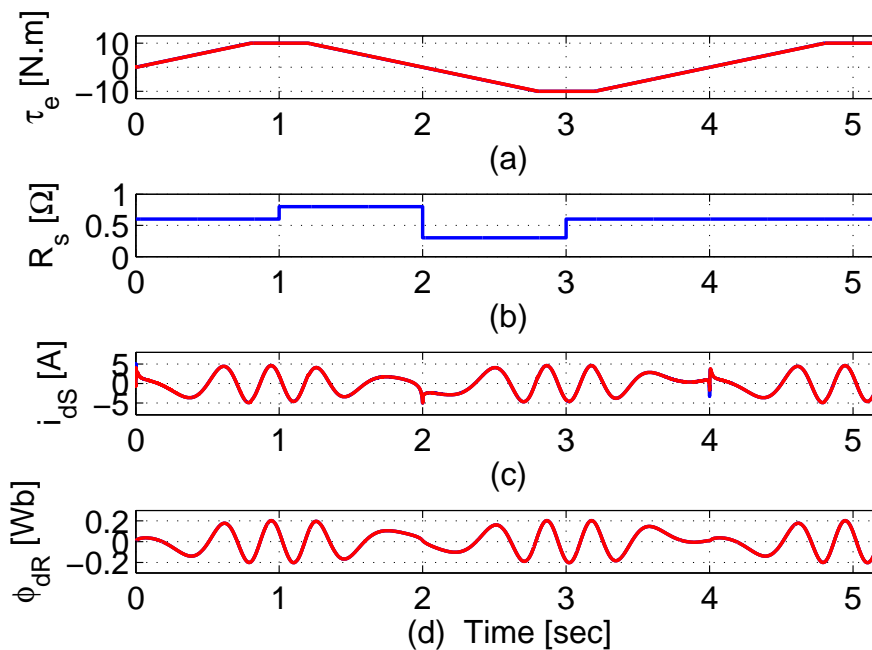


FIGURE 5.15: Actual (blue) and estimated (red) experimental results for a reference (trapezoidal-wave) of  $\pm 10$  Nm. (a) Torque tracking. (b) Stator resistance variation. (c) Stator current. (d) Rotor flux.

### 5.7.4 Torque Derating Compensation against FUDS Cycle

In the third experiment, FUDS driving cycle based speed demand was presented to the LPV Controller under the elevated temperature of  $40^{\circ}\text{C}$ . Figures 5.16, 5.17 and 5.18 show the experimental results for the dynamic performances of the proposed LPV technique for traction induction machine at the raised temperature of  $40^{\circ}\text{C}$ . Figure 5.16 presents the IM speed tracking performance over the entire driving cycle. It is clear from Figure 5.16 that LPV control algorithm provides better performance in the presence of high inertial loads and frequent starts and stops, despite the raised temperature is way above the nominal design temperature. The values for the RMSE and NRMSE are 0.1569 and 0.8431 respectively.

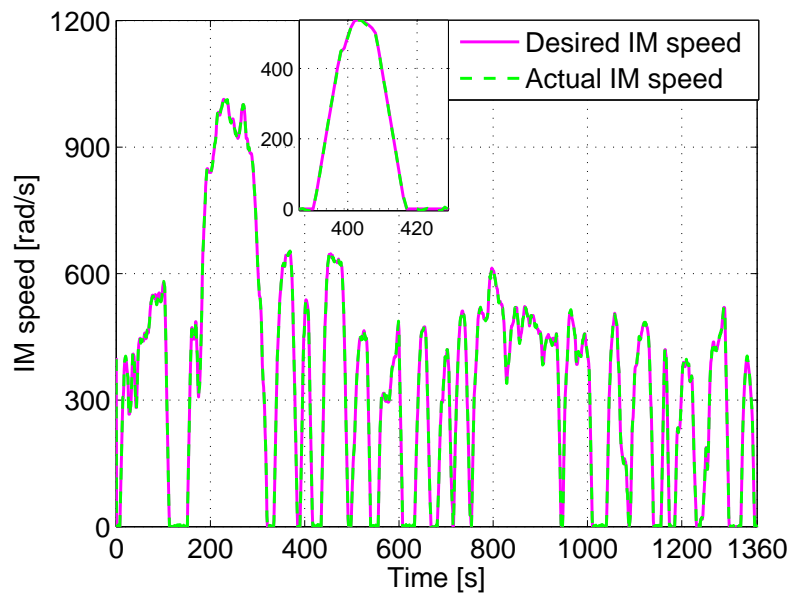


FIGURE 5.16: Experimental result: Tracking of induction machine speed profile via a change profile of temperature (at ambient temperature of  $40^{\circ}\text{C}$ ) with LPV controller observer pair.

The IM torque and flux tracking performance is presented in Figures 5.17 and 5.18.

It is clear that the torque and flux demands are met more precisely in the presence of above mentioned conditions. The RMSE values between the torque and flux tracking of the reference value are 0.2041 and 0.00994 respectively. This also shows

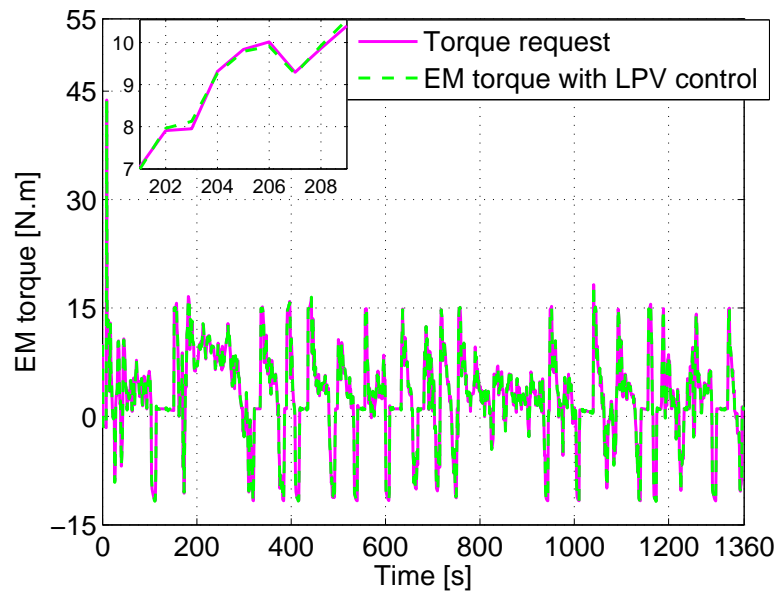


FIGURE 5.17: Experimental results: Tracking of torque request profile via a change profile of temperature (at ambient temperature of  $40^{\circ}C$ ) with LPV controller observer pair.

the accuracy of the estimation of thermally derated torque through LPV observer.

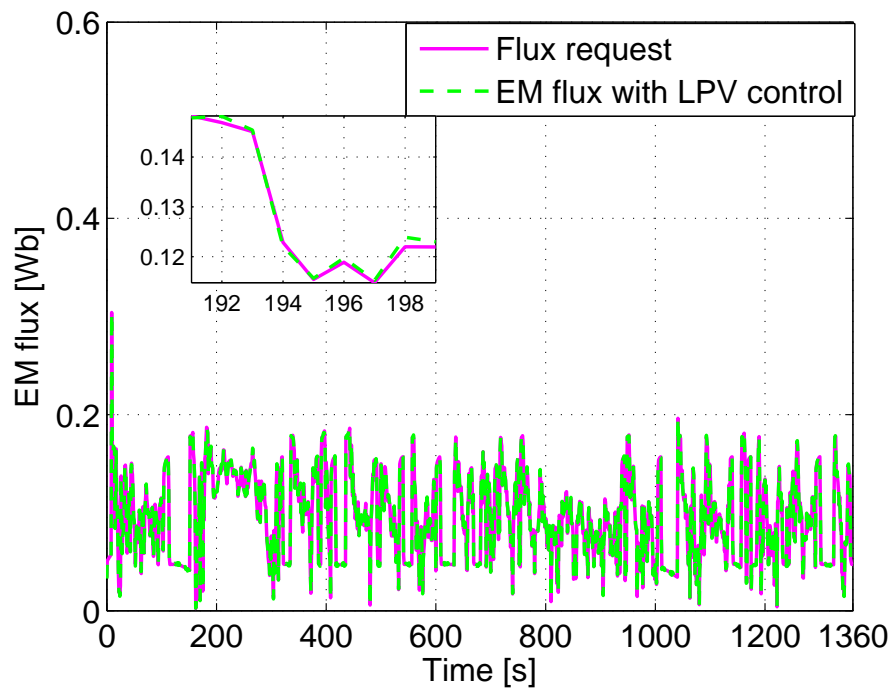


FIGURE 5.18: Experimental results: Tracking of flux request profile via a change profile of temperature (at ambient temperature of  $40^{\circ}C$ ) with LPV controller observer pair.

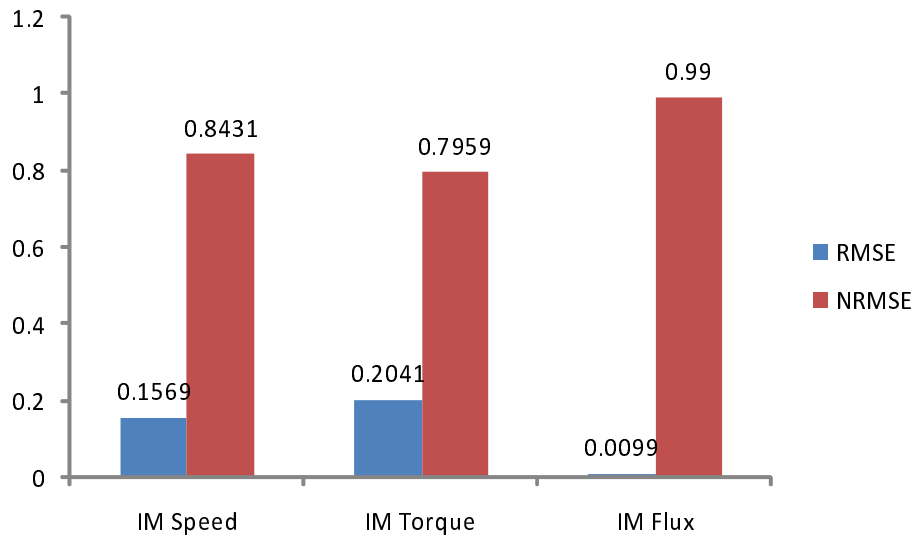


FIGURE 5.19: Experimental results: RMSE and NRMSE values of induction machine: (a) Speed tracking (b) Torque tracking (c) Flux tracking.

The RMSE and NRMSE values of the induction machine speed, torque and flux tracking are shown in Figure 5.19. The experimental results (obtained) prove the effectiveness of the proposed LPV technique.

## 5.8 Conclusion

An LPV observer and controller based robust FOC has been designed and validated for an IM based electrified powertrain in this chapter. The stability of whole LPV scheme is also established. Its efficacy is tested for an electrified powertrain operated in FUDS driving cycle with a dynamic temperature profile. The non-linear simulations confirm the capability of (1) estimating the derated torque and flux and (2) tracking the torque and flux demands for the entire operation of the electrified powertrain. The performance of the proposed controller out performs its SMC counterpart and is experimentally verified on an IM drive controlled by NI myRIO-1900, using the current profile corresponding to FUDS driving cycle. The experimental results confirm that the proposed technique is effective and delivers robust performance. The RMSE and NRMSE values are used as performance

indices to visualize the effectiveness of the LPV control scheme theoretically and practically at different ambient temperatures.

In the coming chapter an LPV based degradation control scheme will be formulated and discussed for EVs and HEVs electric powertrain.

## Chapter 6

# Degradation Control for an Induction Machine based Electrified Powertrain

In this chapter a degradation control technique is proposed to mitigate the electric machine based electrified powertrain degradation while simultaneously providing the desired closed loop performance. The performance of an electrified powertrain in extreme operating conditions is greatly compromised. This is due to the fact that meeting the road loads, ensuring efficient powertrain operation and minimizing the loss of lifetime (aging) of an electric machine are three essential but conflicting targets. In this chapter, a multi-objective Linear Parameters Varying (LPV) based Field-oriented Control (FOC) is proposed to address the problem of conflicting objectives mentioned above. The effectiveness of the proposed control framework is tested for a direct drive electrified powertrain of a three-wheeled vehicle commonly found in urban transportation for Asian countries. The urban driving schedule based simulation results confirm that the lifetime of induction machine can be enhanced by appropriate controller design without compromising its performance.

## 6.1 Introduction

The real world problems offer targets that are often conflicting in nature. In many practical control problems, energy consumption and meeting the desired performance are typical conflicting objectives. For example, a semi-active suspension control offers good separation from road roughness and simultaneously keeps permissible road holding performances, which are two conflicting but essential performance objectives [121].

The automotive industry is rolling out energy-efficient electrified powertrains due to limited energy resources and increasing energy demands,. One of the integral part of electrified powertrain is traction motor, which has considerable impact on the cost and performance of the vehicle. Induction machines (IMs), Permanent Magnet Synchronous Machines (PMSMs) and Switched Reluctance Machines (SRMs) are three possible candidates for traction applications. Among these, IMs are robust, mature, require little maintenance and are inherently de-excited with respect to inverter fault [41] and have been used for electric traction systems, such as Tesla Roadster [88]. In an electrified powertrain, meeting the road torque demands, ensuring the efficient operations and minimizing the aging (loss of lifetime) of traction motor are the desired objectives. However, variation in road loads is met at the cost of motor efficiency and life. Therefore these goals are important to meet but conflicting in nature and make the control problem more challenging. In an electrified powertrain, Induction Machine (IM) is responsible to meet the road loads in all operating conditions. However, due to part load operations and variation in operating temperatures, the rotor and stator resistances change. As a result, torque delivering capability of the motor de-rates [122], [56], [123], [124], unlike an industrial drive which operates at constant loads and temperatures. Under these conditions, IM has to supply the desired torque requested by the driver, thus forcing the IM to operate in in-efficient regions. Similarly, the aging of an IM is accelerated by several stress factors, which include high ambient temperatures, variation in vehicle duty cycle and change in payloads. These stress

factors will create voltage and current imbalance and increase winding temperatures during the IM operation for an electrified powertrain, unlike an industrial drive [125], [126], [127]. This will result in loss of flux generation capability of the windings, thus effecting the torque producing capability of IM. In order to maximize the motor efficiency or to reduce the power loss, the major efforts are seen in better physical design of the motor [128], [110], [129] and improving its performance by means of closed-loop controllers [76]. For a controller design of an on-board motor to be used in an electrified powertrain, the prime concern is efficiency. In fact, main argument behind the use of electric motors in energy efficient vehicles is to take advantage of the high efficiency ratings of an electric motor as compared to that of internal combustion engines. If, in the pursuit of high performance, the controller drives the motor to a low efficiency operating region, the whole design philosophy of electrified powertrain will be jeopardized and thus driving range of the vehicle will be compromised. Therefore, an efficient IM drive, to be used for traction in an electrified powertrain, must address the issues highlighted above.

Conventional Field-Oriented Control (FOC) is commonly used to ensure efficient operation of an IM based electric drive [88]. The performance of conventional FOC is highly dependent on IM rotor and stator parameters. These parameters are adversely affected in extreme operating conditions, part loads and variation in payloads. As a result, efficiency and torque of an electrified powertrain is also affected. This problem has been addressed by [76], [10] and [80] using Sliding-Mode Control (SMC) based FOC. SMC technique is robust but it suffers from chattering problem. Due to the chattering in control, the optimal efficiency is difficult to ensure for traction applications. The LPV control design technique is an efficient tool for the performance improvement of a closed-loop control system in pre-defined operating range. However, it allows the controller to schedule itself based on some measurements in addition to robustness. The key step of the LPV control design technique is the selection of weighting functions. However, in many practical problems, this is not always an easy task to achieve with the help of optimally combined improvement of more than one objective (multi-objective

design). An LPV based control for industrial IM drive has been presented in [86], [85] and [87], where the variation in motor parameters is not significant during the entire operation.

From the above discussion, it is clear that there is a true need of a control scheme to address the conflicting features of an electrified powertrain. In this chapter, an LPV based FOC is proposed for traction IM. The outer loop in FOC generates the desired currents from the torque and flux controllers synthesized using LMIs. The optimal flux is estimated using LPV observer to ensure efficient IM operation [109]. The inner loop of FOC is formulated with the help of a multi-objective LPV controller. The multi objective cost function is proposed based on conflicting goals in an electrified powertrain which are i) meeting the road torque demands, ii) ensuring the IM efficient operations and iii) minimizing the IM aging (loss of lifetime). The optimal weighting functions, which help to maximize the conflicting cost, are selected using LMI based convex optimization approach [130] and are derived from maximum static conditions on the motor voltage inputs and torque. The performance of the proposed control framework is evaluated for a three-wheeled vehicle against Federal Urban Driving Schedule (FUDS), a common controller evaluation approach adapted by automotive community [110], [111]. The results are compared with an LPV based FOC, which does not consider IM aging in the formulation of the cost function. It is observed in the results that the aging of the traction IM is significantly reduced without compromising the overall performance.

This chapter advances as follows. A theoretical background of model based multi-objective control problem is briefly described in Section 6.2 followed by a brief introduction to the proposed control framework in Section 6.3. Section 6.4 presents the vehicle modeling, IM model and its LPV variant. The calculations for the upper limit on the stator voltages are also conducted in Section 6.5. Section 6.6 describes the conflicting cost functions for electrified powertrain. MOC design is conducted and described in Section 6.7 by keeping in view the requirements of three-wheeled vehicle. Section 6.7 also includes the flux and torque estimation. Section 6.8 describes the vehicle specifications, details of simulations, controller

evaluation and result discussion. Summary and concluding comments are presented in Section 6.9.

## 6.2 Brief Theoretical Background of Multi-objective Control Problem

In this section, the abstract form of the multi-objective control problem is presented. Let the plant to be controlled is represented by the state space model

$$\begin{cases} \dot{x}(t) = f(x(t), u(t), t) \\ y(t) = Cx(t) \end{cases} \quad (6.1)$$

where  $x(t) \in R^n$  designates the plant states,  $y(t) \in R^n$  and  $u(t) \in R^m$  are the control outputs and inputs, subject to constraints  $\| u(t) \|_\infty \leq a$ . The purpose of the control is to achieve  $y(t)|_{t \rightarrow \infty} \rightarrow y^*$ .

The LPV state space representation of (6.1) is

$$\begin{cases} \dot{x}(t) = A(\rho(t))x(t) + B(\rho(t))u(t) \\ y(t) = C(\rho(t))x(t) + D(\rho(t))u(t) \end{cases} \quad (6.2)$$

where  $\rho(t) \in R^s$  is the time varying parameter.

Considering two objectives as an example, this work aim to design the multi-objective LPV controller

$$\begin{cases} \dot{\zeta}(t) = A_K(\rho(t))\zeta(t) + B_K(\rho(t))v(t) \\ u(t) = C_K(\rho(t))\zeta(t) + D_K(\rho(t))v(t) \end{cases} \quad (6.3)$$

and to minimize the two conflicting objectives: control error,  $\xi_1$ , and control energy consumption  $\xi_2$ , describes as

$$\begin{cases} \xi_1 = \int_{t_0}^T (y(t) - y^*)^T (y(t) - y^*) dt \\ \xi_2 = \int_{t_0}^T (u(t))^T (u(t)) dt \end{cases} \quad (6.4)$$

Then the multi-objective control problem (6.2)- (6.4) can be converted into the conflicting cost function,  $J$  and can be written as

$$J = \min (\xi_1 (x(t))) + \min (\xi_2 (x(t))) \tag{6.5}$$

s.t.

1. The control in (6.3) exists.
2.  $\| u(t) \|_{\infty} \leq a$
3.  $\xi_1 \leq \xi_1^L$
4.  $\xi_2 \leq \xi_2^L$

In practical control problem, energy consumption and performance error always lie within an acceptable range and are designate by  $\xi_1^L$  and  $\xi_2^L$ . The maximum acceptable values are called the practical objective constraint condition  $L$ . It is notable that  $\xi_1^L$  and  $\xi_2^L$  are only the worst acceptable values and not the control objectives. We will use similar approach to design the inner loop of FOC in the subsequent sections.

### **6.3 Proposed LPV based FOC Framework for Traction Induction Machine**

In this section, the concepts of MOC have been adopted for LPV based FOC to track the desired currents in the inner loop, issued by the torque and flux controllers residing in the outer loop. Fig. 6.1 shows the control framework for the traction IM in an electric vehicle. The traction and braking requests are issued by driver via accelerator ( $\alpha$ ) or brake ( $\beta$ ) pedal in order to follow the driving cycle. The supervisory controller translates the pedal signals into a torque command ( $\tau_{command} = \tau_e$ ), which is then translated to a current reference,  $i_{qref}$ . In an electrified powertrain, it is unusual to operate the electric machine at rated flux due to the change in the road loads. Therefore, the flux command ( $\phi$ ) is

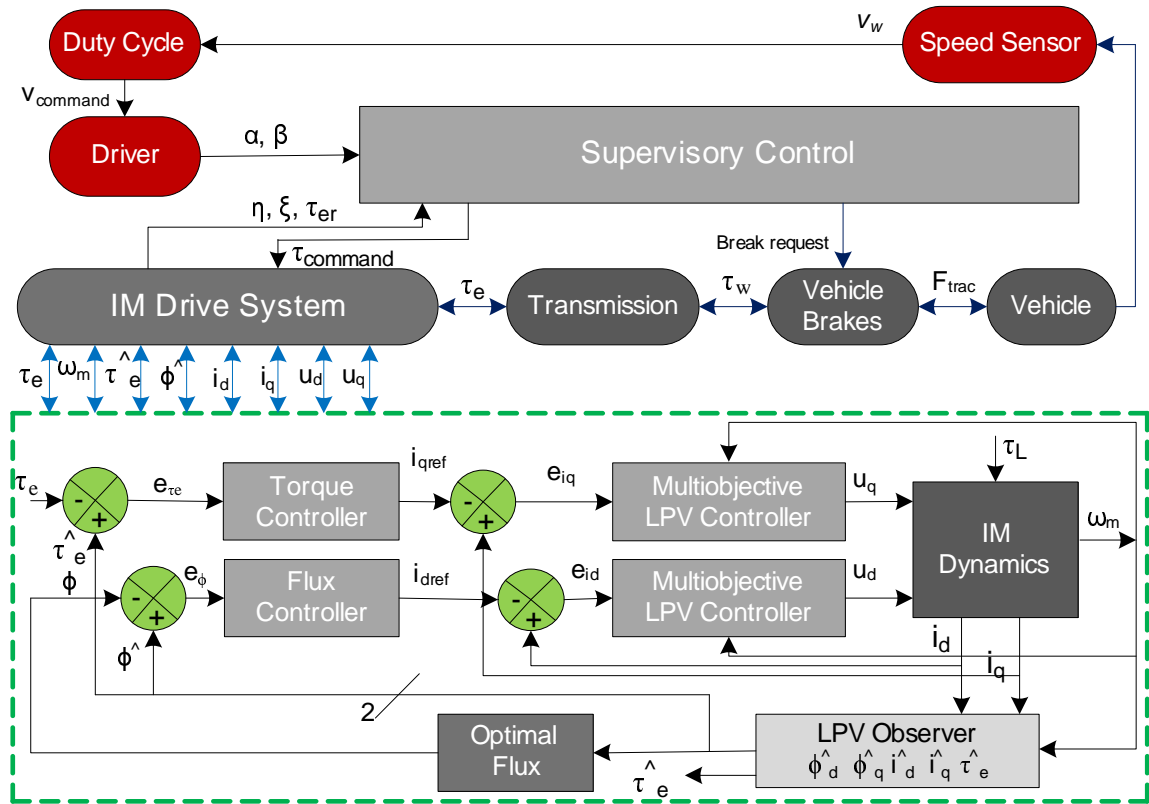


FIGURE 6.1: Proposed LPV based FOC control framework for a traction induction machine.

obtained from the torque command to minimize the energy consumption, which is then translated to a current reference,  $i_{dref}$ . The IM is controlled to deliver the demanded torque, enhance the efficiency and minimize the loss of life using LPV based FOC technique. The IM drive system takes the speed, torque, flux, current and voltage signals which are then used to ensure the torque demand, efficient IM operations and enhance the IM life. A gearbox is employed to amplify the IM torque in order to drive the vehicle. The vehicle and IM dynamics necessary for the synthesis of MOC, are given in the subsequent Sections.

## 6.4 Modeling of Electrified Powertrain

This section describes the vehicle, drivetrain and IM dynamics followed by the LPV variant of IM model.

### 6.4.1 Vehicle Dynamics and Drivetrain Modeling

The proposed MOC strategy takes into consideration the vehicle dynamics, which act as a load torque for IM. The vehicle model is based on mechanics and aerodynamics principles [66].

The load torque ( $\tau_L$ ) of a vehicle is given by

$$\tau_L = \underbrace{(F_a + F_g + F_r + F_w)}_{F_t} R_w \quad (6.6)$$

where,  $F_a$  is the aerodynamic resistance force,  $F_g$  is the grade resistance force,  $F_r$  is the rolling resistance force,  $F_w$  is the acceleration resistance force,  $F_t$  is the total road load, and  $R_w$  is the wheel radius.

The following speed dynamics in the motor referential is used to describe the wheel drive:

$$\frac{dn_M}{dt} = \frac{n_p}{J}(\tau_e - \tau_L - bn_M) \quad (6.7)$$

where,  $n_M$  is the motor mechanical speed,  $\tau_e$  is the motor generated torque,  $n_p$  is the number of pole-pair,  $J$  is the total inertia (rotor and load), and  $b$  is the friction.

Moreover, the vehicle speed ( $v_w$ ) is proportional to the IM speed ( $n_M$ ), which can be expressed in term of wheel radius  $R_w$ , and the gear box ratio ( $G_R$ ) as follows:

$$v_w = \frac{R_w}{G_R} n_M \quad (6.8)$$

and the vehicle torque ( $\tau_w$ ) is given by

$$\tau_w = \tau_e G_R \eta_t \quad (6.9)$$

where,  $\eta_t$  is the transmission efficiency.

### 6.4.2 Mathematical Model of IM

A three-phase IM in synchronously rotating reference frame can be expressed by the mathematical equations, presented in Section 3.2.1.3, as follows, [109]:

$$\begin{cases} \dot{i}_{ds} = -k_1 i_{ds} + n_e i_{qs} + k_2 \phi_{dr} + k_3 n_r \phi_{qr} + k_4 u_{ds} \\ \dot{i}_{qs} = -k_1 i_{qs} - n_e i_{ds} + k_2 \phi_{qr} - k_3 n_r \phi_{dr} + k_4 u_{qs} \\ \dot{\phi}_{dr} = -k_5 \phi_{dr} + n_p (n_e - n_r) \phi_{qr} + k_6 i_{ds} \\ \dot{\phi}_{qr} = -k_5 \phi_{qr} - n_p (n_e - n_r) \phi_{dr} + k_6 i_{qs} \end{cases} \quad (6.10)$$

where

$$\begin{cases} k_1 = \frac{(\chi_M^2 r_r + \chi_r^2 r_s)}{\sigma \chi_s \chi_r^2} \\ k_2 = \frac{M r_r}{\sigma \chi_s \chi_r^2} \\ k_3 = \frac{n_p \chi_M}{\sigma \chi_s \chi_r} \\ k_4 = \frac{1}{\sigma \chi_s} \\ k_5 = \frac{r_r}{\chi_r} \\ k_6 = \frac{\chi_M r_r}{\chi_r} \\ \sigma = 1 - \frac{\chi_M^2}{\chi_s \chi_r} \end{cases} \quad (6.11)$$

$i_{ds}$ ,  $i_{qs}$  and  $u_{ds}$ ,  $u_{qs}$  are the d-axis and q-axis stator currents and voltages respectively,  $\omega$  is the electrical rotor speed,  $n_e$  is the rotating reference frame velocity,  $\phi_{dr}$  and  $\phi_{qr}$  are the d-axis and q-axis rotor fluxes,  $\chi_s$ ,  $\chi_r$  and  $\chi_M$  are the stator, rotor and mutual inductances respectively,  $r_s$  and  $r_r$  are the stator and rotor resistances respectively.

The flux and electromagnetic generated torque are calculated as follows:

$$\begin{cases} n_r = n_p n_M \\ \tau_e = k_9 (\phi_{dr} i_{qs} - \phi_{qr} i_{ds}) \\ \phi = \sqrt{\phi_{dr}^2 + \phi_{qr}^2} \\ i_S = \sqrt{i_{ds}^2 + i_{qs}^2} \\ u_S = \sqrt{u_{ds}^2 + u_{qs}^2} \end{cases} \quad (6.12)$$

where

$$k_9 = \frac{3}{2} n_p \frac{\chi_M}{\chi_r} \quad (6.13)$$

$\phi$  is the rotor flux,  $i_S$  is the stator current and  $u_S$  is the stator voltage vectors.

Since the model is highly nonlinear and it needs to be converted into an LPV one to design a multi-objective LPV controller. Based on Eq. (6.10), an LPV model is obtained by taking  $r_r$ ,  $r_s$  and  $n_r$  as varying parameters and  $n_e = 0$  [13]. The continuous time state-space LPV model can be expressed as follows:

$$\begin{cases} \dot{x} = \underbrace{(A_c + A_\gamma \gamma_1 + A_\gamma \gamma_2 + A_\gamma \gamma_3)}_{A(\rho)} x + B_c u \\ y = C_c x \end{cases} \quad (6.14)$$

where  $A_c$ ,  $B_c$ ,  $C_c$  are the nominal state-space matrices and  $A_\gamma \gamma_1$ ,  $A_\gamma \gamma_2$ ,  $A_\gamma \gamma_3$  are the varying parameter depended matrices. The definition of these matrices are given as

$$A(\rho) = \begin{bmatrix} a_{11}(\rho) & 0 & a_{13}(\rho) & a_{14}(\rho) \\ 0 & a_{22}(\rho) & a_{23}(\rho) & a_{24}(\rho) \\ a_{31}(\rho) & 0 & a_{33}(\rho) & a_{34}(\rho) \\ 0 & a_{42}(\rho) & a_{43}(\rho) & a_{44}(\rho) \end{bmatrix} \quad (6.15)$$

where

$$\begin{cases} a_{11}(\rho) = a_{22}(\rho) = -\frac{\chi_M^2 \rho_1 + \chi_r^2 \rho_2}{\sigma \chi_s \chi_r^2} \\ a_{13}(\rho) = \frac{\chi_M \rho_1}{\sigma \chi_s \chi_r^2} \\ a_{14}(\rho) = \frac{n_p \chi_M \rho_3}{\sigma \chi_s \chi_r^2} \\ a_{23}(\rho) = -\frac{n_p \chi_M \rho_3}{\sigma \chi_s \chi_r^2} \\ a_{31}(\rho) = \frac{\chi_M \rho_1}{\chi_r} \\ a_{24}(\rho) = \frac{\chi_M \rho_1}{\sigma \chi_s \chi_r^2} \\ a_{42}(\rho) = \frac{\chi_M \rho_1}{\chi_r} \\ a_{33}(\rho) = -\frac{\rho_1}{\chi_r} a_{34}(\rho) = -n_p \rho_3 \\ a_{43}(\rho) = n_p \rho_3 \\ a_{44}(\rho) = -\frac{\rho_1}{\chi_r} \end{cases} \quad (6.16)$$

$$B_c = k_4 \begin{bmatrix} I & O \end{bmatrix}^T, C_c = \begin{bmatrix} I & O \end{bmatrix} \quad (6.17)$$

In (6.17),  $I$  is  $2 \times 2$  identity matrix and  $O$  is  $2 \times 2$  zero matrix. The state, time varying signal, input and output vectors of the achieved LPV model are

$$\begin{cases} x(t) = [i_{ds} & i_{qs} & \phi_{dr} & \phi_{qr}]^T \\ y(t) = [i_{ds} & i_{qs}]^T \\ u(t) = [u_{ds} & u_{qs}]^T \\ \rho(t) = [r_r & r_s & n_r]^T \end{cases} \quad (6.18)$$

The time varying parameter  $\gamma$  can be expressed as

$$\gamma = (\gamma_1, \gamma_2, \dots, \gamma_L)^T \quad (6.19)$$

and the range of each parameter  $\gamma_i$  is given as

$$\gamma_i(t) \in [\gamma_{-i} \quad \gamma^{-i}] \quad (6.20)$$

$\mathcal{P}$  is a convex polytopes with vertices,  $\gamma_i, i = 1, 2, \dots, N.$ , and can be defined as

$$\mathcal{P} = Co\{\gamma_{v1}, \gamma_{v2}, \dots, \gamma_{vL}\} \quad (6.21)$$

where  $\gamma_{vi}$  are the vertices,  $i = 1, 2, \dots, L.$   $L = 2^\rho$  are the number of vertices.  $Co$  is a convex hull, i.e, the set of all convex combinations of  $\gamma_{vi}$  (all points inside and on the boundary of the polytopes). The following expression defines the range of  $\gamma_1, \gamma_2$  and  $\gamma_3.$

$$\begin{cases} \gamma_1(r_r) \in [0.2r_r & 1.8r_r] \\ \gamma_2(r_s) \in [0.2r_s & 1.8r_s] \\ \gamma_3(n_r) \in [-180 & 180] \end{cases} \quad (6.22)$$

## 6.5 Calculations for the Upper Limits on Stator Voltages

The selection of weighting functions is the core for the design of proposed MOC. The weighting functions, in this article, are computed by defining the upper limits on stator voltages. In steady-state, the following relationships for d-axis and q-axis stator currents can be defined from (6.10) and (6.12)

$$\begin{cases} i_{ds} = \frac{\phi_{dr}}{\chi_M} \\ i_{qs} = \frac{2}{3} \frac{\tau_e}{p\phi_{dr}} \end{cases} \quad (6.23)$$

The machine steady-state losses on the stator and rotor sides are given by

$$P_{Loss} = \underbrace{\frac{3}{2} r_s (i_{ds}^2 + i_{qs}^2)}_{\text{Stator losses}} + \underbrace{\frac{3}{2} \frac{\chi_M}{\chi_r} (n_e - n_r) \phi_{dr} i_{qs}}_{\text{Rotor losses}} \quad (6.24)$$

The slip-speed characteristics of the machine can be obtained from the (6.10), (6.12) and (6.23)

$$n_r = \frac{\left( 3\phi_{dr}^2 p - \sqrt{9\phi_{dr}^4 p^2 - 16\chi_r^2 \tau_e} \right) r_r}{4\chi_r^2 \tau_e} \quad (6.25)$$

The speed of reference coordinate system  $\omega_e$  can be obtained from (6.10)

$$n_e = \frac{r_r \phi_{dr} + 2\chi_r i_{qs} n_r + \sqrt{r_r^2 \phi_{dr}^2 + 4\chi_r^2 i_{qs}^2 r_r^2}}{2\chi_r^2 i_{qs}} \quad (6.26)$$

The voltage limits can be expressed by assuming that the supplying source has a certain maximum limit where the source is not able to deliver enough voltage to increase the machine's torque. Substitution of (6.23), (6.25) and (6.26) into (6.24)

$$u_{ds} = \frac{r_s \left( \phi_{dr} \sqrt{\phi_{dr}^2 - 4\chi_r^2 i_{qs}^2} + 2\chi_r^2 i_{qs}^2 - \phi_{dr}^2 \right)}{\chi_r \left( -\phi_{dr} \sqrt{\phi_{dr}^2 - 4\chi_r^2 i_{qs}^2} \right)} + \frac{r_s \phi_{dr}}{\chi_s} \quad (6.27)$$

and

$$u_{qs} = \left( n_e + \frac{(3\phi_{dr}^2 n_p \sqrt{\eta_1 - \eta_2}) r_r}{\eta_3} \right) \phi_{dr} + r_s i_{qs} \quad (6.28)$$

where

$$\eta_1 = 9\phi_{dr}^4 n_p^2 \quad (6.29)$$

$$\eta_2 = 36n_p^2 \chi_r^2 \phi_{dr}^2 i_{qr}^2 \quad (6.30)$$

$$\eta_3 = 6n_p \chi_r^2 \phi_{dr} i_{qs} \quad (6.31)$$

## 6.6 The Multi-objective Functions

The efficient operation of a traction IM can be ensured by selecting the objective function that addresses economic or performance features. Consequently, following three conflicting objectives that can affect the operation of IM in an electrified powertrain have chosen.

1. To minimize the traction torque error;
2. To maximize the operating efficiency of electrified powertrain;
3. To minimize the loss of lifetime (aging) of an IM;

However, a right compromise among the different objective functions is required to ensure the good design and this kind of problem is only solvable with multi-objective approach. Therefore, following cost functions formulations have considered in this article:

### 6.6.1 Case-1

In this case, two conflicting objectives, meeting torque demands and ensuring the efficient IM operations are considered in the formulation of conflicting cost function to achieve the optimal performance of electrified powertrain, without taking any bound on the aging (loss of lifetime) of IM objective. The formulation is

$$J_1 = \max(\eta(i_{ds}, i_{qs})) + \max\left(\frac{1}{\tau_{er}(i_{ds}, i_{qs})}\right) \quad (6.32)$$

### 6.6.2 Case-2

In this case, optimal performance of an electrified powertrain is obtained by considering the all three above mentioned conflicting objectives in the formulation of conflicting cost function. The formulation is

$$J_2 = \max(\eta(i_{ds}, i_{qs})) + \max\left(\frac{1}{\xi(i_{ds}, i_{qs})}\right) + \max\left(\frac{1}{\tau_{er}(i_{ds}, i_{qs})}\right) \quad (6.33)$$

where,  $\eta$  is the efficiency of electrified powertrain,  $\xi$  is the loss of lifetime of IM and  $\tau_{er}$  is the torque error.

**Remark:** Case 1 is discussed for the sake of comparison with proposed Case-2 in Section 6.8 to highlight the benefits of proposed framework.

### 6.6.3 Constraints

The constraints are imposed on the conflicting multi-objective control problem to ensure the performance requirements of an IM based electrified powertrain. These constraints are defined as the cost function requirements:

$$i_{ds}^L \leq i_{ds} \leq i_{ds}^M \quad (6.34)$$

$$i_{qs}^L \leq i_{qs} \leq i_{qs}^M \quad (6.35)$$

$$u_{ds}^L \leq u_{ds} \leq u_{ds}^M \quad (6.36)$$

$$u_{ds}^L \leq u_{ds} \leq u_{ds}^M \quad (6.37)$$

where, the superscripts  $L$  and  $M$  stand for the minimum and maximum values respectively.

### 6.6.4 Efficiency of Electrified Powertrain

The efficiency of electrified powertrain can be given as

$$\eta = \frac{\tau_w v_w}{\frac{3}{2}(u_{ds}i_{ds} + u_{qs}i_{qs})} \quad (6.38)$$

### 6.6.5 Road Load Error

The torque error can be written as

$$\tau_{er} = \tau_e - \tau_{eref} \quad (6.39)$$

The Root Mean Square Error (RMSE) value of the torque error  $\tau_{er}$  is computed that is mostly used to evaluate practical implementations.

$$\tau_{erRMSE} = \sqrt{\frac{1}{t_2 - t_1} \int_{t_1}^{t_2} [\tau_{er}(t)]^2 dt} \quad (6.40)$$

where,  $(t_1, t_2)$  is the vehicle operating interval.

### 6.6.6 Aging

The affect on IM winding due to thermal aging is an essential lifetime parameter. Its aging rate, a derived formulation of Arrhenius [127], [57], can be calculated as

$$\xi(T_x) = \xi_0 \times 2^{(T_c - T_x)/HIC} \quad (6.41)$$

where,  $\xi_0$  is the reference lifetime in h and generally set to 20,000h [57],  $\xi$  is the lifetime in h at  $T_x$ ,  $T_c$  is the reference temperature in  $^{\circ}C$  (temperature in the hottest point of the insulation system in the nominal work conditions),  $T_x$  is the reference temperature in  $^{\circ}C$  (temperature in the hottest point of the insulation system in the real work conditions) and  $HIC$  is the halving interval index  $^{\circ}C$  (14, 11, 9.3, 8 and 10 for insulation class A, B, F, H and H' respectively) [127].

For the dynamic operation as in the case of electric vehicle, the percentage aging factor is defined as

$$p(t_1, t_2) = \frac{1}{\xi_0} \int_{t_1}^{t_2} 2^{(T_x - T_c)/HIC} dt \quad (6.42)$$

Then, the lifetime loss of the excess temperature time interval  $(t_1, t_2)$  can be calculated by

$$\iota_{1,2} = p(t_1, t_2) \cdot \xi(T_x) \quad (6.43)$$

### 6.6.7 Temperature Measurement

The temperature  $T_x$  can be estimated from the measurement of rotor and stator resistance and is given as

$$R = R_0 [1 + \alpha (T_x - T_c)] \quad (6.44)$$

where,  $R_0$  is the rotor and stator resistance at nominal work conditions ( $T_0 = 25^\circ C$ ) and  $\alpha$  is the temperature coefficient of resistance.

The rotor resistance can be estimated as

$$r_r = \sqrt{n_{sl}^2 \chi_r \left[ \frac{n_e \chi_M^2}{\frac{Q}{I_s^2} + n_e \chi_s} - \chi_r \right]} \quad (6.45)$$

where,  $n_{sl}$  is the slip frequency, and  $Q$  is the reactive power.

The estimation of stator resistance is given by [113]:

$$\begin{cases} r_s = k r_r \\ k = \frac{r_{s0}}{r_{r0}} \end{cases} \quad (6.46)$$

where,  $r_{r0}$ ,  $r_{s0}$  are the nominal values of rotor and stator resistance, respectively.

## 6.7 LPV based FOC Control Design

In this section, we will expand on the control framework shown in Fig. 6.1.

### 6.7.1 Torque and Flux Estimation

The core requirement for the efficient operation of an IM based electric drive in an electrified powertrain is an accurate estimation of de-rated torque and flux. Therefore, a robust LPV observer [109] is designed to overcome the effects of uncertainties in rotor resistance, stator resistance, and rotor speed. It is further assumed that currents and speed measurements are available for use. The mathematics of the robust LPV estimator is devised as

$$\left\{ \begin{array}{l} \begin{bmatrix} \dot{\hat{i}}_S \\ \dot{\hat{\phi}} \end{bmatrix} = A(\rho) \begin{bmatrix} \hat{i}_S \\ \hat{\phi} \end{bmatrix} + B_c u_S + L(\rho)(i_S - \hat{i}_S) \\ i_S = C_c \begin{bmatrix} i_S \\ \phi \end{bmatrix}, \hat{i}_S = C_c \begin{bmatrix} \hat{i}_S \\ \hat{\phi} \end{bmatrix} \end{array} \right. \quad (6.47)$$

Eq. (6.47) can be rewritten as:

$$\begin{bmatrix} \dot{\hat{i}}_S \\ \dot{\hat{\phi}} \end{bmatrix} = A(\rho) \begin{bmatrix} \hat{i}_S \\ \hat{\phi} \end{bmatrix} + B_c u_S + L(\rho) C_c \left( \begin{bmatrix} i_S \\ \phi \end{bmatrix} - \begin{bmatrix} \hat{i}_S \\ \hat{\phi} \end{bmatrix} \right) \quad (6.48)$$

For carrying out the calculation for the estimator gain, the estimation error is defined as:

$$e = \begin{bmatrix} i_S \\ \phi \end{bmatrix} - \begin{bmatrix} \hat{i}_S \\ \hat{\phi} \end{bmatrix} \quad (6.49)$$

The equation (state-space) of the estimation error,  $e$ , (subtracting the Eq. (6.48) from Eq. (6.14)) is then specified as:

$$\dot{e} = (A(\rho) - L(\rho)C_c)e \quad (6.50)$$

The stability of the estimator error achieved in Eq. (6.50) and formula for computation of estimator gains is outlined in [109]. The gain of the robust polytopic estimator is obtained by solving LMIs formulated as follows:

$$\begin{cases} A_i^T P - C_i^T Q_i^T + P A_i - Q_i C_i \prec 0, i = 1, \dots, 2^p \\ P = P^T \succ 0 \end{cases} \quad (6.51)$$

The computation of estimated torque is done as

$$\hat{\tau}_e = k_g(\hat{\phi}_{dr} i_{qs} - \hat{\phi}_{qr} i_{ds}) \quad (6.52)$$

### 6.7.2 Multi-objective LPV Controller Synthesis

A multi-objective LPV current feedback controller is synthesized for an LPV model of IM presented in Section 6.4.2. LPV control design is a comprehensive form of  $H_\infty$  optimal control to time-varying or nonlinear systems that can be formulated in LPV form [115]. The design specifications are defined by actuator constraints, disturbance rejection, and reference tracking. These are the control sensitivity function (to ensure efficient operations), complementary sensitivity function and sensitivity function (to meet the torque demands) to shape the design specifications.  $H_\infty$  norm can be selected to guarantee these requirements.  $L_2$ -gain of the closed-loop system is an alternate to  $H_\infty$  norm in the LPV structure. The idea of ‘augmented plant’ is commonly used in LPV control to formulate the design specifications. The closed-loop continuous time system architecture is shown in Fig. 6.2, where  $P(\rho)$  is the state-space model given in (6.14);  $K(\rho)$  is the multi-objective LPV output feedback controller. There are two inputs for the system (plant): one is the feedback control  $u$  (from the multi-objective LPV controller), other is the reference  $r$ . The reference input  $r$  is a vector of  $i_d$  and  $i_q$  currents and formulated as

$$\begin{bmatrix} i_{dsref} \\ i_{qsref} \end{bmatrix} = \frac{1}{|M|\phi^2} [M]^{-1} [N] \quad (6.53)$$

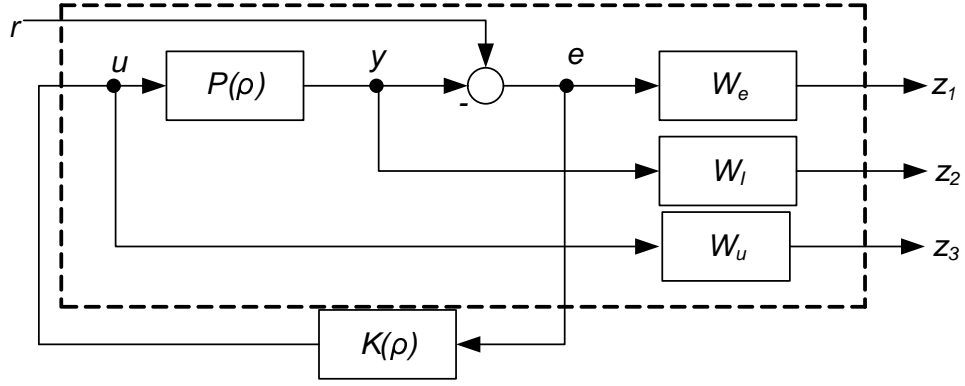


FIGURE 6.2: Closed loop system block diagram

where

$$M = \begin{bmatrix} k_6 \phi_{dr} & k_6 \phi_{qr} \\ -k_5 k_8 \phi_{qr} & k_5 k_8 \phi_{dr} \end{bmatrix}, N = \begin{bmatrix} \phi_r (v_2 + k_5 \phi_r) \\ v_1 + k_7 n_r + \frac{1}{J} \tau_L \end{bmatrix}$$

For multi-objective LPV control design, the weighting function  $W_u$  is selected to meet the actuator constraints without significant degradation of performance. In the drive system of an electrified powertrain, the supplying source (battery) has a certain maximum limit beyond which the source has no ability to supply sufficient voltage to increase electric machine's torque and this limit can be expressed as (from (6.28))

$$-\left( n_e + \frac{(3\phi_{dr}^2 n_p \sqrt{\eta_1 - \eta_2}) r_r}{\eta_3} \right) \phi_{dr} - r_s i_{qs} + u_{qs} = 0 \quad (6.54)$$

where  $\eta_1 = 9\phi_{dr}^4 n_p^2$ ,  $\eta_2 = 36n_p^2 \chi_r^2 \phi_{dr}^2 i_{qs}^2$ ,  $\eta_3 = 6n_p \chi_r^2 \phi_{dr} i_{qs}$

Keeping in view the maximum voltage limit ((6.54)),  $W_u$  is selected as a high-pass filter and formulated as

$$W_u = \frac{c s + \omega_u}{a s + c\omega_u} \quad (6.55)$$

where,  $\omega_u = 10^3$  rad/s, coefficient  $c$  is a large number to place the pole of  $W_u$  at very high frequency, it is  $10^3$  and coefficient  $a$  is selected as a design constant and is tuned during the design process to meet the condition ((6.54)).

To meet the performance objective (robustness and tracking),  $W_e$  and  $W_I$  are selected and filtering frequency is optimized to maintain high bandwidth of the

control system for satisfactory performance. The weighting function  $W_e$  is formulated as a high gain low-pass filter.

$$W_e = \frac{s + \omega_e A}{as + \omega_e} \quad (6.56)$$

where,  $\omega_e = 570$  rad/sec,  $A = 0.002$  and coefficient  $a$  is selected as a design constant.

The weighting function  $W_I$  is also selected as design constant and  $a(W_e)$  and  $W_I$  both are optimized during control design by considering the following maximum torque limit.

$$\tau_{emax} = \frac{3n_p \phi_{dr}^2}{4\chi_r} \quad (6.57)$$

The continuous time polytopic time-varying system is formulated by

$$\begin{bmatrix} \dot{x} \\ z \\ y \end{bmatrix} = \begin{bmatrix} A(\rho) & B_1(\rho) & B_2(\rho) \\ C_1(\rho) & D_{11}(\rho) & D_{12}(\rho) \\ C_2(\rho) & D_{21}(\rho) & 0 \end{bmatrix} \begin{bmatrix} x \\ w \\ u \end{bmatrix} \quad (6.58)$$

where  $w$  and  $z$  are the external input and controlled output vectors, respectively.

The objective is to design the gain schedule LPV output feedback control which will maximize the cost function described in (6.32) in case-1 and (6.33) in case-2.

The state-space representation of the dynamic controller is:

$$\begin{bmatrix} \dot{x}_K \\ u \end{bmatrix} = \begin{bmatrix} A_K(\rho) & B_K(\rho) \\ C_K(\rho) & D_K(\rho) \end{bmatrix} \begin{bmatrix} x_K \\ y \end{bmatrix} \quad (6.59)$$

which guarantees  $L_2$ -gain bound  $\gamma$  for the closed loop system ( (6.58) and (6.59)) and ensures the internal stability.

The LMI convex optimization approach is adopted to compute the multi-objective gain scheduling LPV controller and presented in theorem 1.

**Theorem:** Consider the LPV system ((6.58)) with parameter trajectories constrained as in (6.20). There exists a gain scheduling multi-objective LPV output

feedback controller ((6.59)) imposing closed-loop stability and an upper bound  $\gamma > 0$  on the  $L_2$ -gain of the closed-loop system ((6.58) and (6.59)) from  $w$  to  $z$ , if there exist parameter dependent symmetric matrices  $V(\rho)$  and  $W(\rho)$  and a parameter dependent quadruple of state-space data  $(\tilde{A}_K(\rho), \tilde{B}_K(\rho), \tilde{C}_K(\rho), \tilde{D}_K(\rho))$  such that([116])

$$\begin{bmatrix} AW + B_2\tilde{C}_K + * & * & * & * \\ \tilde{A}_K^T + A & A^T V + \tilde{B}_K C_2 + * & * & * \\ B_1 & V B_1 + \tilde{B}_K D_2 & -\gamma I & * \\ C_1 W + (D_{12}\tilde{C}_K)^T & C_1 & D_{11} & -\gamma I \end{bmatrix} < 0 \quad (6.60)$$

$$\begin{bmatrix} V & I \\ I & W \end{bmatrix} > 0 \quad (6.61)$$

where  $*$  signifies the terms needed to obtain symmetry in matrix and  $\rho$  is omitted for simplicity.

The multi-objective gain scheduling LPV output feedback controller

$$K(\rho) = \sum_{i=1}^{i=L} c_i \begin{bmatrix} A_K(i) & B_K(i) \\ C_K(i) & D_K(i) \end{bmatrix} \quad (6.62)$$

is obtained by solving following optimization problem

$$\min_{V(\rho), W(\rho), \tilde{A}_K(\rho), \tilde{B}_K(\rho), \tilde{C}_K(\rho)} \gamma \quad (6.63)$$

where

$$\begin{cases} D_K = 0 \\ C_K = (\tilde{C}_K - D_K C_2 W)(S^T)^{-1} \\ B_K = (R)^{-1}(\tilde{B}_K - V B_2 D_K) \\ A_K = (R)^{-1}(\tilde{A}_K - R B_K C_2 W - V B_2 C_K S^T \\ -V(A + B_2 D_K C_2)W)(S^T)^{-1} \end{cases} \quad (6.64)$$

In (6.64), the definition of  $R$  and  $S$  is

$$RS^T = I_n - VW \quad (6.65)$$

which can be solved by a singular value decomposition.

### 6.7.3 Robust Flux and Torque Controller

The concept of input-output linearization [102] is used to obtain the nonlinear torque and flux controller. For the control of IM, the relative degree and zero dynamics are well defined and are stable respectively [77]. Thus input-output linearization can be used and evaluated.

The complete derivation and construction of flux and torque controllers are given in Chapter 5 (Section 5.4.4).

### 6.7.4 Calculation for Reference Flux

The IM for an electrified powertrain operates at different torques and speeds over the entire driving cycle. Hence, it is unusual to operate the IM under the rated flux. In this fashion, it is not possible to minimize the energy utilization. In order to consume less energy, reference flux is computed using the stator direct-axis current reference in [76]. However, in this work, torque is the reference instead of stator current. Therefore, in this work a new optimal flux reference is computed by taking into account the steady-state copper and iron losses of the machine on the rotor and stator sides and formulated as [76]:

$$P_{loss} = \underbrace{k_{10} (i_{ds}^2 + i_{qs}^2)}_{\text{Stator loss}} + \underbrace{k_{11} i_{qs}^2}_{\text{Rotor loss}} + \underbrace{k_{12} (\chi_M^2 i_{ds}^2 + k_{13} i_{qs}^2)}_{\text{stator iron loss}} \quad (6.66)$$

where,

$$\begin{cases} k_{10} = \frac{3}{2} r_s \\ k_{11} = \frac{3}{2} r_r \left( \frac{\chi_M}{\chi_r} \right)^2 \\ k_{12} = \frac{1}{r_c} n_e^2 \\ k_{13} = \left( \frac{\chi_M^2 - \chi_M \chi_r}{\chi_r} \right)^2 \end{cases} \quad (6.67)$$

Applying the steady-state value of  $i_{ds}$  and  $i_{qs}$  obtained from (6.10) in (6.66) and minimizing the losses by differentiating the total losses with respect to rotor flux.

$$\begin{cases} \phi_{rref} = K_{opt} \sqrt{|\tau_{e_{ref}}|} \\ K_{opt} = k_{14} \left( \frac{(r_s + n_e^2 \chi_M^2)}{\left( r_s + \left( \frac{r_r \chi_M^2}{\chi_r^2} \right) + \left( \frac{(n_e^2 (\chi_M^2 - \chi_s \chi_r^2)^2)}{r_c \chi_r^2} \right) \right)} \right)^{1/2} \end{cases} \quad (6.68)$$

where

$$k_{14} = \frac{2}{3} \frac{\chi_M}{n_p} \quad (6.69)$$

## 6.8 Performance Evaluation

This section will elaborate the vehicle specifications, details of simulation scenarios and simulation results.

### 6.8.1 Vehicle specifications and simulation detail

The numerical simulations are a flexible and critical tool to comprehensively evaluate the electrified powertrain under different driving cycles and loads. The designed multi-objective LPV controller is also validated in simulations using the nonlinear electrified powertrain model constructed in MATLAB/SIMULINK for an actual electric vehicle shown in Figure 6.1, as commonly exercised by automotive community to evaluate their control frameworks [131], [120] and [119].

The simulations are based on an IM drive system used for traction in a three-wheeled vehicle commonly found in urban transportation of Asian countries. The simulator can evaluate an IM with LPV based FOC technique. FOC current commands for IM control are generated by using the (6.53). A 4.75KW induction machine with class F insulation is used. The parameters of the IM and test vehicle used in simulations are given in Tables 6.1 and 6.2.

TABLE 6.1: Specifications of the three-wheeled vehicle induction machine

Parameter	Value	Parameter	Value
$n_p$	2	$r_s$	0.22 $\Omega$
$r_r$	0.209 $\Omega$	$\chi_s$	0.0425 H
$\chi_r$	0.043 H	$\chi_M$	0.04 H
$J$	0.124 Kg.m <sup>2</sup>	$b$	0.06 N.m.s.rad <sup>-1</sup>

TABLE 6.2: Specifications of a three-wheeled vehicle used in urban transportation for Asian countries

Parameter	Value	Parameter	Value
$M$	350 Kg	$R_w$	0.205 m
$A_f$	2.1 m <sup>2</sup>	$C_r$	0.013
$C_d$	0.42	$G_R$	8.32

Two cases are studied for the IM based electrified powertrain in this work: (1) under the cost function ((6.32)) which maximizes the efficiency and meets torque demands of an electrified powertrain, (2) under the cost function ((6.33)) which maximizes the efficiency, meets the torque demands and minimizes the loss of lifetime of IM for an electrified powertrain. The optimal flux operation for minimum losses on the rotor copper losses, stator copper and iron losses are implemented in simulator for the both cases. For the IM under LPV-FOC technique, the optimal flux calculations are given in Section 6.7.4.

The effectiveness of the multi-objective controller for an electrified powertrain is evaluated in two ways. Firstly, simulations are done for one complete driving cycle to measure the efficiency, torque error of an electrified powertrain and the loss of lifetime for an IM. In the second phase of evaluation, the slow aging process is taken care of by conducting simulations for relatively long time. These simulations are performed by considering the driving cycle profile of 75 minutes. It consists on a complete driving cycle of 22.6 minutes, then there is a rest time of 5 minutes and same driving cycle is repeated twice (45.2 minutes).

## 6.8.2 Simulation Results

A predefined urban driving cycle FUDS, which has number of starts and stops, is used for assessing the performance of proposed multi-objective LPV control strategy. In order to achieve the conflicting goals, a multi-objective LPV controller is obtained by selecting the optimal values of the weighting matrices  $W_u$  (parameter  $a$ ),  $W_e$  (parameter  $a$ ) and  $W_I$  for the both cases. Table 6.3 gives the optimal weighting matrices.

TABLE 6.3: Optimal Value of Weighting Matrices coefficients

Case-1			Case-2		
$a(W_u)$	$a(W_e)$	$W_I$	$a(W_u)$	$a(W_e)$	$W_I$
0.22	2	0.9	0.19	2	0.75

The change in the IM drive system parameters (rotor and stator resistances) and the winding temperature for a one complete cycle for the three-wheeled vehicle are shown in Figure 6.3.

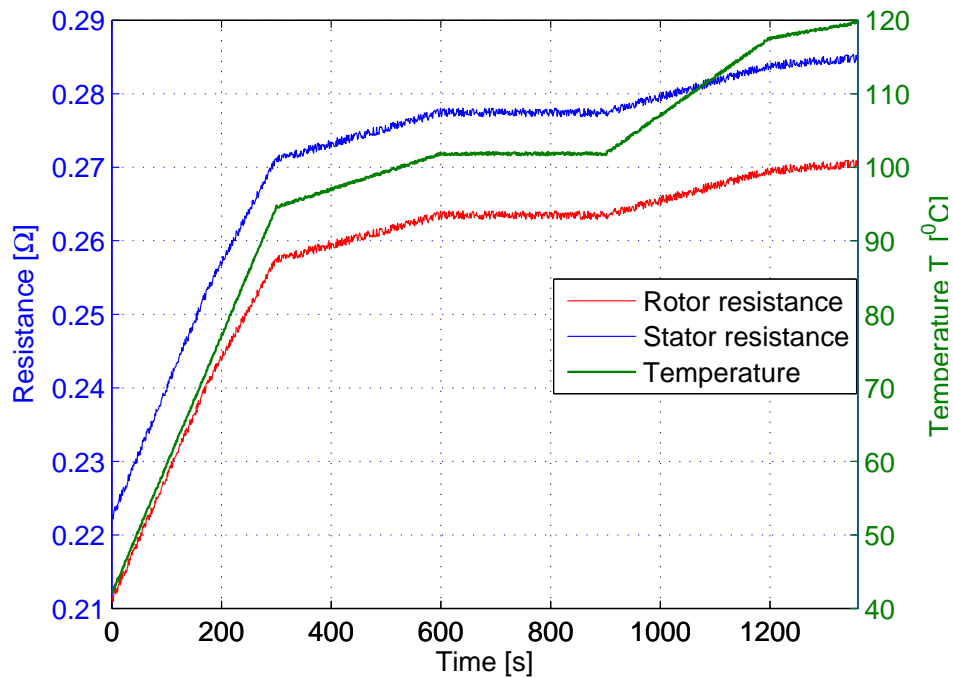


FIGURE 6.3: IM winding temperature and resistance over the entire period of operation.

It is clear that the drive system parameters and winding temperature are greatly influenced by the road load conditions and ambient temperature. To overcome the effects of these changes on the performance of an electrified powertrain, a multi-objective controller is computed using LMI convex optimization approach for two different cases (Section 6.6). The performance evaluation plots are shown through Figure 6.4 through Figure 6.12.

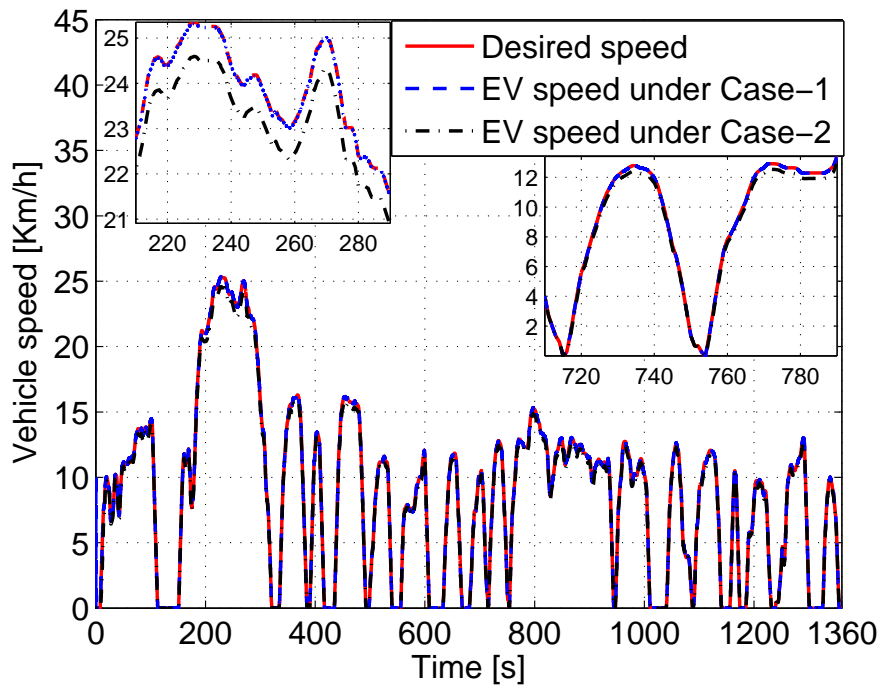


FIGURE 6.4: Vehicle speed profile for the validation of multi-objective LPV controller with and without aging compensation during the operation of electrified powertrain.

As seen in Figure 6.4 that the supervisory controller enables the vehicle to meet the speed demands. The vehicle speed tracking performance is better for the case of without aging compensation at the expense of more energy consumption as shown in Figure 6.4 and the Root Mean Square Error (RMSE) for Case-1 is 0.1451 and for Case-2 is 0.1522. The IM speed in this driving cycle is shown in Figure 6.5.

The torque of an IM based electrified powertrain is greatly effected by the operating temperature and parameter variations, as highlighted in [109] by the term “thermally de-rated torque”. The wheel torque is shown in Figure 6.6.

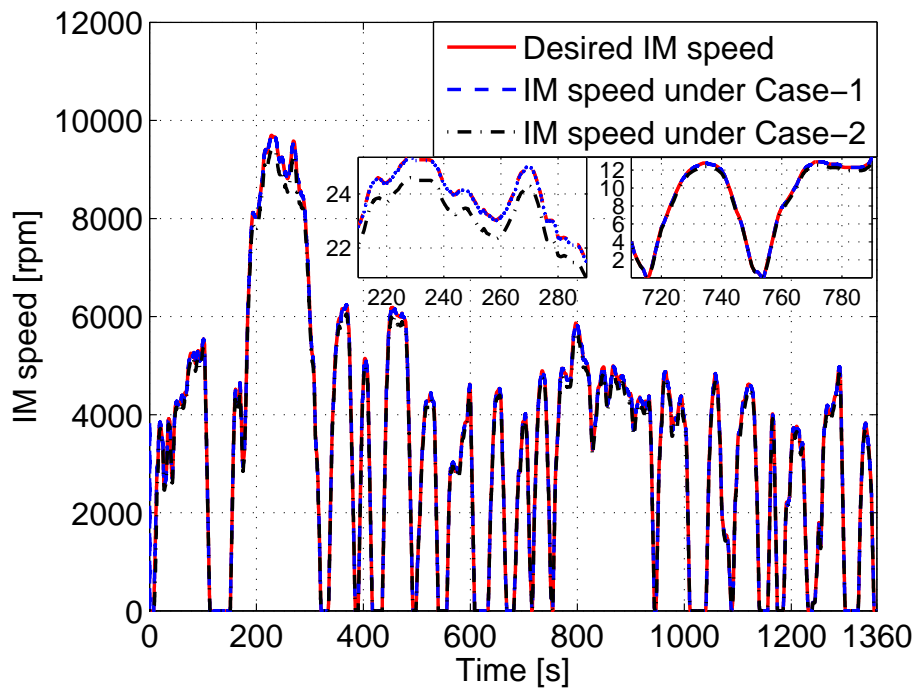


FIGURE 6.5: IM speed under the validation driving schedule with and without aging compensation.

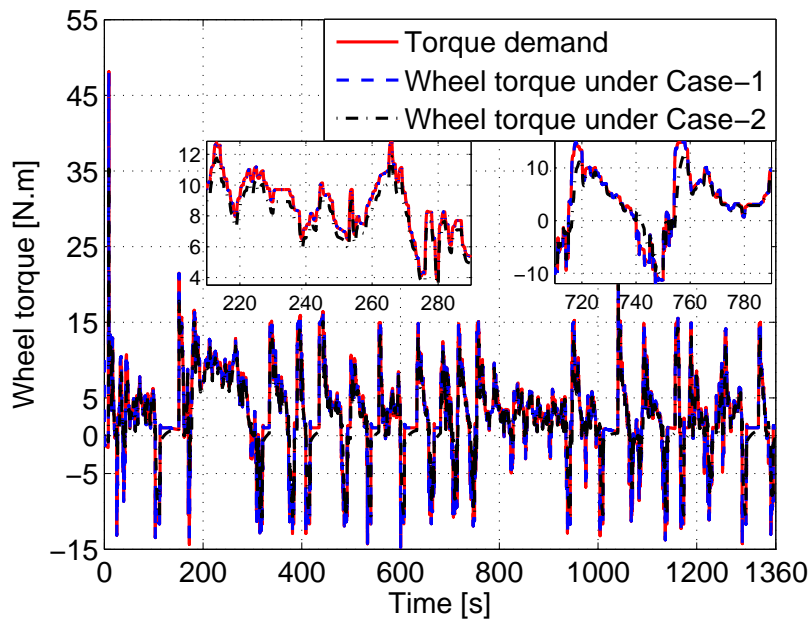


FIGURE 6.6: Vehicle torques with multi-objective LPV controller: without and with aging compensation.

It is clear that the torque demands are met more precisely when the aging objective is not formulated in the cost function. Again, it is possible only at the expense of more current and voltage (more battery utilization and IM aging). The RMSE

values between the torque tracking of the reference value are 0.195 and 0.231 for the case-1 and case-2 respectively. The multi-objective LPV controller also overcomes the de-rating in the torque as vivid in Figure 6.6.

Dynamic efficiency (the instantaneous efficiency value at each sampling instant in a driving cycle) approach is adopted instead of steady-state point efficiency. The power efficiency characteristics of the IM based drive system under the both cases with multi-objective LPV controller is presented in Figure 6.7. The average power efficiency under the both cases, with aging compensation and without aging compensation are 76.4% and 75.3% respectively.

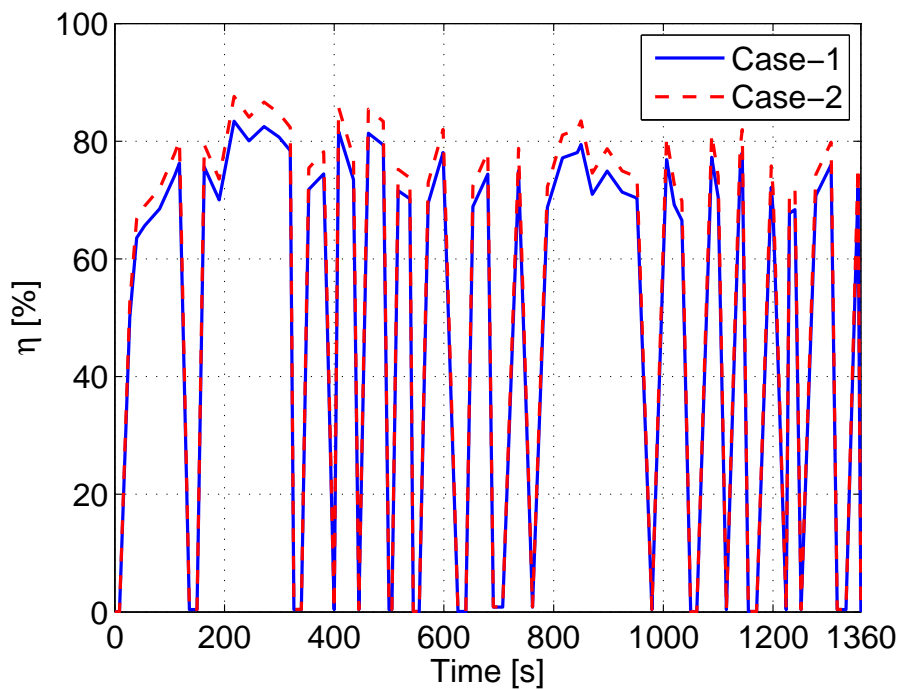


FIGURE 6.7: Power efficiency for an electrified powertrain after the compensation of change in operating conditions with multi-objective LPV controller.

In the second case, (6.33) is considered in the computation of the controller and simulated to measure the efficacy of the proposed controller. The vehicle speed demand and IM torque tracking are within acceptable range when the aging was considered in the cost function and it is clear from Figures 6.4 and 6.6. As a result, the efficiency and life of the electrified powertrain is enhanced as shown in the Figures 6.7 and 6.12. The IM voltages and currents for the both cases are

shown in the Figures 6.8 and 6.9. It can be observed that the current and voltage demands are higher in Case 1 as compared to Case 2.

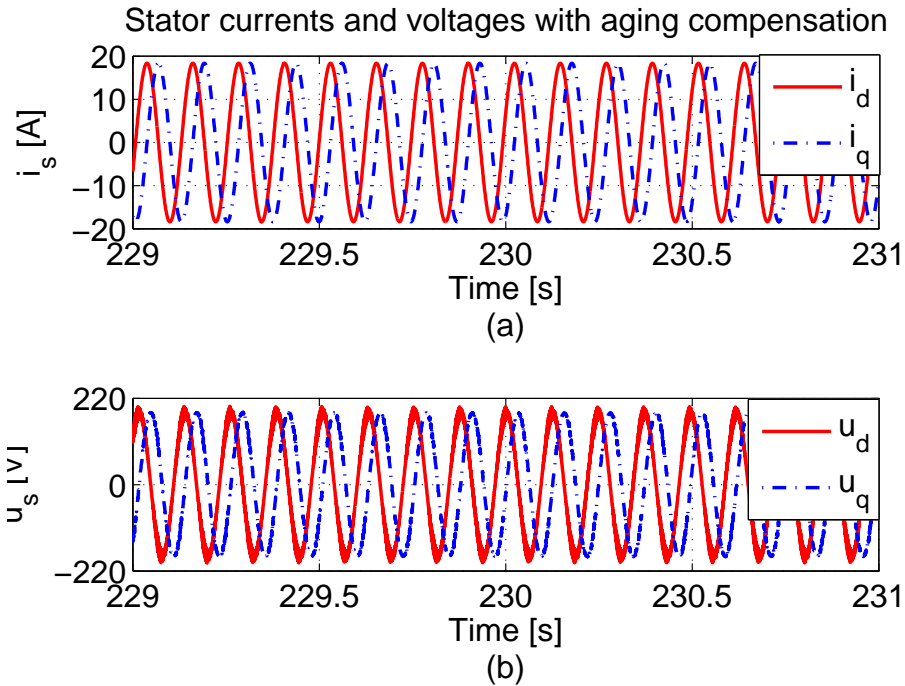


FIGURE 6.8: Induction machine direct and quadrature axis (a) stator currents. (b) stator voltages with aging.

However, IM supply voltages, duty cycles, ambient temperature and parameters change during the operation. Due to these changes, the IM temperature varies. Therefore, IM life is effected, depending on the magnitude of the temperature. IM life scenarios are explained next, to illustrate how IM life is affected when the temperature changes with the time. Figures. 6.10 and 6.11 depicts the result of the simulations that are performed for the evaluation of loss of lifetime of IM. It is evident from the results that the entire driving period is of 75min and subsequent cooling phase is of 3.2h. Due to the motor losses, the winding temperature rose up to the point when the last driving cycles ends. Then, when the vehicle is stationary, the IM emanates its heat to ambience and winding temperature decreases exponentially according to the adopted thermal laws.

The IM in an electrified powertrain is operated for the entire period of driving cycle of span 75 minutes and ambient temperature for this operation was  $40^{\circ}C$

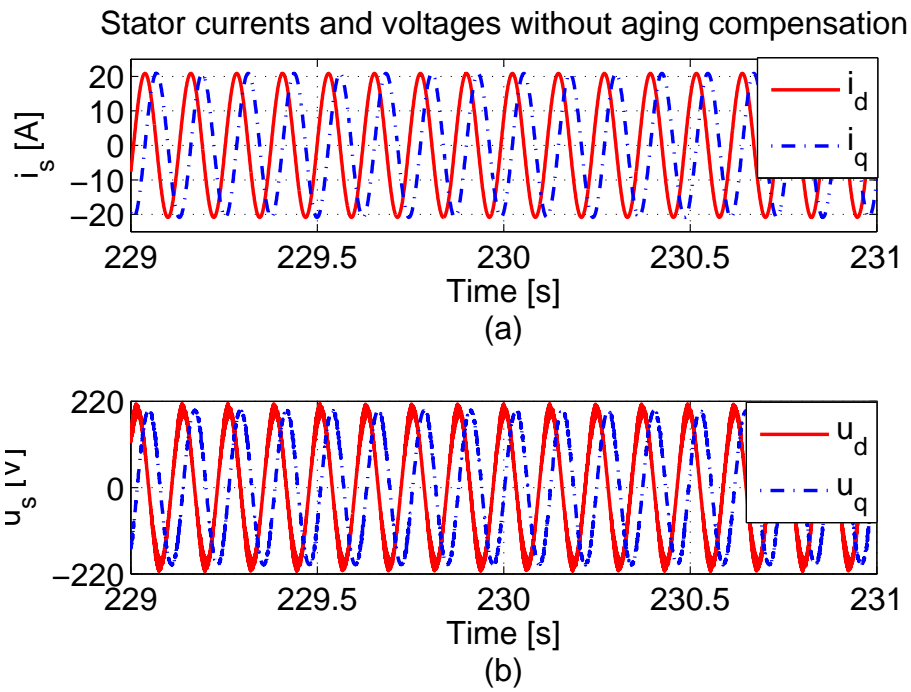


FIGURE 6.9: Induction machine direct and quadrature axis (a) stator currents. (b) stator voltages without aging.

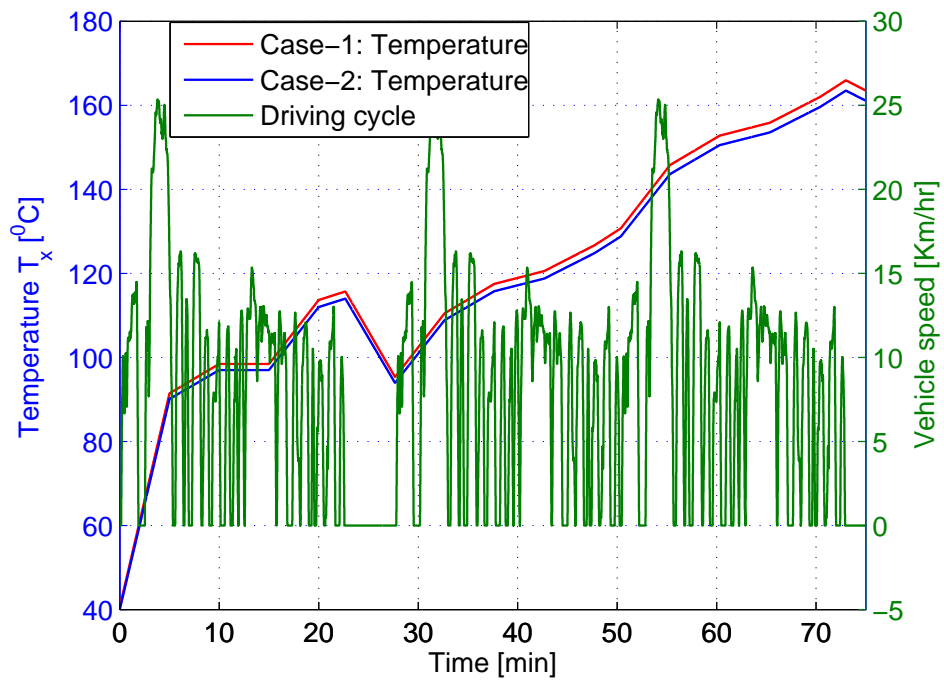


FIGURE 6.10: IM winding temperature: simulation of driving cycle.

which is the nominal temperature during the entire summer. The deterioration rate is given  $(1) / (\xi(T_x)) = (1) / (\xi_0 \cdot 2^{(T_c - T_x) / HIC})$ , where  $\xi(T_x)$  is the expected life

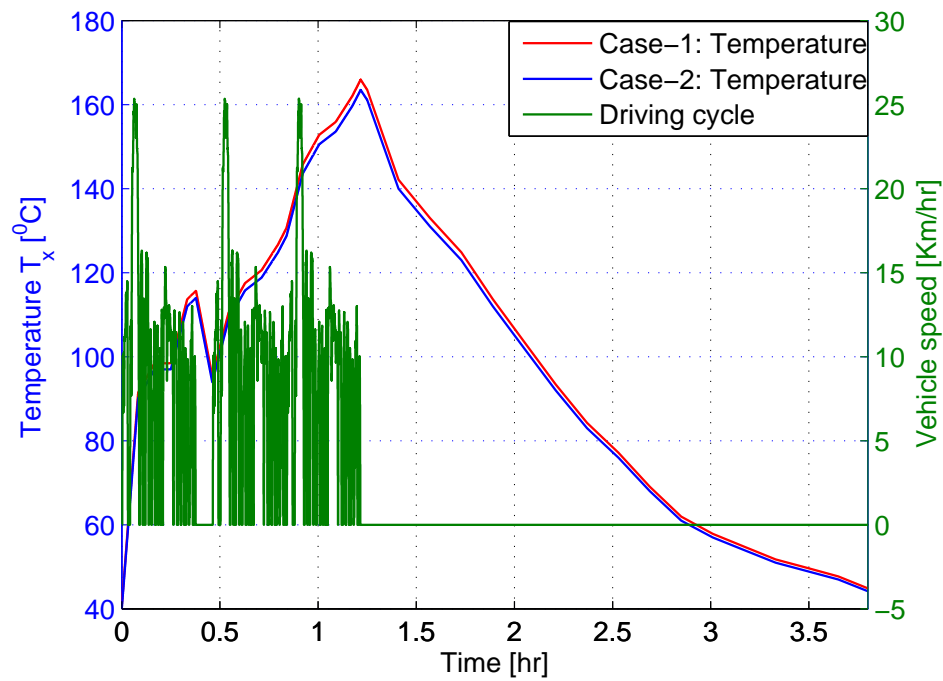


FIGURE 6.11: IM winding temperature: simulation of driving cycle with cooling phase.

at a particular operating temperature  $T_x$ ,  $HIC = 9.3$ ,  $\xi_0$  is the rated life at rated temperature  $T_c$ .

Assume the rated IM life span is  $\xi_0 = 20,000$  h [57]. To find the loss of lifetime for entire driving cycle (43min) in the case-1, the rate of deterioration is  $1/\xi(T_x) = 1/31746.5540 = 0.000031499(1/h)$ . The product of the deterioration rate, period of driving cycle and rated life gives the loss of lifetime  $\iota_{1,2}$ , which in this case is  $(0.000031499 \times 0.7166 \times 20000) = 0.412h$ . In case-2, the rate of deterioration is  $1/\xi(T_x) = 1/39114.4044 = 0.000025566(1/h)$ . The product of the deterioration rate, period of driving cycle and rated life gives the loss of lifetime  $\iota_{1,2}$ , which in this case is  $(0.001143 \times 0.7166 \times 20000) = 0.366h$ .

Similarly, loss of lifetime of the IM operated in an electrified powertrain is also evaluated at  $20^{\circ}C$  and results are summarized in Table 6.4. The difference in loss of lifetime for the both cases is due to the maximum peak temperature for a short period in time.

TABLE 6.4: Loss of lifetime of IM at ambient temperature of  $40^{\circ}C$  and  $20^{\circ}C$ 

Case-1		Case-2	
@ $40^{\circ}C$	@ $20^{\circ}C$	@ $40^{\circ}C$	@ $20^{\circ}C$
0.412h	0.389h	0.336h	0.324h

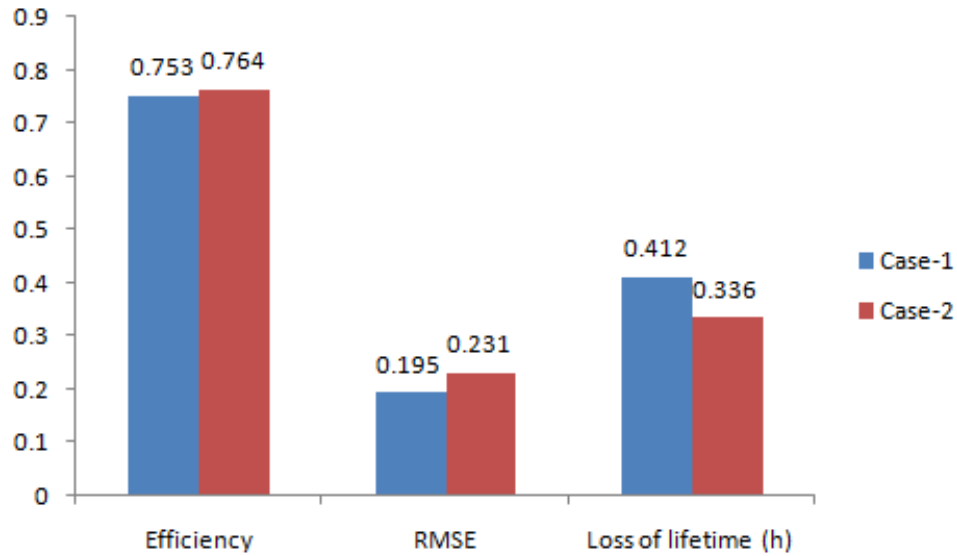


FIGURE 6.12: (a) Average efficiency of an electrified powertrain. (b) RMSE values of vehicle torque. (c) loss of lifetime of an IM.

Consequently, the number of peak temperature overshoots during vehicle operation and short-term part loads are the critical aspects in loss of lifetime of a traction motor due to thermal activity. Therefore, multi-objective LPV controller optimally manages the current limits in order to avoid the further insulation deterioration.

Figure 6.12 shows the comparison of performance in both cases considered in this article. It is clear from the above discussion that multi-objective LPV controller provides better performance to achieve the conflicting objectives (in meeting the torque demands, ensuring efficient electrified powertrain operations and minimizing the loss of lifetime (aging) of an EM over the entire driving cycle). Hence, it was confirmed in this paper that the lifetime of an EM can be enhanced by appropriate controller design without compromising the performance significantly.

## **6.9 Conclusion**

A systematic approach based on LPV control technique for enhancing the performance of an electrified powertrain has been proposed in the chapter. A realistic conflicting cost function was formulated by taking into account the torque demands, efficient operation of an electrified powertrain and loss of an IM lifetime (aging) as three essential but conflicting objectives, which were used to develop a multi-objective LPV-FOC controller. The optimal weighting filters were selected based upon the upper bounds on the supply voltage (battery) and torque. The efficacy of the proposed controller is evaluated for a three-wheeled vehicle driven under the normal and extreme operating conditions. The simulation results confirmed that the aging of the IM was reduced without compromising the performance of the IM drive.

# Chapter 7

## Conclusion and Future Directions

This chapter builds some concluding comments and then opinions for the continuation/expansion of this work will be presented.

### 7.1 Conclusions

The summary of the thesis is disclosed as follow: Chapter 3 explains the LPV modeling of induction machine and its validation. The comparison of the output signals and state signals with non-linear model is done. Root Mean Square Error (RMSE), which is less than  $1.93 \times 10^{-4}$  for all states and then Normalized Root Mean Square Error (NRMSE), which is less than 0.9998 for all states are also investigated. This model is necessarily required for the development of novel control techniques to address the EVs and HEVs problems elaborated in Section 2.3 and Section 2.5.1: namely the ambient and operating temperatures effects on the torque performance, efficiency and the degradation of traction machine winding for EVs and HEVs powertrain.

Chapter 4 explains the thermal derating of torque for an electrified powertrain. A novel and robust LPV based observer is designed for estimating the thermally derated torque and its capability to estimate the thermally derated torque is investigated for HEV powertrain under different ambient temperature.

Chapter 5 describes the design of novel and robust LPV based controller to manage and compensate the thermally derated torque of an induction machine based electrified powertrain. The estimation technique presented in Chapter 4 is used to accomplish it. The performance of designed observer-controller pair is investigating for the EV operating in standard driving cycle (FUDS) under. The proposed control technique ensures good tracking performance in meeting the road loads demands by keeping the the actuator constraints within the desired limits in the presence of rise in operating and surrounding temperatures. The optimal flux calculations using the rotor and stator sides losses are also presented to achieve the efficient operation of traction induction machine under the above mentioned operating conditions.

The efficacy of the proposed control scheme is also investigated using a hardware test set-up consisting of an IM, a Controller Board and a Torque Measurement arrangement. Firstly, practical observation of the open loop thermal torque effects is done using experimental set-up. Secondly, the excellent performance on the test bed of the LPV controller for a step demand on the torque, in contrast to the sliding mode based controller is addressed and this experiment is performed on the raised temperature profile. The third and final experiment, aimed at validating controller for the harsh environment faced by an electrified powertrain in a challenging urban environment, is addressed. For this purpose the speed demand profile was generated from FUDS.

The LPV control method is selected. The main objective of an LPV control (gain scheduling) technique is to control the plant over a predefined operating range. However, it allows the controller to schedule itself based on some measurements in addition to robustness.

Chapter 6 explains the degradation control technique, proposed to mitigate the effects of rise in ambient and operating temperatures on the life time of an traction induction machine for EVs and HEVs while simultaneously providing the desired closed-loop performance. In the synthesis of the degradation controller, meeting the road loads, ensuring efficient powertrain operation and minimizing the loss

of lifetime (aging) of a traction machine are taken as three essential but conflicting targets. The effectiveness of the proposed control framework is tested for a direct drive electrified powertrain of a three-wheeled vehicle commonly found in urban transportation for Asian countries. The urban driving schedule based simulation results confirm that the lifetime of induction machine can be enhanced by appropriate controller design without compromising its performance.

## 7.2 Contributions

After going through a brief discussion on the presented work, the main contributions of the thesis can be enumerated as follows:

1. Development and validation of LPV model of an induction machine by taking rotor resistance, stator resistance and rotor speed as scheduling signals.
2. Estimation of
  - (a) Thermally derated torque of an electrified powertrain
  - (b) Flux of a traction induction machine

from the developed LPV dynamics of a traction induction machine under the rise in operating and surrounding temperatures. These dynamics is used to develop the estimation technique from linear parameter varying control theory. The presented technique needed measurement from voltage sensors, current sensors and speed sensors. These sensors are the compulsory part of traction drive.

3. Development of open loop torque derating confirmation method for a traction machine in an electrified powertrain due to the change in one or both temperatures. This task is accomplished using the developed estimation technique.

4. Design, development and evaluation of a robust LPV control framework for the electrified powertrain in managing the thermally derated torque of an electrified powertrain perspective.
5. Formulation of a conflicting cost functions by considering the following objectives
  - (a) To minimize the traction torque error
  - (b) To maximize the operating efficiency of electrified powertrain
  - (c) To minimize the loss of lifetime (aging) of an IM
6. Design, development and evaluation of a robust multi-objective LPV based field-oriented control framework in mitigating the electric machine based electrified powertrain degradation while simultaneously providing the desired closed loop performance perspective.

### 7.3 Future Directions

The presented research work in this document can be expanded in several directions.

The following future tasks are suggested for estimating and managing the thermally derated torque's control scheme.

1. In this manuscript, electrical equations of a traction induction machine are used to develop the estimation and compensation control techniques for the thermally derated torque of an electrified powertrain. In future, thermal dynamics of a traction induction machine can be developed to make the estimation and control techniques more robust.
2. The proposed estimation and compensation control techniques are evaluated using the developed EV simulator and induction machine based electric drive. These scheme will also be evaluated using the hardware in the loop (HIL) powertrain setup.

3. The operating temperature, in the proposed schemes, is computed from the estimation of induction machine winding's rotor and stator resistances. This can also be computed by development of induction machine thermal dynamics. This will make the estimation and control schemes more simple and robust.

The suggested future tasks for the proposed degradation control for an induction machine based electrified powertrain are;

1. The developed EV simulator is used to investigate the efficacy of degradation control scheme. This control scheme will also be investigated using the hardware in the loop (HIL) powertrain setup.
2. The gains of weighting filters in the design of degradation control scheme are tuned by hit and trial method keeping in view the upper stator voltages and currents bounds. The off line optimization technique can be used to tune the gains of weighting filters to make the design process simple and less time consuming.
3. The performance of this technique in aging perspective should be evaluated by on road testing on actual electric vehicle.
4. The both control schemes are tested and evaluated for the light duty vehicle and three-wheeled electric vehicles used in urban transportation of Asian countries. The high power traction induction machine used in transit buses system faces more temperature effects as compared to medium power traction induction machine. Therefore, the both control schemes should be tested for the high power traction induction machine to evaluate the efficacy of the proposed techniques.

# Chapter 8

## Appendices

### 8.1 Appendix A

#### 8.1.1 Close-loop stability and synthesis of controller

The generalized plant and closed-loop system are shown in Figures 8.1 and 8.2.

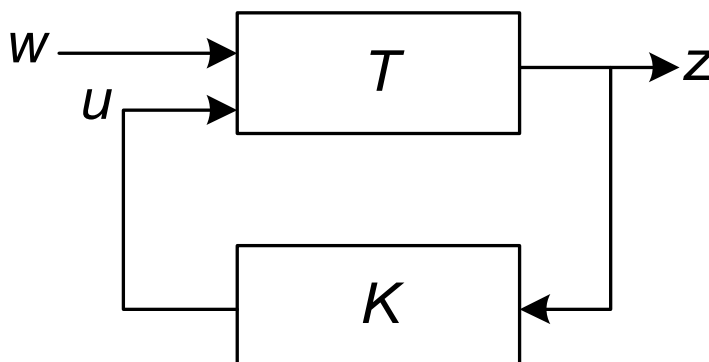


FIGURE 8.1: Generalized plant diagram.



FIGURE 8.2: Closed-loop system.

The state-space representation can be given as:

$$\begin{cases} \dot{x}(t) = Ax(t) + Bw(t) \\ z(t) = Cx(t) + Dw(t) \\ x(0) = 0 \end{cases} \quad (8.1)$$

Assume that  $T(s)$  is stable and the  $H_\infty$  norm of the closed-loop system is given as

$$\|T\|_\infty^2 = \max \frac{\int_0^\infty z^T(t)z(t)dt}{\int_0^\infty w^T(t)w(t)dt}, \quad w \neq 0 \quad (8.2)$$

It is clear from (8.2) that  $\|T\|_\infty < \gamma$  is equivalent to

$$\int_0^\infty (z^T(t)z(t) - \gamma^2 w^T(t)w(t))dt < 0 \quad (8.3)$$

Assuming a Lyapunov function,

$$V(x) = x^T P x, \quad P = P^T > 0 \quad (8.4)$$

Since  $x(0) = x(\infty) = 0$ ,  $\|T\|_\infty < \gamma$  is enforced by the existence of  $P = P^T > 0$  such that

$$\dot{V}(x) + \frac{1}{\gamma} z^T(t)z(t) - \gamma w^T(t)w(t) < 0, \quad \forall x(t), w(t) \quad (8.5)$$

To convert (8.5) in to LMI, putting (8.6) and (8.7) into (8.5)

$$\dot{V}(x) = x^T (A^T P + P A)x + x^T P B w + w^T B^T P x \quad (8.6)$$

$$Z = Cx + Dw \quad (8.7)$$

It yields

$$\begin{bmatrix} x^T & w^T \end{bmatrix} \begin{bmatrix} A^T P + P A + \frac{1}{\gamma} C^T C & P B + \frac{1}{\gamma} C^T D \\ B^T P + \frac{1}{\gamma} D^T C & -\gamma I + \frac{1}{\gamma} D^T D \end{bmatrix} \begin{bmatrix} x \\ w \end{bmatrix} < 0 \quad (8.8)$$

For  $\|T\|_\infty < \gamma$  the (8.8) must hold for all  $x$  and  $w$ . The (8.8) can be rewritten as

$$\begin{bmatrix} A^T P + PA & PB \\ B^T P & -\gamma I \end{bmatrix} + \frac{1}{\gamma} \begin{bmatrix} C^T \\ D^T \end{bmatrix} \begin{bmatrix} C & D \end{bmatrix} < 0 \quad (8.9)$$

The existence of solution to LMI in (8.9) is necessary condition for  $\|T\|_\infty < \gamma$ . Using Schur complement, the (8.9) can also be written as

$$\begin{bmatrix} A^T P + PA & PB & C^T \\ B^T P & -\gamma I & D^T \\ C & D & -\gamma I \end{bmatrix} < 0 \quad (8.10)$$

From Figure 8.1, the state-space representation of closed-loop system is given as

$$\begin{cases} \dot{x}_c(t) = A_c x_c(t) + B_c w_c(t) \\ z(t) = C_c x_c(t) + D_c w_c(t) \end{cases} \quad (8.11)$$

where

$$A_c = \begin{bmatrix} A + B_u C_k C_v & B_u C_k \\ B_k C_v & A_k \end{bmatrix} \quad (8.12)$$

$$B_c = \begin{bmatrix} B_w + B_u D_k D_{vw} \\ B_k D_{vw} \end{bmatrix} \quad (8.13)$$

$$C_c = \begin{bmatrix} C_z + D_{zu} D_k D_v & D_{zu} C_k \end{bmatrix} \quad (8.14)$$

$$D_c = \begin{bmatrix} D_{zw} + D_{zu} D_k D_{vw} \end{bmatrix} \quad (8.15)$$

The closed-loop transfer function  $T(s)$  is given as

$$T_s = \begin{bmatrix} A_c & B_c \\ C_c & D_c \end{bmatrix} = C_c (sI - A_c)^{-1} B_c + D_c \quad (8.16)$$

Further solving for  $H_\infty$  output feedback control results in two LMIs.

$$\begin{bmatrix} AY + YA^T + B_u \tilde{C}_k + (B_u \tilde{C}_k)^T & \tilde{A}_k + A + B_u \tilde{D}_k C_v & B_w + B_u \tilde{D}_k D_{vw} & (C_z Y + D_{zu} \tilde{C}_k)^T \\ * & A^T X + XA + \tilde{B}_k C_v + (B_k \tilde{C}_v)^T & X B_w + \tilde{B}_k D_{vw} & (C_z + D_{zu} \tilde{D}_k C_v)^T \\ * & * & -\gamma I & (D_{zw} + D_{zu} \tilde{D}_k D_{vw})^T \\ * & * & * & -\gamma I \end{bmatrix} < 0 \quad (8.17)$$

$$\begin{bmatrix} Y & I \\ I & X \end{bmatrix} < 0 \quad (8.18)$$

## 8.2 Appendix B

### 8.2.1 Induced L-2 norm of LPV systems

The LPV system in state-space form can be given as:

$$G : \begin{cases} \frac{dx(t)}{dt} = A(\rho(t))x(t) + B(\rho(t))w(t) \\ z(t) = C(\rho(t))x(t) + D(\rho(t))w(t) \end{cases} \quad (8.19)$$

where the system matrices are the continuous function of the parameter  $\rho$ . In addition,  $\rho(\cdot)$  is a piecewise continuous function of time,  $\rho : R^+ \rightarrow R^m$ , that is assumed to satisfy the known bounds

$$\rho_i(t) \in [\rho_{-i}, \rho^{-i}], \quad i = 1, 2, \dots, m \quad (8.20)$$

The set of parameter vectors  $\rho \in R^m$  satisfying the magnitude constraints in (8.20) is denoted by  $P$  and the set of admissible trajectories. The performance of  $G$  can be specified in term of its  $L_2$  gain from input  $w$  to output  $z$  assuming  $x(0) = 0$  [132].

$$\|G\| = \sup_{0 \neq w \in L_2(R^p), \rho(\cdot) \in A} \frac{\|z\|}{\|w\|} \quad (8.21)$$

## 8.3 Appendix C

### 8.3.1 Thermally derated torque's observer gains

The observer gains are selected using (4.22)- (4.24) which were computed by solving the LMI in (4.21). The LMI optimization delivered a LPV observer with 8 vertices, each vertex being an LTI regulator with four states.

The observer gains at each vertex are

@ vertex-1

$$L_1 = \begin{bmatrix} 45.93 & 0 \\ 0 & 45.93 \\ 4 & 51.9 \\ -51.9 & 4 \end{bmatrix}$$

@ vertex-2

$$L_2 = \begin{bmatrix} 49.91 & 0 \\ 0 & 49.91 \\ 5 & -51.9 \\ 51.9 & 5 \end{bmatrix}$$

@ vertex-3

$$L_3 = \begin{bmatrix} 49.91 & 0 \\ 0 & 49.91 \\ 5 & 51.9 \\ -51.9 & 5 \end{bmatrix}$$

@ vertex-4

$$L_4 = \begin{bmatrix} 50.09 & 0 \\ 0 & 50.09 \\ 4 & -51.9 \\ 51.9 & 4 \end{bmatrix}$$

@ vertex-5

$$L_5 = \begin{bmatrix} 50.09 & 0 \\ 0 & 50.09 \\ 4 & 51.9 \\ -51.9 & 4 \end{bmatrix}$$

@ vertex-6

$$L_6 = \begin{bmatrix} 49.89 & 0 \\ 0 & 49.89 \\ 5 & -51.9 \\ 51.9 & 4 \end{bmatrix}$$

@ vertex-7

$$L_7 = \begin{bmatrix} 49.91 & 0 \\ 0 & 49.91 \\ 5 & -51.9 \\ -51.9 & 5 \end{bmatrix}$$

@ vertex-8

$$L_8 = \begin{bmatrix} 45.93 & 0 \\ 0 & 45.93 \\ 4 & -51.9 \\ 51.9 & 4 \end{bmatrix}$$

## 8.4 Appendix D

### 8.4.1 LPV current controllers gains

The LPV controller  $K_{lpv}$  was computed by solving the optimization problem of (5.25) such that (6.60) and (6.61) hold. With the weighting functions defined in (5.31), the LMI optimization gave a LPV controller with eight vertices, each vertex being an LTI controller with six states. Four states come from the plant and two from WS: The achieved optimal value of performance index  $\gamma$  is 1.023.

The controller gains at each vertex are

@ vertex-1

$$A_K(1) = 1 \times 10^6 \cdot \begin{bmatrix} -0.0034 & -0.0001 & -0.0003 & -0.0060 & 1.2085 & -7.2151 \\ -0.0001 & -0.0033 & -0.0069 & 0.0003 & 5.1533 & 1.7220 \\ -0.0000 & 0.0000 & -0.0000 & -0.0002 & -0.0009 & -0.0007 \\ 0.0000 & 0.0000 & 0.0002 & -0.0000 & -0.0004 & 0.0032 \\ 0.0004 & 0.0014 & 0.0031 & 0.0004 & -2.3658 & -0.0131 \\ -0.0021 & 0.0004 & 0.0007 & -0.0038 & -0.0131 & -4.6456 \end{bmatrix}$$

$$B_K(1) = \begin{bmatrix} -0.6402 & -0.4883 \\ 0.4934 & -0.6538 \\ -0.8040 & 0.3800 \\ 0.2492 & 0.7760 \\ 219.2878 & -495.4651 \\ 707.6236 & 313.2384 \end{bmatrix}$$

$$C_K(1) = 1 \times 10^5 \cdot \begin{bmatrix} 0.0015 & -0.0011 & -0.0032 & 0.0011 & 1.2318 & 3.9566 \\ 0.0012 & 0.0015 & 0.0015 & 0.0029 & -2.8186 & 1.7106 \end{bmatrix}$$

$$D_K(1) = \begin{bmatrix} 0 & 0 \\ 0 & 0 \end{bmatrix}$$

The plant matrices  $B$  and  $C$  are not time varying. Therefore, the controller matrices  $B_K(\cdot)$ ,  $C_K(\cdot)$  and  $D_K(\cdot)$  remain same at each vertex. The controller matrix  $A_K(\cdot)$  is only varied and given below.

@ vertex-2

$$A_K(2) = 1 \times 10^6 \cdot \begin{bmatrix} -0.0035 & -0.0001 & 0.0059 & -0.0027 & 1.2085 & -7.2151 \\ -0.0001 & -0.0034 & -0.0036 & -0.0059 & 5.1533 & 1.7220 \\ -0.0000 & 0.0000 & -0.0000 & 0.0002 & -0.0009 & -0.0007 \\ 0.0000 & 0.0000 & -0.0002 & -0.0000 & -0.0004 & 0.0032 \\ 0.0004 & 0.0015 & 0.0009 & 0.0029 & -2.3658 & -0.0131 \\ -0.0021 & 0.0005 & 0.0042 & -0.0007 & -0.0131 & -4.6456 \end{bmatrix}$$

@ vertex-3

$$A_K(3) = 1 \times 10^6 \cdot \begin{bmatrix} -0.0035 & -0.0001 & -0.0003 & -0.0059 & 1.2085 & -7.2151 \\ -0.0001 & -0.0034 & -0.0068 & 0.0003 & 5.1533 & 1.7220 \\ -0.0000 & 0.0000 & -0.0000 & -0.0002 & -0.0009 & -0.0007 \\ 0.0000 & 0.0000 & 0.0002 & -0.0000 & -0.0004 & 0.0032 \\ 0.0004 & 0.0015 & 0.0031 & 0.0004 & -2.3658 & -0.0131 \\ -0.0021 & 0.0005 & 0.0007 & -0.0037 & -0.0131 & -4.6456 \end{bmatrix}$$

@ vertex-4

$$A_K(4) = 1 \times 10^6 \cdot \begin{bmatrix} -0.0035 & -0.0001 & 0.0059 & -0.0027 & 1.2085 & -7.2151 \\ -0.0001 & -0.0033 & -0.0036 & -0.0059 & 5.1533 & 1.7220 \\ -0.0000 & 0.0000 & -0.0000 & 0.0002 & -0.0009 & -0.0007 \\ 0.0000 & 0.0000 & -0.0002 & -0.0000 & -0.0004 & 0.0032 \\ 0.0004 & 0.0015 & 0.0009 & 0.0029 & -2.3658 & -0.0131 \\ -0.0021 & 0.0005 & 0.0042 & -0.0007 & -0.0131 & -4.6456 \end{bmatrix}$$

@ vertex-5

$$A_K(5) = 1 \times 10^6 \cdot \begin{bmatrix} -0.0035 & -0.0001 & -0.0003 & -0.0060 & 1.2085 & -7.2151 \\ -0.0001 & -0.0033 & -0.0069 & 0.0003 & 5.1533 & 1.7220 \\ -0.0000 & 0.0000 & -0.0000 & -0.0002 & -0.0009 & -0.0007 \\ 0.0000 & 0.0000 & 0.0002 & -0.0000 & -0.0004 & 0.0032 \\ 0.0004 & 0.0015 & 0.0031 & 0.0004 & -2.3658 & -0.0131 \\ -0.0021 & 0.0004 & 0.0007 & -0.0038 & -0.0131 & -4.6456 \end{bmatrix}$$

@ vertex-6

$$A_K(6) = 1 \times 10^6 \cdot \begin{bmatrix} -0.0034 & -0.0001 & 0.0059 & -0.0027 & 1.2085 & -7.2151 \\ -0.0001 & -0.0033 & -0.0036 & -0.0059 & 5.1533 & 1.7220 \\ -0.0000 & 0.0000 & -0.0000 & 0.0002 & -0.0009 & -0.0007 \\ 0.0000 & 0.0000 & -0.0002 & -0.0000 & -0.0004 & 0.0032 \\ 0.0004 & 0.0014 & 0.0009 & 0.0029 & -2.3658 & -0.0131 \\ -0.0021 & 0.0004 & 0.0042 & -0.0007 & -0.0131 & -4.6456 \end{bmatrix}$$

@ vertex-7

$$A_K(7) = 1 \times 10^6 \cdot \begin{bmatrix} -0.0035 & -0.0001 & -0.0003 & -0.0059 & 1.2085 & -7.2151 \\ -0.0001 & -0.0033 & -0.0068 & 0.0003 & 5.1533 & 1.7220 \\ -0.0000 & 0.0000 & -0.0000 & -0.0002 & -0.0009 & -0.0007 \\ 0.0000 & 0.0000 & 0.0002 & -0.0000 & -0.0004 & 0.0032 \\ 0.0004 & 0.0014 & 0.0031 & 0.0004 & -2.3658 & -0.0131 \\ -0.0021 & 0.0004 & 0.0007 & -0.0037 & -0.0131 & -4.6456 \end{bmatrix}$$

@ vertex-8

$$A_K(8) = 1 \times 10^6 \cdot \begin{bmatrix} -0.0034 & -0.0001 & 0.0059 & -0.0027 & 1.2085 & -7.2151 \\ -0.0001 & -0.0033 & -0.0036 & -0.0059 & 5.1533 & 1.7220 \\ -0.0000 & 0.0000 & -0.0000 & 0.0002 & -0.0009 & -0.0007 \\ 0.0000 & 0.0000 & -0.0002 & -0.0000 & -0.0004 & 0.0032 \\ 0.0004 & 0.0014 & 0.0009 & 0.0029 & -2.3658 & -0.0131 \\ -0.0021 & 0.0004 & 0.0042 & -0.0007 & -0.0131 & -4.6456 \end{bmatrix}$$

### 8.4.2 Torque and flux controllers gains

The torque and flux controllers were computed by solving the linear matrix inequality in (5.53) and Equation (5.54) gives us the gains of controllers.

The gains of torque and flux controllers are  $\text{diag}(-300; -230)$ .

# Bibliography

- [1] U. E. I. Administration, “The annual energy review.” Technical report, 2008. (Available at <http://www.eia.doe.gov/aer/>), 2008.
- [2] M. K. J. Adeel Ahmad, “Status of petroleum sector in pakistan - a review,” School of Environment, Resources and Development Asian Institute of Technology, Bangkok 12120, Thailand, (<http://www.ogbus.ru/eng/>), 2010.
- [3] F. D. F. K. H. Allen, M., “The exit strategy, in climate change,” N. reports, Editor. p. 56-58, 2009.
- [4] F. Porsche, “The first hybrid vehicle built in 1898.”
- [5] E. Hesla, “Electric propulsion [history],” *Industry Applications Magazine, IEEE*, vol. 15, no. 4, pp. 10–13, July 2009.
- [6] J. M. Miller, *Propulsion Systems for Hybrid Vehicles*. The Institution of Engineering and Technology, United Kingdom: Springer, 2010.
- [7] K. agatay Bayindir, M. A. Gzkk, and A. Teke, “A comprehensive overview of hybrid electric vehicle: Powertrain configurations, powertrain control techniques and electronic control units,” *Energy Conversion and Management*, vol. 52, no. 2, pp. 1305 – 1313, 2011. [Online]. Available: <http://www.sciencedirect.com/science/article/pii/S0196890410004309>
- [8] P. S. Caiying Shen and T. Gao, “A comprehensive overview of hybrid electric vehicles,” *International Journal of Vehicular Technology*, vol. 2011, no. 3, pp. 463–469, March 2012.

- 
- [9] S. Dilmi and S. Yurkovich, "Nonlinear torque control of the induction motor in hybrid electric vehicle applications," in *American Control Conference, 2005. Proceedings of the 2005*, June 2005, pp. 3001–3006 vol. 5.
- [10] H. Rehman and L. Xu, "Alternative energy vehicles drive system: Control, flux and torque estimation, and efficiency optimization," *Vehicular Technology, IEEE Transactions on*, vol. 60, no. 8, pp. 3625–3634, 2011.
- [11] Z. Rahman and et al., "An investigation of electric motor drive characteristics for ev and hev propulsion systems," *SAE Technical Paper Series, Paper no. 2000-01-3062*, 1990.
- [12] J. de Santiago, H. Bernhoff, B. Ekergrd, S. Eriksson, S. Ferhatovic, R. Waters, and M. Leijon, "Electrical motor drivelines in commercial all-electric vehicles: A review," *Vehicular Technology, IEEE Transactions on*, vol. 61, no. 2, pp. 475–484, Feb 2012.
- [13] B. K. Bose, *Modern power electronics and AC drives*. Prentice Hall, 2002.
- [14] I. Boldea and S. A. Nasar, *Vector Control of AC Drives*. CRC Press, NY, 1992.
- [15] M. Valenzuela, J. Tapia, and J. Rooks, "Thermal evaluation of tefc induction motors operating on frequency-controlled variable-speed drives," *Industry Applications, IEEE Transactions on*, vol. 40, no. 2, pp. 692–698, March 2004.
- [16] T. H. Bishop, "Temperature monitoring is key to motor reliability," *Maintenance Technology Magazine*, vol. 40, no. 2, pp. 34–F, July 2004.
- [17] J. Estima and A. Marques Cardoso, "Efficiency analysis of drive train topologies applied to electric/hybrid vehicles," *Vehicular Technology, IEEE Transactions on*, vol. 61, no. 3, pp. 1021–1031, March 2012.
- [18] C. Mi, "Field-oriented control of induction motor drives with direct rotor current estimation for applications in electric and hybrid vehicles," *Journal of Asian electric vehicles*, vol. 5, no. 2, pp. 989–992, 2007.

- [19] Y. Liu and C. Shao, "Sensorless torque control scheme of induction motor for hybrid electric vehicle," *Journal of Control Theory and Applications*, vol. 5, no. 1, pp. 42–46, 2007.
- [20] F. Zhu, L. Chen, and C. Yin, "Design and analysis of a novel multimode transmission for a hev using a single electric machine," *IEEE Transactions on vehicular technology*, vol. 62, no. 3, pp. 1097–1110, 2013.
- [21] S.-I. Kim, J. Cho, S. Park, T. Park, and S. Lim, "Characteristics comparison of a conventional and modified spoke-type ferrite magnet motor for traction drives of low-speed electric vehicles," *IEEE Transactions on Industry Applications*, vol. 49, no. 6, pp. 2516–2523, 2013.
- [22] P. Werynski, D. Roger, R. Corton, and J. F. Brudny, "Proposition of a new method for in-service monitoring of the aging of stator winding insulation in ac motors," *IEEE Transactions on Energy Conversion*, vol. 21, no. 3, pp. 673–681, 2006.
- [23] N. Lahoud, J. Faucher, D. Malec, and P. Maussion, "Electrical aging of the insulation of low-voltage machines: Model definition and test with the design of experiments," *IEEE Transactions on Industrial Electronics*, vol. 60, no. 9, pp. 4147–4155, 2013.
- [24] A. Soualhi, K. Medjaher, and N. Zerhouni, "Bearing health monitoring based on hilbert–huang transform, support vector machine, and regression," *IEEE Transactions on Instrumentation and Measurement*, vol. 64, no. 1, pp. 52–62, 2015.
- [25] F. Rufus, S. Lee, A. Thakker, S. A. Field, and N. Kumbar, "Advanced diagnostics of aircraft electrical generators," *SAE International Journal of Aerospace*, vol. 1, no. 2008-01-2923, pp. 1064–1070, 2008.
- [26] J. D. McFarland and T. Jahns, "Influence of d-and q-axis currents on demagnetization in pm synchronous machines," in *Energy Conversion Congress and Exposition (ECCE), 2013 IEEE*. IEEE, 2013, pp. 4380–4387.

- [27] C. Chan and K. Chau, "An overview of power electronics in electric vehicles," *Industrial Electronics, IEEE Transactions on*, vol. 44, no. 1, pp. 3–13, 1997.
- [28] Z. Zhu and D. Howe, "Electrical machines and drives for electric, hybrid, and fuel cell vehicles," *Proceedings of the IEEE*, vol. 95, no. 4, pp. 746–765, 2007.
- [29] M. Terashima, T. Ashikaga, T. Mizuno, K. Natori, N. Fujiwara, and M. Yada, "Novel motors and controllers for high-performance electric vehicle with four in-wheel motors," *Industrial Electronics, IEEE Transactions on*, vol. 44, no. 1, pp. 28–38, 1997.
- [30] K. Chau and Y. Wong, "Hybridization of energy sources in electric vehicles," *Energy Conversion and Management*, vol. 42, no. 9, pp. 1059–1069, 2001.
- [31] —, "Overview of power management in hybrid electric vehicles," *Energy Conversion and Management*, vol. 43, no. 15, pp. 1953–1968, 2002.
- [32] M. Ehsani, Y. Gao, and A. Emadi, *Modern electric, hybrid electric, and fuel cell vehicles: fundamentals, theory, and design*. CRC press, 2009.
- [33] M. Zeraoulia, M. E. H. Benbouzid, and D. Diallo, "Electric motor drive selection issues for hev propulsion systems: A comparative study," *Vehicular Technology, IEEE Transactions on*, vol. 55, no. 6, pp. 1756–1764, 2012.
- [34] S. Hasan, "Hybrid electric vehicle powertrain: On-line parameter estimation of an induction motor drive and torque control of a a pm bldc starter-generator," Ph.D. dissertation, University of Akron, 2008.
- [35] I. Husain, *Electric and hybrid vehicles: design fundamentals*. CRC press, 2011.
- [36] A. Hanif, F. Pervaiz, W. Shabbir, A. Abbas, and Z. Qamar, "Plug in type series hybrid vehicle: Concept, design and implementation," in *Proceeding of the International Conference on Mechanical and Electrical Technology, ICMET-2011*, vol. 1, 2011, pp. 159–165.

- [37] K. Chau, C. C. Chan, and C. Liu, "Overview of permanent-magnet brushless drives for electric and hybrid electric vehicles," *IEEE Transactions on industrial electronics*, vol. 55, no. 6, pp. 2246–2257, 2008.
- [38] C. Chan, "The state of the art of electric and hybrid vehicles," *Proceedings of the IEEE*, vol. 90, no. 2, pp. 247–275, 2002.
- [39] T. M. Jahns and V. Blasko, "Recent advances in power electronics technology for industrial and traction machine drives," *Proceedings of the IEEE*, vol. 89, no. 6, pp. 963–975, 2001.
- [40] D. W. Novotny and T. A. Lipo, *Vector Control and Dynamics of AC Drives*. Clarendon Press, Oxford, 1996.
- [41] G. Pellegrino, A. Vagati, B. Boazzo, and P. Guglielmi, "Comparison of induction and pm synchronous motor drives for ev application including design examples," *Industry Applications, IEEE Transactions on*, vol. 48, no. 6, pp. 2322–2332, 2012.
- [42] H. L. Husted, "A comparative study of the production applications of hybrid electric powertrains," SAE Technical Paper, Tech. Rep., 2003.
- [43] M. Jalalifar, A. F. Payam, B. Mirzaeian, and S. Nezhad, "Dynamic modeling and simulation of an induction motor with adaptive backstepping design of an input-output feedback linearization controller in series hybrid electric vehicle," in *Power Electronics, Drives and Energy Systems, 2006. PEDES'06. International Conference on*. IEEE, 2006, pp. 1–6.
- [44] P. Caratozzolo, M. Serra, C. Ocampo, and J. Riera, "A proposal for the propulsion system of a series hybrid electric vehicle," in *Power Electronics Specialist Conference, 2003. PESC'03. 2003 IEEE 34th Annual*, vol. 2. IEEE, 2003, pp. 586–591.
- [45] C. Mi, "Field-oriented control of induction motor drives with direct rotor current estimation for applications in electric and hybrid vehicles," *Journal of Asian electric vehicles*, vol. 5, no. 2, pp. 989–992, 2007.

- [46] K. Engelen, S. De Breucker, and J. Driesen, "Implementation aspects of field oriented control of an induction machine for a hybrid electric vehicle," in *Proceedings of" The 25th World Battery, Hybrid and Fuel Cell Electric Vehicle Symposium & Exhibition"*, 2010.
- [47] M. Osama and T. A. Lipo, "A new inverter control scheme for induction motor drives requiring wide speed range," *Industry Applications, IEEE Transactions on*, vol. 32, no. 4, pp. 938–944, 1996.
- [48] S. Jiang, K. Chau, and C. Chan, "Spectral analysis of a new six-phase pole-changing induction motor drive for electric vehicles," *Industrial Electronics, IEEE Transactions on*, vol. 50, no. 1, pp. 123–131, 2003.
- [49] J. F. Gieras, *Permanent magnet motor technology: design and applications*. CRC press, 2002.
- [50] N. Demerdash and T. Nehl, "Dynamic modeling of brushless dc motors for aerospace actuation," *Aerospace and Electronic Systems, IEEE Transactions on*, no. 6, pp. 811–821, 1980.
- [51] F. Deng, "Commutation-caused eddy-current losses in permanent-magnet brushless dc motors," *Magnetics, IEEE Transactions on*, vol. 33, no. 5, pp. 4310–4318, 1997.
- [52] T. M. Jahns, "Flux-weakening regime operation of an interior permanent-magnet synchronous motor drive," *Industry Applications, IEEE Transactions on*, no. 4, pp. 681–689, 1987.
- [53] J. Malan and M. J. Kamper, "Performance of hybrid electric vehicle using reluctance synchronous machine technology," in *Industry Applications Conference, 2000. Conference Record of the 2000 IEEE*, vol. 3. IEEE, 2000, pp. 1881–1887.
- [54] K. M. Rahman, B. Fahimi, G. Suresh, A. V. Rajarathnam, and M. Ehsani, "Advantages of switched reluctance motor applications to ev and hev: design

- and control issues,” *Industry Applications, IEEE Transactions on*, vol. 36, no. 1, pp. 111–121, 2000.
- [55] C. Pollock, H. Pollock, R. Barron, J. R. Coles, D. Moule, A. Court, and R. Sutton, “Flux-switching motors for automotive applications,” *Industry Applications, IEEE Transactions on*, vol. 42, no. 5, pp. 1177–1184, 2006.
- [56] R. Rothe and K. Hameyer, “Life expectancy calculation for electric vehicle traction motors regarding dynamic temperature and driving cycles,” in *Electric Machines & Drives Conference (IEMDC), 2011 IEEE International*. IEEE, 2011, pp. 1306–1309.
- [57] H. Oraee and A. Emanuel, “Induction motor useful life and power quality,” *IEEE Power Engineering Review*, vol. 20, no. 1, pp. 47–47, 2000.
- [58] D. Montone, “Temperature effects on motor performance,” Technical report, 2008. (Available at <http://www.Pittman-Motors.com>), 2008.
- [59] F. A. Khalifa, S. Serry, M. M. Ismail, and B. Elhady, “Effect of temperature rise on the performance of induction motors,” in *Computer Engineering & Systems, 2009. ICCES 2009. International Conference on*. IEEE, 2009, pp. 549–552.
- [60] J. Faiz and H. Ebrahimpour, “Precise derating of three phase induction motors with unbalanced voltages,” *Energy Conversion and Management*, vol. 48, no. 9, pp. 2579–2586, 2007.
- [61] P. Gnacinski, “Derating of an induction machine under voltage unbalance combined with over or undervoltages,” *Energy Conversion and Management*, vol. 50, no. 4, pp. 1101–1107, 2009.
- [62] A. Hanif, A. I. Bhatti, and Q. Ahmed, “Managing the thermally derated torque of an electrified powertrain through lqv control,” *IEEE Transactions on mechatronics*, vol. 23, no. 1, pp. 364–376, 2018.
- [63] A. Hanif, S. M. Nawazish Ali, Q. Ahmed, A. I. Bhatti, G. Yin, and M. H. Jaffery, “Effect of variation in rotor resistance on the dynamic performance of

- induction motor,” in *Control Conference (CCC), 2016 35th Chinese*. IEEE, 2016, pp. 9524–9529.
- [64] A. M. Trzynadlowski, *Control of induction motors*. Academic press, 2000.
- [65] H. Kubota, K. Matsuse, and T. Nakano, “Dsp-based speed adaptive flux observer of induction motor,” *IEEE Transactions on Industry Applications*, vol. 29, no. 2, pp. 344–348, 1993.
- [66] B. Tabbache, M. E. H. Benbouzid, A. Kheloui, and J.-M. Bourgeot, “Virtual-sensor-based maximum-likelihood voting approach for fault-tolerant control of electric vehicle powertrains,” *IEEE transactions on vehicular technology*, vol. 62, no. 3, pp. 1075–1083, 2013.
- [67] G. C. Verghese and S. Sanders, “Observers for flux estimation in induction machines,” *Industrial Electronics, IEEE Transactions on*, vol. 35, no. 1, pp. 85–94, 1988.
- [68] S.-H. Jeon, K. K. Oh, and J.-Y. Choi, “Flux observer with online tuning of stator and rotor resistances for induction motors,” *Industrial Electronics, IEEE Transactions on*, vol. 49, no. 3, pp. 653–664, 2002.
- [69] H. Rehman, A. Derdiyok, M. Guven, and L. Xu, “A new current model flux observer for wide speed range sensorless control of an induction machine,” *Power Electronics, IEEE Transactions on*, vol. 17, no. 6, pp. 1041–1048, 2002.
- [70] H. Rehman, “Design of voltage model flux observer,” *Electric Power Applications, IEE Proceedings -*, vol. 151, no. 2, pp. 129–134, 2004.
- [71] P. Jansen, R. Lorenz, and D. Novotny, “Observer-based direct field orientation: analysis and comparison of alternative methods,” *Industry Applications, IEEE Transactions on*, vol. 30, no. 4, pp. 945–953, 1994.
- [72] L. Zhen and L. Xu, “Sensorless field orientation control of induction machines based on a mutual mras scheme,” *Industrial Electronics, IEEE Transactions on*, vol. 45, no. 5, pp. 824–831, 1998.

- [73] H. Tajima and Y. Hori, "Speed sensorless field-orientation control of the induction machine," *Industry Applications, IEEE Transactions on*, vol. 29, no. 1, pp. 175–180, 1993.
- [74] C. Schauder, "Adaptive speed identification for vector control of induction motors without rotational transducers," *Industry Applications, IEEE Transactions on*, vol. 28, no. 5, pp. 1054–1061, 1992.
- [75] Y.-R. Kim, S.-K. Sul, and M.-H. Park, "Speed sensorless vector control of induction motor using extended kalman filter," *Industry Applications, IEEE Transactions on*, vol. 30, no. 5, pp. 1225–1233, 1994.
- [76] M. Farasat, A. M. Trzynadlowski, and M. S. Fadali, "Efficiency improved sensorless control scheme for electric vehicle induction motors," *IET Electrical Systems in Transportation*, vol. 4, no. 4, pp. 122–131, 2014.
- [77] V. I. Utkin, J. Guldner, and J. Shi, *Sliding Mode Control in Electromechanical Systems*. London: Taylor and Francis, 1999.
- [78] A. Derdiyok, M. Guven, H. Rehman, N. Inanc, and L. Xu, "Design and implementation of a new sliding-mode observer for speed-sensorless control of induction machine," *Industrial Electronics, IEEE Transactions on*, vol. 49, no. 5, pp. 1177–1182, 2002.
- [79] L. Zhao, J. Huang, H. Liu, B. Li, and W. Kong, "Second-order sliding-mode observer with online parameter identification for sensorless induction motor drives," *IEEE Transactions on Industrial Electronics*, vol. 61, no. 10, pp. 5280–5289, 2014.
- [80] J. R. Domínguez, C. Mora-Soto, S. Ortega-Cisneros, J. J. R. Panduro, and A. G. Loukianov, "Copper and core loss minimization for induction motors using high-order sliding-mode control," *IEEE Transactions on Industrial Electronics*, vol. 59, no. 7, pp. 2877–2889, 2012.

- [81] S. Di Gennaro, J. R. Domínguez, and M. A. Meza, “Sensorless high order sliding mode control of induction motors with core loss,” *IEEE Transactions on Industrial Electronics*, vol. 61, no. 6, pp. 2678–2689, 2014.
- [82] S. Zak, “On the stabilization and observation of nonlinear/uncertain dynamic systems,” *Automatic Control, IEEE Transactions on*, vol. 35, no. 5, pp. 604–607, 1990.
- [83] C. Kwon, S. D. Sudhoff, S. H. Zak, and S. Hui, “Rotor flux and speed observers for induction motors,” in *International Conference on Power Electronics and Intelligent Control for Energy Conservation*, 2005, pp. 1–2.
- [84] S. H. Zak, “On the stabilization and observation of nonlinear/uncertain dynamic systems,” *Automatic Control, IEEE Transactions on*, vol. 35, no. 5, pp. 604–607, 1990.
- [85] K. Dalila, M. Abdessalem, D. Said, and L. Chrifi-Alaoui, “Robust linear parameter varying induction motor control with polytopic models,” *Serbian Journal of Electrical Engineering*, vol. 10, no. 2, pp. 335–348, 2013.
- [86] E. Prempain, I. Postlethwaite, and A. Benchaib, “A linear parameter variant h8 control design for an induction motor,” *Control Engineering Practice*, vol. 10, no. 6, pp. 633–644, 2002.
- [87] A. Salem and A. S. Tlili, “On the polytopic and multimodel state observers of induction motors.”
- [88] V. T. Buyukdegirmenci, A. M. Bazzi, and P. T. Krein, “Evaluation of induction and permanent-magnet synchronous machines using drive-cycle energy and loss minimization in traction applications,” *IEEE Transactions on Industry Applications*, vol. 50, no. 1, pp. 395–403, 2014.
- [89] R. Marino, S. Peresada, and P. Tomei, “Adaptive observer-based control of induction motors with unknown rotor resistance,” *International journal of adaptive control and signal processing*, vol. 10, no. 4-5, pp. 345–363, 1996.

- [90] M. Bodson, J. Chiasson, and R. Novotnak, "High-performance induction motor control via input-output linearization," *Control Systems, IEEE*, vol. 14, no. 4, pp. 25–33, 1994.
- [91] J. Chiasson, "A new approach to dynamic feedback linearization control of an induction motor," *Automatic Control, IEEE Transactions on*, vol. 43, no. 3, pp. 391–397, 1998.
- [92] R. Marino, S. Peresada, and P. Tomei, "Output feedback control of current-fed induction motors with unknown rotor resistance," *Control Systems Technology, IEEE Transactions on*, vol. 4, no. 4, pp. 336–347, 1996.
- [93] G.-W. Chang, G. Espinosa-Perez, E. Mendes, and R. Ortega, "Tuning rules for the pi gains of field-oriented controllers of induction motors," *Industrial Electronics, IEEE Transactions on*, vol. 47, no. 3, pp. 592–602, 2000.
- [94] G. Espinosa-Perez, R. Ortega, and J. Nicklasson, "Torque and flux tracking of induction motors," in *Proc. of the European Control Conference*, 1995, pp. 342–347.
- [95] R. Ortega and G. Espinosa, "Torque regulation of induction motors," *Automatica*, vol. 29, no. 3, pp. 621–633, 1993.
- [96] V. I. Utkin, "Sliding mode control design principles and applications to electric drives," *Industrial Electronics, IEEE Transactions on*, vol. 40, no. 1, pp. 23–36, 1993.
- [97] K. B. Mohanty, "Sensorless sliding mode control of induction motor drives," in *TENCON 2008-2008 IEEE Region 10 Conference*. IEEE, 2008, pp. 1–6.
- [98] J. Guzinski and H. Abu-Rub, "Sensorless induction motor drive for electric vehicle application," *International Journal of Engineering, Science and Technology*, vol. 2, no. 10, 2010.
- [99] M. Ghanes and G. Zheng, "On sensorless induction motor drives: Sliding-mode observer and output feedback controller," *IEEE Transactions on Industrial Electronics*, vol. 56, no. 9, pp. 3404–3413, 2009.

- [100] P. Krause, O. Wasynczuk, and S. D. Pekarek, *Electromechanical motion devices*. John Wiley & Sons, 2012, vol. 90.
- [101] G. I. Bara, J. Daafouz, F. Kratz, and J. Ragot, “Parameter-dependent state observer design for affine lpv systems,” *International journal of control*, vol. 74, no. 16, pp. 1601–1611, 2001.
- [102] J. E. Slotine and W. Li, *Applied Nonlinear Control*. Englewood Cliffs, NJ: Prentice-Hall, 1991.
- [103] C. Chan, A. Bouscayrol, and K. Chen, “Electric, hybrid, and fuel-cell vehicles: Architectures and modeling,” *Vehicular Technology, IEEE Transactions on*, vol. 59, no. 2, pp. 589–598, 2010.
- [104] G. Murtaza, A. Bhatti, and Q. Ahmed, “Control-oriented model of atkinson cycle engine with variable intake valve actuation,” *Journal of Dynamic Systems, Measurement, and Control*, vol. 138, no. 6, p. 061001, 2016.
- [105] T. D. Do, H. H. Choi, and J.-W. Jung, “Nonlinear optimal dtc design and stability analysis for interior permanent magnet synchronous motor drives,” *IEEE/ASME Transactions on Mechatronics*, vol. 20, no. 6, pp. 2716–2725, 2015.
- [106] M. Zeraoulia, M. Benbouzid, and D. Diallo, “Electric motor drive selection issues for hev propulsion systems: A comparative study,” *Vehicular Technology, IEEE Transactions on*, vol. 55, no. 6, pp. 1756–1764, 2006.
- [107] J. Yu, W. Pei, and C. Zhang, “A loss-minimization port-controlled hamilton scheme of induction motor for electric vehicles,” *IEEE/ASME Transactions on Mechatronics*, vol. 20, no. 6, pp. 2645–2653, 2015.
- [108] V. A. Katić, B. Dumnić, Z. Čorba, and D. Milićević, “Electrification of the vehicle propulsion system—an overview,” *Facta Universitatis, Series: Electronics and Energetics*, vol. 27, no. 2, pp. 299–316, 2014.

- [109] A. Hanif, A. I. Bhatti, and Q. Ahmed, “Estimation of thermally de-rated torque of an hev drive using robust lpv observer,” in *American Control Conference, 2016. Proceedings of the 2016*, July 2016, pp. 1530–1535.
- [110] Z. Yang, F. Shang, I. P. Brown, and M. Krishnamurthy, “Comparative study of interior permanent magnet, induction, and switched reluctance motor drives for ev and hev applications,” *IEEE Transactions on Transportation Electrification*, vol. 1, no. 3, pp. 245–254, 2015.
- [111] L. Fang, S. Qin, G. Xu, T. Li, and K. Zhu, “Simultaneous optimization for hybrid electric vehicle parameters based on multi-objective genetic algorithms,” *Energies*, vol. 4, no. 3, pp. 532–544, 2011.
- [112] R. Marino, S. Scalzi, P. Tomei, and C. Verrelli, “Fault-tolerant cruise control of electric vehicles with induction motors,” *Control Engineering Practice*, vol. 21, no. 6, pp. 860–869, 2013.
- [113] P. Zhang, Y. Du, T. G. Habetler, and B. Lu, “A survey of condition monitoring and protection methods for medium-voltage induction motors,” *IEEE Transactions on Industry Applications*, vol. 47, no. 1, pp. 34–46, 2011.
- [114] R. Beguenane and M. E. H. Benbouzid, “Induction motors thermal monitoring by means of rotor resistance identification,” *IEEE Transactions on Energy Conversion*, vol. 14, no. 3, pp. 566–570, 1999.
- [115] K. Zhou, J. C. Doyle, K. Glover *et al.*, *Robust and optimal control*. Prentice hall New Jersey, 1996, vol. 40.
- [116] H. Werner, “Optimal and robust control,” 2007.
- [117] H. K. Khalil, E. G. Strangas, and S. Jurkovic, “Speed observer and reduced nonlinear model for sensorless control of induction motors,” *IEEE Transactions on Control Systems Technology*, vol. 17, no. 2, pp. 327–339, 2009.
- [118] J. Rivera, C. Mora-Soto, A. De La Mora, S. Di Gennaro, and J. Raygoza, “Field oriented control of induction motors with core loss.”

- [119] S. S. Williamson, A. Emadi, and K. Rajashekara, "Comprehensive efficiency modeling of electric traction motor drives for hybrid electric vehicle propulsion applications," *IEEE Transactions on Vehicular Technology*, vol. 56, no. 4, pp. 1561–1572, 2007.
- [120] S. Williamson, M. Lukic, and A. Emadi, "Comprehensive drive train efficiency analysis of hybrid electric and fuel cell vehicles based on motor-controller efficiency modeling," *IEEE Transactions on power electronics*, vol. 21, no. 3, pp. 730–740, 2006.
- [121] C. Poussot-Vassal, O. Sename, L. Dugard, P. Gaspar, Z. Szabo, and J. Bokor, "A new semi-active suspension control strategy through lpv technique," *Control Engineering Practice*, vol. 16, no. 12, pp. 1519–1534, 2008.
- [122] J. R. M. D. Reyes, R. V. Parsons, and R. Hoemsen, "Winter happens: the effect of ambient temperature on the travel range of electric vehicles," *IEEE Transactions on Vehicular Technology*, vol. 65, no. 6, pp. 4016–4022, 2016.
- [123] D. Huger and D. Gerling, "On the effects of high-temperature-induced aging on electrical machine windings," in *Electric Machines & Drives Conference (IEMDC), 2015 IEEE International*. IEEE, 2015, pp. 1018–1021.
- [124] J. Zhang, H. Yao, and G. Rizzoni, "Fault diagnosis for electric drive systems of electrified vehicles based on structural analysis," *IEEE Transactions on Vehicular Technology*, 2016.
- [125] S. N. Ali, A. Hanif, and Q. Ahmed, "Review in thermal effects on the performance of electric motors," in *Intelligent Systems Engineering (ICISE), 2016 International Conference on*. IEEE, 2016, pp. 83–88.
- [126] P. Pillay and M. Manyage, "Loss of life in induction machines operating with unbalanced supplies," *IEEE transactions on energy conversion*, vol. 21, no. 4, pp. 813–822, 2006.

- 
- [127] P. Gnani *et al.*, “Windings temperature and loss of life of an induction machine under voltage unbalance combined with over-or undervoltages,” *IEEE Transactions on Energy Conversion*, vol. 23, no. 2, pp. 363–371, 2008.
- [128] P. Lazari, J. Wang, and L. Chen, “A computationally efficient design technique for electric-vehicle traction machines,” *IEEE Transactions on Industry Applications*, vol. 50, no. 5, pp. 3203–3213, 2014.
- [129] Z. Huang, “Modeling and testing of insulation degradation due to dynamic thermal loading of electrical machines,” Ph.D. dissertation, Lund University, 2017.
- [130] S. Zhang, J. J. Yang, and G. G. Zhu, “Lpv gain-scheduling control of an electronic throttle with experimental validation,” in *American Control Conference (ACC), 2014*. IEEE, 2014, pp. 190–195.
- [131] M. Amrhein and P. T. Krein, “Dynamic simulation for analysis of hybrid electric vehicle system and subsystem interactions, including power electronics,” *IEEE transactions on vehicular technology*, vol. 54, no. 3, pp. 825–836, 2005.
- [132] T. Peni and P. J. Seiler, “Computation of lower bounds for the induced  $l_2$  norm of lpv systems,” *International Journal of Robust and Nonlinear Control*, vol. 26, no. 4, pp. 646–661, 2016.